# Heavy Oil Upgrading through Oxidative Cracking in Near-critical and Supercritical Water

**Pedro Manuel Arcelus Arrillaga**

Imperial College London

Chemical Engineering Department

Thesis submitted for the degree of Doctor of Philosophy (PhD)
to Imperial College London

Supervised by:

Dr. Marcos Millan Agorio

Prof. Klaus Hellgardt

**Declaration of Originality:**

The author declares that the contents of this work are the product of his original effort and that anything else has been appropriately referenced.

Pedro Manuel Arcelus Arrillaga

# Abstract

The gradual decline in conventional oil production combined with an increasing world energy demand has made the production and upgrading of heavy and extra heavy oil feedstocks crucial for the future of the global energy market. Properties of heavy oil such as high viscosity and high specific gravity as well as the high percentage of asphaltenes, heteroatoms and metals cause severe problems during extraction and refining processes. As a result, traditional upgrading technologies are not suitable as a standalone method to process these feedstocks. This makes necessary the development of alternative or complementary technologies to process heavy oil feedstocks in a more efficient and environmentally friendly way.

This work is aimed to study an alternative heavy oil upgrading process that takes advantage of the unique properties of water at near-critical and supercritical conditions as reaction medium to perform the oxidative cracking of heavy oil feedstocks. The process consists of three main stages including the partial oxidation, cracking of the molecule, and removal of part of the oxygen incorporated from the final product. The process was studied using phenanthrene and methyl naphthalene as heavy oil model compounds and also Maya oil vacuum residue as real feedstock. This was performed in a purposely built microbomb batch reactor and an oxidative cracking flow reactor. The effect of the main process variables and the potential reaction pathways were studied with model compounds. Then the process was tested with real feedstock and the inclusion of a zeolite based catalyst to enhance yields to light oil was considered.

It was found that process conditions have an important influence in the yield and selectivity to different product fractions. Optimum conditions to maximize the production of organic soluble products were determined. It was observed that polycyclic aromatic hydrocarbons were not reactive in the absence or at low concentration of reactive oxygen species. However, oxygenated intermediates continued to react in water alone. In addition, it was observed that intermediate products were mainly oxygenated compounds and that the oxygenation proceeded preferentially through central rings. A hydrogen rich gas product was obtained. Experiments with vacuum residue showed that high yields to liquid products with low boiling point are obtained keeping low yields to coke at most conditions studied. The addition of a zeolite based catalyst showed improvement in the process, increasing the yield to light oil and reducing the average molecular weight of the product. Heteroatoms and metals present were mainly removed as coke and showed to be relatively stable.

# Acknowledgement

This thesis not only represents five years of absolute dedication, hard work and sacrifices, but the attainment of years of efforts by many professionals and friends who deserve to be acknowledged and recognized. I extend my complete gratitude to all these people that in a way or another assisted me in this quest and without whom the accomplishment of this work would have just been impossible.

Throughout these years in Imperial, I have had moments of great happiness, great disappointments, moments of complete frustration and great satisfactions, which would not have meant the same if it was not for the remarkable individuals with whom I shared them. Doing a PhD in Imperial has been an amazing experience full of challenges and life lessons that have tested my character and have shaped me into the person I am today. It has also given me the opportunity to meet people from different nationalities and backgrounds from which I have not just learnt about science and engineering but have also opened my world into a whole load of different opinions, traditions and ideas enriching me not just academically but most importantly as a person.

I want to take this opportunity to thank and give recognition in no particular order to the people that have helped me into the finish line and have made this dream possible.

First and foremost, I want to thank my mom and sister that have been a source of inspiration every second of this great experience. They have suffered as much as I have from the distance and have remained an inexhaustible source of love and affection throughout these years.

I also want to thank the rest of my family for their encouragement and support, which has been crucial throughout my life in the achievement of my goals.

I would like to extend my total gratitude and give a special recognition to my supervisor and academic mentor Dr. Marcos Millan without whom the accomplishment of this thesis would have not been possible. I am indebted with Dr. Millan, whose support, advice, knowledge and kind help whenever needed, guided me to successfully finish my PhD and have opened me the doors to pursue a career in science.

I also want express my gratitude to my supervisor Prof. Klaus Hellgardt from whom I have learnt a lot and whose knowledge and critical contributions have nurtured this work and have showed me the path to excel in academic research.

I want to specially thank Dr Khairul Rostani, Dr Elias Martinez and Mr David Flores who I consider my brothers and in the distance have lived and suffered the experience as much I have done and have remained a constant source of encouragement throughout these years.

I want to thank Dr Holda Puron and Dr Manuel Piñuela who have been a family in London to me. I have no words to thank you enough.

A special thanks to Dr Beatriz Fidalgo, Dr Jose Luis Pinilla, Dr Cesar Berrueco and Dr Esther Llorente for their unconditional friendship, contributions and guidance at early stages of my PhD and especially at difficult times when things got supercritical. Thank you for all the advice and also for pulling my ear every time I lost focus.

I also want to thank my friends and colleagues Dr Jose Bermudez, Dr Tomas Ramirez, Dr Yatika Somrang, Mr Daniel Torres, Dr Javier Remon, Dr Matt Boot-hanford, Dr John Blamey, Ms Eneritz Fernandez, Ms Xiangyi Long, Dr Jie Yu, Dr Tomas Hills, Dr Zili Zang, Dr Mario Villanueva, Mr Marco Jano, Dr Vicky Skoulou, Dr Emilio Bejarano, Mr Jonathan Ball, Mr Aderlanio da Silva, Mr Bhavish Patel, Dr Rafizan Daud, Mr Joseph Yao and Mr Peter Clough with whom I have shared amazing times and have always been there for me.

I am grateful with Susi Underwood and Anusha Sri-Pathmanathan for the support, assistance and help throughout my PhD, especially for their help to arrange and clarify details on the multiple interruption of studies occurred throughout my PhD.

My gratitude to Tony Meredith, Richard Wallington, Paul Mayer, Paul Crudge, Chin Lang, Patricia Carry, Sarah Payne, Dr Severine Toson, Pim Amrit, Jesus Gomez and Ben Kistnah for their technical assistance and help in innumerable occasions throughout my PhD.

I thank Dr Tatiana Klimova for her support, guidance and council since my undergraduate studies.

I also want to thank my MSc students Ms Carla de Sa Martins, Mr Leonard Van Thiele and Mr Arran Marais-Gilchrist whose projects were related to this PhD thesis and who performed an outstanding work in our research group.

I am very grateful with Dr Isabel Suelves and Dr Jose Luis Pinilla for giving me the opportunity to develop a short research stay in their facilities at the Institute of Carbochemistry in Zaragoza, Spain.

I am thankful with Imperial College Trust who granted me economical support in two occasions to present my work in two important international conferences.

Finally I want to acknowledge the economic support provided by the National Council of Science and Technology in Mexico, CONACYT for the partial funding of this PhD.

And above all, I want to dedicate this to you who have always been at my side. Cannot thank you enough!!

# Table of Contents

# List of Tables

# List of Figures

# List of Abbreviations

| | |
|---|---|
| **A** | Cross sectional tube area |
| **Ã** | Pre-exponential factor |
| **Å** | Ångström |
| **API** | American Petroleum Institute |
| **ASTM** | American Society for Testing and Materials |
| **BET** | Brunauer Emmet and Teller |
| **BHJ** | Barrett Joyner and Halenda |
| **bp** | Boiling point |
| **C** | Concentration |
| **$C_{mol}$** | Carbon moles |
| **DI** | De-ionized |
| **$d_T$** | Tube internal diameter |
| $\delta$ | Density |
| **E** | Error percent |
| **Ea** | Activation energy |
| **EDX** | X-ray spectroscopy |
| **FID** | Flame ionization detector |
| **GC** | Gas chromatography |
| **h** | Heat transfer coefficient |
| **H** | Heating time constant |
| **H/C** | Hydrogen to carbon molar ratio |
| **HOMO** | Highest occupied molecular orbital |
| **HPLC** | High performance liquid chromatography |
| **ICP** | Induced coupled plasma |
| **k** | Kinetic constant |
| **$l_t$** | Length of tube |
| **LUMO** | Lowest unoccupied molecular orbital |
| **m** | Mass |
| **M** | Mean value |
| **mbpd** | Million barrels per day |
| **MS** | Mass spectrometry |
| **NCW** | Near-critical water |
| **NIST** | National Institute of Standards and Technology |
| **NMP** | N-methyl pyrrolidone |
| **OCR** | Oxidative cracking reactor |
| **OES** | Optical emission spectroscopy |
| **O/C** | Oxygen to carbon molar ratio |
| **$O/O_{stoich}$** | Moles of oxygen fed respect to the stoichiometric oxygen |

| | | | |
|---|---|---|---|
| **O/VR** | Mass of oxygen respect to the mass of vacuum residue fed | **VR** | Vacuum residue |
| **P** | Pressure | **X** | Conversion |
| **PAH** | Polycyclic aromatic hydrocarbon | **XRD** | X-ray diffraction |
| **ppm** | Parts per million | | |
| **PTFE** | Polytetrafluoroethylene | | |
| **q** | Volumetric flow rate | | |
| **ROS** | Reactive oxygen species | | |
| **SCW** | Supercritical water | | |
| **SCWO** | Supercritical water oxidation | | |
| **SD** | Standard deviation | | |
| **SE** | Standard error | | |
| **SEC** | Size exclusion chromatography | | |
| **SEM** | Scanning electron microscopy | | |
| **SS** | Stainless steel | | |
| **T** | Temperature | | |
| **T** | Residence time | | |
| **Θ** | Heating time | | |
| **TCD** | Thermal conductivity detector | | |
| **TGA** | Thermogravimetric analysis | | |
| **u** | Unit of atomic mass | | |
| **Vr** | Volume of reactor | | |

# Chapter 1
# Introduction

An overview of the current world energy outlook and the need to process heavy oil feedstocks in order to meet the energy requirements in the decades to come is given in the present chapter. Moreover, the concepts behind the upgrading of heavy oil through oxidative cracking in supercritical water are introduced. Finally, the fundamental research questions that are addressed in this work as well as the aims and structure of this thesis are presented.

## 1.1. INTRODUCTION

According to the International Energy Agency, world energy consumption is expected to increase forty three percent between the years 2015 and 2040 as shown in Figure 1.1. Nowadays, most of the energy consumed is obtained from liquid fuels derived from fossil sources accounting for thirty two percent of the total world energy demand. Although the share of liquid fuels in the energy market is expected to drop from thirty two percent to twenty eight percent in 2040, they will continue to be the main energy supply worldwide in the decades to come, as seen in Figure 1.1 (1).

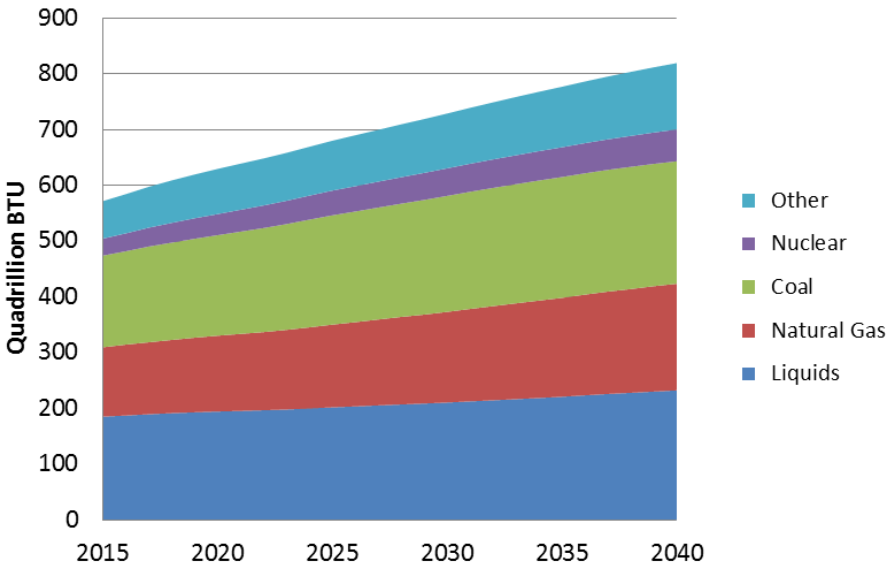


*Figure 1.1 World energy consumption by fuel type between 2015 and 2040 adapted from (1)*

It is estimated that in order to meet the future energy demand, liquid fuel production will have to increase to approximately 119 million barrels per day (mbpd) by the year 2040, which represents an increment of thirty percent of the actual production. In order to achieve this, an increment in the production of liquid fuels from different sources is expected as shown in Figure 1.2 (2).

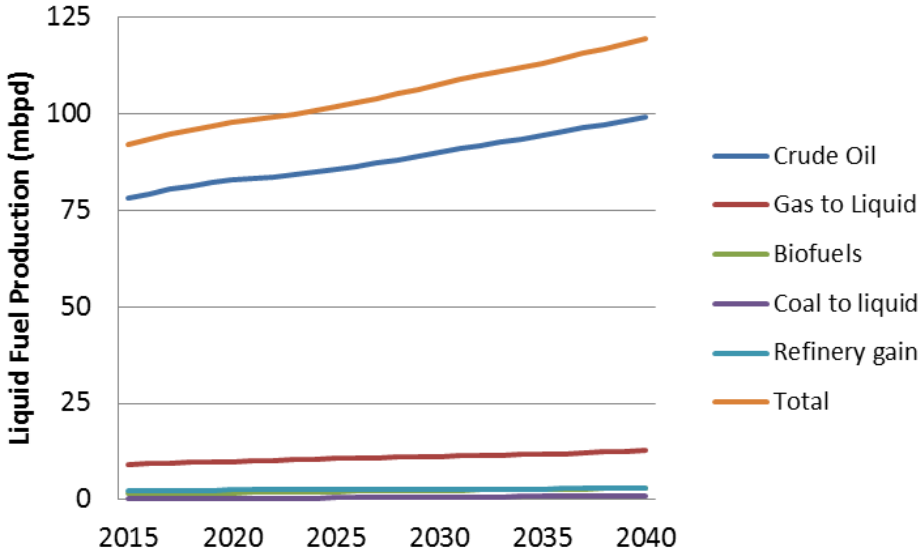


*Figure 1.2 World liquid fuel production between 2015 and 2040 adapted from (2).*

Crude oil is expected to remain the main source of liquid fuels in the upcoming years. It is estimated that it will account for eighty three percent of the total liquid fuel production by the year 2040. However, in order to meet the required fuel supply, crude oil production has to increase thirty percent from the actual production to reach 99 mbpd (2).

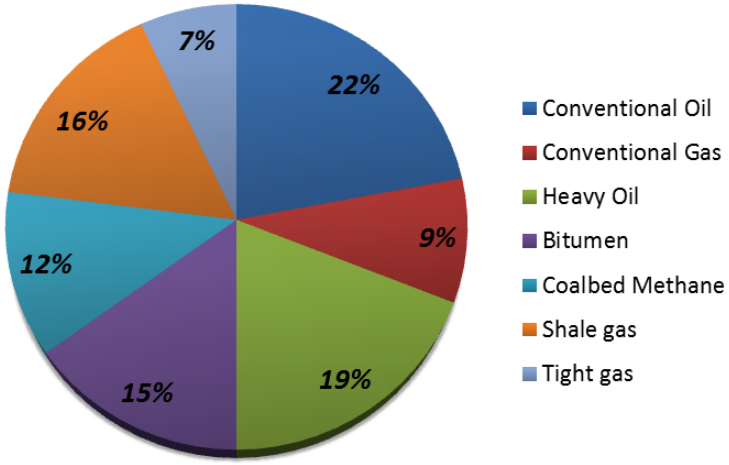


*Figure 1.3 World's hydrocarbon reserves distribution adapted from (3).*

A detailed classification of the world's hydrocarbon reserves is shown in Figure 1.3. The figure shows that thirty four percent of the total hydrocarbon reserves are composed by heavy oil and bitumen (unconventional resources) compared to twenty two percent of crude oil (conventional resource) (3). The abundance of heavy oil feedstocks combined with the continuous decline of conventional crude oil reserves makes the development of technologies to process and upgrade heavy oil of great importance for the future of the energy market. In fact, estimations show that oil production from unconventional sources has to increase to 13 mbpd by the year 2035 in order to meet future energy demand (4). This cannot be achieved with the actual extraction and upgrading technologies in operation and will require the development and implementation of new and complementary technologies to enable efficient heavy oil processing. Research in the development of these new technologies can be boosted by the increasing necessity to process these feedstocks as well as by a potential increase in oil prices expected to occur in the years to come (5,6).

Some of the main challenges to address during the processing of unconventional oil feedstocks are the high heteroatom and metal content and their highly asphaltenic nature as well as their high viscosity and density (4,7–9). These characteristics, common in heavy oils, cause major problems during upgrading processes like catalyst poisoning due to metal deposition and coke formation that results in lower yields to higher value fuel (10). Normally, crude oil refining consists of a series of processes based on carbon rejection and hydrogen addition that can be performed in the presence or absence of a catalyst, depending on the nature of the oil fraction being upgraded. A generic process flow diagram of an oil refining process adapted from literature is shown in Figure 1.4.

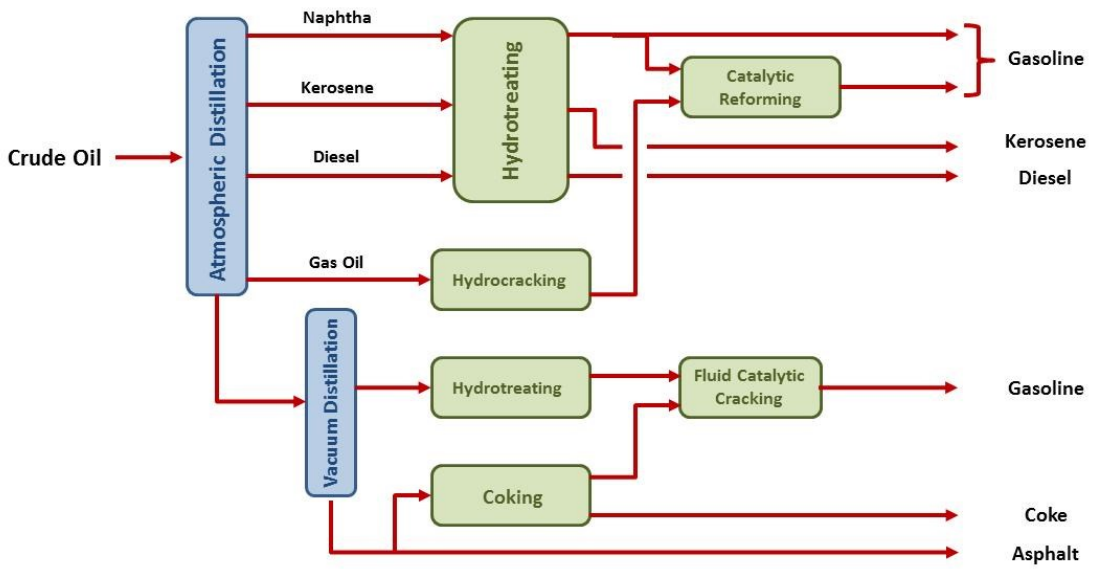


*Figure 1.4 Simplified oil refining process scheme adapted from (11).*

Upgrading processes based on hydrogen addition are meant to make the feedstock lighter in order to decrease its boiling point range (hydrocracking) and to remove impurities such as metals and heteroatoms from its structure (hydrotreating). On the other hand, processes based on carbon rejection (coking, vis-breaking and fluid catalytic cracking) use heat and in occasions an added catalyst to fractionate the structure of heavy hydrocarbons present in heavy oil into lighter fractions without the need of adding hydrogen into the process. These technologies are not effective as a standalone refining method to process heavy oil feedstocks due to disadvantages such as catalyst de-activation and poisoning, high yields to coke, poor conversions and yields to light fractions, high volumes of hydrogen required as well as large amounts of catalyst needed, which represent high operational costs (12,13). In spite of this, it has been suggested that the best alternative to meet these challenges is the integration of upgrading technologies in order to increase the yields to valuable high quality products in refineries (14). In addition, fundamental technology challenges like catalyst de-activation and coking, development of selective catalysts and the optimization of process conditions have to be further addressed (15). The abovementioned issues provide an opportunity to conduct research on new technologies that can provide alternatives to the actual processes or be used as complementary technologies to upgrade heavy oil feedstocks in a more effective way.

Asphaltenes are the most complex species found in heavy oil. They are composed of polycyclic aromatic hydrocarbons (PAHs), which contain heteroatoms like sulfur or nitrogen and metals such as vanadium and nickel in their structure. It has been reported that enzymes found in certain fungi species are capable of degrading PAHs in an energy efficient way (16–18). Experimental results by Hammel KE using short chain PAHs such as phenanthrene and anthracene, have shown that the reaction pathway of PAH fungi degradation proceeds through the oxidation of the central ring (19). This was used as a fundamental concept for the development of the proposed process in this work.

The novelty of this work lies in the development of a process that takes advantage of the characteristic properties near-critical water (NCW) and supercritical water (SCW) have as reaction medium, to be implemented in a process that integrates the concept of oxidation of PAHs previously discussed with the upgrading heavy oil feedstocks. The process denominated as oxidative cracking is schematically represented in Figure 1.5. It consists of three main stages of reaction. First heavy hydrocarbons present in the original heavy oil are partially oxygenated in NCW or SCW. In this stage the process takes advantage of the complete solubility that oxygen has in near-critical and supercritical water and also the homogeneous dispersion of heavy hydrocarbons in the reaction medium, which greatly reduces mass transfer limitations in the process. Second, the oxygenated intermediates

crack into lighter species at the oxygenated sites weakened by the presence of the heteroatom. Finally, part of the oxygen initially incorporated into the organic product is removed through carbon and oxygen rejection processes improving the quality of the product and reducing the need of further refining.

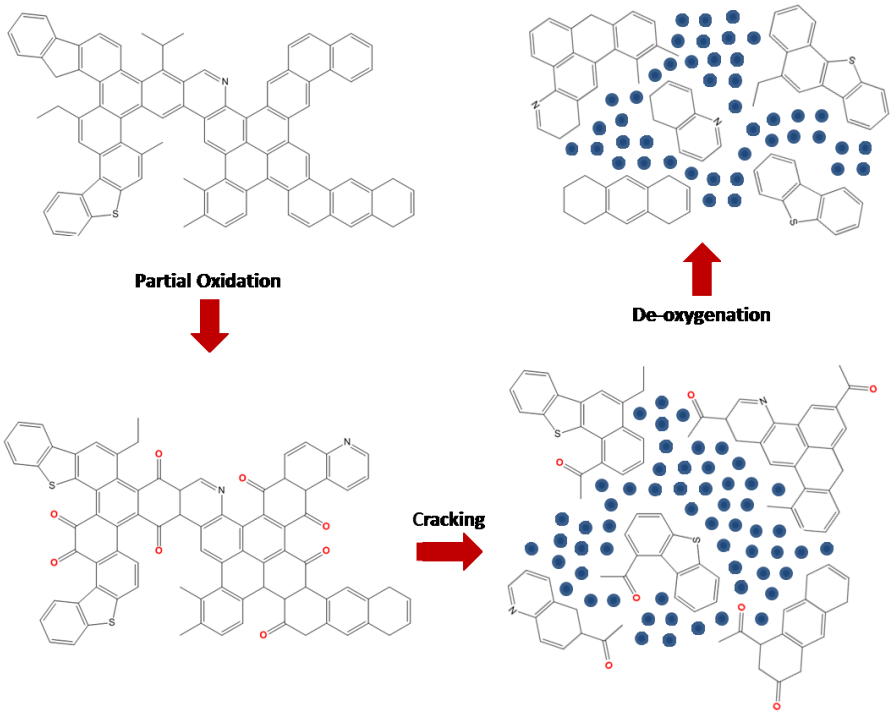


*Figure 1.5 Conceptual representation of the process to upgrade heavy oil through oxidative cracking in water at near-critical and supercritical conditions.*

## 1.2. AIM OF THE THESIS

This work aimed to develop and assess a heavy oil upgrading process through oxidative cracking in NCW and SCW. The approach of this project is twofold, 1) the use of PAHs such as phenanthrene and methyl naphthalene to perform the proof of concept, in depth study of the fundamentals of the process as well as the study and optimization of process variables, and 2) process evaluation with an extra heavy oil feedstock, Maya oil vacuum residue (VR).

The PAHs selected as heavy oil model compounds for this work are considered a good representation of the main building blocks of asphaltenes commonly present in heavy oil feedstocks. The work performed with model compounds enabled the detailed study of the process by identifying the main reaction products as well as the potential reaction pathways.

The use of model compounds also delivered a good understanding of the effect of process conditions such as pressure, temperature, initial oxygen loading and reaction time in the system, which can be implemented in the optimization of reaction conditions to be used in reactions with real heavy oil feedstocks.

In order to achieve this aim, a series of objectives enlisted below were set.

1) To design and commission a batch and a flow reaction systems as well as to develop an experimental methodology to study the hydrothermal oxidative cracking of heavy oil at different reaction conditions. This included the following tasks:
   - Modification and optimization of an in-house designed microbomb batch reactor.
   - Design and commissioning of a continuous flow reactor.
   - Development of an experimental method to recover and analyze the different products obtained from reactions with heavy oil model compounds as well as from reactions with real heavy oil feedstocks.

2) To study the effect of process conditions such as pressure, temperature and initial oxygen loading in the process using heavy oil model compounds in order to:
   - Understand how changes in reaction conditions affect conversion and product distribution in the process.
   - Determine the optimum reaction conditions to achieve high conversions while maintaining a high selectivity to organic soluble products.
   - Identify the main products of reaction and study how these are determined by the different reaction conditions studied.

3) To determine the potential reaction pathways using heavy oil model compounds and gain insight on the reactivity of the different species in the system. The objective was covered with the following activities:
   - Determine the role of the different species (water and oxygen) in the process.
   - Study the reactivity of the products according to their nature (PAHs and oxygenated products) at different stages of the process.

4) To evaluate the process with real heavy oil feedstocks with special emphasis on :
   - Maximizing conversion to light fractions with a boiling point below 450 °C while maintaining low yields to coke.
   - Evaluating the potential of the process to decrease the average molecular weight of the oil recovered.

- Assessing the capacity of the process to remove heteroatoms and metals from the original oil.

5) To develop and test catalysts aiming at enhancing cracking and oxidation capacity of the system in order to improve the upgrading of heavy molecules like asphaltenes commonly present in heavy oils.

During this project, a collaboration with the Institute of Carbochemistry (CSIC) in Zaragoza, Spain was established for the design, synthesis and characterization of catalysts used in the upgrading of heavy oil as part of the joint project I-LINK-0439.

## 1.3. THESIS STRUCTURE

The thesis is divided in eleven chapters including a) the background and introduction, b) the design and commissioning of the reaction set ups as well as the experimental procedure, c) the experimental results, d) the conclusions derived from this work including recommendations for future work and e) the references and appendix of the thesis.

An outline of the chapters that composes this work with a brief description of the main content on each of them is given below.

Chapter 2 presents a comprehensive survey of literature focused on relevant concepts needed for the development of this project. Topics such as heavy oil, supercritical water, hydrothermal oil upgrading and catalysis in SCW are extensively discussed.

Chapters 3 and 4 are dedicated to the design and commissioning of the batch and continuous reaction set ups as well as to provide a detailed description of the experimental procedures and product analysis techniques.

Chapter 5 presents the results obtained from the oxidative cracking of phenanthrene in the microbomb batch reactor. In this chapter, an extensive evaluation of the effect that process conditions (temperature, pressure, $O/O_{stoich}$ ratio and reaction time) have in conversion, selectivity and product yields has been discussed. Moreover, the evolution of reaction products at different reaction times and temperatures was studied and a potential reaction pathway has been proposed.

Chapter 6 is dedicated to present the results of the work performed using methyl naphthalene as model compound in the continuous oxidative cracking reactor. The process

was analyzed at short residence times in order to identify intermediate species present at early reaction stages. In addition a potential reaction pathway has also been proposed.

Chapter 7 and 8 are focused in the analysis of the oxidative cracking process using Maya oil vacuum residue as feedstock. As part of the work results obtained in the presence and absence of a zeolite based catalyst were compared to assess the impact of the catalyst in the process. Moreover, the evolution with reaction time and temperature of the different products of reaction as well as the concentration of metals (V) and heteroatoms (S and N) in the liquid product fraction were analyzed.

Chapter 9 is dedicated to the general conclusions obtained from this work as well as to discuss some particular conclusions of the work performed with heavy oil model compounds and heavy oil feedstock. In addition, some recommendations for future work have been made.

# Chapter 2
# Background

In this chapter, relevant background information on heavy oil properties, hydrothermal oil upgrading, supercritical water and some relevant analytical techniques are discussed. First, properties and composition of heavy oil feedstocks as well as the traditional heavy oil upgrading processes are addressed. This is followed by a brief discussion on the reactivity of PAHs. Then, a detailed review of the main properties of SCW and some chemical reactions relevant for this work is provided. Moreover, relevant literature on the upgrading of heavy oil feedstocks in water at near-critical and supercritical conditions is discussed with special emphasis on the role that water plays in the reaction as well as the effect it has in the removal of heteroatoms and metals. Some literature on heterogeneous catalysis in SCW is also reviewed. Finally, a brief description of the operation principles of the analytical techniques used in this project to analyze the products of reaction is provided.

## 2.1. HEAVY CRUDE OIL

Crude oil, also known as petroleum, is commonly defined as a complex mixture of hydrocarbons containing different amounts of heteroatoms (S, N and O), metals (Ni and V) and salts depending on the nature of the feedstock. Therefore, properties of crude oils such as density, viscosity and volatility may vary largely between feedstocks (20,21). A complete agreement in an adequate classification of crude oil is complicated due to the complex composition and diverse nature of the oils. It is commonly accepted that it can be classified depending on its physical properties such as viscosity and density (API gravity). Based on these criteria, heavy oil can be defined as a feedstock with an API gravity below 20° and 100 cP at reservoir conditions. Crude oils that at reservoir conditions have an API gravity below 10° and high viscosities up to 10,000 cP are classified as extra heavy oil. Extra heavy oil that at reservoir conditions presents a viscosity over 10,000 cP is categorized as bitumen (4,8,12,20).

Light and heavy crude oil feedstocks present important differences. The latter, is characterized by low API gravities, high concentrations of impurities such as metals and heteroatoms and by the low yields to distillate fractions with higher quality and value

obtained after refining. A comparison of the properties of different types of oil is shown in Table 2.1.

*Table 2.1 Crude oil properties adapted from (8,22).*

| | Light Crude Oil | Heavy Crude Oil | Extra Heavy Crude Oil |
|---|---|---|---|
| **API gravity (°API)** | > 20 | 10 - 20 | <10 |
| **Viscosity (cP)** | <100 | >100 | <10,000 |
| **Asphalthene content (%w/w)** | 0.1 - 12 | 11 - 25 | 15 - 40 |
| **Total sulfur (%w/w)** | 0.05 - 4 | 0.1 - 5 | 0.8 - 6 |
| **Total nitrogen (%w/w)** | 0.02 – 0.5 | 0.2 – 0.8 | 0.1 – 1.3 |
| **Metal content V & Ni (ppm)** | 10 - 200 | 50 - 500 | 200 - 600 |

Moreover, oils can also be classified according to their solubility into four different categories: saturates, aromatics, resins and asphaltenes (SARA). Saturates are mainly composed of non-polar structures, which include linear, branched and saturated cyclic hydrocarbons. The aromatic fraction is normally polarizable and is mainly composed by species containing one or more fused aromatic rings. However, differentiating between resin and asphaltene fractions is difficult as both have chemical similarities presenting polar substituents in their structure. The common way to distinguish one from the other relies on the complete miscibility of resins and the insolubility of asphaltenes in short chain alkane solvents (pentane, hexane and heptane) (23,24). As a result, crude oil samples can be classified into maltenes and asphaltenes based on their solubility or insolubility in these solvents (25). In this work, asphaltenes are defined as the fraction of crude oil that precipitates in the presence of an excess of n-heptane as graphically explained in Figure 2.1.

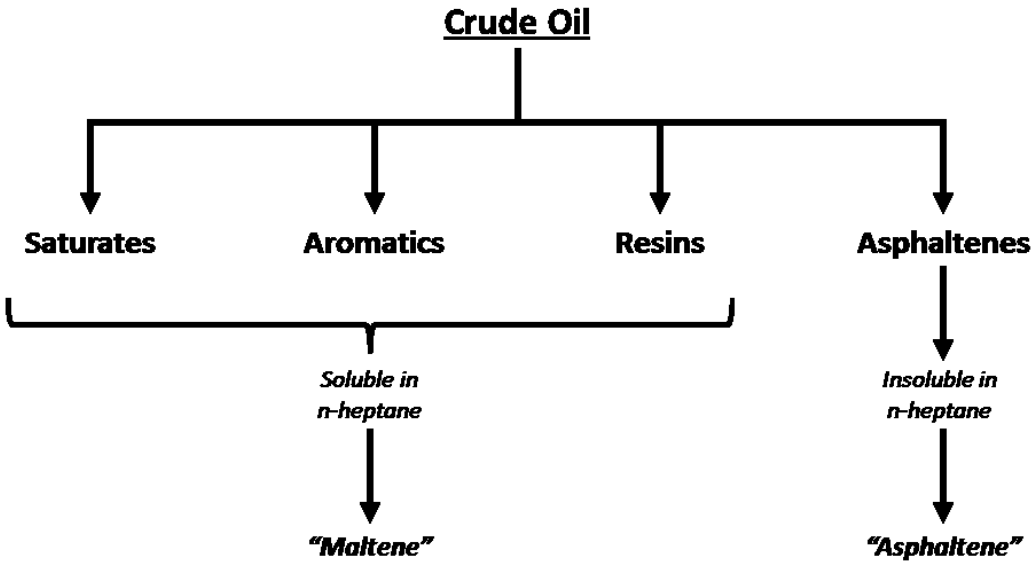


*Figure 2.1 Crude oil fractionation graphic representation.*

Important processing difficulties derived from a complex chemical nature (high heteroatom and metal contents) and from physical properties such as high viscosity and density are presented by heavy oil feedstocks. Chemical composition of different heavy oil resources in the world are shown in Table 2.2.

*Table 2.2 Elemental analysis of different heavy oil feedstocks adapted from (7,26–28) .*

| | Maya (Mexico) | Morichal (Venezuela) | Athabaska (Canada) | Paraho (United States) |
|---|---|---|---|---|
| **C (%w/w)** | 83.96 | 80.60 | 83.20 | 85.30 |
| **H (%w/w)** | 11.80 | 8.10 | 9.70 | 11.20 |
| **O (%w/w)** | 0.35 | 4 | 1.70 | 1 |
| **N (%w/w)** | 0.32 | 1.80 | 0.40 | 2 |
| **S (%w/w)** | 3.57 | 5.50 | 5.30 | 0.50 |
| **Metals (ppm)** | 351.5 | 274 | 340 | 75 |
| **Asphaltene (%w/w)** | 11.32 | 10 | 18.60 | nd |

These characteristics of heavy oil present great processing challenges such as low mobility in the reservoir, difficult and costly transportation and low processing capacity in refineries (14). Moreover, low yields to high value fractions as well as high rates of catalyst deactivation due to metal deposition and coke formation are commonly found during refining stages (10).

### 2.1.1. Asphaltenes

Asphaltenes are the heaviest, most highly polar and complex molecules that are present in crude oil (29). They normally present high solubility in aromatic hydrocarbons such as toluene, but are found to be insoluble when short chain alkanes (n-pentane or n-heptane) are used as solvent. It is thought that the solubility properties of asphaltenes are mainly due to the strong presence of polar groups, the degree of condensation of the fused ring aromatic structures and their high molecular mass that result in poor solubility in alkane solvents (30).

Asphaltenes are normally defined based on their chemical composition as a condensed polycyclic aromatic compound that contains heteroatoms in small amounts and traces of metals suspended in crude oil (7,31). General consensus agrees that an asphaltene can be represented by a condensed fused polyaromatic core with cyclo-alkyl substituents as part of its structure (32,33). Moreover, asphaltenes are formed of polycyclic aromatic clusters with side chains of up to thirty carbon molecules. Heteroatoms such as sulfur and nitrogen are commonly found in the form of aromatic rings with thiophenes and pyrrole/pyridine

structures, nitrogen-containing molecules in the form of amides / amines, oxygen in the form of ketones / phenols / oxanes and metals in a porphyrin ring structure (34).

The definition of asphaltenes based on their chemical structure has been a subject of great debate among the scientific community. Proposed structures have evolved with time and vary according to the analytical technique used in their determinations. When research on this topic commenced, asphaltenes were proposed to be large organic structures composed of a maximum of ten aromatic rings fused together and connected through sulfur and alkyl bonds in order to constitute oligomers (35). It is believed that a model asphaltene molecule contains from forty to seventy aromatic rings and between seven to twenty one heteroatoms in its structure (35,36). Recently, studies performed with non-destructive analytical techniques have suggested that the most likely chemical structure of an asphaltene is better represented by small clusters of five to seven fused aromatic rings joined together by means of heteroatom and aliphatic chains (37). The chemical structure of asphaltene molecules has been represented in two different ways, the continental and archipelago models. The continental model shows asphaltenes as molecules composed of a polycyclic aromatic core surrounded by aliphatic chains (38,39), while the archipelago model is represented by small groups of aromatic cores joined together by aliphatic chains (40,41) as shown in Figure 2.2.

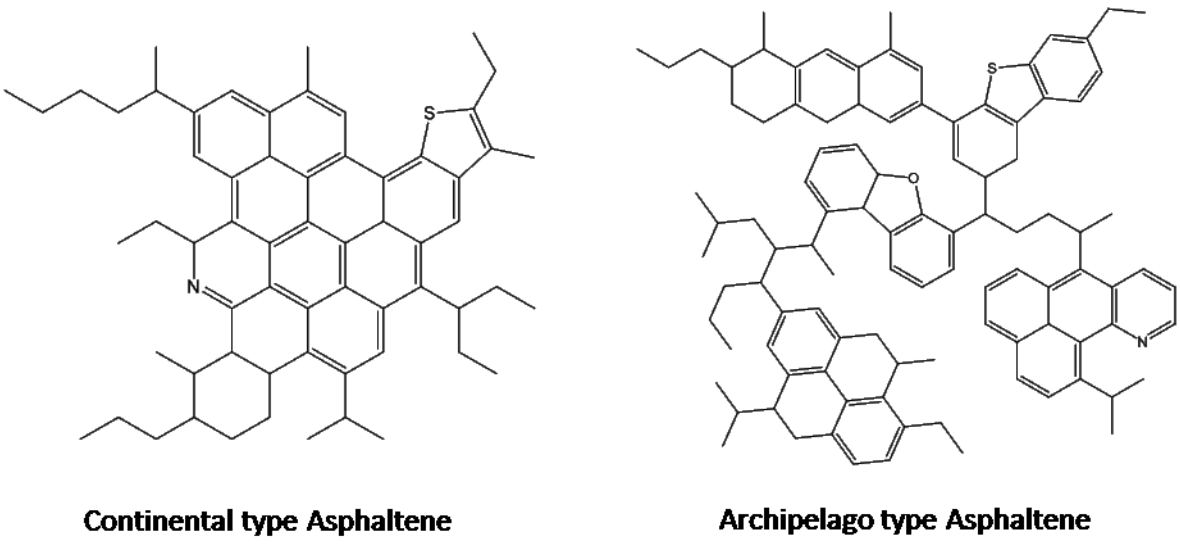


*Figure 2.2 Hypothetical structures of asphaltene molecules (adapted from 38, 39-41).*

### 2.1.2. Traditional upgrading processes

Oil refining involves a series of thermal and catalytic processes intended to convert heavy organic molecules found in crude oil into lighter fractions of higher quality and value in the

market. During refining, processes involving cracking of aromatic rings, changes in the number of carbon atoms and important changes in the molecular structure of the compounds take place (20). To date, the most effective refining processes available to upgrade heavy oil feedstocks are those based on increasing the H/C ratio of the oil. In order to achieve this, technologies based on carbon rejection and hydrogen addition, which present advantages and disadvantages on economic and technical grounds are normally implemented (14,42).

Carbon rejection processes (thermal processes) are those in which large molecules found in heavy oil crack into two molecules, a small one with a high H/C ratio commonly denominated as distillate and a second one with a low H/C ratio (PAHs) that can condense into coke. On the other hand, hydrogen addition processes such as hydrocracking and hydrotreating increase the H/C ratio of the molecule by adding hydrogen, which results in lower coke yields and higher yields to lighter liquid hydrocarbons (21,43). Commercially available processes to upgrade oil and their main operating conditions are listed in Table 2.3.

Nowadays, the increasing necessity to process heavy oil feedstocks have made traditional oil refining technologies based on hydrogen addition and carbon rejection (coking, catalytic cracking or hydrotreating) insufficient and not suitable as a standalone refining method. Therefore, it has been proposed that in order to obtain greater yields of good quality oil the combination of different technologies in an integrated process is the best alternative (14). Moreover, important technical challenges such as process optimization, catalyst poisoning and deactivation, high levels of coking and lower yields to higher value products need to be addressed. The above-mentioned issues present an opportunity for the development and application of new technologies as the implementation of hydrothermal processes in water at near-critical and supercritical conditions as an alternative technology to upgrade heavy oil resources.

*Table 2.3 Traditional oil upgrading processes commercially available, adapted from (15,20,44–48).*

| | **C Rejection** | | | **H Addition** | |
|---|---|---|---|---|---|
| | **Visbreaking** | **Coking** | **Fluid Catalytic Cracking** | **Hydrotreating** | **Hydrocracking** |
| **Temperature (°C)** | 455 - 515 | 480 - 520 | 480 - 540 | 260 - 345 | 370 - 450 |
| **Pressure (bar)** | 3 - 20 | 1 - 10 | < 2 | 35 - 70 | 100 - 300 |
| **Catalyst** | No catalyst | No catalyst | Zeolites | Bimetallic catalysts | Bimetallic catalysts |
| **Challenges** | -Coke | -High coke yield<br>-Low liquid yields | -High coke yield<br>-High catalyst consumption | -Catalyst deactivation<br>-High $H_2$ Pressure | -Catalyst deactivation<br>-High $H_2$ Pressure |

### 2.1.3. Reactivity of polycyclic aromatic hydrocarbons

Understanding the kinetic and thermodynamic behavior of PAHs is of great relevance to predict to some extent the reactivity of the system. Three main approaches on how to determine reactivity in these systems have been formulated and will be briefly explained in the following sections.

#### *2.1.3.1. Clar theory of polycyclic aromatic structures stability*

Clar's rule state that in systems composed of more than one fused aromatic rings forming a straight structure, two π electrons of a sextet present greater mobility than the remaining four electrons and can migrate from one ring to another within the structure. Therefore, the π electrons in a double bond shared by two aromatic rings are considered to belong to both. However, in order for a further migration of the π electrons into a third aromatic ring to take place, two positive charges need to be transferred into the double bond located between the second and third aromatic rings, which makes all double bonds mobile. This enables the migration of the two π electrons as well as the two positive charges throughout the whole molecule moving the position of the sextet and keeping two double bonds localized within the rings. If the structure is big, the π electrons have the possibility to move throughout the larger structure, which represents a dilution of the sextet resulting in a reduction of the benzenoid character of the molecule increasing its reactivity (49).

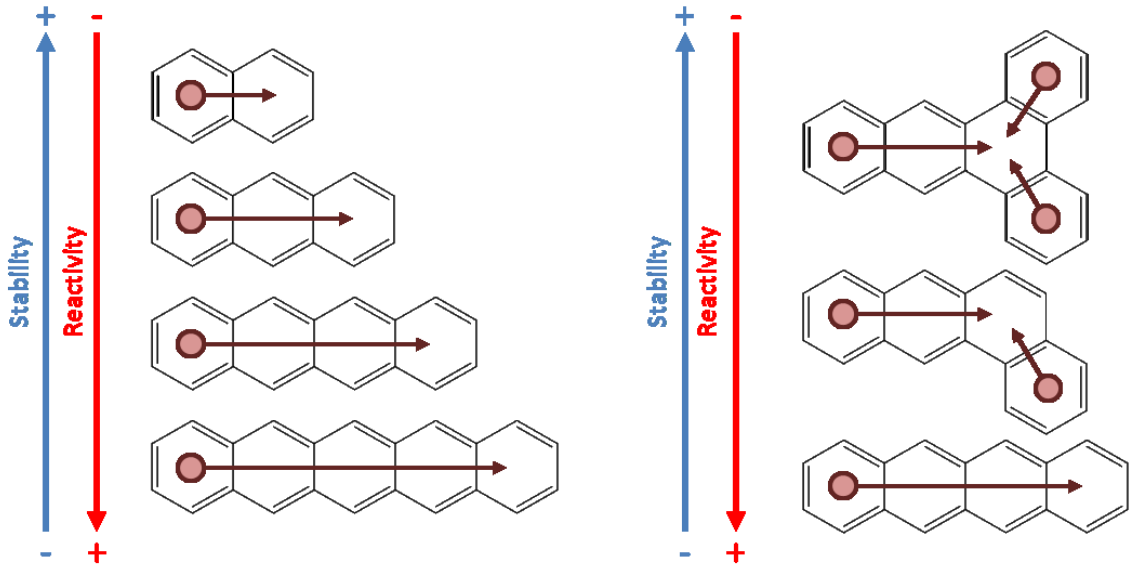


*Figure 2.3 Reactivity of PAH molecules according to size and number of sextets in its structure adapted from (49).*

However, if there are aromatic rings disposed angularly throughout the molecule, more than one aromatic ring will have three double bonds conforming a sextet in the structure, which increases the stability of the molecule and decreases its reactivity (49). In summary, if the number of aromatic rings in the structure of a molecule increases, its benzenoid character decreases, resulting in a reduction of the molecular stability, which increases its reactivity. The same behavior is observed with the number of sextets in a molecule. Molecules with more sextets have greater stability and are less reactive than the ones with less sextets as shown in Figure 2.3. Based on these properties it can be concluded that PAHs do react and tend to retain their conjugated aromatic ring systems (50). Some typical reactions commonly occurring with this type of molecules are addition, oxidation, substitution, cracking and hydrocracking reactions (51).

#### *2.1.3.2. Reduced HOMO-LUMO gap as measure of reactivity*

Kinetic stability is defined as the stability that a compound has compared to the one that an activated complex has in a further chemical reaction. The highest occupied molecular orbital (HOMO) to lowest unoccupied molecular orbital (LUMO) energy gap is commonly used as an indicator of the kinetic stability of PAHs. If a PAH has a large HOMO-LUMO gap signifies that the kinetic stability of the molecule is high and will present a low chemical reactivity. This occurs as the addition of electrons into a high lying LUMO is energetically unfavorable as well as the extraction of electrons from a low lying HOMO, which makes difficult the formation of an activated complex for a potential reaction to occur (52).

In order to establish a proper comparison between the stability of two molecules, the value of the HOMO-LUMO gap of both compounds has to be multiplied by the number of conjugated atoms in their structures to give an index of the kinetic stability of each molecule corrected by its size. In addition, the HOMO-LUMO energy gap of a PAH can be correlated to the stability theory proposed by Clar through the density of aromatic sextets in the molecule ($D_{AS}$). PAHs with a HOMO-LUMO gap value below 1.3 have been found to be highly reactive. It has been reported that most PAHs have $D_{AS}$ values below 0.4 showing that not all polyaromatic systems are kinetically stable (52).

#### *2.1.3.3. Thermodynamic stability of polycyclic aromatic systems*

Thermodynamic stability of a PAH is the result of the aromaticity produced from the cyclic conjugation of its structure. A PAH that possess high aromaticity will be highly stable and

consequently will show very low reactivity. Quantification of aromaticity in a compound is by no means easy. In order to quantify aromaticity in a compound, the resonance energy is normally considered a good indicator. Resonance energy is defined as the difference between the total $\pi$ electron energy of a molecule and the one of a hypothetical reference compound. Haddon and Fukanga related the HOMO-LUMO gap with the value of resonance energy in a molecule demonstrating that a connection between the kinetic and thermodynamic criteria of aromatic character in a molecule exists (53). Therefore, if a molecule is not reactive it can be stated that it is both kinetically and thermodynamically stable (54). Values of Clar's density of aromatic sextets, kinetic stability and thermodynamic stability of PAH's are reported in Table 2.4.

*Table 2.4 Values of HOMO-LUMO energy gap, $D_{AS}$ and resonance energy as a measure of kinetic and thermodynamic stability of PAH molecules. Adapted from (52).*

| PAH | Density of aromatic sextets ($D_{AS}$) | HOMO-LUMO energy gap | Resonance Energy |
|---|---|---|---|
| **Naphthalene** | 0.60 | 1.75 | 0.055 |
| **Anthracene** | 0.43 | 1.57 | 0.047 |
| **Phenanthrene** | 0.86 | 2.08 | 0.055 |
| **Pyrene** | 0.75 | 1.81 | 0.051 |

## 2.2. SUPERCRITICAL WATER

Water turns into a supercritical fluid when it reaches or surpasses a temperature of 374 °C, a pressure of 221 bar and a density of 0.32 g/ml (55). Properties of water in the vicinity or above the critical point present great differences if compared to the ones observed at ambient conditions. Hydrogen bonding, characteristic of water at ambient conditions is completely disrupted when surpassing the critical point, turning water into an excellent solvent for non-ionic species and a poor solvent for ionic species. In addition, important changes in physical properties of water such as heat capacity, thermal conductivity, density and viscosity occur near or above the critical point as shown in Figure 2.4.

Moreover, changes in properties like the ionic product and the dielectric constant are also observed. An important increase in the ionic product is obtained when water approaches its critical point. However, when the critical point is surpassed, the ionic product of water dramatically decreases (56). The dielectric constant decreases with an increase in temperature and increases with an increase in density meaning that when water reaches the critical point, the value of the dielectric constant is lower than the one observed at ambient conditions. Therefore, SCW behaves more like a non-polar solvent rather than a polar one, which explains its capacity to dissolve non-polar organic compounds (57). Apart from these

properties, water at near-critical and supercritical conditions is regarded as a non-hazardous and non-toxic green solvent that can act as solvent, catalyst and reactant in the same chemical process (58).

SCW has an analogous behavior to many organic solvents in which organic compounds show almost complete miscibility and high solubility. An additional advantage that SCW presents is that gases are completely solubilized in it. This enables the development of chemical reactions in a single phase reaction system, which presents important advantages over other heterogeneous systems such as the absence of mass transfer limitations and high reactant concentrations in the system. Therefore, a series of organic chemical reactions such as hydrogenation, ring cleavage, elimination, oxidation and hydrolysis have been readily identified in hydrothermal processes at near-critical and supercritical water conditions.

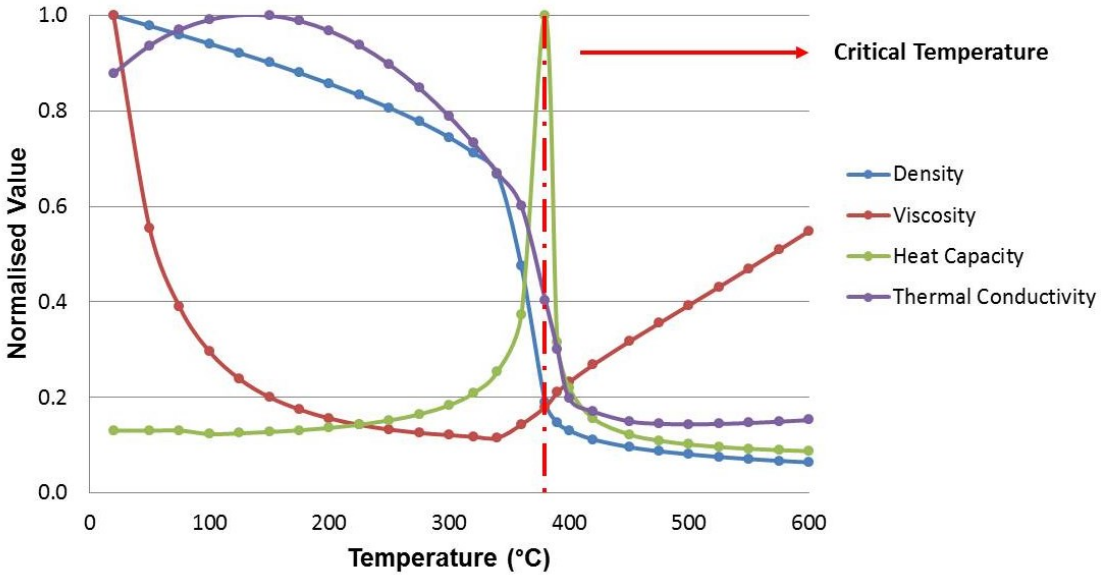


*Figure 2.4 Changes in physical properties of water with temperature.*

## 2.2.1. Chemical reactions in supercritical water

### *2.2.1.1. Hydrolysis reaction*

Water at near-critical or supercritical conditions is a highly reactive medium where hydrolysis reactions involving the rupture by water of one or more bonds of an organic compound occur. Hydrolysis reactions proceed as shown in the general reaction below (59).

$$R – R' \quad + \quad H – OH \quad \longrightarrow \quad R – H \quad + \quad R' – OH$$

Hydrolysis and thermal decomposition reactions in SCW proceed simultaneously and the selectivity to one or the other is determined by the process conditions. Thermal decomposition is favored by higher reaction temperatures while the hydrolysis reaction depends on the concentration of water in the system (59,60). It is clear that the thermal decomposition in SCW proceeds via a free radical mechanism. However, the reaction mechanism of hydrolysis is not fully understood. Klein et al, conducted a kinetic study, which suggests that potentially the reaction mechanism for the hydrolysis in SCW proceeds through a $S_N2$ nucleophilic substitution with water as nucleophile (60).

#### *2.2.1.2. Water gas shift reaction*

In situ production of hydrogen in near-critical and supercritical water processes is of great importance for the potential implementation of the technology in established industrial processes such as biomass gasification, waste destruction, bio-oil upgrading, oil upgrading, among others. At these conditions, hydrogen production through water gas shift reaction (WGSR) shown in the reaction below emerges as a potential route to achieve it.

$$CO \quad + \quad H_2O \quad \leftrightarrow \quad CO_2 \quad + \quad H_2$$

The WGSR is closely linked to the partial oxidation of organic compounds where CO is produced. The presence of CO promotes WGSR, shifting the equilibrium towards the formation of $H_2$. If these reactions, take place in hydrothermal processes (NCW or SCW) where water is present in great excess, the reaction could proceed through a non-catalytic route to the formation of $H_2$ (61). However, one of the main drawbacks that WGSR presents at industrially accessible reaction temperatures (approximately 400 °C) and in the absence of a catalyst is the slow reaction rates achieved. Although, evidence strongly suggest that a dependence exists between the rate of reaction and the water density in the system. In addition, water molecules modify the energy of activation as they participate in the conformation of the transition state complex in the absence of a catalyst (62). It has been proposed that in hydrothermal processes, the water-gas shift reaction mechanism proceeds via two steps. The first step consists of the formation of formic acid as reaction intermediate and the second step is its further decomposition into $CO_2$ and $H_2$, as follows.

$$CO + (n+1)H_2O \longrightarrow HCOOH + nH_2O \longrightarrow CO_2 + H_2 + nH_2O$$

As shown in the previous reaction, water participates in the formation of the transition state, which results in an important reduction of the reaction's activation energy (63).

#### *2.2.1.3. Oxidation*

Hydrothermal oxidation in SCW, also known as supercritical water oxidation (SCWO), takes advantage of the high solubility of oxygen and the almost complete miscibility of organic compounds to form a single phase reaction system, where reactions proceed in the absence of mass transfer limitations. Furthermore, the high temperatures required for the process ensure that high rates of reaction are achieved leading to high conversions of organic compounds to carbon dioxide, water and other intermediate organic molecules (56,57,64).

SCWO kinetics are considered to have a global pseudo first order of reaction with first order kinetics with respect to the organic substrate. In addition, it is well accepted that reaction rates of SCWO are independent from the oxygen concentration in the system. However, it is unclear the way that water participates in the rate of reaction as it has been observed that it is strongly dependent on the amount of water present in the system. Normally, authors consider water to be always in great excess during the entire reaction leaving its concentration unchanged so it can be omitted from the reaction rate expression (65–69).

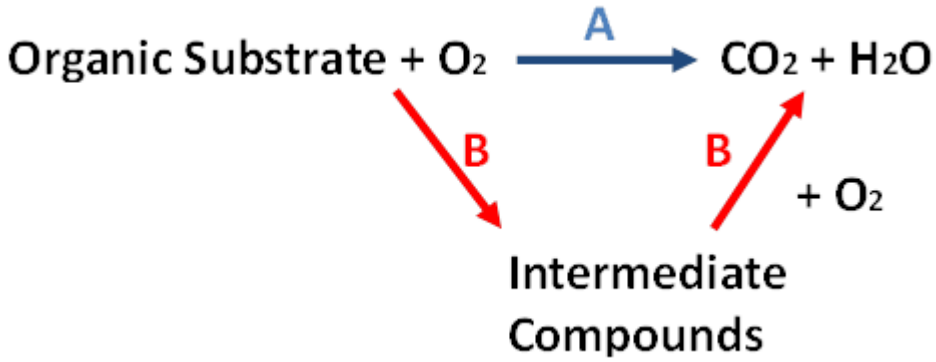


*Figure 2.5 Simplified SCWO reaction pathway model considering the formation of intermediates during the process adapted from (70).*

A simplified representation of the SCWO reaction pathway is shown Figure 2.5. The model considers that the formation and further oxidation of reaction intermediates can be taken as the controlling step of the overall reaction kinetics of the process. Two main reaction pathways for the SCWO of organic compounds in SCW are considered. First, the organic substrate can be directly oxidized into carbon dioxide and water as shown in route A. Second, route B considers the formation of stable reaction intermediates from the partial oxidation of the organic substrate followed by subsequent oxidation reactions into carbon dioxide and water as shown in Figure 2.5 (70). Post reaction analysis into the nature of these intermediate products showed that they were mainly alcohols, ketones, aldehydes and short chain carboxylic acids (64).

Furthermore, it has been reported that the reaction mechanism for the SCWO of organic compounds proceeds through a chain of radical reactions (64,71,72). The reaction mechanism is thought to proceed through three different phases denominated initiation, propagation and termination phases. The initiation phase, also known as the induction phase, is the one in which the concentration of radicals namely OH and $HO_2$ in the medium increases rapidly. During this phase negligible conversion of organic substrates is achieved due to the slow reaction rates observed. The initiation stage is followed by the propagation stage where reactions between organic substrate and radicals in the medium take place and can be described using a first order reaction model. The moment either the organic substrate or the oxygen have been totally consumed, organic radicals react with each other forming stable products, which slow down the rates of reaction in the so called termination phase (73).

## 2.3. HYDROTHERMAL UPGRADING OF HEAVY OIL IN NEAR-CRITICAL AND SUPERCRITICAL WATER

There is great potential in the application of hydrothermal processes in the oil refining sector. The implementation of technologies such as steam assisted gravity drainage (SAGD) have proven that great benefits can be obtained from the incorporation of water into the recovery processes, which results in greater oil recovery yields and in the in-situ upgrading of the feedstock to some extent (74–76). However, some concerns like the high energy requirements and the low efficiency that the process presents have delayed the widespread application of water in heavy oil recovery and processing. In order to improve the overall performance of the process, water-solvent mixtures (77–79), water-gas mixtures (80–82) and the addition of surfactants show to increase heavy oil recovery yields improving its quality.

To date, hydrothermal processes have been successfully implemented in upstream applications including the extraction of bitumen and shale oil and their in situ upgrading into lighter oil fractions (83,84). In addition, it was reported that the presence of water at near-critical and supercritical conditions enhances further heavy oil extraction, and provides some degree of upgrading with conversions up to twenty four percent and sulfur removal ranging from sixteen to twenty percent (85). In addition, highly asphaltenic and kerogene rich hydrocarbons have been effectively extracted using SCW as extraction medium (86). Moreover, it has been observed that process conditions (temperature and pressure) impact directly the overall efficiency of the oil extraction process and determines the yields and composition of the extracted product. An increase in temperature and pressure results in higher yields to extracted oil as a result of two main effects. First, an increase in the solubility of heavy hydrocarbons in water and second the decomposition of these compounds into lighter products due to higher process temperatures. Both effects together result in an overall increase in the extraction and formation rates (87). It was concluded that small changes in process condition defines the selectivity of the process towards different product fractions (87).

### 2.3.1. Role of supercritical water in the upgrading of heavy oil

Hydrothermal upgrading of heavy oil in near-critical and supercritical conditions has shown improvements compared to traditional thermal based upgrading methods mainly due to the higher yields to light fuels obtained and an important reduction in the yields to coke produced (88). In addition, during the upgrading of heavy oils in hydrothermal conditions, it has been reported that high heteroatom (89,90) and metal (91,92) removal were achieved.

Water at near-critical or supercritical conditions is responsible of the solubilization, dispersion and dehydrogenation of heavy oil components, as well as for the prevention of recombination reactions between heavy organic radicals.

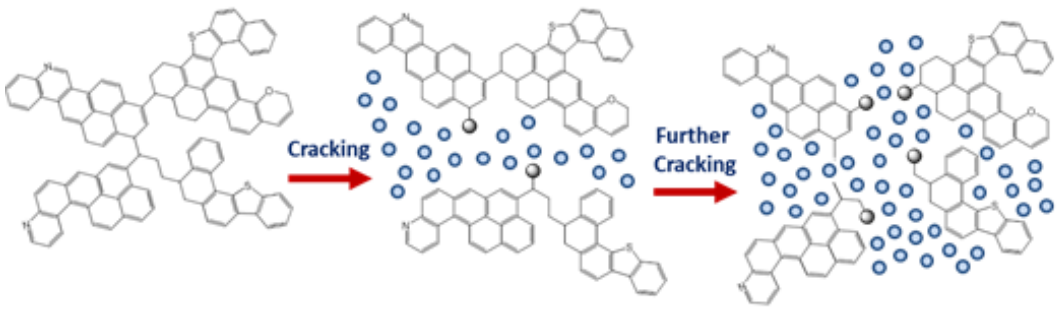


*Figure 2.6 Supercritical water as reaction medium "Cage Effect"*

This occurs due to the cage effect in which water molecules surround an activated organic complex forming a perimeter that stabilizes it. The presence of water around the complex slows down considerably the occurrence of radical reactions radical reactions in the system (93,94). However, taking advantage of the cage effect, heavy molecules continue to crack into lighter compounds of greater value, which are also stabilized by the effect of water preventing recombination reactions and suppressing coke formation as seen in Figure 2.6.

Water density has been found to exert an important influence in the performance of hydrothermal upgrading of heavy oil. It was reported that increments in water density result in higher asphaltene conversions and higher yields to coke. Moreover, the nature of the coke produced is also to water density in the process. Coke produced at higher water densities have a more porous nature than the one obtained at lower water densities (95,96). Nevertheless, water density has a minor effect in the process when oxygen is added to the system. This is mainly due to the considerably larger effect that temperature and oxygen loading have on asphaltene conversion and coke yields that shadow the effect of changes in water density. Interestingly, in hydrothermal oxidation processes variations in the water density do show an important influence in the yields to gas produced (97).

#### *2.3.1.1. Coke suppression*

Coke forms as a result of condensation and polymerization reactions that occur in thermal oil upgrading processes. Coke formation is accomplished through the reaction between two heavy organic free radicals formed during asphaltene cracking reactions (98). Moreover, it has been reported that interactions between asphaltene molecules and the solvent have are determining in the amount of coke produced. These are mainly based on the ability of the solvent to donate hydrogen and also in the capacity of the asphaltene molecules to receive it (99).

Water is a key player in the reduction of coke yields in hydrothermal processes. Its role consists of three main processes such as the dispersion of heavy hydrocarbons, hydrogen donation and the extraction of cracking products, which prevent the occurrence of polymerization reactions. The reaction pathway of coke formation in high and low levels of coke precursor extraction is schematically represented in Figure 2.7.

This figure shows that initially asphaltene molecules crack in the organic rich phase to produce lighter aromatic fractions denominated cracking products. If the reaction takes place in a medium with high extraction capacity, cracking products are extracted into the water rich phase, which prevents the occurrence of polymerization reactions that can potentially lead

into coke formation. Cracking products solubilized in the water rich phase continue to crack into even lighter products denominated maltenes. On the contrary, if the reaction takes place in a medium with low extraction capacity, most of the cracking products remain in the oil rich phase where two main reactions can occur. Cracking products could either react through condensation and polymerization to form coke or they can continue to crack into maltene products. In addition, the small fraction of cracking products extracted into the water rich phase when reaction takes place in a low extraction capacity medium, can be further upgraded into maltenes or can react through recombination with other cracking products to form asphaltenes that return into the oil rich phase (100). Since NCW or SCW are considered good solvents with a high extraction capacity, low yields to coke are expected in hydrothermal oil upgrading processes.

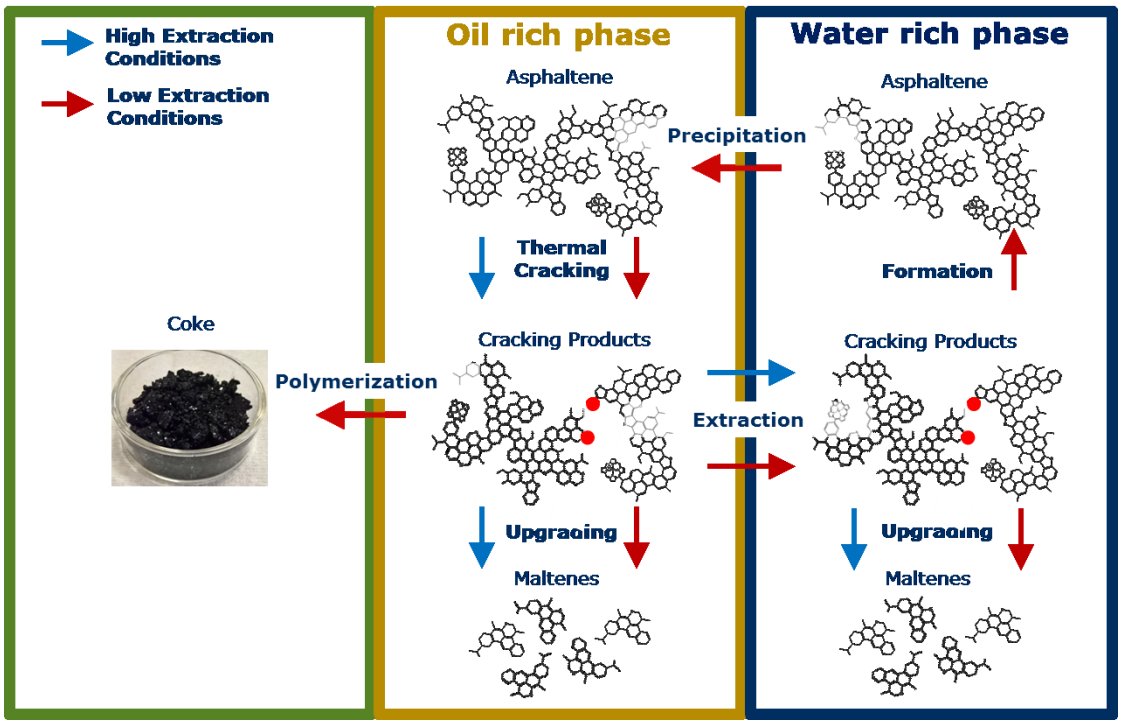


*Figure 2.7 Mechanism of coke formation and suppression in low or high aromatic extraction medium. Adapted from (100).*

### *2.3.1.2. Upgrading of asphaltene fractions*

Asphaltene molecules decompose when exposed to a heating source breaking into smaller organic radicals that can recondense to produce coke as an undesirable by-product (101). However, as previously stated, coke production is greatly inhibited in hydrothermal upgrading processes making them a really attractive medium to process highly asphaltenic

feedstocks. Few processes where highly asphaltenic oil feedstocks are upgraded using water as reaction medium are currently available. Brons et al developed a process to thermally treat asphaltenes in near-critical and supercritical water at temperatures ranging between 300 °C and 425 °C. The authors claim that high yields to light hydrocarbons with a low sulfur content, low molecular weight and a low fixed carbon can be obtained (102). In addition, it was reported that cracking of asphaltene molecules proceeds through a series of chemical reactions such as dealkylation and aromatization to mainly produce gas, maltenes and coke (90,103).

Operating pressure and temperature have an important influence in the conversion and sulfur removal capacity of the system when reactions take place at supercritical conditions in the absence of an oxidizer. Overall, high temperatures and pressures result in high oil conversions. Interestingly, in the presence of an externally added oxidizer asphaltene conversion obtained was lower than in SCW alone but greater desulfurization was achieved. A potential explanation could be that with the addition of oxygen higher polymerization rates are reached, which aid in the removal of sulfur as part of the solid fraction produced (104).

#### *2.3.1.3. Studies on the upgrading of polycyclic aromatic hydrocarbons in supercritical water*

The use of PAHs as a representation of asphaltene structures provides with the opportunity to study different reactions in a controlled environment without the risk of interference of other molecules. This is extremely useful to better understand the effect that process conditions have in the reaction system as well as in evaluating the potential reaction pathways.

Studies on the stability of PAHs in NCW have shown that low conversions are achieved mainly to produce oxygenated products as ketones and quinones. This indicates that water can act as a mild oxidizer at these conditions to a certain extent. These results were compared with the ones obtained in the presence of an added oxidizer, which resulted in an important increase in conversion. This shows that conversion of PAHs is highly dependent on the presence of an additional oxidizing agent (105).

Extensive studies on the reactivity of different hydrocarbons and heterocycles in near-critical and supercritical water conditions have been performed by Katrinsky et al (106,107). Experiments to assess the reactivity of different PAH molecules, aryl oxides and aryl carbonyl structures in SCW were performed showing that low yields to ring opening and reduction products are obtained even at long reaction times and high temperatures.

However, evidence that hydrolysis proceeds in the presence of acid and basic catalysts was found. This suggests that the only difference between reactions occurring at near-critical or supercritical conditions is an increase in radical based reactions in SCW (106,107).

Moreover, it was observed that the destruction of PAHs through complete combustion in SCW is achieved with high efficiencies in the presence of a strong oxidizer such as hydrogen peroxide at high temperatures and pressures (108). Moreover, it was reported that aliphatic hydrocarbons present higher reactivity in SCWO process when compared to the highly stable nature of aromatic hydrocarbons. Similar conclusions as the once obtained with asphaltenes have been reached regarding the great influence that process conditions have in the final product distribution and reaction pathway observed in the SCWO of PAHs (109).

### 2.3.2. Heteroatom and metal removal

As has been previously commented, asphaltene molecules are polycyclic aromatic structures containing an important amount of heteroatoms such as sulphur, nitrogen and oxygen and traces of metals like nickel and vanadium in its structure. Heteroatoms and metals can be normally found in an asphaltene in the form of heterocyclic sulfur and nitrogen compounds and porphyrin metal-organic compounds represented in Figure 2.8.

Nitrogen containing heterocyclic compounds are more stable than sulfur containing heterocycles in hydrothermal reactions at supercritical conditions. In addition, molecules that contain more than one heteroatom in their structure tend to be more reactive than the ones with a single heteroatom (110).

Highly asphaltenic heavy oil feedstocks containing an important amount of heteroatoms and metals represent one of the main processing challenges in the current oil refining processes. These feedstocks, cause great problems when processed through traditional methods, which opens the possibility to develop research focused in the implementation of emerging oil processing technologies such as hydrothermal treating. Hydrothermal processes applying near-critical (111) or supercritical water (112) conditions for the removal of heteroatoms and metals have been assessed.

In addition, the inclusion of additives or catalysts in the process with the aim of increasing the upgrading capacity and heteroatom/metal removal capability of the process has been considered. Compounds of different natures such as olefins and halides (113,114) as well as sulfur/nitrogen resistant catalysts (115,116) have been tested with positive results in the absence of external hydrogen supply. Regardless of the promising results and the great

potential displayed by the technology further improvement and research in the process is still required to convert it into a fully commercially available process.

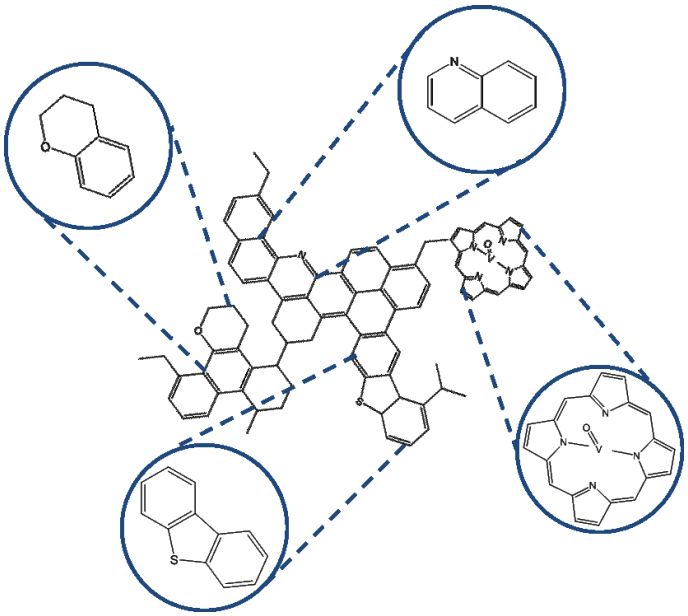

*Figure 2.8 Heteroatom (S, N and O) and metals (Ni and V) structures found in asphaltene molecules.*

#### *2.3.2.1. Sulfur removal*

Implementation of hydrothermal processes at near-critical and supercritical water conditions in heavy oil desulfurization has received little attention despite the great potential of the research field. Removal of sulfur from the oil fraction can be achieved in NCW and SCW without the need of any added catalyst. It has been reported that hydrolysis and thermolysis reactions of sulfur-containing organic compounds occur in NCW, mainly to produce short chain hydrocarbons and a gas product mainly composed of $CO_2$, $CH_4$ and $H_2S$ (117).

An extensive study comparing the reactivity of different sulfur-bearing organic molecules such as sulfides, disulfides, sulfonic acids, thiophenols, thiophenes as well as alkyl and aryl sulfides in hydrothermal and thermal exclusive conditions has been performed by Katritzky et al. Their results showed that reactivity of the molecule depended on the nature of the model compound studied. As an example, sulfides and disulfides presented higher reactivity in thermal conditions over hydrothermal conditions. This led them to the conclusion that reaction mechanisms with this type of molecule are mainly free radical based rather than ionic based (118). In contrast, reactions performed with mercaptans showed that these molecules had a greater reactivity in hydrothermal rather than thermal conditions suggesting the opposite behavior (119). Low reactivities were registered in experiments performed with

arenethiols, diaryl sulfides and especially with aromatic sulfur compounds, which remained unreactive in the tested conditions (120). Heterocyclic sulfur model compounds such as thiophenes showed no reactivity in water at near-critical conditions suggesting that the high stability of these molecules impedes desulfurization to occur through hydrothermal processes in the absence of additives or catalysts (121,122). Similar trends in behavior were observed when the severity of reaction conditions was increased to P and T over the critical point of water. Experiments with model compounds such as thiophenols, alkyl and aryl sulfides showed high degrees of desulfurization while thiophenes were completely unreactive (123).

Current research focuses on the understanding of fundamental concepts of the hydrothermal desulfurization in NCW and SCW. Studies on the role that water plays in the process, the effect that the presence of an additive or a catalyst has in the reaction and the fundamental reaction pathways are of great importance for the development of the technology (124). A study on the potential of hydrothermal processes at supercritical conditions to remove sulfur from oil feedstocks showed that low degrees of desulfurization can be achieved when the process is performed in the absence of a catalyst or an external hydrogen source. Moreover, it was concluded that aromatic sulfur is almost unreactive whilst achieving a marginal degree of hydrolysis (125). Figure 2.9 presents the findings of a kinetic study that related the reactivity of the sulfur-containing organic compounds and its chemical structure when reaction took place in SCW (126).

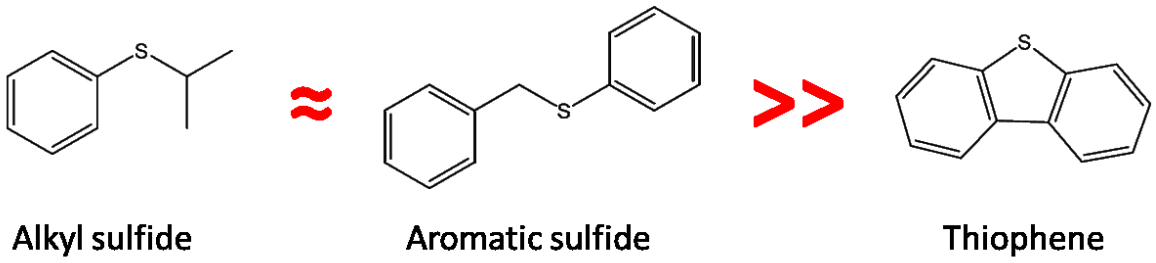


*Figure 2.9 Reactivity trend of sulfur organic compounds in SCW adapted from (126).*

It has been reported that water in hydrothermal conditions plays the role of reactant in hydrolysis reactions, of hydrogen transfer catalyst and also of hydrogen donor during desulfurization reactions (127).

As has been briefly mentioned, one of the options currently being assessed to increase sulfur removal in hydrothermal processes is the addition of a catalyst. The implementation of a traditional bi-functional hydrotreating catalyst such as $CoMo/Al_2O_3$ and $NiMo/Al_2O_3$ in a

hydrogen enriched SCW reaction medium has proven to effectively remove sulfur from organic compounds. In addition, it was observed that in situ generated hydrogen possess a greater hydrogenation capacity than the one of externally supplied hydrogen as it produces highly reactive intermediate species (128,129). Finally, the use of metal oxides and metal sulfides as catalysts was assessed for the desulfurization of heavy oil and heavy oil model compound in SCW. A series of catalysts including $MoS_2$, $Mo_2O_3$ and ZnO were tested. It was concluded that the sole presence of a catalyst resulted in higher degrees of desulfurization than in the absence of one. However, analysis of the spent catalysts showed that all catalysts tested with the exception of $MoS_2$ were unstable in supercritical water conditions and presented major structural changes during the process (89).

#### *2.3.2.2. Nitrogen removal*

Nitrogen removal from oil feedstocks is normally achieved through hydrogenation in the presence of traditional hydrotreating catalysts such as metal supported catalysts in its sulfidated form. Recently, the use of cataysts such as metal carbides or nitrides have increased in popularity (130). As with sulfur-bearing compounds, a potential alternative to traditional hydrotreating processes is the hydrothermal upgrading and de-nitrogenation of oil in near-critical or supercritical conditions.

An analogous study to the one previously presented for sulfur bearing compounds, was developed by Katritzky et al with nitrogen-containing molecules such as indoles, pyrroles and pyridine in water at near-critical conditions. They concluded that at these reaction conditions, nitrogen bearing organic compounds are non-reactive based on the negligible de-nitrogenation levels achieved. Moreover, they observed that the addition of an acid into the system presented no changes for most of the model compounds tested with the exception of pyrroles and indoles that showed higher conversions (131,132). In addition, they performed a series of experiments in SCW and cyclohexane as reaction mediums in order to compare the performance of hydrothermal and thermal processes. Similar reactivity was observed in both processes, which suggests that in SCW the reaction mechanism is mainly radical based. In addition, it indicates that SCW is not reactive enough to remove nitrogen from the structure of the organic compound without the inclusion of externally supplied additives into the system (133,134).

In order to enhance denitrogenation in the system, hydrogen addition through in-situ generation in SCW has been extensively studied by Yuan et al (135). They observed that high degrees of nitrogen removal were achieved through a two-step process based on the

partial oxidation of the organic compound followed by WGSR in the presence of a traditional hydrotreating catalyst (135). Process conditions exert an important influence in the overall de-nitrogenation capacity of processes based on partial oxidation reactions in hydrothermal conditions. It was reported that the effect of temperature and the initial oxygen loading have a high impact compared to pressure in the performance of the process at supercritical conditions. In addition, kinetic studies by Pinto et al on the partial oxidation of quinoline as model compound have shown that the process follows a pseudo first order of reaction for the organic substrate and showed to be dependent in the concentration of oxygen to some extent while water present in great excess did not have an influence in the observed rate of reaction (136,137).

Quinoline and isoquinoline have been also used in a study to assess the effect that the addition of an acid catalyst ($ZnCl_2$) has in the hydrothermal de-nitrogenation process. Results of this study show that the presence of the catalyst increased the conversion of the nitrogen-bearing model compounds and also had a positive effect on the level of de-nitrogenation achieved. A kinetic analysis was also developed showing that the reaction rate follows a pseudo-first order of reaction for the organic compounds and also for the catalyst (138,139).

#### *2.3.2.3. Metal removal*

Similarly, traditional hydrotreating processes are regarded as the most popular de-metallization process for the upgrading of heavy oil feedstocks. Hydrodemetallization requires the addition of a traditional hydrotreating catalyst such as $FeMo/Al_2O_3$ or $CoMo/Al_2O_3$, which are susceptible to poising and de-activation. The process is limited by factors in the feedstock such as asphaltene content, large molecular size and high contents of metals and heteroatoms as well as by the morphological characteristics of the catalyst like surface area, pore diameter and pellet size (140,141).

Alternatively, hydrothermal processes in NCW and SCW represent a promising complementary or substitute technology for upgrading and metal removal from heavy oil feedstocks. The use of nickel and vanadium metalloporphyrins as model compounds showed that high degrees of demetallization as well as high conversions can be achieved in water at supercritical conditions (91,92,142). Moreover, it was also stated that vanadium porphyrins are more stable than nickel porphyrins in SCW. This shows that the chemical structure of the molecule also influences the degree of de-metallization achieved as shown in Figure 2.10. In addition, the authors concluded that conversion and metal removal in

SCW is strongly linked to the reaction temperature and time. A two-step reaction mechanism for the de-metallization of metalloporphyrins in SCW involving hydrogenation and hydrogenolysis reactions was proposed. It is also reported that the process is best described by an overall pseudo first order of reaction (91,92,142).

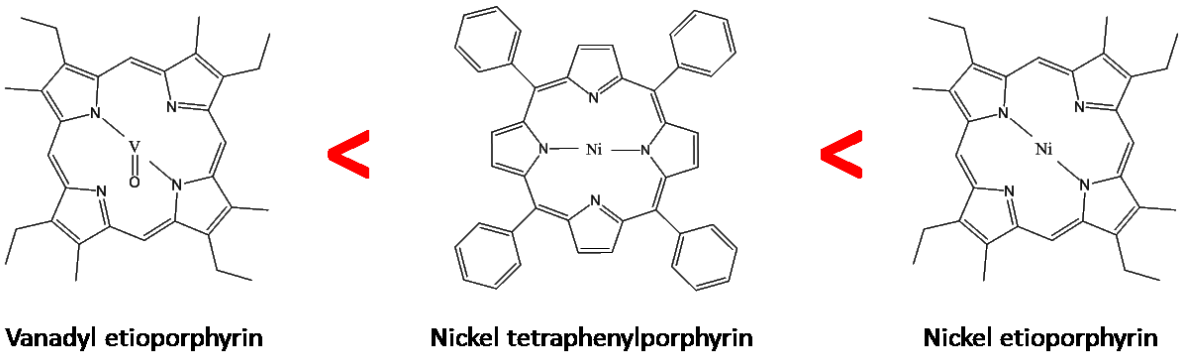


*Figure 2.10 Reactivity of metaloporphyrins in SCW depending on metal and structure adapted from (91,92,142).*

## 2.4. CATALYSIS IN SUPERCRITICAL WATER

Catalytic hydrothermal processes in NCW and SCW have been extensively used in chemical synthesis, waste destruction, generation of renewable fuels, synthesis of materials and biomass conversion (143). Therefore, finding a suitable catalyst capable of enhancing the main reactions such as hydrolysis, partial and total oxidation and WGSR in hydrothermal systems is of great importance. The main challenge behind the implementation of catalytic processes at hydrothermal conditions lies in the development of a material that can provide catalytic activity and show sufficient stability to withstand the harsh conditions of the reaction medium (144).

The use of transitional metals like ruthenium and iron in solution as catalysts for the hydrothermal upgrading of heavy oils improves considerably the properties of the oil produced. The addition of the catalysts resulted in an important reduction in viscosity and also in a decrease in the average molecular weight of the asphaltene fraction. However, contrasting results were observed regarding the formation of insoluble materials with the choice of metal. In the presence of iron, the amount of insoluble material obtained was greatly reduced while the opposite effect was observed with ruthenium that increased the production of insoluble material. The authors related this phenomenon with the capacity of ruthenium to cleave C-S bonds, which promotes recombination reactions between the different reaction fragments increasing the formation of high molecular weight insoluble

material (145). Moreover, a similar study showed that the use of metallic catalyst precursors in solution in a SCW-syngas reaction medium promoted the in-situ formation of hydrogen through WGSR. The hydrogen produced aids in the upgrading of heavy oil feedstocks improving the performance of the process through the reduction of asphaltene contents and prevention of coke formation if compared to the efficiency shown in the non-catalytic process (146).

The potential implementation of an iron oxide catalyst supported over zirconium or zirconium/alumina for the hydrothermal upgrading of heavy oil process was studied by Fumoto et al (147-152). They observed that reactive oxygen species (ROS) are generated in great quantities from the interaction between water, catalyst and heavy oil resulting in the formation of light oil fractions with low coke yields. In addition, the authors developed a kinetic model from where kinetic parameters were determined. They observed that the activation energy values obtained were lower than the ones commonly found in traditional upgrading processes like hydrocracking (147–152).

Furthermore, it was reported that the use of metallic waste shavings from zinc and aluminum have a positive effect when used in hydrothermal processes to upgrade heavy oil. An increase in conversion and in the H/C ratio of the oil produced was observed when these metals were added for the upgrading of bitumen fractions (153). The improvement observed in the process is mainly attributed to the occurrence of a parallel reaction where $H_2$ is formed in-situ from the oxidation of metal shavings into metal oxide nanoparticles (154–156). Contrasting results were obtained depending on the metal used. The addition of zinc resulted in an increase in the yields to resins and also in an increase in the amount of oxygen incorporated into the organic product compared to the non-catalytic process. The opposite effect was obtained with the addition of aluminum, which decreased the yield to resins and the amount of oxygen incorporated into the product if compared with the process in the absence of any metal (153).

## 2.5. ANALYTICAL TECHNIQUES

### 2.5.1. Size exclusion chromatography

Size exclusion chromatography (SEC) is an analytical technique composed of a liquid chromatographic column that separates molecules in solution according to their molecular size. A detailed diagram of a size exclusion chromatography system including its main components is shown in Figure 2.11.

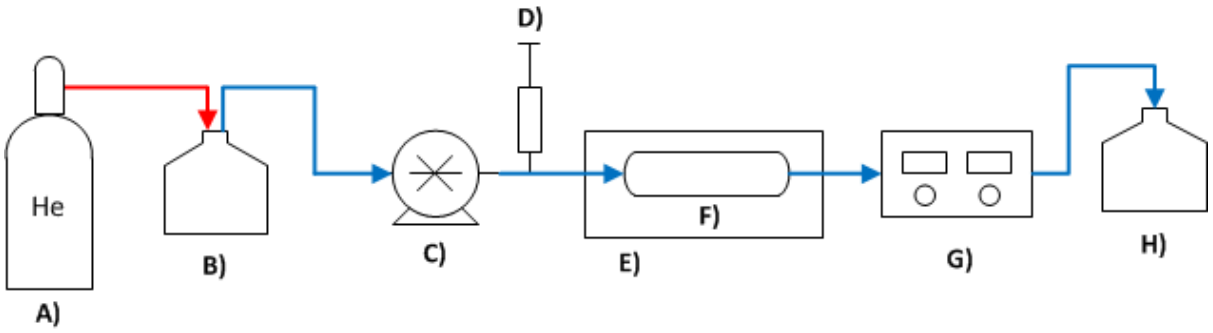


*Figure 2.11 Detailed diagram of an SEC system comprised of gas supply (A), solvent reservoir (B), HPLC pump (C), injector (D), oven (E), SEC packed column (F), detector (G) and spent solvent reservoir (H).*

The analyte is introduced into the SEC column by means of a solvent as carrier, which is denominated as the mobile phase. The mobile phase is fed into the column with a positive displacement pump [C]. The column [F] is composed of a rigid porous material that presents a wide pore size distribution. Size separation in the SEC system occurs through a constant exchange between solute molecules in the mobile phase and a stagnant liquid contained in the pores of the column. The pore size distribution will determine the molecular size range at which separation occurs (157).

SEC operation is based on the absence of interaction between the analyte and the column packing. If this condition is met, the analysis depends solely on the ability of molecules to penetrate the different size pores that conforms the column packing. Molecules with larger size are the first to elute due to their incapacity to penetrate through the porosity of the chromatography column. On the contrary, molecules of smaller size are able to penetrate the porosity of the packing and travel a longer path that results in longer elution times (158). As a result, SEC chromatograms of high molecular weight coal or oil derived molecules present a bimodal distribution showing two principal elution fractions. The first peak corresponding to the fraction of molecules that were not able to penetrate through the column denominated as excluded peak, and the second that appears at longer elution times that corresponds to the fraction of molecules that permeated through the column known as the retained peak. An important parameter of this technique is the selection of an adequate solvent, as the structure dependence and the solubility of the analyte may interfere and modify the elution times obtained (159,160).

### 2.5.2. Gas chromatography

Gas chromatography (GC) enables the analysis of complex mixtures of compounds through fractionation. The technique relies on the affinity that each individual component in the mixture have with the mobile or the stationary phase, enabling its separation at different times throughout the determination. A diagram of the main components of the technique is shown in Figure 2.12.

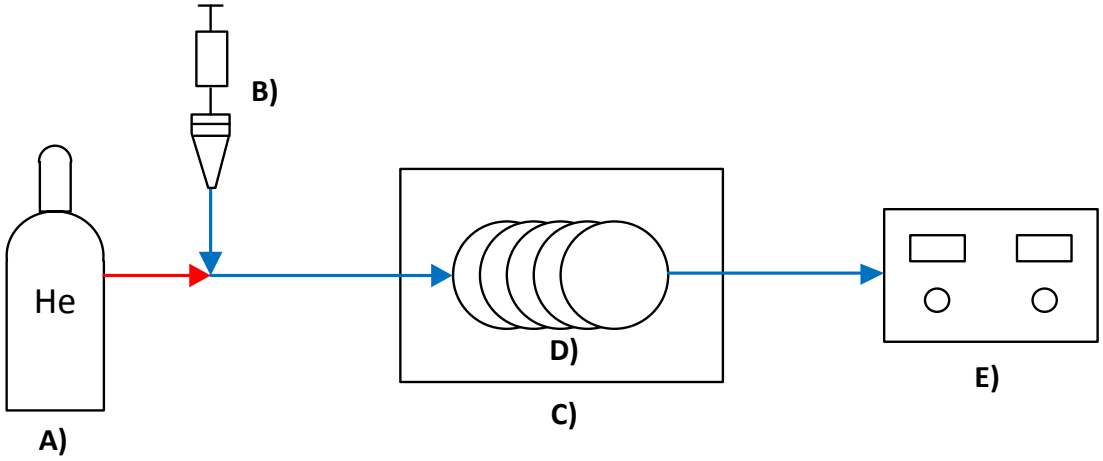


*Figure 2.12 Detailed diagram of a GC system comprised of an inert gas inlet "mobile phase" (A), sample injector (B), oven (C), chromatography column (D) and a detector (E).*

First, the analyte is introduced through the injector [B] where it is vaporized. The vaporized compounds are then transported by means of a carrier gas into the column [D] where the different compounds in the sample separate. The separation principle is based on the velocity at which the different compounds travel across the column due to the level of interaction that they experience with the stationary phase. The higher the interaction a compound presents, the longer the time it takes for it to pass through the column. Finally, after the compound leaves the column, it is conducted into a detector for its identification and quantification. For this purpose detectors of different kinds such as flame ionization detector (FID), thermal conductivity detector (TCD) or mass spectrometry detector (MS) are commonly used with this technique.

### 2.5.3. CHNS elemental analysis

Elemental analysis (CHNS) is used to determine the content of carbon, hydrogen, nitrogen and sulfur in organic samples. The fundamental principle of operation is based on the instantaneous and complete oxidation of the analyte through flash dynamic combustion into

their principal combustion products. A detailed scheme of the elemental analysis set-up is shown in Figure 2.13.

The combustion chamber [C] is purged with helium before the sample is introduced. Samples are contained inside a tin capsule at the moment they are introduced into the analysis chamber. Once the sample has been placed, helium is switched to an oxygen enriched gas to facilitate the combustion of the sample. The combustion chamber is maintained at a temperature around 1000 °C, which enables the melting of the tin container promoting a violent combustion reaction of the sample. During combustion carbon, hydrogen, nitrogen and sulfur are turned into $CO_2$, $H_2O$, NOx and $SO_2$ respectively. Combustion gases are removed from the chamber and conducted to a reduction stage. In this stage, combustion gases pass over a heated high purity copper bed at a temperature of around 600 °C. The copper bed is normally located below the combustion chamber and is meant to remove any remaining oxygen in the gas stream as well as to convert the $NO_x$ into nitrogen gas. Then, the gas stream passes through a GC column [E] where the different gases are separated and analyzed in a TCD [F] for quantification (161).

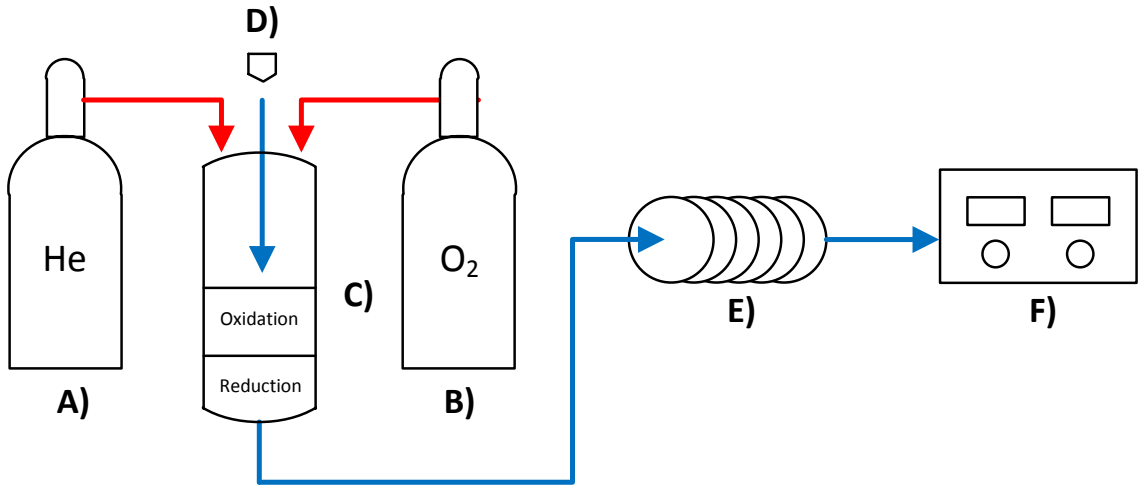


*Figure 2.13 CHNS elemental analysis set up consisting on an inert gas (A) and oxygen supply (B), combustion chamber (C), sample feed (D), gas chromatography column (E) and a TCD detector (F).*

### 2.5.4. Inductively coupled plasma optical emission spectroscopy

Inductively Coupled Plasma Optical Emission Spectroscopy (ICP-OES) is used to determine the concentration of elements in a sample. The fundamental principle lies on the thermal excitation of atoms that drive them into their excited states, followed by the subsequent

decay of their energy level through energy emission at a certain wavelength. This emission can be measured and is used to determine the concentration of the element being analyzed. A detailed diagram of the system is shown in Figure 2.14.

The sample is normally introduced in the form of an aqueous solution with a pump [B]. Once inside the equipment, the solution is turned into an aerosol through a process known as nebulization. The aerosol is then transported into the plasma torch [D] where it is vaporized, atomized and excited by the plasma. The plasma is maintained by the energy provided by a radio frequency generator.

Finally, the characteristic radiation emitted by the excited atoms is collected in a spectrometer [E] that sorts radiation by wavelength emitted and turns it into signals. These signals can be processed and translated into values of concentration of the element being analyzed (162).

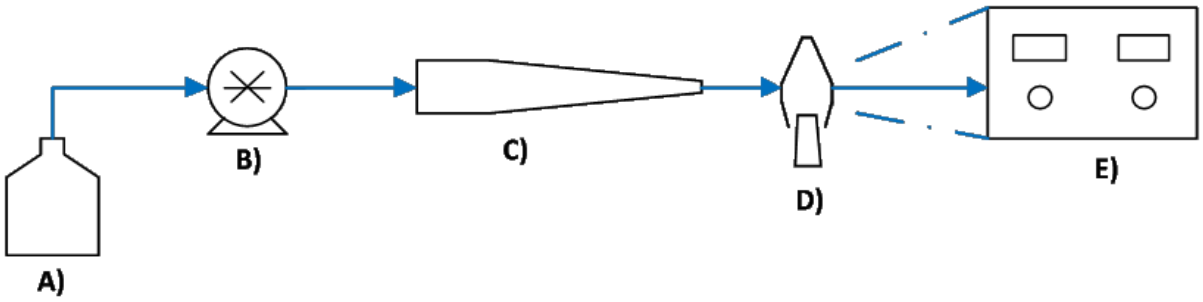


*Figure 2.14 ICP-OES analysis set-up comprised of a sample vessel (A), injection pump (B), nebulizer (C), plasma torch (D) and a spectrometer (E).*

# Chapter 3
# Reaction Set Up

The present chapter is dedicated to the design, construction, commissioning and improvement of a batch (microbomb reactor) and a flow (oxidative cracking reactor) reaction systems. Both systems have been used for experiments on the oxidative cracking in both NCW and SCW. A detailed description including process flow diagrams, design considerations, rationales behind the choice of material of construction and measures to ensure safe operation are extensively discussed throughout the chapter.

## 3.1. MATERIALS OF CONSTRUCTION

Apart from the high pressure and temperature at which hydrothermal processes in near-critical and supercritical water take place, problems related to the design of the reactor such as corrosion and salt deposition were observed (64). In order to prevent from salt deposition, experiments in this work were carried out with deionized water (DI). However, an adequate selection of construction materials was considered crucial to deal with the effect of corrosion in the equipment, which becomes more relevant in processes involving oxidation or partial oxidation reactions. An evaluation of construction materials commercially available was performed. As previously mentioned, certain characteristics of SCWO processes such as elevated pressures and temperatures, high dissolved oxygen concentrations and sharp density changes increase the possibility of corrosion in the system, which compromises the long term operation of the equipment (64,163). Specific properties of the reaction medium such as density, ion product and dielectric constant have an important effect in the extent of corrosion of the system. These properties play an important role in the dissociation of corrosive species as well as in the removal of a metal oxide protective layer that coat the metal preventing from further corrosion (164). In addition, the presence of areas in the reactor that remain hot but in subcritical conditions was reported. These areas are potentially susceptible of corrosion due to a higher dissociation of ionic species (165). Detailed studies focused on the assessment of the resistance of different materials of construction to corrosion in hydrothermal processes at supercritical conditions have been published. A diagram summarizing the main findings of these works is presented in Figure 3.1. It was reported that corrosion rates in F/M steel are enhanced by the presence of dissolved oxygen

in the medium and that its effect is strongly dependent on the temperature of the process (166,167). Moreover, a comparative assessment on the resistance that SS-316 and Ni based alloys present to corrosion in hydrothermal oxidative processes in supercritical conditions showed that the degree of corrosion obtained in both materials was similar (168). However, contrasting results on the weight loss of SS-316 and Ni based alloys after exposure to SCW were reported (169,170).

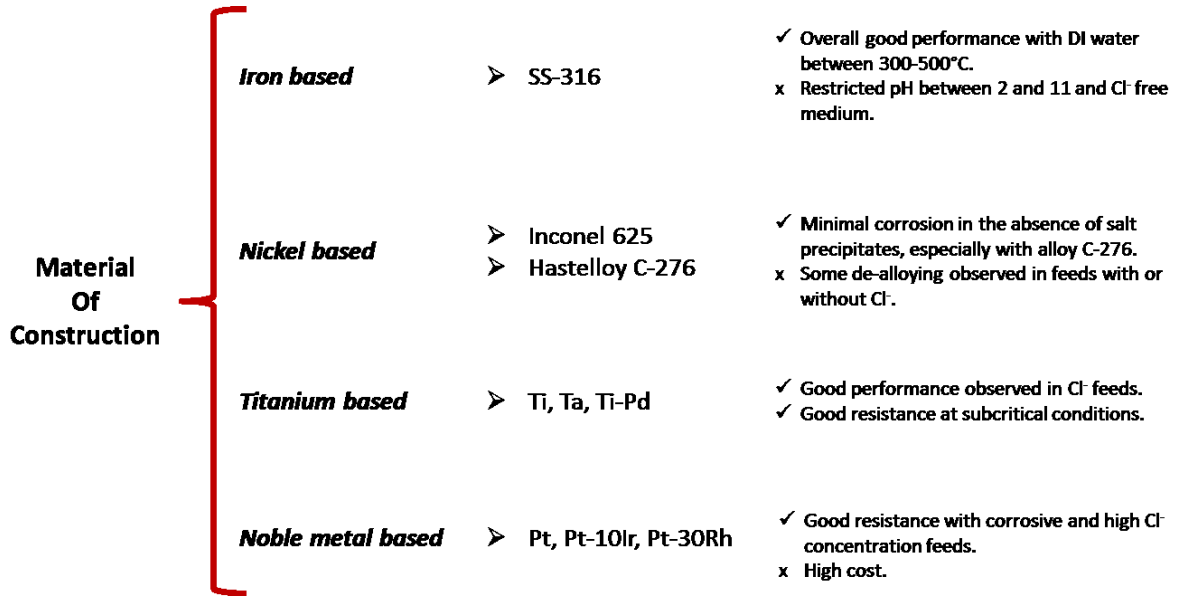


*Figure 3.1 Materials of construction adapted from (171).*

The possibility of corrosion due to salt deposition in reactor sections at subcritical conditions was not considered for this work as all experiments were performed with DI water. Moreover, reactants used in this project such as pure PAHs and VR are also free from salts and species like Cl- that have the potential to cause corrosion in the system. However, the presence of dissolved oxygen in the medium was considered for the selection of the material of construction. Taking into consideration factors such as reaction medium, nature of reactants, material cost and information on the performance of each material in hydrothermal conditions in literature, the reaction systems were built with SS-316. Overall, it was reported that SS-316, presented a good performance during continuous operation at hydrothermal conditions for a period of approximately 100 h at temperatures ranging from 360 to 400 °C (165). As an additional precautionary measure to ensure safety of operation, reactor components exposed to SCW conditions were replaced on a regular basis to prevent any de-alloying from occurring. The reaction section in the microbomb reactor was replaced after

a maximum of 6 experiments and in the case of the oxidative cracking flow reactor, the reaction section was replaced after 30 h of continuous operation.

## 3.2. REACTION SET-UPS

### 3.2.1. Microbomb batch reactor

Batch experiments were performed in a microbomb reactor equipped with a gas sampling section. The reactor is an adapted version of two previously used reaction systems (172,173), designed for experiments with model compounds in near-critical and supercritical water conditions. The system was built and designed for operation at a maximum pressure of 275 bar and a maximum temperature of 500 °C in the presence of dissolved oxygen in the medium. The reactor was built with Swagelok high pressure and high temperature resistant SS 316L fittings and tubing. A complete inventory of fittings and tubing lengths that compose the system can be consulted in Appendix 11.1.1. Based on the temperature and pressure ratings reported by the supplier, operating conditions were set to ensure that an over specification of at least 100% was kept. Swagelok type fittings have a design based on the overlapping of two ferrules, which provides thermal shock resistance and also compensates from rapid expansion-contraction as a result of rapid changes in temperature that may result in leaks (174,175).

#### *3.2.1.1. Reactor description*

Figure 3.2 shows a detailed diagram of the microbomb reactor with its main components. The reactor is comprised of two main sections: A) a gas recovery section used to collect the gas produced for further analysis and B) a reaction section that operates at high temperature and pressure in the presence of dissolved oxygen. The gas recovery section has a total volume of 6 mL and is composed of two needle valves [a,d], which control the inlet and outlet of purging gas. In addition, a ball valve [c] with a septum placed in its outlet enables gas sampling for analysis. This section of the reactor is equipped with an Omega digital pressure gauge [b] used to record the pressure of the gas produced. The reaction section has a total volume of 12 mL and is composed of a bored through 1/2” tee [h] where the original sample, $H_2O$, $H_2O_2$ solution and catalyst are loaded. The rationale behind the use of a bored through tee is its flat surface that facilitates product recovery, reducing greatly the experimental error in the procedure. Temperature in the reactor is measured by means of a type k thermocouple [g] located in the center of the tee. The reaction section is isolated from

the gas sampling section by means of a heavy duty needle valve [e] that withstands high pressure and high temperature environments. As an added safety feature, this section is connected to a safety release valve [f], calibrated to open at a pressure of 300 bar in the case of a sudden increase in the reactor pressure. The reaction section is immersed into a fluidized sand-bath that provides the heating as will be further explained.

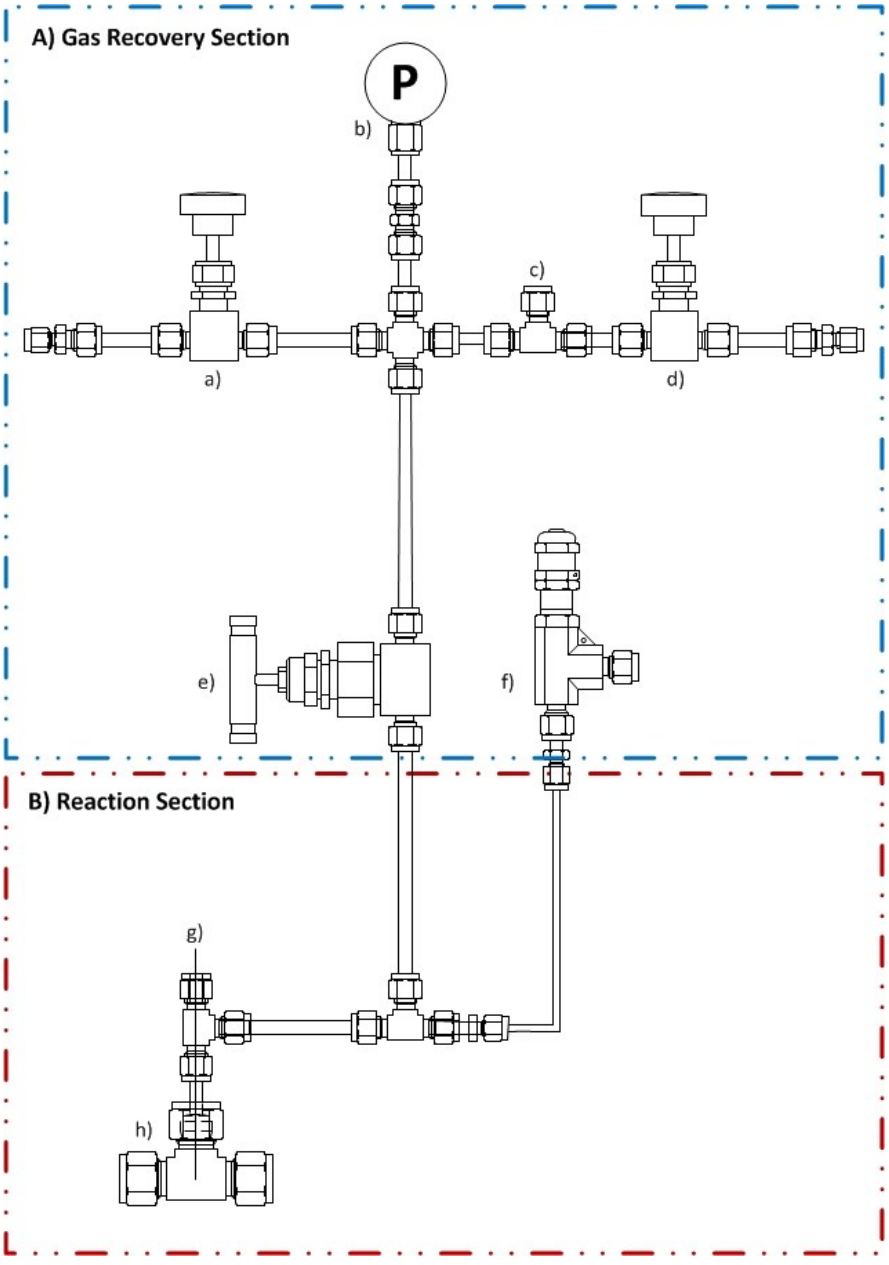


*Figure 3.2 Microbomb reactor scheme: a) purge inlet valve, b) gas pressure gauge, c) gas sampler, d) purge outlet valve, e) high pressure – high temperature valve, f) pressure relief valve, g) type K thermocouple, h) ½" bored though tee.*

#### 3.2.1.2. Heating source

Heating is provided to the microbomb reactor by means of a TECHNE 2BL-2D sand-bath. The sand-bath is composed of an internal SS vessel with a depth of 35 cm and an internal diameter of 22.8 cm. The vessel is thermally insulated with fiberglass for safety reasons and to avoid heat loss. Heating is provided by four 1 kW electric elements located near the bottom of the vessel. The inner vessel is filled with an initial heat transfer medium loading of approximately 30 kg. The heat transfer medium is composed of aluminum oxide particles “alundum” fluidized by a stream of pressurized air at approximately 0.1 bar. Pressurized air is fed through a porous plate distributor located at the bottom of the vessel. At complete fluidization conditions, a uniform temperature profile and good heat transfer are achieved. The sand-bath has a heat up time of approximately 105 min to reach from 20 °C to 600 °C. Heating control as well as the monitoring of temperature in the sand-bath was performed from a custom made control box.

#### 3.2.1.3. Safety cabinet, shaking mechanism and fast release system

In order to ensure safe operation with the microbomb reactor, an existing SS cabinet was upgraded and refurbished. The safety cabinet shown in Figure 3.3 is composed of two sections: A) the top section where the reactor is guarded and B) the bottom section where the sand-bath controls and air supply are guarded.

Both sections are separated by a 3 mm SS sheet, welded to the cabinet structure, with a hole where the sand-bath is located as shown in Figure 3.3. An aluminum skirt is fitted into the hole to align the inner vessel of the sand-bath and the SS sheet isolating both sections of the cabinet. The top section has two doors with vision panels made out of 6 mm perspex acrylic to enable visual control of the reactor throughout the experiments. The cabinet is equipped with an air extraction system provided by an in-line Vent Axia ACM100 mixed flow fan with an extraction capacity of 220 $m^3$/h.

A shaking mechanism detailed in Figure 3.3 was designed to attach the reactor and provide homogeneity to the system through mechanical shaking. The structure of the mechanism is built with two ½” SS rods, each of them attached to two aluminum blocks with a space for the rod to slide. The space on each block is covered with nylon 66 modified with $MoS_2$ that provides low friction and self-lubrication. The rods go across the right wall of the cabinet and are attached to a SS structure that join them with a Parvalux 95 W motor that gives movement to the structure. Moving parts and SS sections are covered by rubber elements to protect the structure avoiding contact with the alundum, which prevents corrosion. The

shaking mechanism frequency is controlled from the same custom made control box mentioned in Section 3.2.1.2.

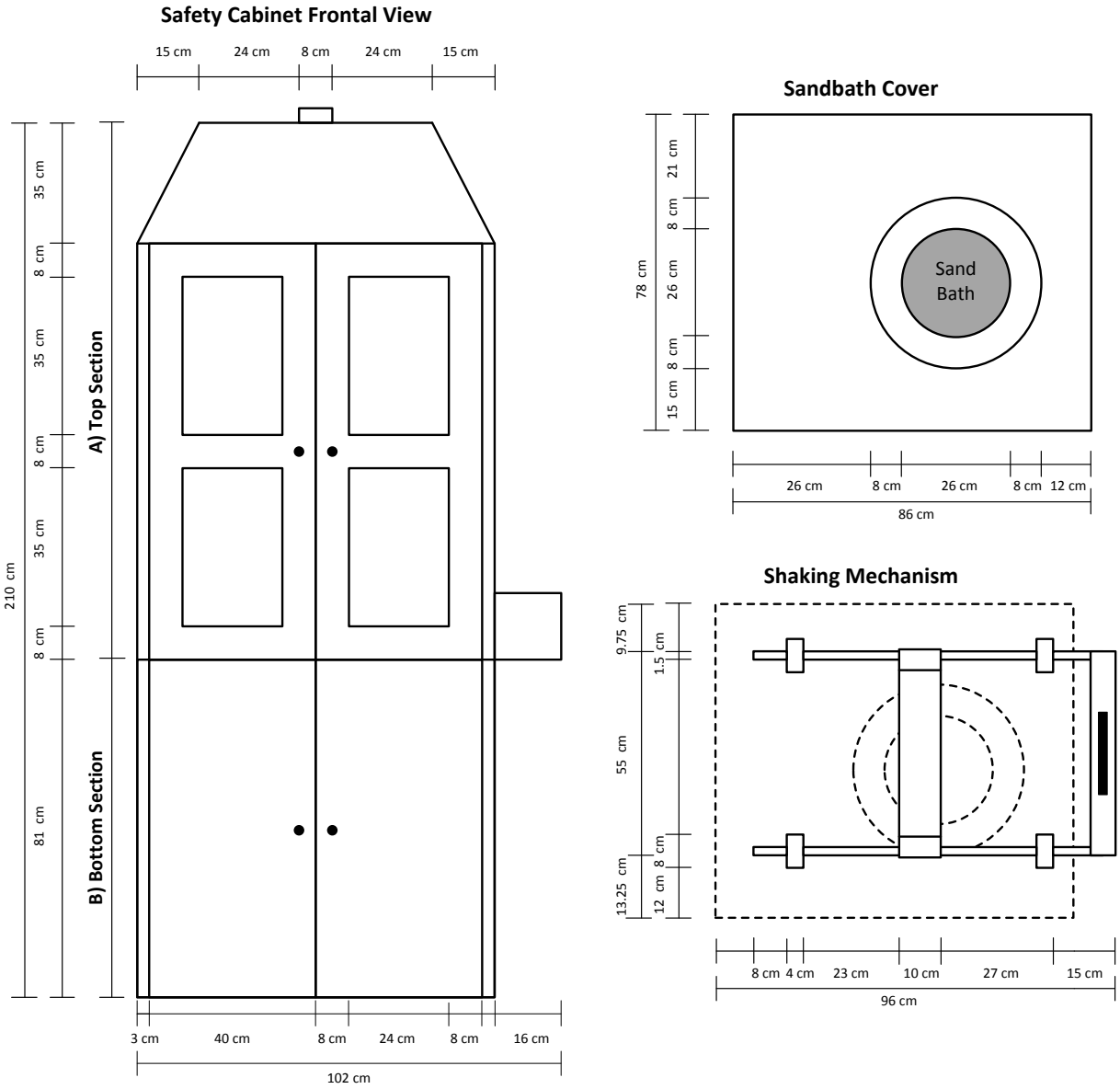


*Figure 3.3 Microbomb reactor safety cabinet and shaking mechanism.*

The most critical moments for the safety of the microbomb reactor operator are the insertion and removal of the system to and from the heating source. In previous designs, the reactor was attached to an aluminum base plate by means of G type clamps, which required long exposure times from the operator while the system was secured in place. This system was replaced by a fast release mechanism detailed in Figure 3.4. It consists of two parts: 1) a base plate attached to each of the SS rods on the shaking mechanism and 2) an assembly

plate where the reactor is located. The base plate has the shape of an inverted C that leaves space for the reactor to be positioned and matches the geometry of the assembly plate. It is also equipped with a lock made of a piece of aluminum that slides over the assembly plate to secure the reactor in position. The assembly plate is made of aluminum and holds the reactor in two positions, where the high pressure and high temperature valve is located and on the tube leading to the pressure gauge by means of a clamp. The average time to attach or detach the reactor from the fast release mechanism is 10 s, which greatly reduces the exposure time decreasing the risks of operation.

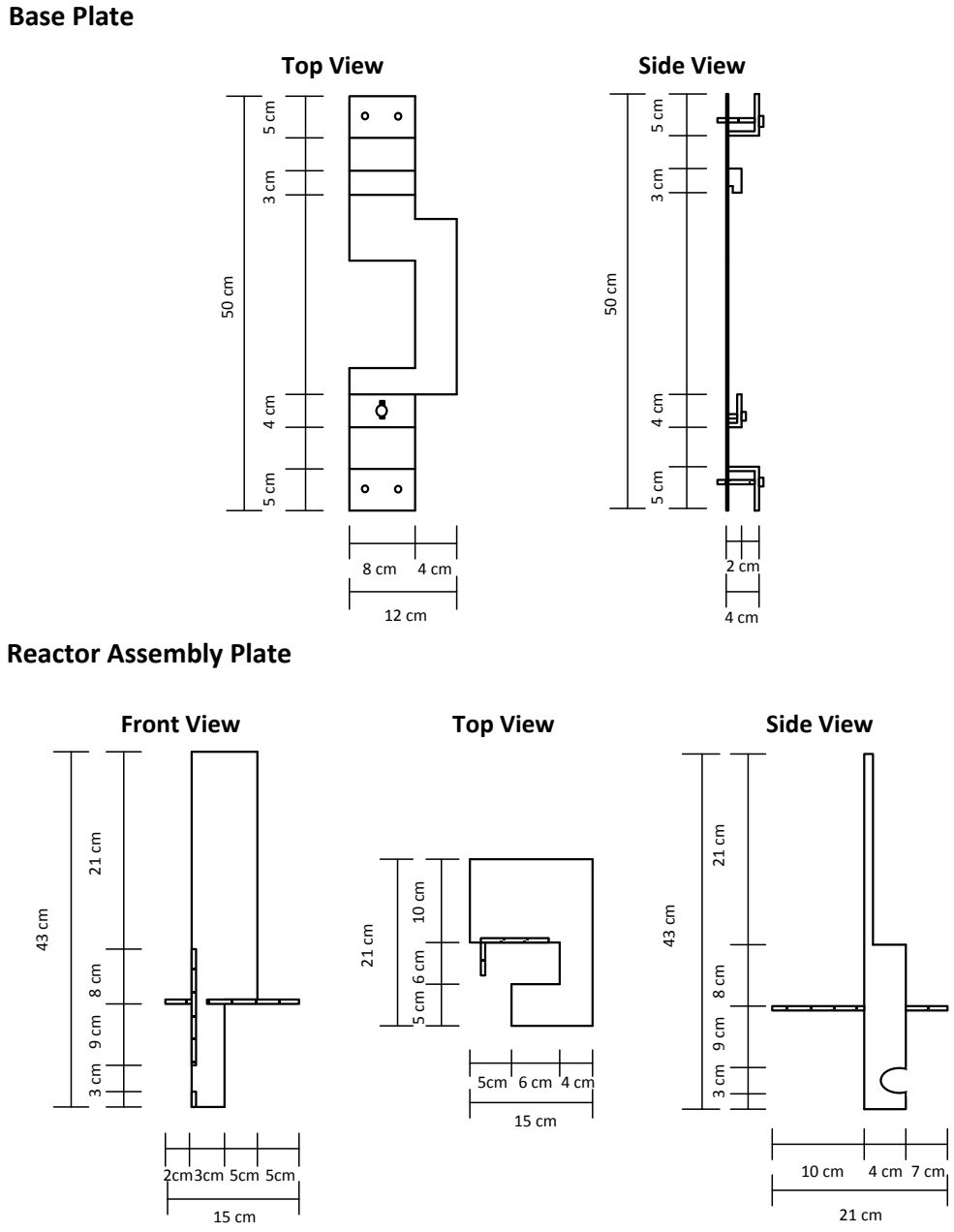


*Figure 3.4 Microbomb reactor fast release mechanism*

### 3.2.2. Oxidative cracking reactor

A continuous flow reactor to perform oxidative cracking of heavy oil model compounds in SCW was designed and commissioned. The system was designed in order to enable the study of oxidative cracking processes at short residence times (early reaction stages) between 10 and 60 s. The system has the capacity to operate at pressures up to 275 bar and temperatures of 500 °C. Following the same criteria as during the design of the batch reactor, the materials of construction were selected in order to have an over specification of 100% at all operating conditions. Reactor components were chosen according to specifications on pressure and temperature ratings from the supplier. The whole system was built with Swagelok high pressure and high temperature resistant SS 316L fittings and tubing. A complete list of the reactor components can be consulted in Appendix 11.1.2. As previously mentioned, the sections of the system that are exposed to SCW conditions, were designed in a way they can be replaced for brand new fittings after 30 h operation to prevent any failure in the structure. These precautionary measures are aimed to ensure the safe operation of the equipment and increase operation efficiency as mentioned in Section 3.1.

#### *3.2.2.1. Reactor description*

The oxidative cracking reactor described in Figure 3.5, is composed of three sections: A) reactant feed section, B) reaction section and C) product recovery section.

The reactant feed section is subdivided into two subsections, an organic feed and a $H_2O$ with $H_2O_2$ solution feed. The organic solution is fed to the system with a Varian LC Star 9002 HPLC pump capable of delivering a volumetric flow between 0.1 and 10 mL/min at a maximum pressure of 400 bar. The organic feed section has two manual purges used to remove any air trapped in the system prior to operation. In addition, it also has a safety pressure relief valve calibrated to open in case the system reaches a pressure of 275 bar or over. $H_2O$ and $H_2O_2$ solution are fed into the system by means of a Varian LC Star 9010 HPLC pump with capacity to deliver a solution at a volumetric flow between 0.5 and 5 mL/min and pressures up to 400 bar. Similar to the organic feed, the water and peroxide solution feed section has a manual purge to remove air trapped in the system and a safety relief valve calibrated to open in case the system reaches a pressure of 275 bar or over.

The reaction section operates at supercritical conditions and is subdivided into three main sections, the peroxide decomposition section (D), the mixing section (M) and the supercritical water partial oxidation section (R) as shown in Figure 3.5. The system is designed in a way that the oxygen required is supplied in the form of aqueous $H_2O_2$ solution,

which fully decomposes in D prior to mixing with the organic feed stream. D is built of 1/8" SS tube with a 0.028" wall thickness bent to form a coil of 20 cm diameter.

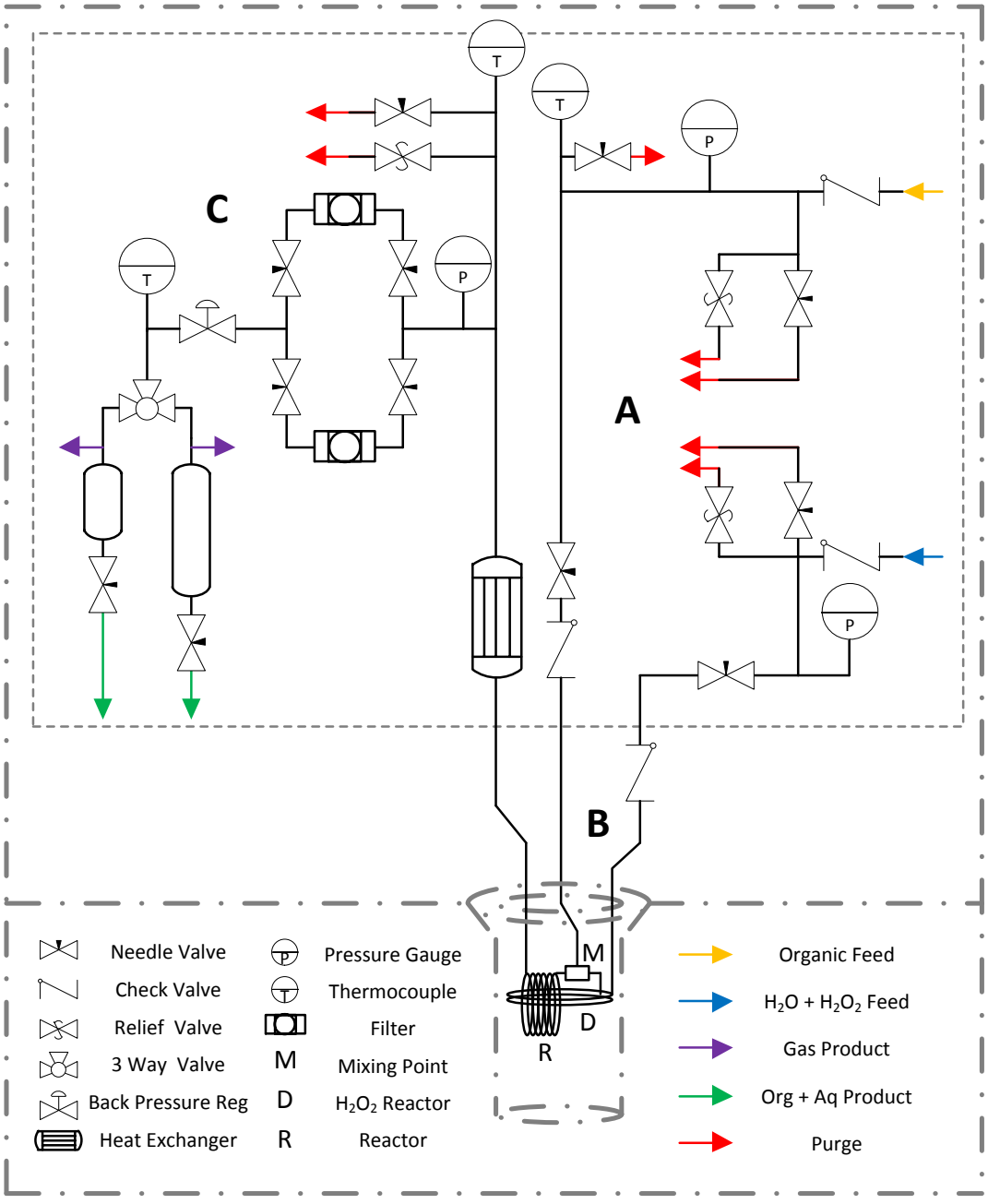


*Figure 3.5 Oxidative cracking reactor process flow diagram: A) reactant feed section, B) reaction section and C) product recovery section.*

The mixer (M) consists of a SS 1/4" bored through tee piece coupled with two 1/4" to 1/8" reducers that connect the mixer to the organic feed and to the outlet of D. The tee is oriented in a way that the flow of organic is fed from the bottom and the $H_2O + O_2$ from D is fed from

one of the side connections as shown in Figure 3.6. The mixer operates at the same process conditions than D and R, which aids in the mixing of reactants as SCW is a good solvent for gases and organic compounds. The use of a bored through tee as main body of the mixer as well as the orientation of the fitting, aid to the mixing process preventing the accumulation of $O_2$ and avoiding the formation of eddies that may lead to experimental error and a potential operational hazard.

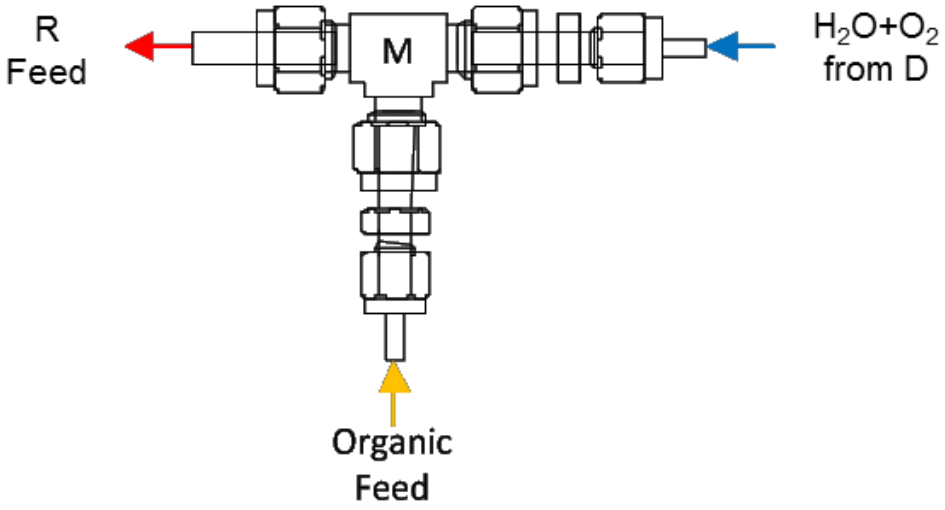


*Figure 3.6 Oxidative cracking reactor mixing section.*

After mixing, the reactants are fed into the partial oxidation reactor (R). R that is built of 1/4" SS tube with a 0.065" wall thickness bent to form a coil of 8 cm diameter. Heating into the reaction section is provided by means of a TECHNE 2BL-2D sand-bath described in section 3.2.1.2. Similarly as in the microbomb reactor, temperature in the system is controlled from a custom made control box with capacity to register temperature in five different sections of the reactor (organic feed, $H_2O_2$ solution feed, R, product recovery section and sand-bath temperature). The product stream that leaves the reactor is directed to a heat exchanger where it is cooled down to room temperature in order to fully stop the reaction. The heat exchanger consists of two concentric straight tube sections with a water flow as heat transfer fluid between them. The inner tube is composed of a 1/4" SS tube where the products of reaction flow. The outer shell is made of 1/2" SS tube closed at each side by a 1/4" to 1/2" SS bored though reducers. Cold water flows inside the shell co-currently to the direction of the reaction products.

The product stream continues to flow into the filters located in the product recovery section as shown in Figure 3.5. The system operate alternately with two tee type 7 μm filters, which

enables two different experiments to be carried out in a day. In addition it serves as an additional safety feature in case of a sudden increase in pressure due to blockage in one of the filters. Coke formed during reaction is retained in the filters and recovered after the system has been de-pressurized. After filtration the solid-free product stream flows through a back pressure regulator where pressure is reduced to ambient conditions. Then, the organic soluble, aqueous soluble and gas products are directed into the product recovery section. The product stream flows through a 3 way valve into a 1/4" SS tube that extends concentrically through a bored through tee piece that connects the system with the vessels. Reaction products flow into a continuous operation vessel (c) or a sampling vessel (b) as shown in Figure 3.7. The continuous operation vessel has a volume of 150 mL while the sampling vessel 50 mL.

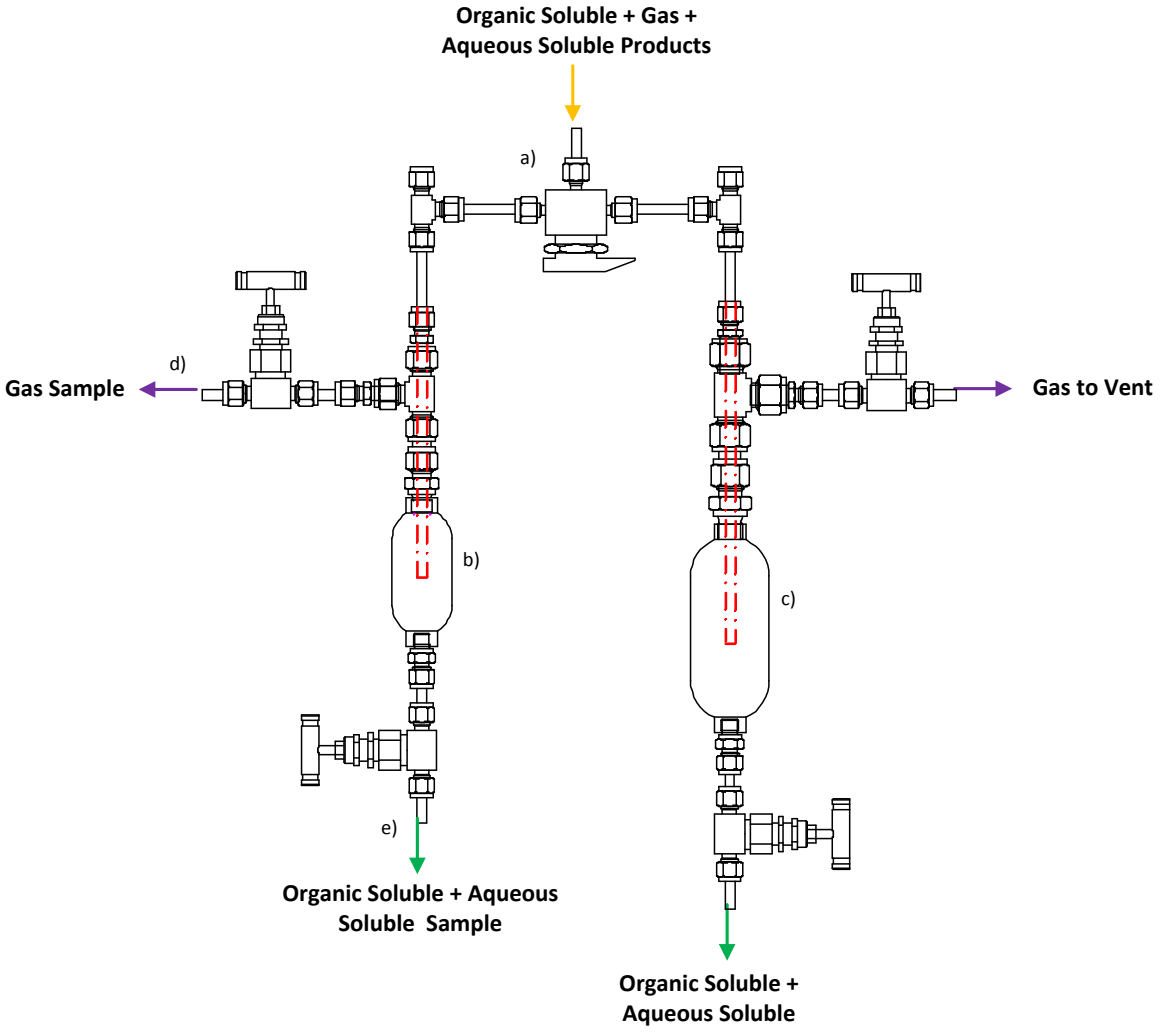


*Figure 3.7 Oxidative cracking reactor product recovery section: a) three way valve, b) sampling vessel, c) continuous operation vessel, d) gas sampling point and e) organic and aqueous products sample recovery.*

Products collected in the continuous operation vessel are treated as waste and disposed, while the products collected in the sampling vessel are recovered for further analysis. Once in the sampling vessel, reaction products separate into organic, aqueous and gas phases. The organic soluble and aqueous soluble products settle at the bottom of the vessel where they can be recovered for analysis. Gas products flow through the space between the 1/4" tube and the bored through tee into the gas sampling point. The flow of gas is measured with an Agilent ADM 1000 flow meter and the sample is collected in a tedlar gas-bag for further analysis.

#### *3.2.2.2. Oxidative cracking reactor design*

As described in Section 3.2.2.1, once the organic and the $H_2O$ with $O_2$ flows blend in the mixing section, they are directed straight into the partial oxidation reactor (R). The high solubility shown by organic compounds and the complete miscibility $O_2$ has in SCW enable a highly homogeneous and well dispersed solution at the inlet of R. The reactor was built in the shape of a coil of 8 cm diameter using 1/4" SS tube with a wall thickness of 0.065". Design considerations and calculations are explained in great detail in this section.

The total volume of the reactor is defined by the length of the coil, which in turn is determined by the residence time required as well as by the process conditions. In this project, experiments were performed within a range of operating conditions specified in Table 3.1.

*Table 3.1 Oxidative cracking reactor operating conditions.*

| Parameter | Range |
|---|---|
| Temperature (°C) | 380 - 450 |
| Pressure (bar) | 230 - 275 |
| $O/O_{stoich}$ ratio | 0 - 0.2 |
| Water/Organic ratio | 15 |
| Residence time (s) | 10 - 60 |

The design strategy is graphically detailed in the process flow diagram shown in Figure 3.8. The starting point for calculation is the determination of the desired operating conditions in R and the selection of an initial reactor length estimate.

Once the operating conditions were specified, a fixed amount of 1 g of $H_2O$ was taken as base of calculation to determine the mass fraction of each compound (organic compound,

$H_2O$ and $O_2$) at the inlet of R. With these data, it was possible to calculate a density ($\delta$) value for the reactant stream using a Peng Robinson – Soave (PRSV) equation of state in Aspen Hysis.

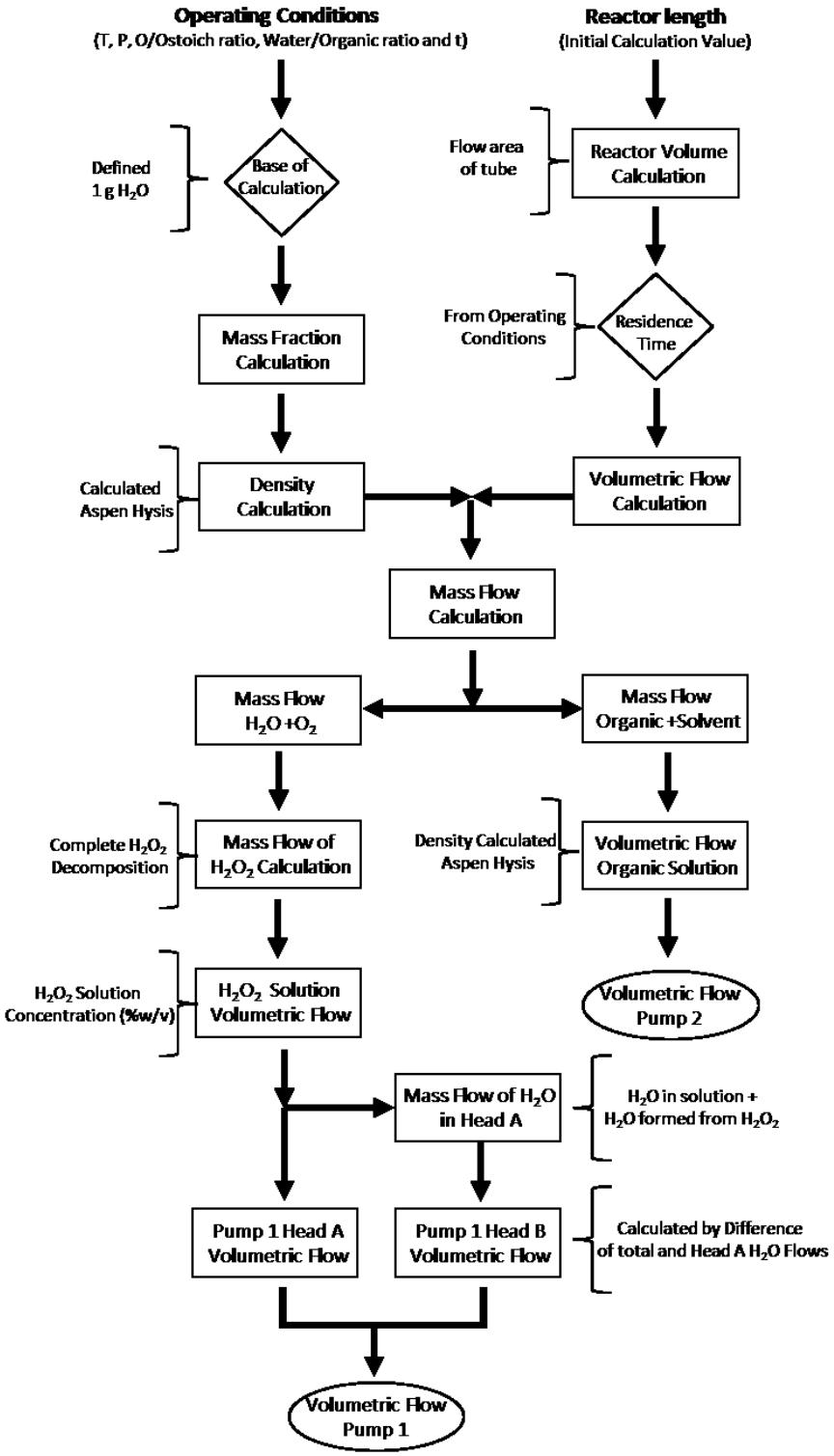


*Figure 3.8 Oxidative cracking reactor design calculations flow chart.*

The total volume of the reactor ($V_R$) was calculated with the fixed reactor length ($l_t$) and the SS 1/4" tube cross sectional area of flow (A) using Equation 3.1.

$$V_R = l_t * A \tag{3.1}$$

Once the volume of the reactor was determined, the volumetric flow rate (q) was calculated based on the desired residence time ($\tau$) using Equation 3.2.

$$q = \frac{V_R}{\tau} \tag{3.2}$$

Both, the volumetric flow rate and the fluid density are then used to calculate the mass flow (m) at the inlet of R from Equation 3.3.

$$m = \delta * q \tag{3.3}$$

The individual mass flow of each component was calculated with the total mass flow and the mass fraction previously determined. Once the individual mass flows were obtained they were divided into organic flow ($m_{org}$) and $H_2O$ + $O_2$ flow ($m_{H2O+O2}$) fed into the mixing section in Figure 3.6. Once $m_{H2O+O2}$ was determined, the flow of $H_2O_2$ solution at the inlet of D was calculated considering a complete conversion of $H_2O_2$ in D. Hydrogen peroxide is decomposed as shown in the following reaction.

$$2\ H_2O_2 \rightarrow O_2 + 2\ H_2O$$

The $O_2/H_2O_2$ molar relation and the molecular weight of the reactants were considered in Equation 3.4 to calculate the mass flow of $H_2O_2$ ($m_{H2O2}$) at the inlet of D from the known mass flow of oxygen ($m_{O2}$) at the outlet of D.

$$m_{H_2O_2} = 2.125 * m_{O_2} \tag{3.4}$$

In addition, the mass flow of $H_2O$ at the outlet of D ($m_{H2Otot}$) is composed of the $H_2O$ formed from the decomposition of $H_2O_2$ and the $H_2O$ originally being fed into D ($m_{H2O}$). Similarly, the mass flow of water fed into D was calculated by difference from the one leaving D and the one produced from the decomposition of $H_2O_2$. The $H_2O/H_2O_2$ molar relation in the reaction and the molecular weights were considered to calculate the mass flow of water fed using Equation 3.5.

$$m_{H_2O} = m_{H_2O_{tot}} - 0.47 m_{H_2O_2} \quad (3.5)$$

Once both mass flows were determined, the volumetric flow of the HPLC pump at room temperature was determined. Furthermore, the volumetric flow of organic solution was calculated from $m_{org}$ and the density of the compound at room temperature.

Finally, the volumetric flows determined for pump 1 and pump 2, as denominated in Figure 3.8, were compared with the flow capacity of the HPLC pumps to confirm whether they were within operational range, or if process parameters had to be modified to fit the equipment's capacity. Once the calculations were made and the operating parameters were within the equipment's capacity, two coils (specifications in Table 3.2) were built in order to enable operation at all conditions required in this work.

*Table 3.2 Supercritical water partial oxidation reactor (R) specifications.*

| | **Reactor Specifications** | |
|---|---|---|
| Reactor length (cm) | 150 | 200 |
| Tube External/Internal Diameter (in) | 0.25 / 0.12 | 0.25 / 0.12 |
| Reactor volume (mL) | 11 | 15 |

### *3.2.2.3. Hydrogen peroxide decomposition reactor design*

As has been briefly mentioned in Section 3.2.2.1, the $H_2O_2$ decomposition reactor (D) was designed and built in the shape of a coil of 20 cm diameter made out of SS 1/8" tube with a wall thickness of 0.028". D is divided in two lengths of tube, the first to preheat the fluid to SCW conditions and the second to provide the necessary residence time to fully decompose $H_2O_2$ into $H_2O$ and $O_2$ at the reaction. Design considerations and calculation procedures are explained in great detail in the following sections.

#### 3.2.2.3.1. Design of preheating section

For design purposes, it is considered as preheater the length of tube required to increase the temperature of the fluid to 380 °C slightly above the critical temperature of water. Moreover, $H_2O_2$ decomposition has been reported to be low at this temperature interval, reason why it was assumed that any potential decomposition of $H_2O_2$ in the preheating section was negligible (176).

The change in reaction conditions from sub-critical to supercritical results in great variations in the physicochemical properties of the reaction medium such as density, viscosity, heat capacity and conductivity. These changes were taken into account during the calculation of the heating time and the length of preheater required. Additional process parameters such as temperature of the heat source, external heat transfer coefficient, volumetric flow, and tube diameter have an impact in the length of preheater required. A model developed by Azadi et al was used to calculate the heating time required for the solution to reach supercritical water conditions (177). This was then used to estimate the length of tube required to reach the required operating temperature. The validity of the model is limited to certain range of operating parameters shown in Table 3.3.

*Table 3.3 Operating parameters of the model to predict heating time constants for SCW flow reactors, adapted from (177)*

| Parameter | Range |
|---|---|
| Volumetric flow (mL/min) | 0.5 - 10 |
| Tube external diameter (mm) | 3 - 13 |
| External heat transfer Coefficient (W/m$^2$K) | 10 - ∞ |
| Heating medium temperature (K) | 673 - 873 |

The first step of calculation was the determination of the heating time constant, which is defined as the time required to achieve 63% of the operation temperature required. This calculation was done using Equation 3.6 (177) where H is the heating time constant (s), $d_t$ is the internal diameter of the tube (mm), $q_p$ is the volumetric flow rate in the pump (mL/min) and $h_{out}$ is the external heat transfer coefficient (W/m$^2$K).

$$H = 75.41 {d_t}^{1.71} \left[\frac{487 {q_p}^{0.3} h_{out}}{487 {q_p}^{0.3} + h_{out}}\right]^{-0.886} \quad (3.6)$$

Following Azadi's procedure, the heating time constant obtained was used to calculate the time required for the reactants to reach the desired operating temperature. For this purpose, Equation 3.7 (177) was implemented where Θ stands for heating time (s), $T_{ext}$ for temperature of the heating source (K), $T_0$ for the initial temperature (K) and T for the target temperature (K).

$$\theta = H \ln\left[\frac{T_{ext}-T_0}{T_{ext}-T}\right] \quad (3.7)$$

Once the heating time was calculated the required length of tube for the pre-heating section was determined. It was taken into account that changes in process conditions affect greatly the density of the feed, which is directly linked with the volumetric flow rate. In addition, the mass flow of the feed was pre-established by the requirements of R (temperature, $O/O_{stoich}$ ratio, $H_2O$/organic ratio and residence time). Therefore, the length of the pre-heater was designed in order to ensure that the $H_2O_2$ solution being fed reached the required operating temperature at all conditions studied. This section operates with a HPLC pump with the capacity to deliver $H_2O_2$ solution in a range of volumetric flows between 0.5 and 5 mL at room temperature. This was used as base of calculation to determine the required volume of preheater. The mass flow of solution for a fixed volumetric flow of $H_2O_2$ solution was obtained using Equation 3.8, where m stands for mass flow (g/min), q for volumetric flow rate (mL/min) and $\delta$ for density (g/mL). It is worth highlighting that the mass flow was determined from the volumetric flow at room temperature set on the HPLC pump.

$$m = q * \delta \quad (3.8)$$

As briefly mentioned, changes in temperature have an important impact in the density of the fluid and hence in the volumetric flow rate obtained. In order to account for these changes, the volume of the preheater was divided into three temperature regions (25-250 °C, 250-340 °C, 340-380 °C) where density changes are linear and an average fluid density can be obtained from Aspen Hysis. A volumetric flow rate was then calculated with the mass flow previously calculated with Equation 3.8 and the average density at each temperature region. Likewise, a heating time for each temperature region was determined using Equation 3.7. Finally, the required tube volume to increase the temperature from the initial temperature to

the final temperature within each region was calculated with Equation 3.9 where V stands for volume (mL).

$$V = \theta * q \tag{3.9}$$

Then the length of tube required in each temperature was obtained with the volume previously determined and the cross sectional area of flow with Equation 3.10.

$$l_t = \frac{V}{A} \tag{3.10}$$

After calculating the required length of tube for each individual temperature region, all lengths were added in order to obtain the total length of preheater required. It was determined that at the highest volumetric flow rate of 5 mL/min (pump at ambient temperature), the length of preheater required to reach SCW temperatures over 380 °C is 18 cm, which was taken as the design length when the peroxide decomposition reactor was built.

#### *3.2.2.3.2. Design of hydrogen peroxide decomposition section*

As previously mentioned, it has been reported that the rate of $H_2O_2$ decomposition is slow at temperatures below the supercritical (176). According to this assumption and for design purposes, negligible $H_2O_2$ decomposition was considered during the preheating stage. Therefore, the concentration of $H_2O_2$ leaving the HPLC pump was used as the initial $H_2O_2$ concentration for the calculations to design the peroxide decomposition section.

The kinetics of $H_2O_2$ decomposition are assumed to follow first order of reaction (176). Kinetic parameters (activation energy and pre-exponential factor) for the decomposition of $H_2O_2$ in SCW conditions are shown in Table 3.4.

*Table 3.4 Kinetic parameters for the decomposition of $H_2O_2$ in SCW, adapted from (176).*

| Parameter | Value |
|---|---|
| Energy of Activation (kJ/mol) | 182 |
| Pre-exponential Factor ($s^{-1}$) | $10^{13.9}$ |

Similarly as in the case of the preheater, the $H_2O_2$ decomposition section was designed to operate at temperatures above 380 °C and volumetric flows of $H_2O_2$ solution between 0.5 and 5 mL/min at room temperature. First, the volumetric flow at different operating conditions was calculated from the mass flow that remains the same as the one used to calculate the preheater. The density of the fluid was also considered to remain constant as the process is isothermal (reaction starts once reaction temperature is achieved) and variations in the composition can be assumed to cause negligible changes in the fluid properties.

The kinetic constant for the temperatures considered (380, 400, 425 and 450 °C) was determined using Equation 3.11, where k stands for the kinetic constant ($s^{-1}$), Ã for the pre-exponential factor ($s^{-1}$), Ea for activation energy (kJ/mol), R for the universal gas constant (kJ/molK) and T is the reaction temperature (K).

$$k = \tilde{A} e^{\frac{-E_a}{R*T}} \tag{3.11}$$

Residence time in the $H_2O_2$ decomposition reactor was calculated with Equation 3.9 for different reaction volumes at all temperatures studied. Once the residence time and the kinetic constants for different temperatures were obtained, the concentration of $H_2O_2$ at the outlet of D was determined from Equation 3.12 where $C_f$ stands for outlet concentration (mol/L), $C_0$ for initial concentration (mol/L) and $\tau$ for residence time (s).

$$C_f = \frac{C_0}{e^{(k*\tau)}} \tag{3.12}$$

Finally, the conversion of $H_2O_2$ was calculated using Equation 3.13.

$$X = \frac{C_0 - C_f}{C_0} \tag{3.13}$$

It was determined that the length of reactor required to ensure conversions over 90% at all operating temperatures was 300 cm, which was taken as the design length during the construction of the reactor.

#### 3.2.2.3.3. Hydrogen peroxide decomposition experimental test

In order to confirm the theoretical calculations made during the design of the $H_2O_2$ decomposition reactor presented in Section 3.2.2.3.2, an experimental determination of the extent of $H_2O_2$ decomposition in the reactor was performed. Samples from the outlet of the reactor were analyzed through UV-VIS Spectrophotometry using a $Ti(SO_4)_2/H_2SO_4$ solution. The chemical principle behind this technique is based on the chemical reaction between $H_2O_2$ in the sample with the titanium sulfate acid solution. These compounds react to produce a yellow color solution, which varies in intensity depending on the concentration of peroxide in the original sample. The intensity of the color can be quantified in a UV-VIS spectrophotometer and correlated to the concentration of $H_2O_2$ in the original sample. The experimental methodology and sample preparation procedure were adapted from literature (178–180) and are briefly described in the following paragraphs.

In order to prepare the $Ti(SO_4)_2/H_2SO_4$ solution, 82.8 g of Titanium (IV) sulfate solution were measured and added to a 500 mL volumetric flask. Then, 99.5 g of sulfuric acid 95% were added. Finally DI water was used to fill the flask to a set volume of 500 mL.

The concentration of $H_2O_2$ in the sample was determined in an Agilent UV-VIS Spectrophotometer using a set wavelength of 410 nm. A volume of 5 mL of $Ti(SO_4)_2/H_2SO_4$ solution was placed in a quartz cell and 50 µL of peroxide sample were added to the solution. The sample was shaken vigorously in order to achieve homogeneity before the determination. A calibration curve, shown in Equation 3.14, was built by determining the absorbance value of known concentration $H_2O_2$ standards that can be consulted in Appendix 11.1.3.

$$C_{H_2O_2} = 0.4233 * [Absorbance] \quad (3.14)$$

A purposely built reaction set-up was used to perform the $H_2O_2$ decomposition tests. The system consists of a 300 cm coil built from 1/8” SS tube with a 0.028” wall thickness as shown in Figure 3.9. $H_2O_2$ solution is fed into the coil at 230 bar by means of a Varian LC Star 9010 pump, with the same specifications as the one used in the oxidative cracking reaction set-up. The end of the coil passes through a concentric tube heat exchanger that uses chilled water as coolant to decrease the temperature in order to fully stop the reaction. After the heat exchanger, the product flows through a back pressure regulator that decreases the pressure into atmospheric pressure. Samples can be taken once the fluid has been depressurized.

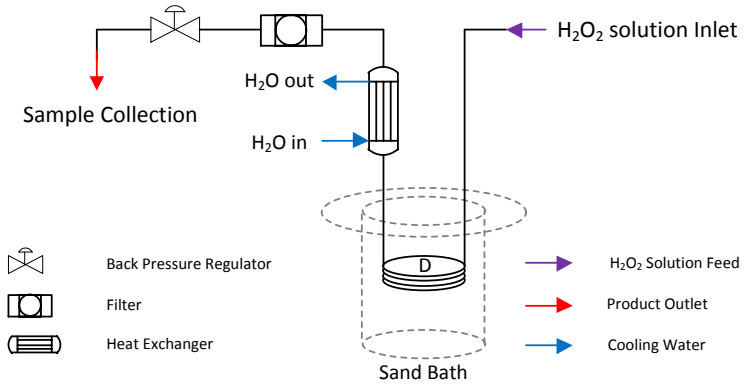


*Figure 3.9 $H_2O_2$ decomposition tests, reaction set-up.*

$H_2O_2$ decomposition experiments were initially performed at 380 °C and 230 bar varying the concentration of $H_2O_2$ in the feed (5, 10 and 15 %) as well as the volumetric flow in the pump (2, 5 mL/min). Samples of the outlet of the reactor were taken for analysis in the UV-VIS spectrophotometer. A total of three samples at each experimental condition were taken and measured five times each. The average values obtained are reported in Table 3.5.

*Table 3.5 Hydrogen peroxide concentration in % w/v detected after reaction at 380 °C and 230 bar at different pump volumetric flow rates.*

| **$H_2O_2$ Initial Concentration (%w/v)** | **$H_2O_2$ Final Concentration (%w/v)** | |
|---|---|---|
| | **Flow 2 (ml/min)** | **Flow 5 (ml/min)** |
| **$H_2O_2$ 5%** | 0.05% | 0.06% |
| **$H_2O_2$ 10%** | 0.00% | 0.00% |
| **$H_2O_2$ 15%** | 0.00% | 0.00% |

Based on the high sensitivity of the analytical technique and the final concentrations of $H_2O_2$ reported in Table 3.5, it was concluded that $H_2O_2$ was completely decomposed at all experimental conditions studied. Furthermore, taking into consideration that 380 °C is the lowest operating temperature studied, the determination of $H_2O_2$ decomposition at 400, 425 and 450 °C is considered unnecessary as the decomposition is expected to proceed at higher reaction rates with any increment in temperature, which would result in higher conversions.

### 3.2.2.4. Safety cabinet and lifting mechanism

In order to ensure safe operation with the oxidative cracking reactor, a safety cabinet to enclose high pressure and high temperature sections of the reactor was designed and built according to the specifications in Figure 3.10. The cabinet consists of two main sections, the top section where the reactor was assembled and the bottom section that gives access to the sand-bath controls and waste disposal drums.

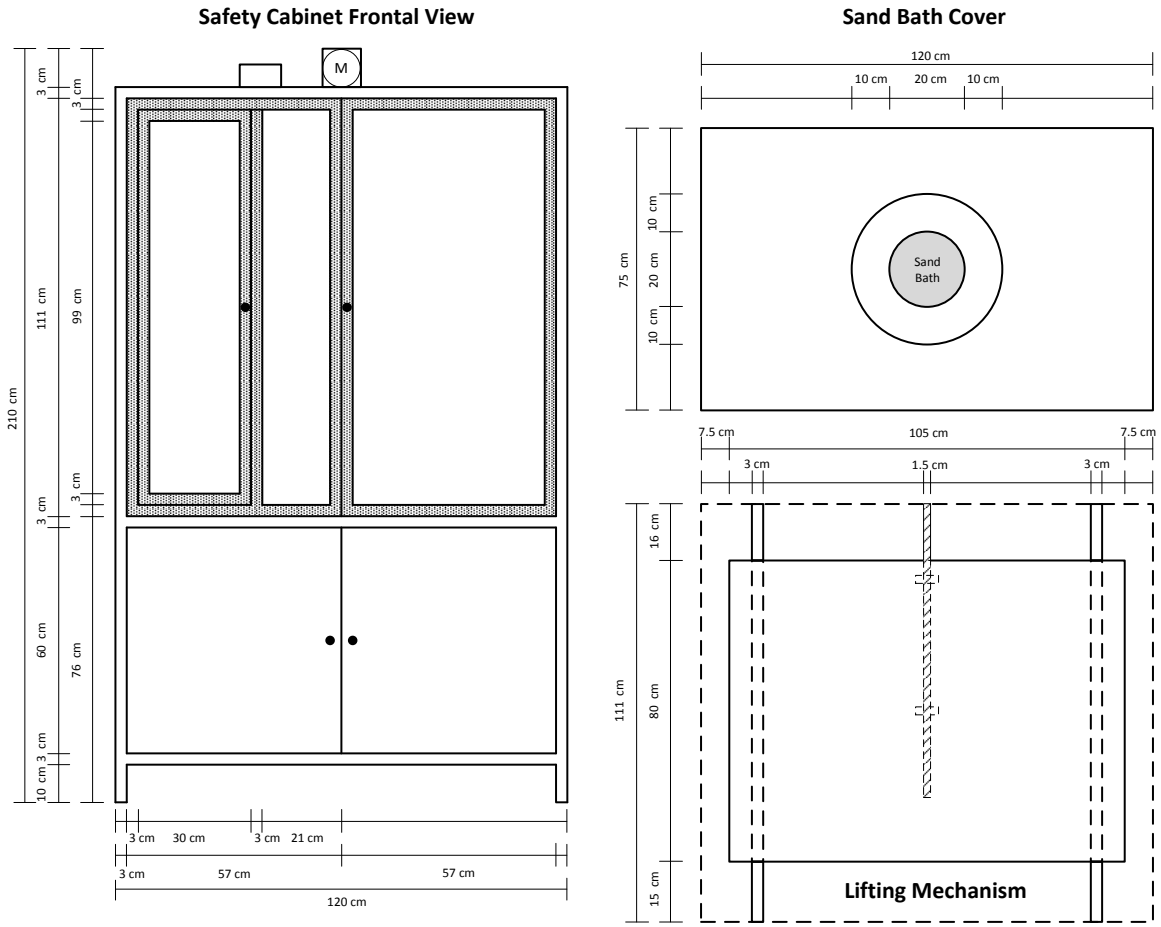


*Figure 3.10 Oxidative cracking reactor safety cabinet and lifting mechanism.*

The two sections are separated by a SS sheet cover with a 40 cm hole located in the middle of the cabinet. The hole is aligned with the sand-bath cover by means of an aluminum skirt, which isolates both sections of the cabinet as shown in Figure 3.10. The top section is fitted with two doors built out of 6 mm perspex acrylic vision panels that enable visual control of the reactor and are resistant to impact. The left door is suited with a window that provides access exclusively to the non-pressurized section of the reactor and enables the operator to take samples safely while the system is pressurized. Extraction in the top section of the

cabinet is provided by a Vent Axia ACM100 in-line mixed flow fan with an air extraction capacity of 220 $m^3$/h.

A mechanism to lift or immerse the reactor to and from the sand-bath was commissioned. The lifting mechanism consists of two guide columns made out of 1" SS tube where a 4 mm SS steel panel (105 cm x 80 cm) is attached by means of 4 nylon 66 holding structures as shown in Figure 3.10. The nylon 66 modified with $MoS_2$ provides low friction and self-lubrication to the structure, which enables it to slide up and down the columns without friction. The SS panel is attached to a lead screw, which rotates on its own axis by means of a Parvalux 150 W motor (M) shown in Figure 3.10. The lead screw provides the panel with vertical movement that enables the reaction section to be immersed or emerged from the sand-bath. The motor is connected to a level switch and to a door switch, which stops the engine when the panel reaches the preset height or cabinet doors are not completely closed to ensure safe operation.

# Chapter 4
# Experimental

In this work experiments to study the hydrothermal oxidative cracking of heavy oil in near-critical and supercritical conditions were performed. In order to gain a deep understanding of the process, both PAH's as heavy oil model compounds and Maya oil VR as real feedstock were used. As described in Chapter 3, two reaction set-ups, a microbomb batch reactor and an oxidative cracking flow reactor, were designed, modified and built. An overview of the operation procedures designed for each reaction set-up and the product recovery procedures employed for each particular feedstock is provided in Section 4.1. A series of experiments in order to test the effect of the addition of a zeolite based catalyst to the oxidative cracking of VR was also considered. The catalyst synthesis procedure and the analytical techniques used to characterize it are explained in Section 4.2

## 4.1. OXIDATIVE CRACKING EXPERIMENTS

### 4.1.1. Batch experiments in the microbomb reactor

A microbomb reactor described in Section 3.2.1 was used in experiments to determine the effect of process conditions such as pressure, temperature, $O/O_{stoich}$ ratio, reaction time and catalyst addition in the process. For this purpose, Sigma-Aldrich phenanthrene 98% w/w as heavy oil model compound and Maya oil VR as heavy oil real feedstock were used. In addition, VWR $H_2O_2$ solution 30% w/v as oxygen source and deionized water were used. The helium used as inert gas to purge and leak test the system was supplied by BOC.

#### *4.1.1.1. Microbomb operating conditions*

Microbomb reaction set-ups have been previously used in hydrothermal oxidative processes with heavy oil model compounds in near-critical and supercritical conditions (172,173). At these conditions, the reactor structure is susceptible of damage due to the highly corrosive environment and stress of operation. After several experiments some degree of de-alloying and damage to the structure caused by corrosion were observed. In addition, the constant tightening and untightening of fittings during the loading and product recovery procedures,

damage the fittings threads making them prone to failure and leakage. Drastic changes in temperature during immersion in the sand-bath and quenching in cold water also contribute to the quick degradation of the reactor components. In order to prevent a potential failure during operation, it was established that the reaction section exposed to the highly corrosive reaction environment and subject to constant stress had to be replaced for new fittings every six experiments where not considerable damage to the threads or reactor walls has yet been observed.

#### *4.1.1.1.1. Reaction temperature*

Experiments at different reaction temperatures between 360 °C and 450 °C were performed in order to study the process at near-critical and supercritical water conditions. Reaction temperature was controlled from a custom made control box and heating was provided by a fluidized bed sand-bath as detailed in Section 3.2.1.2. This heating medium provides with homogeneous heating of the system, which prevents the formation of hot spots or colder sections in the reactor.

The system can operate at temperatures up to 500 °C and can fluctuate within a range of +/- 3 °C. A temperature gradient of 5 °C between the sand-bath and the reactor was determined. This was considered when selecting the temperature controller set point in order to ensure that reaction temperature was reached. It should be noted that after the reactor is immersed in the sand-bath, there is a period between 3 and 3.5 min (heating time) until reaction temperature is reached. This was experimentally determined at all conditions studied and a temperature versus heating time curve was built as shown in Appendix 11.1.4.

#### *4.1.1.1.2. Reaction time*

Different reaction times ranging from 0 to 90 min were studied in experiments with phenanthrene and VR. The aim was to study the evolution of products with time and determine potential reaction pathways. Time zero is defined as the moment when the reaction system reaches a temperature within 5 °C from the set reaction temperature. At this moment, reaction time in every experiment started counting. The reaction time was stopped at the moment that the reactor was quenched in a cool water-bath when the reaction stopped.

#### 4.1.1.1.3. Reaction pressure

Pressure in the microbomb reactor is determined by the amount of water initially loaded into the system. As mentioned in Section 3.2.1.1, the reaction section has a fixed volume of 12 mL. Therefore, pressure in the system increases with temperature until it reaches the desired pressure at the pre-established reaction temperature. It is then of great importance that an adequate temperature control is kept throughout the whole experiment as slight changes in temperature result in an important variation of the system's pressure. This is particularly relevant in experiments aimed to study oxidative cracking in the vicinity of the critical pressure as small changes in temperature may result in a change between near-critical and supercritical conditions. Experiments were performed in a range of pressures between 210 and 275 bar. In order to achieve these conditions, a fixed volume of 1.2 mL of $H_2O_2$ 30% w/v was added into the reactor followed by different de-ionized (DI) water loadings depending on the reaction pressure desired. The amount of DI water to reach the required pressure was determined from a calibration curve that relates DI water loading with the set temperature and target pressure as shown in Appendix 11.1.5.

#### 4.1.1.1.4. $O/O_{stoich}$ ratio

Experiments in the microbomb reactor can be performed at different initial oxygen loading, which is represented by the $O/O_{stoich}$ ratio. $O/O_{stoich}$ ratio is defined as the relation between the amount of oxygen fed into the system and the required oxygen to achieve the complete oxidation of phenanthrene into $H_2O$ and $CO_2$ according to the following reaction.

$$C_{14}H_{10} + 16.5\ O_2 \longrightarrow 14\ CO_2 + 5\ H_2O$$

Oxygen for the reaction was obtained from the thermal decomposition of $H_2O_2$. A fixed volume of 1.2 mL of $H_2O_2$ 30% w/v solution was initially loaded into the microbomb reactor for every experiment. In order to achieve the required $O/O_{stoich}$ ratio, the initial phenanthrene loading was varied between experiments. Varying the initial phenanthrene loading while maintaining the volume of $H_2O_2$ solution constant, ensures that other variables like the pressure are not affected by changes in the $O/O_{stoich}$ ratio. In this work $O/O_{stoich}$ ratios between 0.1 and 0.75 were studied.

#### 4.1.1.1.5. Feed

As has been mentioned previously, experiments with phenanthrene as heavy oil model compound and VR as real feedstock were performed. The rationale behind the choice of

phenanthrene lies in the nature of its structure that resembles the polycyclic aromatic chains that compose real asphaltene molecules. In this work, phenanthrene 98% supplied by Sigma-Aldrich was used. In addition, experiments with real heavy oil were performed with a sample of Maya oil VR supplied by the Mexican Institute of Petroleum. The composition and main properties of this fraction are reported in Table 4.1.

*Table 4.1 Maya crude VR properties and elemental composition*

| Oil Properties | | Elemental Analysis | |
|---|---|---|---|
| Asphaltene content (%) | 33 | C (%w/w) | 82.07 |
| Maltene content (%) | 67 | H (%w/w) | 9.88 |
| Boiling point (°C) | >540 | N (%w/w) | 0.66 |
| API gravity | 0 | S (%w/w) | 6.74 |
| Conradson number (%) | 25.5 | Ni (ppm) | 207 |
| Viscosity (cSt) | 265,546 | V (ppm) | 211 |

#### *4.1.1.2. Microbomb reactor operation*

The general operation of the microbomb reactor regardless of the organic substrate used is schematically explained in Figure 4.1. It has to be noted that as it was mentioned in Chapter 3.1, the reaction section of the experimental set up was replaced for new fittings every 6 experiments. When a new reactor was used for the first time, it was treated in order to passivate its inner walls to prevent from any potential catalytic activity that may lead to deviations in the results obtained. The passivation process consists in exposing the reaction section to an oxygen rich environment at hydrothermal conditions to oxidize any potentially active metal site before any experiment is performed. In order to do this, the reactor was loaded with 2 mL of $H_2O_2$ 30 % w/v and immersed in the fluidized sand-bath for two hours at 300 °C. Once the system has been treated, it was rinsed with $CHCl_3$ / $CH_3OH$ 4:1 v/v solution and left to dry in a hot cabinet at 40 °C.

Figure 4.1 shows that at the start of every experiment, the mass of a clean and dry 1/2” tee with two ends plugged was measured in a Sartorius CPA3245 balance. Then, the tee was loaded with the required amount of organic substrate phenanthrene or VR. In experiments involving a catalyst, the tee was also loaded with the required amount of catalyst in its oxidized state at a 1:4 $g_{cat}/g_{org}$ ratio. Once the mass of substrate and catalyst was measured, the required volume of $H_2O_2$ 30% w/v solution and DI water to reach the desired pressure and $O/O_{stoich}$ ratios were added as explained in Sections 4.1.1.1.3 and 4.1.1.1.4.

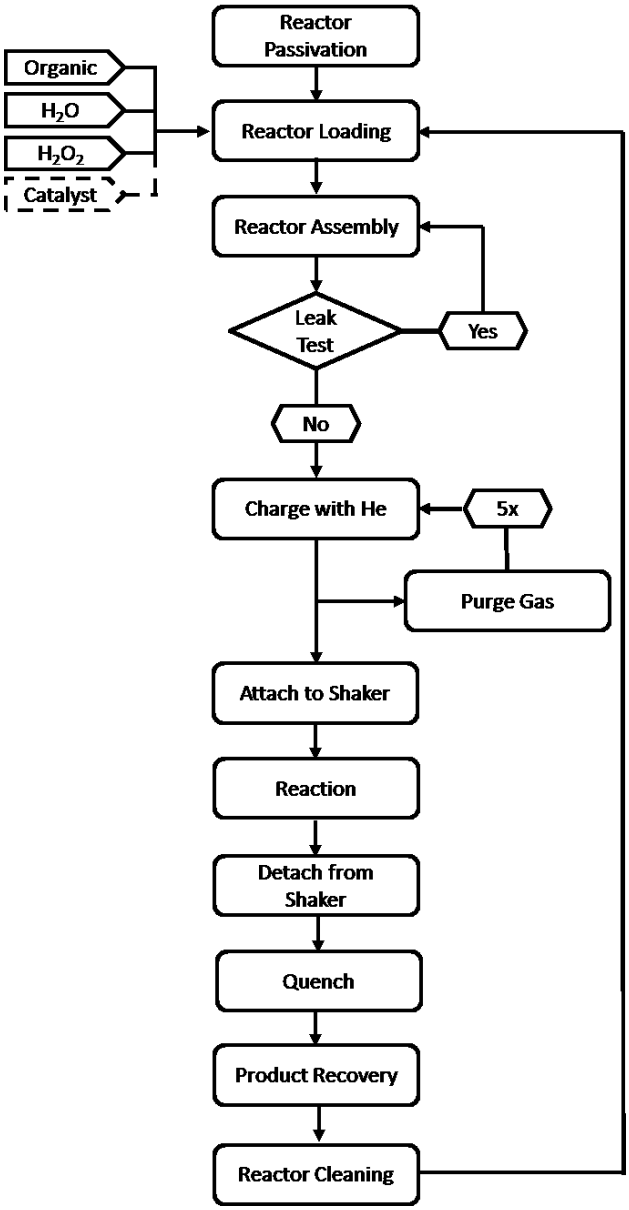


*Figure 4.1 Microbomb reactor operating procedure flow chart.*

Once loaded, the 1/2“ tee was assembled to the main body of the reactor through a 1/2” to 1/4" reducing port connector with a 1/2" nut that closes the system.

The reactor was then connected to a helium cylinder with a line built of 1/8” SS tubing. The reactor was pressurized to 200 bar with helium and tested for any leaks. If a leak was found, pressure was released and the origin of the leak was investigated and suppressed. The procedure was repeated until no leaks were found in the system as described in Figure 4.1. Repeating the leak test is of great importance as regardless if a leak was found and suppressed, it could have masked other minor leaks in different sections of the reactor that need to be resolved as well. After no leaks were detected, the system was purged with

helium at low pressure (20-30 bar) to remove any air that could have remained inside the reactor. This procedure was repeated five times to ensure an oxygen free atmosphere at the start of the reaction. Finally, the high pressure - high temperature valve, which separates the reaction section from the gas recovery section, was closed. This leaves the reaction section loaded and filled with inert helium at room temperature and pressure.

Then, the reactor was immersed into the sand-bath and attached to the shaking mechanism as indicated in Figure 4.1. Immediately after, the doors of the safety cabinet were secured firmly and the shaking mechanism was switched on. As mentioned in Section 4.1.1.1.2, reaction time started the moment the temperature inside the reactor reached a temperature 5 °C below the reaction temperature. When reaction time was reached, the reactor was detached from the shacking mechanism and quenched in a chilled water-bath in order to stop the reaction. Once at room temperature, the gas sampling section was purged with helium to remove any air trapped in the gas recovery section of the reactor. Helium is used as purging gas as its presence does not interfere with the analysis through gas chromatography. After the system was purged, a 1/4" SS nut with a septum incorporated was placed in the gas sampling zone (c) in Figure 3.2. Then, the high pressure - high temperature valve was opened and the pressure of the gas produced recorded. Products of reaction were then recovered and analyzed following the procedures explained in detail in Sections 4.1.1.3 and 4.1.1.4. Finally the whole system was cleaned with $CHCl_3$ / $CH_3OH$ 4:1 v/v solution and left to dry in a hot cabinet at 40 °C.

### *4.1.1.3. Product recovery*

Once the reactor has cooled down to room temperature and it has been purged with helium, the products of reaction were recovered for further analysis. Different product recovery procedures were followed depending on the nature of the feedstock (model compound or real feed) as explained below.

#### *4.1.1.3.1. Experiments with heavy oil model compounds*

A diagram of the detailed product recovery procedure for experiments performed with heavy oil model compound phenanthrene is presented in Figure 4.2. The gas product was analyzed through gas chromatography with thermal conductivity detector (GC-TCD) to determine its composition. After analysis, the remaining gas was vented in a fume hood and the reactor was opened. A solvent solution composed of $CHCl_3$ / $CH_3OH$ 4:1 v/v was used to carefully rinse the interior of the 1/2" tee reactor as well as the plugs to recover the products

of reaction. Furthermore, the interior of the remaining parts that compose the reaction section were also rinsed with solvent solution pumped by means of a HPLC pump.

The recovered products were then filtered in a Sartorius vacuum filtration kit using a 1 μm pore size Whatman PTFE membrane filter. The solid retained in the filter was dried in an oven for three hours at 100 °C and its weight was recorded after it cooled down to room temperature. The solid recovered was then analyzed through thermogravimetric analysis (TGA) to determine the amount of coke produced in the reaction.

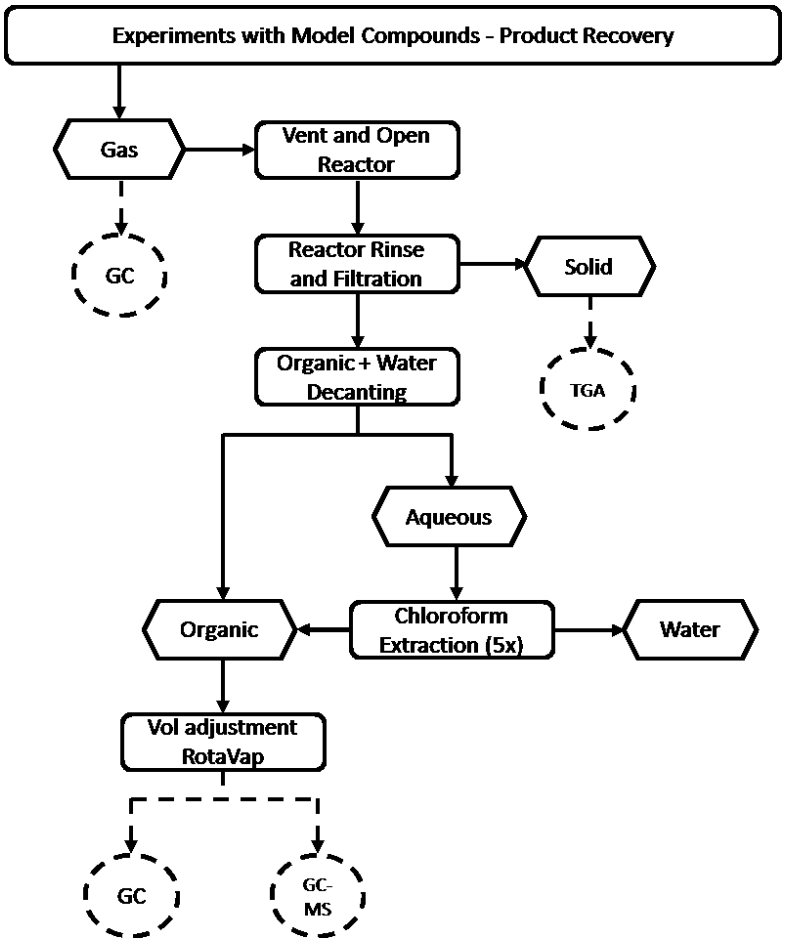


*Figure 4.2 Experiments with phenanthrene product recovery flow chart.*

The liquid fraction recovered was composed of two phases (organic and aqueous), which were separated through decantation in a separation funnel. An organic solvent extraction was performed to the aqueous phase using chloroform to recover any organic product remaining in the aqueous phase. The procedure was repeated five times to ensure that any organic product left was extracted. The organic extracts were combined with the original organic phase to form a single organic phase. Then, the volume of the organic phase was

adjusted in a Buchi rotatory evaporator with a set temperature of 75 °C. Finally, the organic phase was analyzed by gas chromatography with flame ionization detection (GC-FID) and gas chromatography with mass spectrometry (GC-MS).

#### *4.1.1.3.2. Experiments with heavy oil real feedstock*

The detailed product recovery procedure followed in experiments with VR is graphically explained in the flow chart shown in Figure 4.3. One of the main differences between working with model compounds and VR is that the gas product from the latter cannot be analyzed through GC due to the presence of sulfur in the gas product, which is detrimental to the equipment.

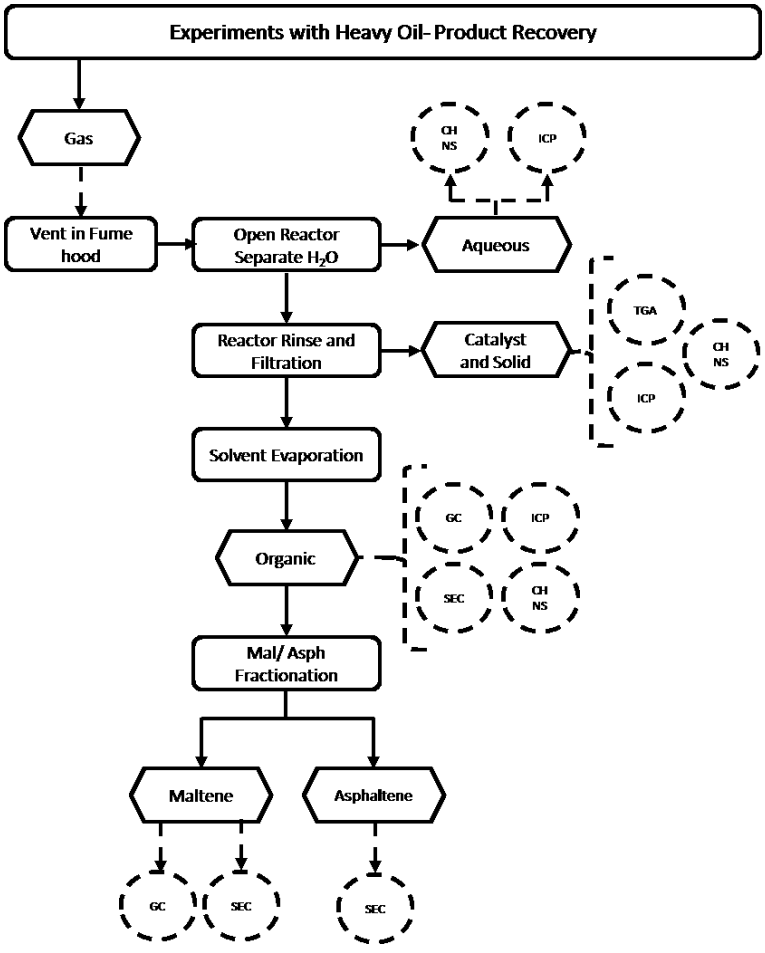


*Figure 4.3 Experiments with heavy oil real feedstock product recovery flow chart.*

Once the reactor has reached room temperature, the high temperature - high pressure valve was opened and the pressure of the gas product was registered in an omega pressure

gauge. Then, the gas was vented inside a fume hood prior to opening the reaction section of the system. The aqueous phase was decanted into a separate glass vial. Then, it was extracted using a 2mL disposable syringe and passed through a Whatman puradisc 13 PTFE syringe filter with 1.0 μm pore diameter to retain any organic or suspended solid. The recovered aqueous phase was then analyzed by induced coupled plasma (ICP) and elemental micro analysis (CHNS) to identify any aqueous soluble product and determine the presence of any heteroatom or metal (S, N, V, Ni) in solution.

The 1/2" bored through tee, which represents most of the reactor body, was thoroughly rinsed with $CHCl_3$ / $CH_3OH$ 4:1 v/v solution to recover the organic and solid products of reaction. The remaining components of the reaction section were rinsed by means of a HPLC pump that passed solvent mixture through them to ensure no product was left. In addition, the syringe previously used to filter the aqueous phase was filled with $CHCl_3$ / $CH_3OH$ 4:1 v/v solution, which was then passed through the syringe filter to recover any organic soluble product retained within the filtrate. Then, the whole solvent mixture was vacuum filtered in a Sartorius filtration kit using a 1 μm pore size Whatman PTFE membrane filter to retain the solids. Solids were then dried for three hours at 100 °C and left to cool down to room temperature before its weight was measured. The dry solid was then analyzed through TGA to determine the amount of coke present. Furthermore, ICP and CHNS analysis were performed to determine the amount of heteroatoms and metals present in the solid product.

Separately, the solvent containing the organic soluble product recovered was evaporated in two steps. The first step was performed in a Buchi rotatory evaporator at 75 °C, where most of the solvent was removed. The product recovered was transferred into a 14 mL glass vial for further drying. The second step was performed in a purposely built $N_2$ drying system shown in Appendix 11.2.1. The remaining solvent in the sample was dried under $N_2$ flow until constant weight was observed. The weight was considered constant once its change within an hour was less than 1%, which indicates that the sample was completely dry. The organic soluble product was then analyzed through size exclusion chromatography (SEC), ICP and CHNS analysis.

The organic soluble product recovered was further fractionated into maltene and asphaltene fractions following a procedure adapted from the ASTM D3279 standard (181). Initially, a 0.1 +/- 0.02 g sample of organic product were placed in a 14 mL glass vial and 6-7 mL of n-heptane were added. The glass vial with the sample was then placed in a Vortex Genie 2 T shaker from Scientific Industries for two hours for the extraction of the maltenes from the recovered oil. The vial was removed from the shaker and placed in a vial holder for

centrifugation in a MSE Centaur 2 centrifuge at 2000 rpm for 20 min. After centrifugation two clear phases were observed: a reddish solution (n-heptane soluble), which corresponds to the maltene fraction and a solid that settles at the bottom (n-heptane insoluble) corresponding to the asphaltene fraction. The maltene fraction was carefully extracted with a disposable syringe and passed through a Whatman puradisc 13 PTFE syringe filter with 1.0 μm pore diameter into another vial. The syringe used was then filled with toluene, which was passed through the filter into the vial containing the solid asphaltenes to recover any retained asphaltene from the filter. The whole process was repeated twice with the remaining solid fraction to ensure that all maltenes were extracted. The two fractions were dried to constant weight under $N_2$ flow as previously explained. Similarly, the final mass of each fraction was recorded once the change in the weight within an hour was less than 1%. Finally, the maltene fraction was analyzed through SEC and simulated distillation in the GC-FID and the asphaltene fraction through SEC.

### 4.1.2. Continuous flow experiments in the oxidative cracking reactor

Experiments to assess the oxidative cracking of heavy oil at early stages of reaction were performed in the oxidative cracking flow reactor using methyl naphthalene as model compound. The experimental set-up, design and commissioning of the reactor are extensively described in Section 3.2.2. In this work, Sigma Aldrich methyl naphthalene 97% w/w was used as heavy oil model compound, VWR $H_2O_2$ 30% w/v was used as oxygen source and DI water as reaction medium. Helium used to purge and leak test the system during start-up and also to remove any air contained in the sampling vessel was supplied by BOC.

#### *4.1.2.1. Reaction conditions*

The oxidative cracking reactor was designed to operate in hydrothermal conditions in the presence of oxygen. As explained in Chapter 3.1, NCW or SCW with dissolved oxygen are highly corrosive reaction media that can damage the structure of the reactor if exposed for long operation periods. In order to prevent any damage to the structure of the reactor, the reaction section was replaced after 30 h of continuous operation. This aimed to ensure safety of operation and prevent from any de-alloying and changes in the reactors surface that may affect the repeatability of the experiments.

#### *4.1.2.1.1. Reaction temperature*

Heating to the oxidative cracking reactor is provided by a Techne fluidized sand-bath. In this work experiments in the flow reactor were performed at supercritical temperatures in the range between 400 °C and 450 °C. A temperature gradient of 2 °C between the temperature in the sand-bath and the internal temperature of the reactor was determined. This temperature difference was considered when adjusting the set point in the systems control box. Maximum fluctuations in temperature of +/- 3 °C were registered throughout the experiments. Temperature was recorded in different sections of the reactor (reactant feed sections, reactor, product recovery section and sand bed) for control.

#### *4.1.2.1.2. Residence time*

Residence time in the reactor is determined by the reactor volume, process conditions and the volumetric flow range that the HPLC pumps can deliver as extensively explained in Section 3.2.2.2. The oxidative cracking flow reactor enabled operation at residence times ranging between 10 and 60 s. Moreover, before any experiment, it was ensured that the volumes of reactants loaded into the feed reservoirs at the start of each experiment were sufficient to maintain the required flows in the experiment for over 120 min of continuous operation.

#### *4.1.2.1.3. $O/O_{stoich}$ ratio*

The reactor was designed to operate at $O/O_{stoich}$ ratios ranging from 0.05 to 0.2. Similarly as in the microbomb reactor, $O/O_{stoich}$ ratio was defined as the relation between the amount of oxygen fed into the system and the necessary one to achieve the complete oxidation of the methyl naphthalene into $CO_2$ and $H_2O$ according to the following reaction:

$$C_{11}H_{10} + 13.5\ O_2 \rightarrow 11\ CO_2 + 5\ H_2O$$

The amount of oxygen fed into the system was controlled by adjusting the $H_2O$-$H_2O_2$ feed stream composition fed by the HPLC pump.

### *4.1.2.2. Reactor operation*

A schematic representation of the general operation procedure of the oxidative cracking reactor is shown in Figure 4.4. Similarly as in the microbomb system operation, when a reactor was replaced, it was pretreated in order to passivate the surface of its inner walls

that can have some degree of catalytic activity. The procedure to passivate the reactor consisted on passing a 2 mL/min flow of $H_2O_2$ 10% w/v solution through the reactor at 300 °C and 150 bar for two hours. After pretreatment time concluded, the flow of $H_2O_2$ solution was switched to 100% DI water and the volumetric flow was increased to 5 mL/min in order to flush the reactor and remove any oxide particles formed. Solids formed were retained in one of the 7 μm inline tee type filters, which were then cleaned before performing any experiment.

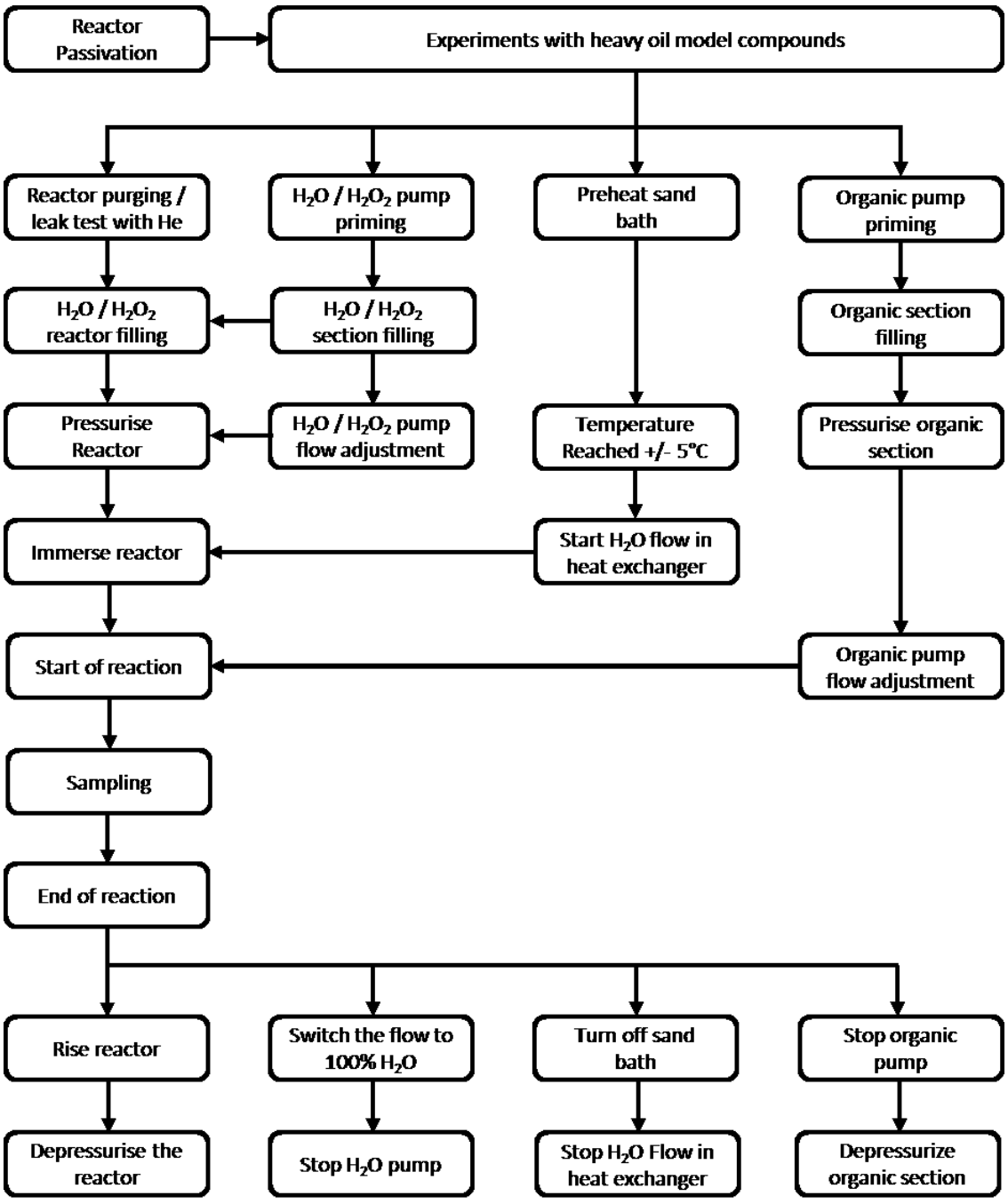


*Figure 4.4 Oxidative cracking reactor operating procedure.*

The reactor was leak tested and purged with helium prior to any experiment as shown in Figure 4.4. Each section of the reactor was individually leak tested using helium at 200 bar to facilitate the identification of leaks. The gas cylinder was connected separately into both the organic and the $H_2O$-$H_2O_2$ feeds to leak test each section independently. Once both sections were tested, the rest of the reactor was filled with helium and the procedure was repeated. When no leaks were found, the gas contained in the system was released from the purge valve into the ventilation system.

Both HPLC pumps were primed to ensure that any air trapped in the pump lines was removed. In order to do this, the purge valve in each pump was opened and solvent was pumped at maximum flow until there were no visible air bubbles in the tubing and constant flow through the purge was observed. Parallel to the priming of the pumps and in preparation for the reaction, the fluidized sand-bath started to be preheated to reaction temperature.

The organic feed section was filled with methyl naphthalene; while the remaining sections of the reactor were filled with DI water. In a similar approach to the one of the leak test, the reactor was filled by sections in order to ensure that helium was entirely displaced from the reactor. Each section of the reactor has a purge valve connected to a pipe network that enables the removal of helium into the vent and directs the surplus of water or organic compound into a mixed waste drum. First the organic and $H_2O$ feed sections were filled with methyl naphthalene or DI water respectively. Once the organic section was filled, the purge valve was closed and the organic feed stopped until the beginning of the experiment. In the case of the $H_2O$-$H_2O_2$ feed section, the purge valve was closed and the valve that connects it to the remaining sections was opened to allow the rest of the sections in the reactor to be entirely filled with DI water. As soon as all sections were filled, purge valves were closed and the pressure in the system was regulated with the back pressure regulator. Then, the flow required in both HPLC pumps were fixed to the required experimental conditions and the composition in the $H_2O$-$H_2O_2$ solution pump was adjusted.

Once the sand-bath reached reaction temperature, before the start of the experiment, a constant flow of water into the heat exchanger was set in order to cool the product stream to room temperature at the outlet of the reactor. Finally, the doors of the cabinet were secured and the reactor was immersed into the sand-bath by means of a mechanical lifting mechanism described in Section 3.2.2.4. In the first few minutes after immersion, fluctuations in temperature and pressure were registered in different sections of the reactor. The system was left to stabilize until variations in experimental conditions settled. At this time, the flow of the organic feed pump was started. The experiment began the moment the needle valve that separates the organic feed section and the rest of the reactor was opened allowing the flow of organic solution into the system. Once the organic reactant started to be

fed, variations in process conditions were monitored and registered throughout the experiment. Experiments had a minimum reaction time of 120 min in which 4 samples were taken at intervals of 15 to 20 min. The first sample was taken 25 to 30 min after the start of the reaction in order to allow the system to reach steady state and the products of reaction to arrive at the product sampling section. The procedure followed for sampling and product recovery will be explained in great detail in Section 4.1.2.3.

After reaction time reached completion, the reactor was removed from the sand-bath by means of the mechanical lifting system and the composition of the $H_2O/H_2O_2$ flow changed to 100% $H_2O$. Immediately after, the organic flow into the system was interrupted and the valve that separates the organic feed section with the rest of the reactor was closed. Then, the sand-bath set point was set to ambient temperature to allow the cooling of the equipment. The flow of water through the reactor was maintained until the system cooled down completely. This also allowed the remaining products to leave the reactor and all the solids to be retained in the solid recovery filters. Then the water pump was turned off and the flow of cooling water through the heat exchanger interrupted. Finally, the reactor was depressurized.

#### *4.1.2.3. Sampling and product recovery*

A flow chart of the procedure on how to take samples in the oxidative cracking reactor is shown in Figure 4.5. Before any sample was taken, a tedlar gas-bag and 8 glass vials with cap were prepared and labelled. Vacuum was applied into the tedlar gas-bag in order to ensure the removal of all air contained. In parallel, the glass vials were thoroughly rinsed with acetone and dried at 60 °C for 30 min to ensure they were completely clean. Both gas-bag and glass vials were labelled with the experiment and sample number.

The sampling vessel in the reactor was rinsed with chloroform and then acetone to ensure that the walls were clean before the collection of any sample. Then, it was left to dry for a few minutes before it was purged with helium to remove any air present prior to the collection of the sample.

Sampling time started the moment the flow of product was diverted into the sampling vessel. Sampling time was fixed based on the initial volumetric flows set in the pumps and the volume of the collection vessel in order to prevent from over filling. The volumetric flow of gas was measured at the gas sampling point with an Agilent ADM1000 mass flow meter. When small variations in the mass flow readings were registered, the reading was recorded. Then, the flow meter was disconnected from the sampling point and the connection was

switched to the tedlar gas-bag for sample collection. Once the sampling time was completed, the product flow was switched back to the continuous operation vessel. At this time the tedlar gas-bag was closed and placed aside to be further used when the next sample was taken. Moreover, the organic and aqueous products were collected in one of the glass vials from the bottom of the sampling vessel. The sampling vessel was thoroughly rinsed with chloroform, which was then collected in a second glass vial. The whole procedure was repeated for all samples taken.

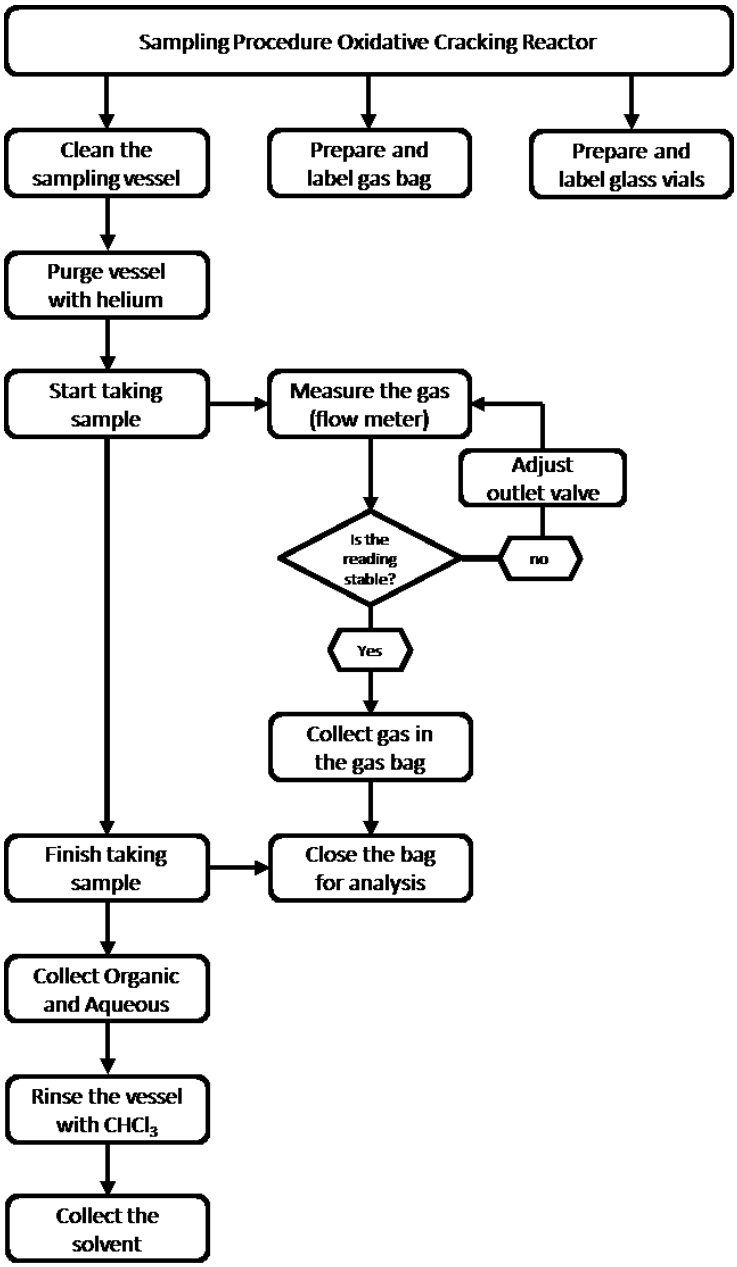


*Figure 4.5 Oxidative cracking reactor sampling procedure.*

Once the samples were taken and the reactor was switched off, the products of reaction were recovered and analyzed following the procedure graphically described in Figure 4.6.

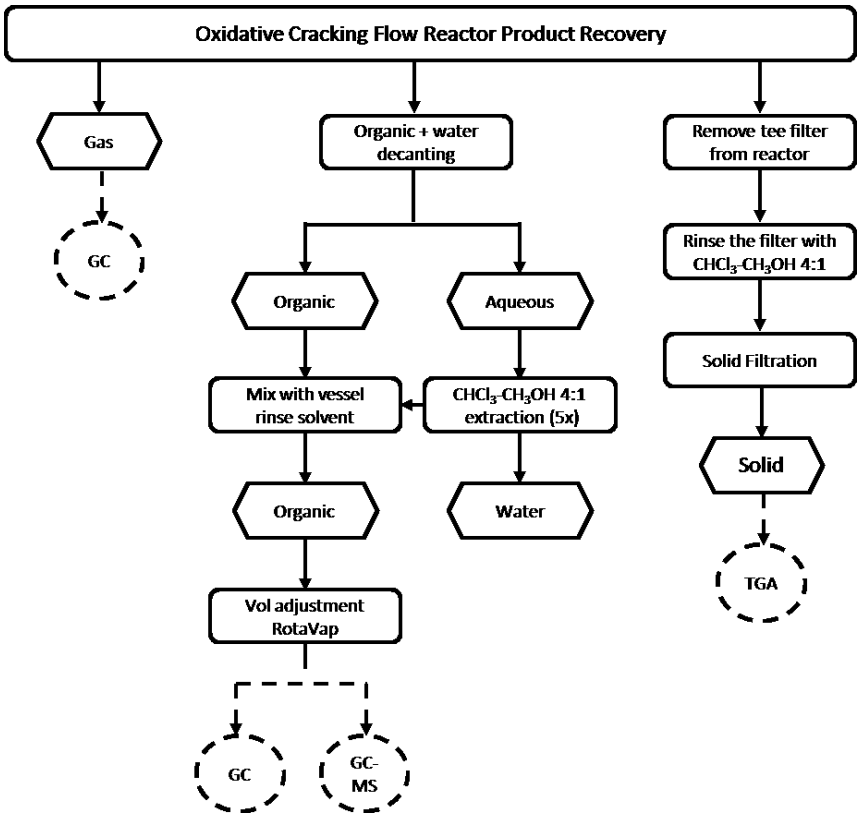


*Figure 4.6 Oxidative cracking reactor product recovery procedure.*

The gas recovered in the tedlar gas-bag was analyzed through GC-TCD to determine its composition.

In addition, the organic and the aqueous fractions recovered were separated through decantation in a separation funnel. Similarly as performed with the aqueous phase recovered in batch experiments, an organic solvent extraction with chloroform was performed using an equal volume of chloroform and water to recover any organic product remaining. This procedure was repeated in five occasions in order to ensure that all the organic products present in the aqueous phase were extracted. The solvent with the extracts was combined with the organic product previously recovered and the solvent obtained from rinsing the sampling vessel to compose a single organic fraction. The volume of the organic fraction was then adjusted in a Buchi rotatory evaporator at 75 °C. The organic phase was then analyzed through GC-FID to quantify the products obtained and GC-MS to identify each individual product.

The tee filter was removed from the reactor and rinsed with $CHCl_3$ / $CH_3OH$ 4:1 v/v solution to recover the solid products of reaction. In addition, the ceramic filter was cleaned in a sonicator bath for 30 min to remove any solid left. The solvent and solid suspension were then filtered in a Sartorius vacuum filtration kit with a Whatman PTFE 1 μm pore size membrane filter. The retained solid was then dried in an oven at 100 °C for three hours. After the solid was dried, its mass was recorded and then it was analyzed using a TGA to determine the amount of coke produced.

### 4.1.3. Product analysis

Product analysis and characterization was mainly performed at Imperial College with the exception of the elemental analysis C, H, N and S and the inductively coupled plasma that were outsourced to Medac Ltd.

#### *4.1.3.1. Gas chromatography*

Gas chromatography was used to analyze the gas and organic soluble products recovered from experiments with both heavy oil model compounds and heavy oil real feedstock. The principle of operation is described in Section 2.5.2.

The gas products recovered were analyzed in a Perkin Elmer Clarus 500 chromatograph equipped with a thermal conductivity detector (GC-TCD). As previously mentioned, gas products from experiments with VR were not analyzed due to the impossibility of the column to withstand the presence of $H_2S$. The GC-TCD was equipped with a Carboxen 1010 plot capillary column (30 m long, ID 0.53 mm and 30 μm thickness). The method and detailed analysis conditions are reported in Table 4.2. A calibration to obtain the response factors of the different gases analyzed was performed using a known composition standard gas mixture supplied by BOC. The composition of the standard as well as the response factors obtained can be consulted in Appendix 11.2.2. A volume of 100 μl of gas sample was analyzed using helium as carrier gas.

The organic fraction recovered from experiments with heavy oil model compounds and the maltene fractions of experiments with VR were analyzed in a Perkin Elmer Clarus 500 equipped with a flame ionization detector (GC-FID). The GC-FID was fitted with a SGE HT5 aluminum clad fused silica capillary column (25 m length, ID 0.32 mm and 0.1 μm film thickness). Samples for analysis were prepared using $CHCl_3$ / $CH_3OH$ 4:1 v/v as solvent and injection volumes were fixed to 1 μl. The carrier gas used for the analysis was helium.

The analysis conditions for products from experiments with heavy oil model compounds are detailed in Table 4.2. In addition, the calibration curves of phenanthrene, naphthalene and the main products of reaction were built using standards from Sigma Aldrich and can be consulted in Appendix 11.2.3.

Maltene products obtained from the fractionation of the liquid fraction from experiments with VR were analyzed through simulated distillation to determine its boiling point distribution through GC-FID. A standard gas oil was used, following the ASTM D2887 standard (182), to relate the retention times (oven temperature) in the chromatograph with the real boiling points of the product as shown in Appendix 11.2.4. In addition, a calibration using different concentrations of gas oil standard was built to relate the area obtained from the GC-FID with the concentration in the product sample. The analysis was done at the conditions reported in Table 4.2 as previously done in literature (183).

*Table 4.2 Gas chromatography analysis conditions.*

| | **Analysis of Gas** | **Analysis organic fraction from model compounds** | **Analysis of Maltenes from VR** |
|---|---|---|---|
| Injector T (°C) | 120 | 300 | 350 |
| Detector T (°C) | 150 | 380 | 370 |
| Split | 1:20 | 1:20 | 1:20 |
| Carrier (ml/min) | 5 | 20 | 10 |
| Oven Initial T (°C) | 30 °C hold for 5.5 min | 50 °C | 35 °C hold for 1 min |
| Ramp 1 | 20 °C/min to 90 °C hold for 2.5 min | 5 °C/min to 100 °C hold for 1 min | 15 °C/min to 350 °C hold for 2 min |
| Ramp 2 | 20 °C/min to 100 °C hold for 3.5 min | 10 °C/min to 320 °C hold for 10 min | 25 °C/min to 380 °C hold for 10 min |

#### *4.1.3.2. Gas chromatography with mass spectrometry*

The organic fraction recovered from experiments with heavy oil model compounds was analyzed through gas chromatography with mass spectrometry (GC-MS) to identify individual products of reaction. The analysis was performed in a Varian Star 3400 - Saturn 2000 GC/MS fitted with a HT5 aluminum clad fused silica capillary column (25 m length, ID 0.32 mm and 0.1 μm film thickness). Analysis conditions are reported in Table 4.3 and helium was used as carrier gas.

The GC-MS is equipped with a Varian 8200 auto sampler capable of delivering automatically 10 μl of sample per injection. Product identification was made by comparison of the spectrum obtained with the ones in the library of spectra of the National Institute of Standards and Technology (NIST) using the software provided by the supplier.

*Table 4.3 Gas chromatography with mass spectrometry analysis conditions.*

| | GC-MS Analysis Conditions |
|---|---|
| Transfer line temperature (°C) | 300 |
| Manifold temperature (°C) | 100 |
| Trap temperature (°C) | 200 |
| Split | 1:20 |
| Carrier (ml/min) | 20 |
| Oven Initial T (°C) | 50 |
| Ramp 1 | 5 °C/min to 100°C hold for 1 min |
| Ramp 2 | 10 °C/min to 320°C hold for 10 min |

#### *4.1.3.3. Thermogravimetric analysis*

The solid products from all reactions with heavy oil model compounds or real feedstock in the presence or absence of a catalyst were analyzed through thermogravimetric analysis (TGA) to determine the amount of coke produced. This was performed in a Perkin Elmer Pyris 1 TGA equipped with a thermal analysis gas unit. Samples of 3 mg +/- 0.5 were loaded into the equipment under $N_2$ atmosphere and left to stabilize until weight variations were negligible. At the start of the analysis, the gas fed was switched to air and the method described in detail in Table 4.4 was followed.

*Table 4.4 Thermogravimetric analysis conditions.*

| | TGA Analysis Program |
|---|---|
| Oven Initial T (°C) | 50 |
| Step 1 | Hold at 50 °C for 15 min in $N_2$ |
| Step 2 | Switch gas to 100% air at 40 ml/min |
| Step 3 | Heat from 50 °C to 900 °C at 10 °C/min |
| Step 4 | Hold at 900 °C for 30 min |

The amount of coke in the sample was determined by difference between the initial weight of the sample and the one after the analysis.

#### *4.1.3.4. Size exclusion chromatography*

Samples of the liquid fraction recovered from experiments with VR as well as the maltene and asphaltene fractions obtained from the fractionation procedure were analyzed through size exclusion chromatography (SEC), described in Section 2.5.1. Prior to the analysis, an aliquot of the recovered sample (liquid product, asphaltene fraction or maltene fraction) was dissolved in a mixture of n-methyl-pyrrolydone (NMP) and chloroform 6:1 v/v solution. The SEC system is equipped with a polystyrene / polydivinylbenzene Mixed-D packed column supplied by Polymer Laboratories UK and a Knauer 2600 UV detector. The column was

heated to 80 °C in a Jones chromatographic oven with the objective of reducing the viscosity of the mixture to enable adequate flow through the column. The solvent mixture is pumped through the column at a flow of 0.5 ml/min with a Knauer HPLC pump.

A calibration curve was built with a series of standards such as PAHs, polystyrene compounds, nitrogen-containing compounds and oxygen-containing compounds, which provide a wide range of molecular weights. The elution time for each standard was registered in order to build two calibration curves as shown in Appendix 11.2.5. The first curve was built with the PAH, nitrogen and oxygenated compounds, which have a lower molecular weight in a range between 80 to 530 g/mol. The second, with standards of polystyrene of different molecular weights in a range between 600 to 52,000 g/mol.

#### *4.1.3.5. Inductively coupled plasma optical emission spectroscopy*

Analysis to determine metals (Ni and V) in the solid, aqueous and organic soluble product fractions from experiments with VR was outsourced to MEDAC ltd. The analysis was performed through inductively coupled plasma with optical emission spectroscopy (ICP-OES), which detects vanadium and nickel at a wavelength of 292.4 nm and 231.6 nm respectively. The operation principle of the technique is detailed in Section 2.5.4.

Samples for analysis were prepared through digestion in a $HNO_3/H_2O_2$ to achieve a homogeneous solution. The concentration of the solution was then adjusted using milli-Q water. A calibration curve prepared from a standard solution of a fixed concentration of 1000 ppm was built. The concentration of each metal was determined by comparison of the values obtained from the sample solution against the calibration curve.

#### *4.1.3.6. Elemental analysis*

Determination of sulfur and nitrogen content in solid, organic soluble and aqueous soluble product fractions obtained in experiments with heavy oil were outsourced to MEDAC Ltd. The analytical technique used was elemental analysis in a Thermo Scientific Flash EA 1112 analyzer. C, H, N and S were determined in a single analysis through a flash dynamic combustion method. This method is based on the instantaneous and complete combustion of the sample into gases. These gases are then transported with helium as carrier through a reduction furnace and through a chromatography column connected to a TCD as described in Section 2.5.3. The signal produced in the TCD is related to the concentration of each component in the original sample.

### 4.1.4. Experimental error estimation

A series of experiments to determine the experimental error and the repeatability of the results was performed for each reaction set-up. An individual error analysis in the microbomb was done for operation with phenanthrene and VR. A fixed experimental condition was repeated four times in experiments done in the microbomb and three times in the ones completed in the oxidative cracking reactor. From these experiments the mean value, standard deviation and standard error were calculated in order to determine the experimental error percent. The following equations where $X_i$ stands for a single measurement, M for the mean value, S for the standard deviation, SE for the standard error, N for the number of experiments and E for the error percent were used.

Mean Value (M), $\boldsymbol{M = \frac{\sum X_i}{N}}$ Standard Deviation (SD), $\boldsymbol{SD = \sqrt{\frac{\sum (X_i - M)^2}{N-1}}}$

Standard Error (SE), $\boldsymbol{SE = \pm \frac{SD}{\sqrt{N}}}$ Error Percent (E), $\boldsymbol{E = \pm \frac{SE}{M} * 100}$

The error percent values for the operation in the microbomb and the oxidative cracking reactors are reported in Table 4.5. Details on the error calculation can be consulted in Appendix 11.2.6.

*Table 4.5 Experimental error for operations with the microbomb reactor (model compounds and heavy oil) and the oxidative cracking reactor (model compounds).*

| Microbomb (Model Compounds) | Error (%) | Microbomb (Heavy Oil) | Error (%) | OCR (Model Compounds) | Error (%) |
|---|---|---|---|---|---|
| Phenanthrene recovery | 1.98 | Liquid organic products yield | 2.14 | Met Naphthalene recovery | 4.27 |
| Liquid organic products yield | 2.04 | Coke yield | 3.16 | Liquid organic products yield | 4.23 |
| Coke yield | 1.92 | Gas yield | 3.71 | Coke yield | 3.18 |
| Gas yield | 3.49 | Maltene yield | 2.12 | Gas yield | 3.05 |
| | | Asphaltene yield | 2.89 | | |
| | | Sulfur removal | 3.89 | | |
| | | Nitrogen removal | 4.24 | | |
| | | Vanadium removal | 2.08 | | |

## 4.2. CATALYST SYNTHESIS AND CHARACTERIZATION

In this work, the use of an added catalyst in the oxidative cracking of heavy oil in SCW was considered. The aim was to promote further cracking of high molecular weight polyaromatic structures to reduce its molecular weight and facilitate the removal of metals and heteroatoms from its structure. It has been reported that heavy oil is effectively converted into lighter fractions through catalytic processes using zeolites as catalyst (184). Y-type zeolite “faujasite” is widely used in oil conversion processes due to its wider pore cavity, which aids in the conversion of oil reducing mass transfer limitations and hence increasing the yields to lighter oil fractions (185,186). Moreover, it was also reported that Mn ion exchanged zeolites are highly efficient catalysts for oxidation reactions of aromatic benzene rings (187), which are the building blocks of heavy oil molecules like asphaltenes. Based on the previous information, an ion exchanged Mn-Y-zeolyte was synthetized to be tested as catalyst in the oxidative cracking of Maya oil VR in SCW.

### 4.2.1. Catalyst synthesis

The experimental procedure for the synthesis of the Mn-Y-zeolite catalyst was adapted from literature and is graphically explained in Figure 4.7 (187–191). Sigma Aldrich Manganese (II) acetate tetrahydrate 99.99 %w/w, Sigma Aldrich Molecular Sieves (ammonium Y zeolite) and DI water were used as reactants for the synthesis of the catalyst.

Two batches of catalyst were synthetized resulting in approximately 5 g of catalyst per batch. First, 250 ml of Mn (II) acetate solution 0.25 M were prepared. The solution was placed in a 500 mL round flask and 5 g of $NH_4$-Y-zeolite were added. The flask with the zeolite and the solution was placed in an IKA reaction block system that provides stirring to the mixture and maintain a constant temperature. The zeolite was ion exchanged at 80 °C for 4 h at constant stirring.

After reaction time was completed, the product was filtered in a Sartorius vacuum filtration kit using 1 μm pore size Whatman PTFE membrane filters. The filtration cake was left to dry overnight in an oven at 70 °C. Finally, the solid recovered was calcined in an air atmosphere for 4 h at 500 °C in a Thermolyne furnace supplied by Thermo Scientific.

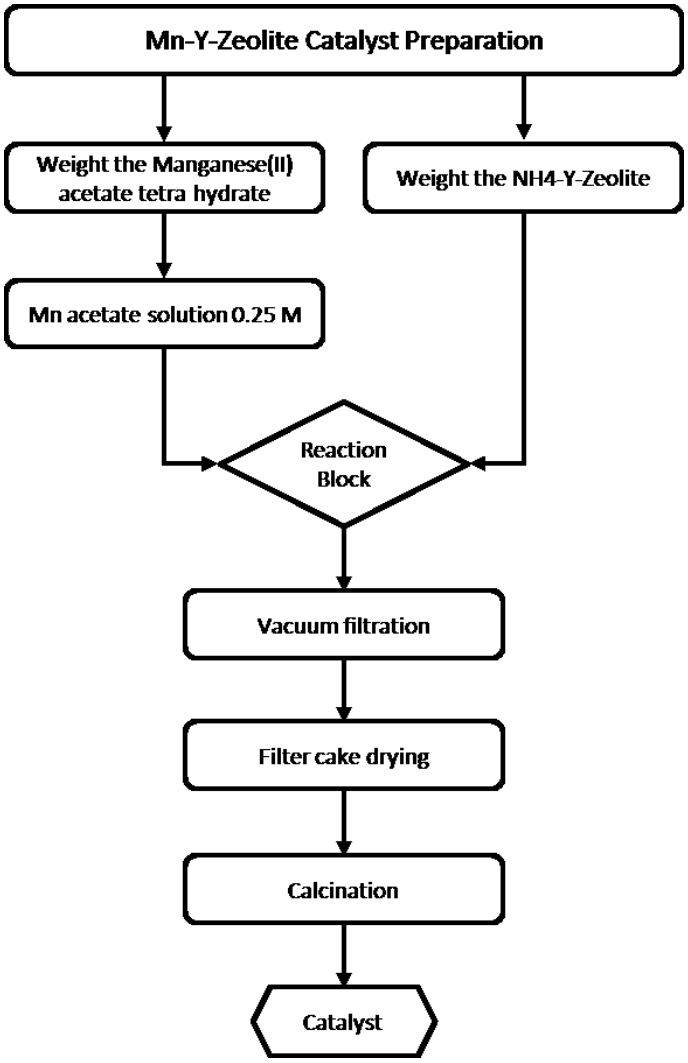


*Figure 4.7 Mn-Y-zeolite catalyst synthesis procedure.*

### 4.2.2. Catalyst characterization

#### *4.2.2.1. Nitrogen adsorption*

Textural properties such as surface area and porosity of the Mn-Y-zeolite catalyst were analyzed through $N_2$ adsorption in a Micromeritics Tristar analyzer. A sample of approximately 200 mg +/- 20 mg of catalyst was degased at 120 °C under $N_2$ atmosphere in a Micrometrics Flow Prep 060 degaser. The degased sample was then placed in the equipment where it was analyzed through a $N_2$ adsorption standard test method at -196 °C. Results were obtained using the Brunauer, Emmett and Teller (BET) method to determine surface area for adsorption incorporating multilayer coverage and the Barrett, Joyner, and Halenda (BHJ) method to calculate the pore size distribution in the catalyst from the experimental isotherms.

#### 4.2.2.2. X-ray diffraction

X-ray diffraction (XRD) patterns of the catalysts were obtained using a Bruker AXS D8 advance diffractometer with a θ–θ configuration using Cu Kα radiation at a λ = 0.15406 nm. Scans were performed for 2θ values from 3° to 80°. Counts were accumulated every 0.05º at a step time of 3 s. The crystal size of the zeolite catalyst was calculated using Scherrer's equation. XRD analysis of the catalyst was performed in the Institute of Carbochemistry CSIC in Zaragoza (Spain).

#### 4.2.2.3. Scanning electron microscopy – X-ray spectroscopy

The morphology and metal dispersion of the catalyst were studied in a JEOL JSM 6400 scanning electron microscope (SEM) equipped with an Oxford Instruments energy dispersive X-ray spectroscopy system (EDX). Catalyst samples were placed in a SEM slab for imaging. A gold coating was applied to improve the quality of the image. A qualitative elemental analysis of a fraction of the sample was performed through EDX at 1.5k magnification.

#### 4.2.2.4. Elemental analysis inductively coupled plasma

Metal loading in the catalyst was determined through inductively coupled plasma optical emission spectroscopy (ICP-OES) in the Institute of Carbochemistry CSIC in Zaragoza (Spain). The determination was made in a Jobin Ybon 2000 ICP-OES, which detected manganese, silica and aluminum at wavelengths of 257.6 nm, 251.6 nm and 396.2 nm respectively.

Samples were prepared through digestion in $H_2O_2$/$HNO_3$/HCl solution. The concentration of the solution was adjusted with milli-Q water. The concentrations of metal in the sample were compared to standards of known concentration to determine the total amount found in the catalyst

# Chapter 5
# Phenanthrene Oxidative Cracking in Near-critical and Supercritical Water

The work presented in this chapter focuses in the study of the hydrothermal oxidative cracking of heavy oil in near-critical and supercritical conditions in the microbomb reactor. For this purpose phenanthrene was used as model compound to represent model chemical structures found in asphaltenes. The aim of this work is twofold 1) the evaluation of the effect of process conditions such as pressure, initial oxygen loading ($O/O_{stoich}$ ratio), temperature and reaction time on phenanthrene conversion and product distribution, 2) the study of the evolution of intermediate products to propose a potential reaction pathway. Section 5.3.1 presents a detailed screening of process conditions, varying an individual condition while the rest were kept constant, to assess their effect on conversion, yield and product selectivity. In Section 5.3.2, optimum conditions found for which the yield and selectivity to organic soluble products were maximized. These conditions were used to study the reaction system at different reaction times and temperatures. The evolution of the main products of reaction was studied and a potential reaction pathway was proposed.

## 5.1. INTRODUCTION

Commercial upgrading of highly asphaltenic oil feedstocks is achieved through conventional hydrogen addition processes such as hydrotreating and hydrocracking (14,183). The main operation disadvantages found in these processes are the high temperatures and high hydrogen pressures required. Moreover, hydrogenation reactions of polyaromatic structures found in asphaltenes are known to start at aromatic rings located in the periphery of the molecule and then proceed further towards rings located at central positions. This results in low atom efficiencies and requires high amounts of hydrogen during the upgrading process. In contrast, it was reported that hydrothermal partial oxidation of PAHs preferentially proceeds starting at central ring positions and readily occur at lower temperatures around 300 °C (192). The oxygen incorporated into the aromatic structure weakens its aromaticity, destabilizing the molecule and making it more reactive. As a result, weaker reactive sites located in central positions of the molecular structure are formed, which are prone to cracking and ring opening reactions.

Moreover, it has been observed that hydrothermal reactions are effective for the decomposition of PAHs and can be applied in processes like water treatment, soil remediation and waste destruction (193–195). Complete conversion of PAHs such as phenanthrene, naphthalene, fluorene, pyrene and biphenyl, has been reported in different SCWO studies available in literature (108,196). In addition, hydrothermal oxidation processes are regarded as environmentally friendly as they do not require the use of any chemicals apart from water and oxygen as reactants (195,197). Widespread interest has been developed in the study and application of the complete oxidation of organic substrates in NCW and SCW in laboratory and commercial scale. However, the oxidative cracking process studied in this work focuses on the assessment of the hydrothermal partial oxidation process to produce valuable intermediate products from the oxidation of polycyclic aromatic compounds.

Two main objectives were pursued. First, to evaluate the effect that process conditions (pressure, $O/O_{stoich}$ ratio, temperature and reaction time) have on phenanthrene conversion, yields and selectivity to product fractions as well as in the O/C molar ratio in the organic soluble fraction. Second objective was to study the evolution of reaction products in order to propose a potential reaction pathway in the process.

## 5.2. EXPERIMENTAL

Oxidative cracking experiments were performed in a SS microbomb reactor extensively described in Section 3.2.1 and Section 4.1.1. Briefly, the reactor was loaded with 1.2 mL of VWR $H_2O_2$ 30% w/v and varying amounts of Sigma-Aldrich phenanthrene 98% according to the $O/O_{stoich}$ ratio required. Then, different volumes of DI water were added to achieve the desired operating pressure according to a calibration curve presented in Appendix 11.1.5. Reaction products were recovered and analyzed following the procedures and specifications detailed in Section 4.1.1.3. and Section 4.1.3.

## 5.3. RESULTS AND DISCUSSION

### 5.3.1. Effect of reaction conditions

In this section, a detailed discussion of the results obtained from experiments conducted to study the effect that changes in operating conditions have on the oxidative cracking reaction is presented. Experimental conditions for this study are reported in Table 5.1. Results were analyzed and reported as phenanthrene conversion, yield and selectivity to different product

fractions and O/C molar ratio in the organic soluble fraction. Total gas production was calculated by mass balance difference.

*Table 5.1 Experimental conditions to study the effect of process variables in the oxidative cracking of phenanthrene in NCW and SCW.*

| Parameter Studied | Pressure (bar) | $O/O_{stoich}$ ratio | Temperature (°C) | Time (min) |
|---|---|---|---|---|
| Pressure | 210 - 275 | 0.40 | 450 | 60 |
| $O/O_{stoich}$ ratio | 230 | 0.1 - 0.75 | 450 | 60 |
| Temperature | 230 | 0.2 | 360 - 450 | 60 |

Phenanthrene conversion was calculated with Equation 5.1, where $Cmol^0_{ph}$ stands for the carbon moles in the initial phenanthrene and $Cmol^f_{ph}$ as carbon moles in the phenanthrene recovered post reaction.

$$Conversion_{ph} = \frac{Cmol^0_{ph} - Cmol^f_{ph}}{Cmol^0_{ph}} \quad (5.1)$$

The yields obtained for the different product fractions and individual products were calculated with Equation 5.2 where $Cmol_i$ stands for the carbon moles present in each product fraction or individual product.

$$Yield_{prod} = \frac{Cmol_i}{Cmol^0_{ph}} \quad (5.2)$$

Equation 5.3 was used for the determination of selectivity towards a product fraction.

$$Selectivity_{prod} = \frac{Cmol_i}{Cmol^0_{ph} - Cmol^f_{ph}} \quad (5.3)$$

Experimental results showed that most of the organic soluble products obtained were oxygenated aromatic compounds such as quinones and furans with minor production of other PAHs. The GC-MS identification of reaction products is shown in Figure 5.1. Products

of similar nature have been reported in literature for the hydrothermal oxidation of PAHs in near-critical and supercritical conditions (105,173,196,198).

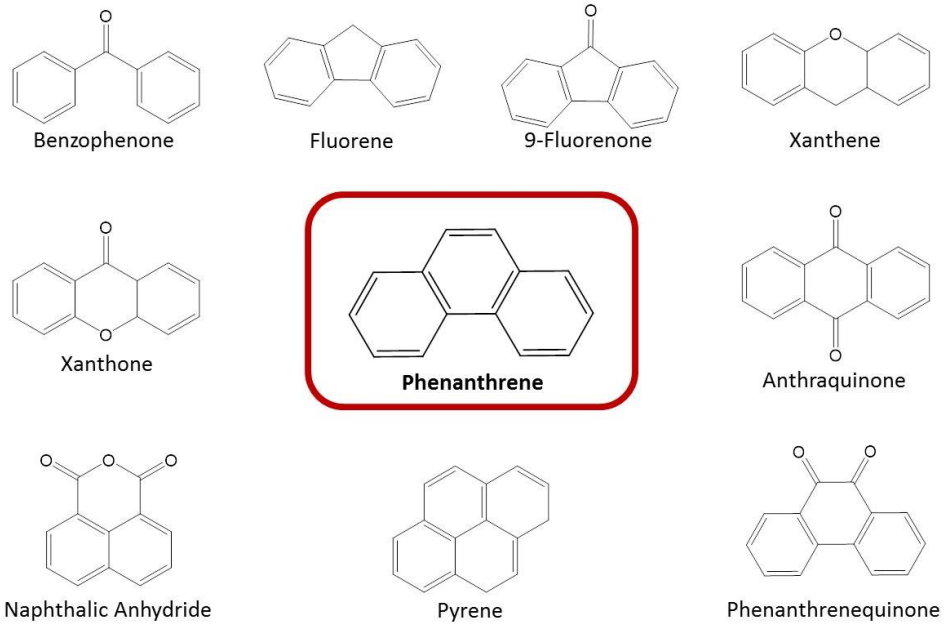


*Figure 5.1 Organic soluble products from the oxidative cracking of phenanthrene in NCW and SCW identified through GC-MS.*

### *5.3.1.1. Effect of pressure*

Experiments to assess the effect of pressure were performed at the reaction conditions shown in Table 5.1. Pressures considered for this work (210, 230, 250 and 275 bar) enabled the development of experiments below and above the critical pressure of water as schematically explained in Figure 5.2. A temperature of 450 °C above the critical temperature as well as a fixed reaction time of 60 min and an $O/O_{stoich}$ ratio of 0.4 were selected for the study.

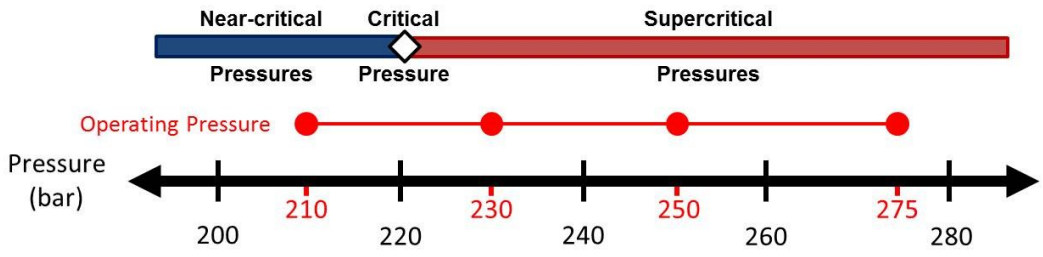


*Figure 5.2 Operating pressures studied within the near-critical – supercritical pressure conditions.*

It was observed that changes in the system's pressure had a minor impact in phenanthrene conversion regardless of whether the reaction was carried out at near-critical or supercritical water conditions. A small increase in conversion was observed when pressure increased from 210 to 230 bar surpassing the critical pressure of water. Once at supercritical conditions increments in pressure had no effect in conversion as shown in Figure 5.3.

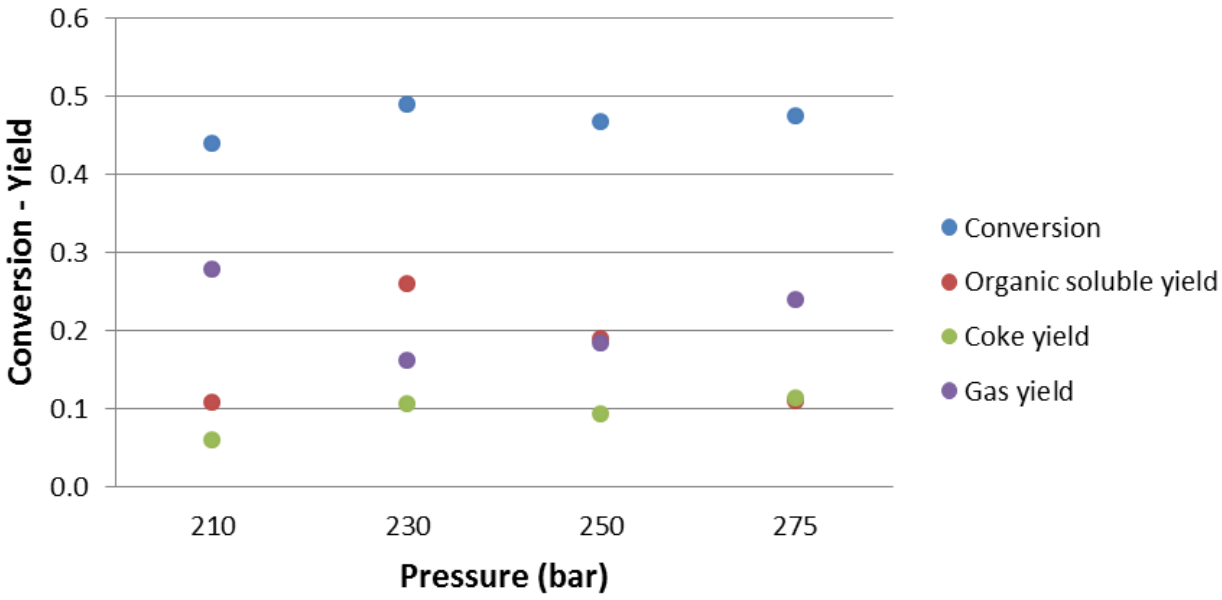


*Figure 5.3 Effect of pressure on phenanthrene conversion and product yields at 450 °C, 0.4 $O/O_{stoich}$ ratio and 60 min reaction time.*

Similar trends with changes in pressure have been reported in SCWO studies with model compounds such as acetic acid and 2,4 dichlorophenol (199). Although pressure changes had a marginal effect in phenanthrene conversion, it was observed that it had an important impact in the yields to products and the selectivities obtained. An increase in operating pressure from 210 to 230 bar, slightly above the critical pressure, resulted in higher yields to organic soluble fractions. From that point, it was observed that further increments in pressure had a negative effect mainly to produce gas, decreasing the yields to organic soluble products.

High yields to gas were obtained at 210 bar, which then decreased with an increase in operating pressure to find a minimum gas yield at 230 bar. Further increments in pressure resulted in higher yields to gas as seen in Figure 5.3. These observations are in good agreement with the trends observed in the yields to organic soluble products and show that the selectivity towards organic soluble or gas products can be controlled with small changes

in the system's pressure. Interestingly, a maximum in the yield to organic soluble products and a corresponding minimum in the yields to gas were obtained at 230 bar, which is in close proximity to the critical pressure of water.

Marginal changes in the yield to coke were registered with changes in pressure. A slight increase was observed when pressure increased from 210 to 230 bar where the critical pressure was surpassed. Similar trends have been reported in literature regarding the effect of process conditions in the SCWO of quinoline (136).

It was mentioned that one of the aims of this work is the identification of optimum reaction conditions at which yields and selectivities to organic soluble products are higher. Pressure has a great impact on selectivity to organic soluble products as shown in Figure 5.4. Higher selectivity to organic soluble products was obtained at 230 bar, which suggests that operating at pressures slightly above the critical prevents over cracking of intermediates favoring the production of organic soluble products over gas products.

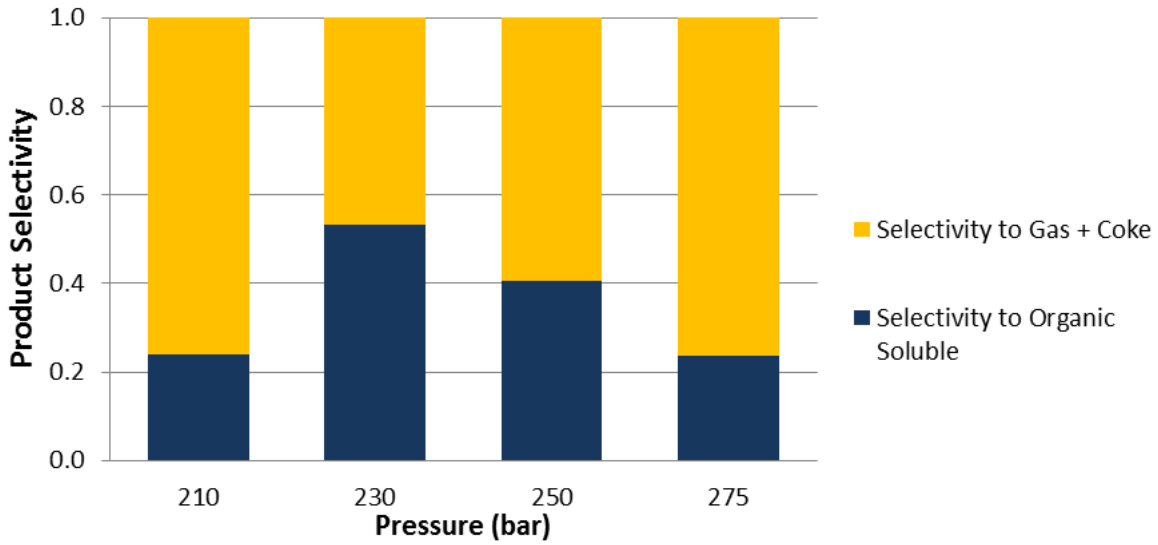


*Figure 5.4 Effect of pressure on the selectivity to organic soluble products at 450 °C, 0.4 $O/O_{stoich}$ ratio and 60 min reaction time.*

The trends observed can be explained based on the role of water as reaction medium and the big changes in its properties with small changes in pressure especially near or above the critical pressure. When pressure surpasses the critical point, the reaction medium turns into a pseudo-homogeneous phase that presents low mass transfer limitations, resulting in high rates of reaction. This may lead to increased conversions and to promote higher yields to organic soluble products derived from oxidation and cracking reactions. Moreover, it is

believed that products of reaction are well dispersed and effectively diffused throughout the reaction medium due to the high miscibility and favorable transport properties found in water at supercritical conditions. As a result, low yields to coke were obtained, as the reaction medium aids in the prevention of condensation and polymerization reactions (93).

Further increments in reaction pressure can result in some additional effects that had an important impact in the selectivity to different product fractions. Higher pressures resulted in higher rates of reaction due to an increase in the collision frequency of small free radicals present in the system (93). This is highly relevant as the oxidation reaction rates with small free radicals can be accelerated leading to a potential increase in gas yields. The opposite effect occurs in reactions with organic radicals of greater size, which are slowed down as a result of the cage effect created by water molecules surrounding the active complex. Basically, the collision frequency between organic radicals and water molecules has a much higher frequency than the one between two organic molecules, which prevents the occurrence of bi-molecular reactions between heavy organic radicals (93,200). An increase in pressure increases the frequency of collisions between organic radicals and water molecules, which results in the radical de-activation. As a result, the organic radical is stabilized preventing it from continued recombination reactions, as suggested in literature (94). This gives an understanding of the reason why changes in the system pressure have negligible effects on the yields observed to coke. However, small oxidation radicals such as •OH and $•HO_2$ can diffuse through the barrier of water molecules surrounding the organic radicals and react with them to form smaller molecules leading to the formation of gas. An important dependence was observed between the product distribution in the organic soluble fraction and reaction pressure as shown in Figure 5.5.

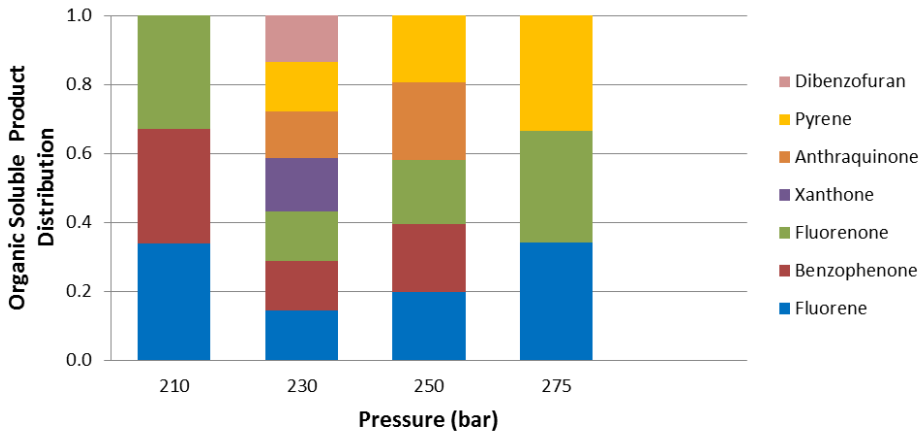


*Figure 5.5 Effect of pressure on the organic soluble product distributon at 450 °C, 0.4 $O/O_{stoich}$ ratio and 60 min reaction time.*

The largest product distribution occurred at 230 bar, slightly over the critical pressure. An increase or decrease in pressure resulted in a reduction in the number of species recovered as part of the organic soluble fraction. It is thought that this trend is also related to the properties of SCW as previously discussed.

As it has been mentioned, one of the aims of the oxidative cracking reaction is to incorporate oxygen into the intermediate product fraction as part of the activation process. This is of great relevance as the presence of oxygen weakens the polyaromatic structure, which facilitates its cracking. It was found that the O/C molar ratio of the organic soluble product fraction was maximized at 230 bar when the process was in the vicinity of the critical pressure of water. Any further increase in the system's pressure resulted in a decrease in the O/C molar ratio as shown in Figure 5.6. This shows that the performance of the process and the nature of the products are directly linked to the reaction pressure. Moreover, it was observed that the O/C molar ratio in the organic soluble product fraction is strongly related with the yields to gas produced. High yields to gas were obtained at conditions where low O/C molar ratio in the organic soluble fraction was registered. This is thought to happen due to an increase in carbon and oxygen rejection processes that result in higher concentrations of CO and $CO_2$ in the gas fraction.

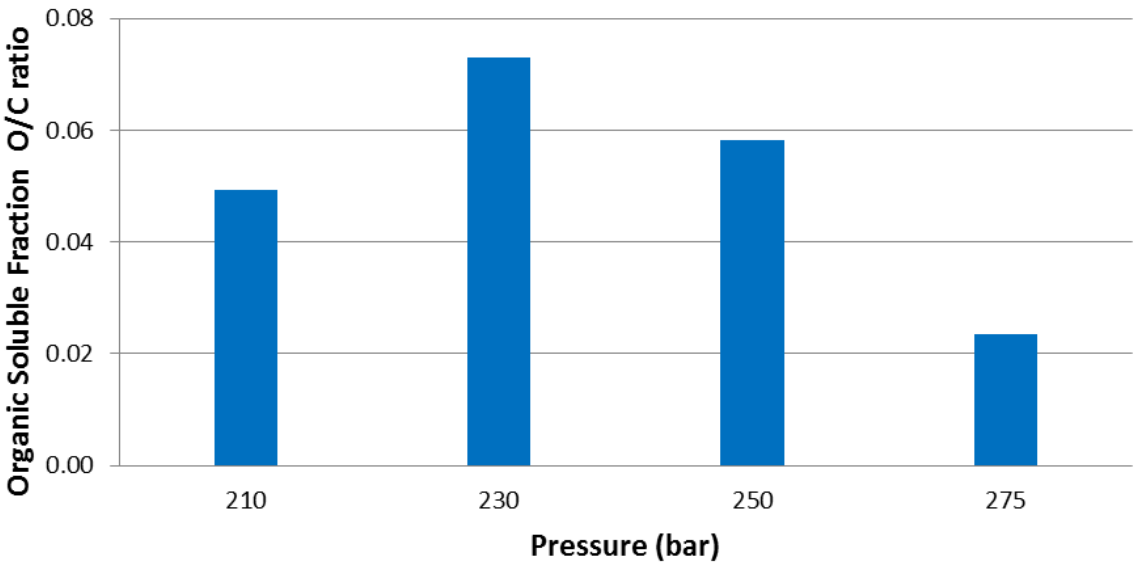


*Figure 5.6 Effect of pressure on the organic soluble product molar O/C ratio at 450 °C, 0.4 $O/O_{stoich}$ ratio and 60 min reaction time.*

Analysis of the gas fraction showed that pressure variations in the system had an important impact in the gas composition obtained. The gas product fraction was mainly composed of $H_2$ and $CO_2$ as shown in Figure 5.7. It was observed that an increment in pressure resulted in a considerable decrease in $H_2$ concentration. The opposite effect was observed with CO, which increased rapidly with pressure until it reached 250 bar and then levelled off with any further pressure increments. $CO_2$ concentration slightly decreased when the system changed from near-critical to supercritical conditions, where a minimum was found at 230 bar. Further increments in pressure within the supercritical range resulted in an important increase in $CO_2$ concentration. Concentrations of $CH_4$ below 10% v/v were registered at all pressures studied and a maximum was found at a pressure of 250 bar.

Experimental evidence regarding the composition of the gas fraction suggests that an increase in pressure negatively impacts gasification and pyrolysis reactions while it enhances oxidation reactions. These results are in good agreement with what has been reported in literature (93). It is highly desirable to obtain a gas fraction mainly composed of $H_2$ and $CH_4$, by-products that have a high commercial value. Therefore, based on experimental results, 230 bar appears to be an optimum reaction pressure based on gas composition, as a $H_2$ rich gas (around 50% v/v) with lower $CO_2$ concentration was obtained. The gas product can be further treated or used in-situ in the hydrogenation and deoxygenation of hydrocarbons, increasing the overall performance of the process.

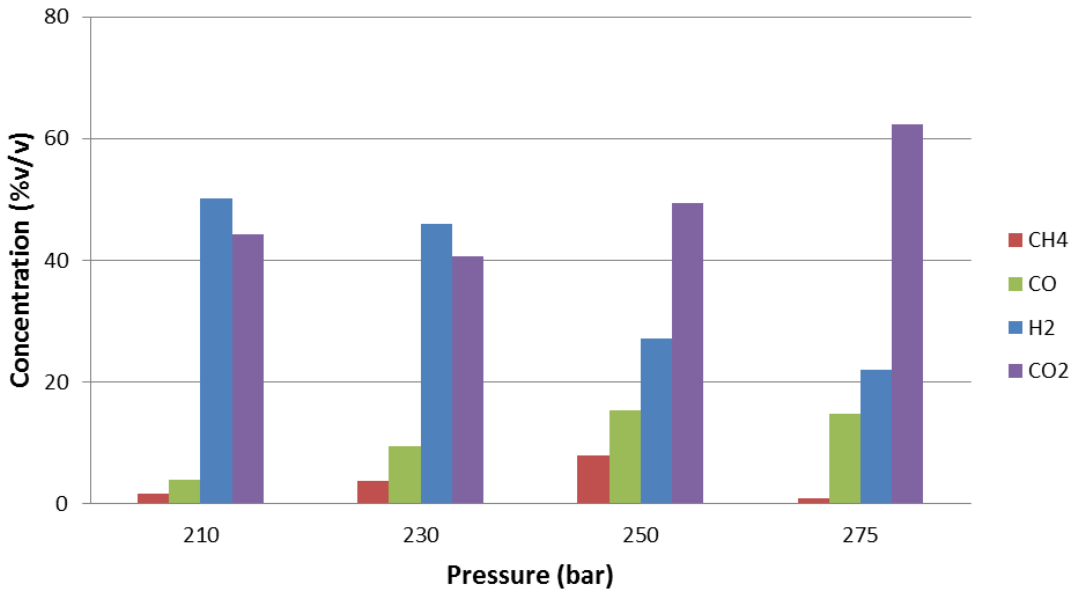


*Figure 5.7 Effect of pressure on the gas product composition at 450 °C, 0.4 $O/O_{stoich}$ ratio and 60 min reaction time.*

### 5.3.1.2. Effect of $O/O_{stoich}$ ratio

Experiments to assess the effect of $O/O_{stoich}$ ratio were performed at a constant pressure of 230 bar, temperature of 450 °C and 60 min reaction time. The rationale behind the selection of the system's pressure was based on the higher yields and selectivity to organic soluble products obtained in experiments discussed in the previous section. Changes in the $O/O_{stoich}$ ratio of the system were achieved with variations in the amount of phenanthrene loaded into the reactor while keeping a constant volume of 1.2 mL of $H_2O_2$ solution fed. $O/O_{stoich}$ ratios of 0.1, 0.2, 0.4 and 0.75 were considered.

Experimental results in Figure 5.8 show that variations in the $O/O_{stoich}$ ratio have an important influence in phenanthrene conversion as well as in the yields to different product fractions as seen in Figure 5.8.

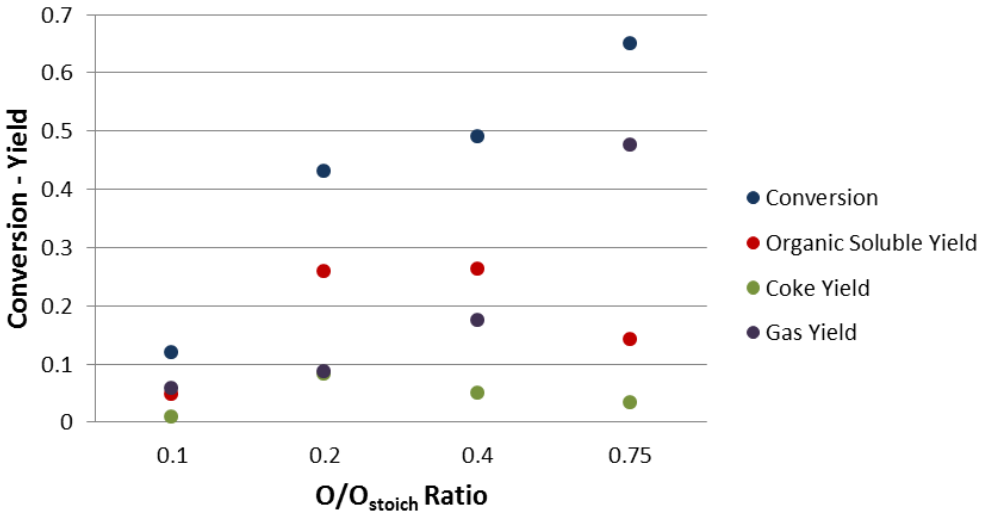


*Figure 5.8 Effect of $O/O_{stoich}$ ratio on phenanthrene conversion and product yields at 450 °C, 230 bar and 60 min reaction time.*

Phenanthrene conversion increased greatly when $O/O_{stoich}$ ratio increased from 0.1 to 0.2. Further increments in the initial oxygen loading resulted in a less pronounced increase in conversion. It was observed that changes in the $O/O_{stoich}$ ratio had an important impact in the yield to different product fractions. An important increase in the yield to organic soluble products took place when the $O/O_{stoich}$ ratio increased from 0.1 to 0.2. Interestingly, the yield to organic soluble products levelled off with a further increase in the $O/O_{stoich}$ ratio to 0.4, to then decrease with any further increments in the $O/O_{stoich}$ ratio as shown in Figure 5.8. The

results suggest that a maximum yield to organic soluble products was reached at an $O/O_{stoich}$ ratio between 0.2 and 0.4.

Yields to coke followed a similar trend where a maximum was obtained at an $O/O_{stoich}$ ratio of 0.2. Experiments at higher $O/O_{stoich}$ ratios resulted in an important decrease in the yields to coke. In addition, it was observed that any increase in the initial oxygen loading resulted in higher yields to gas. The decrease observed in the yields to organic soluble products and coke at high initial oxygen loadings is strongly related with an important increase observed in the yields to gas. This is thought to be due to the high concentrations of oxygen in the system that approaches the stoichiometric oxygen needed for the complete combustion of phenanthrene into $CO_2$ and $H_2O$. Therefore, it is highly relevant to determine the selectivity towards different product fractions in order to determine an optimum $O/O_{stoich}$ ratio for the process.

A higher selectivity to organic soluble products was obtained with an $O/O_{stoich}$ ratio of 0.2, as shown in Figure 5.9. This is mainly due to the difference between the yields to gas obtained at $O/O_{stoich}$ ratios of 0.2 and 0.4, which was higher in the latter case. Nevertheless, the analysis of selectivity is not entirely conclusive to select an optimum $O/O_{stoich}$ ratio as the composition of the gas fraction may be rich in valuable gases such as $H_2$ and $CH_4$ as will be further addressed.

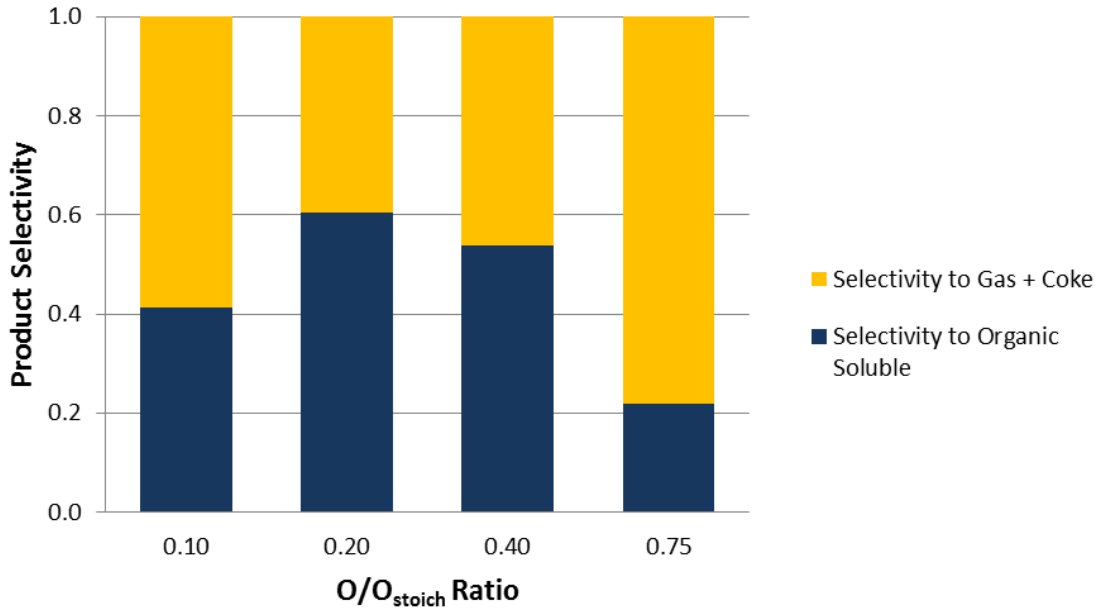


*Figure 5.9 Effect of $O/O_{stoich}$ ratio on the selectivity to organic soluble products at 450 °C, 230 bar and 60 min reaction time.*

As in the study on the effect of pressure, the organic soluble fraction was analyzed to determine its product distribution and is illustrated in Figure 5.10 . It was observed that with an $O/O_{stoich}$ ratio of 0.2 a broader product distribution was obtained. In addition, higher $O/O_{stoich}$ ratios showed to narrow the product distribution, making the organic soluble product more selective to lighter oxygenated products such as benzophenone and fluorenone. These products are likely to continue to react into gas, which is in good agreement with the increase in gas yields observed.

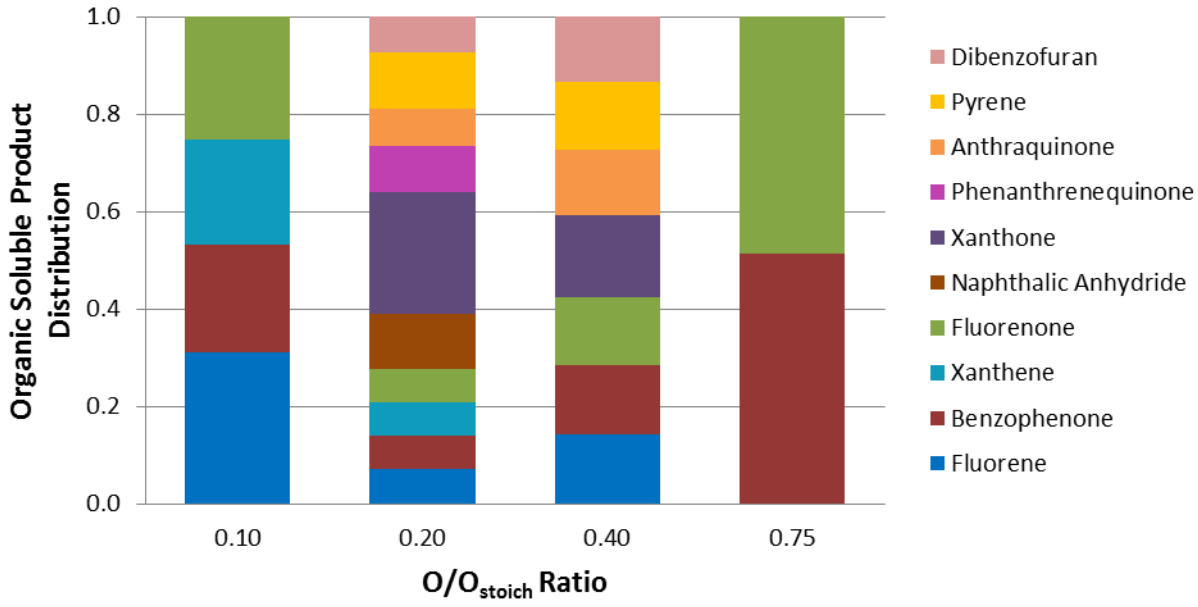


*Figure 5.10 Effect of $O/O_{stoich}$ ratio on the organic soluble product distributon at 450 °C, 230 bar and 60 min reaction time.*

From these results it can be implied that when high oxygen concentrations are present, oxidation reactions predominate over any other reactions occurring. However, when reaction takes place at low $O/O_{stoich}$ ratios, it is thought that oxidation reactions are dominant at early reaction stages until the amount of oxygen is entirely consumed. Once the oxygen in the system has depleted, the reactivity of the medium decreases, and only reactions between the organic intermediates and either water or hydrogen (formed in-situ) continue to take place. This could explain the high concentration of fluorene and benzophenone obtained at an $O/O_{stoich}$ ratio of 0.1 as seen in Figure 5.10.

An interesting trend was observed for the O/C molar ratio in the organic soluble product, which was found to be dependent of the $O/O_{stoich}$ ratio in the system, as shown in Figure 5.11. An increase in the $O/O_{stoich}$ ratio from 0.1 to 0.2 had an important increase in the O/C

molar ratio where a maximum was found. Further increments in the $O/O_{stoich}$ ratio resulted in a decrease in O/C molar ratio in the organic soluble fraction. It is thought that this is mainly due to the higher yields to gas obtained at high initial oxygen loadings as previously shown in Figure 5.8.

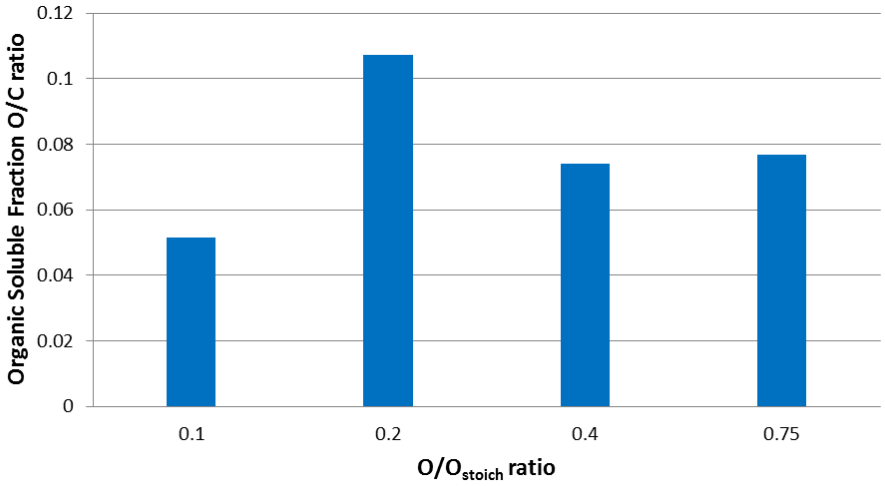


*Figure 5.11 Effect of $O/O_{stoich}$ ratio on the organic soluble product molar O/C ratio at 450 °C, 230 bar and 60 min reaction time.*

Great dependence was observed between the composition of the gas product and the $O/O_{stoich}$ ratio as seen in Figure 5.12.

An increase in the $O/O_{stoich}$ ratio resulted in an important decrease in the concentration of $H_2$ in the gas fraction. However, the opposite effect was observed with $CO_2$, whose concentration increased greatly with $O/O_{stoich}$ ratio. Similarly to $H_2$, the concentration of $CH_4$ decreased with increments in the $O/O_{stoich}$ ratio. A different trend was observed with CO that initially increased with an increase in the $O/O_{stoich}$ ratio to find a maximum at 0.4. However, a further increment in the $O/O_{stoich}$ ratio to 0.75 resulted in an important decrease in CO concentration to negligible values as shown in Figure 5.12.

It is believed this was mainly the result of the high initial oxygen loading, which approaches condition of complete combustion as was mentioned previously. Two competing reactions were identified from the analysis of the gas fraction, namely oxidation and gasification-reforming. At lower initial oxygen loadings it was concluded from the higher $H_2$ concentrations that the second reaction becomes more relevant. At high oxygen loadings, it was concluded that mainly oxidation reactions take place, as seen from the higher $CO_2$

concentration obtained. Similar trends in gas composition have been reported in literature (201).

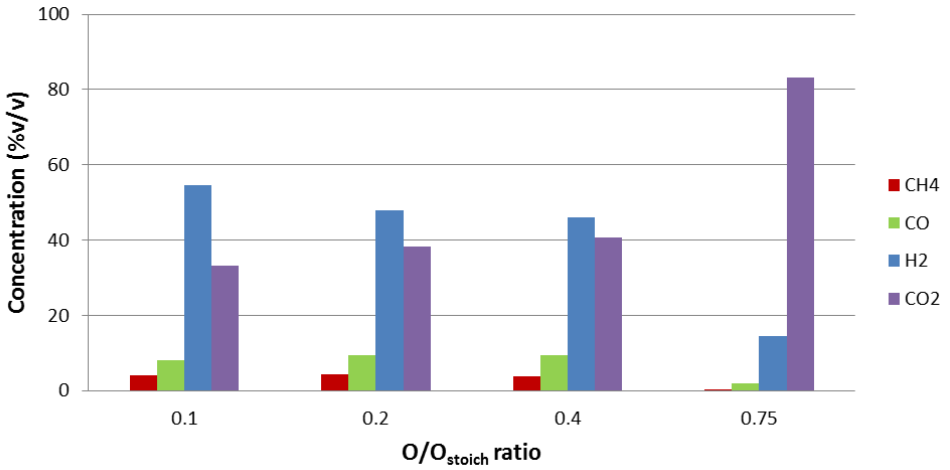


*Figure 5.12 Effect of $O/O_{stoich}$ ratio on the gas product composition at 450 °C, 230 bar and 60 min reaction time.*

In conclusion, based on the higher selectivity to organic soluble products obtained and the higher O/C molar ratio, it was decided that an optimum $O/O_{stoich}$ ratio was found at 0.2, which was used in further studies.

### *5.3.1.3. Effect of temperature*

Experiments to determine the effect of temperature in the process were performed at a fixed pressure of 230 bar and an $O/O_{stoich}$ of 0.2 and 60 min reaction time based on results obtained in previous sections. Process temperatures of 360, 380, 400, 425 and 450 °C were selected to assess the process at both near-critical and supercritical conditions as graphically represented in Figure 5.13.

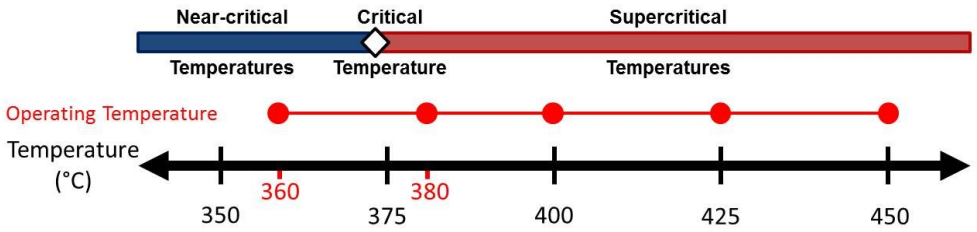


*Figure 5.13 Operating temperatures studied within the near-critical – supercritical temperature conditions.*

It was observed that an increase in temperature resulted in higher phenanthrene conversions. Yields to different product fractions showed to increase with temperature. A greater effect with increments in temperature was observed for the yields to organic soluble products than for the rest as shown in Figure 5.14.

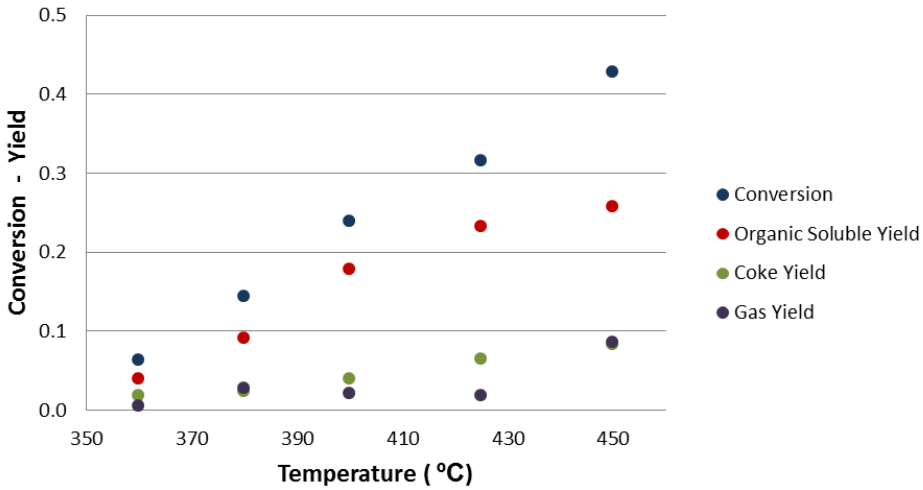


*Figure 5.14 Effect of temperature on phenanthrene conversion and product yields at 230 bar, 0.2 $O/O_{stoich}$ ratio and 60 min reaction time.*

Figure 5.14 shows that increments in temperature between 360 °C and 400 °C resulted in an almost linear increase in the yield to organic soluble products, keeping yields to coke and gas lower than 4%. However, at temperatures above 400 °C, yields to organic soluble products started to gradually level off while the yields to gas started to increase gradually. It was observed that yields to coke linearly increased with temperature and remained below 10% at all temperatures studied. However, gas production showed to be unaffected by temperature increments until temperature reached 450 °C, where it increased considerably to values close to 10%.

Selectivity to organic soluble products showed little changes with temperature compared to the ones observed in the previous sections analyzing pressure and $O/O_{stoich}$ ratio changes. High selectivities over 60% were achieved at all reaction temperatures studied as shown in Figure 5.15. Higher selectivities to organic soluble products with values around 70% were obtained at temperatures between 400 and 425 °C. When temperature was further increased to 450 °C, a reduction in the selectivity to organic soluble products was registered. It is thought that this is mainly due to the increase observed in the yield to gas, as has been previously discussed.

Experiments at temperatures below 400 °C resulted in lower selectivities to organic soluble products mainly due to the considerably lower organic soluble product yields obtained.

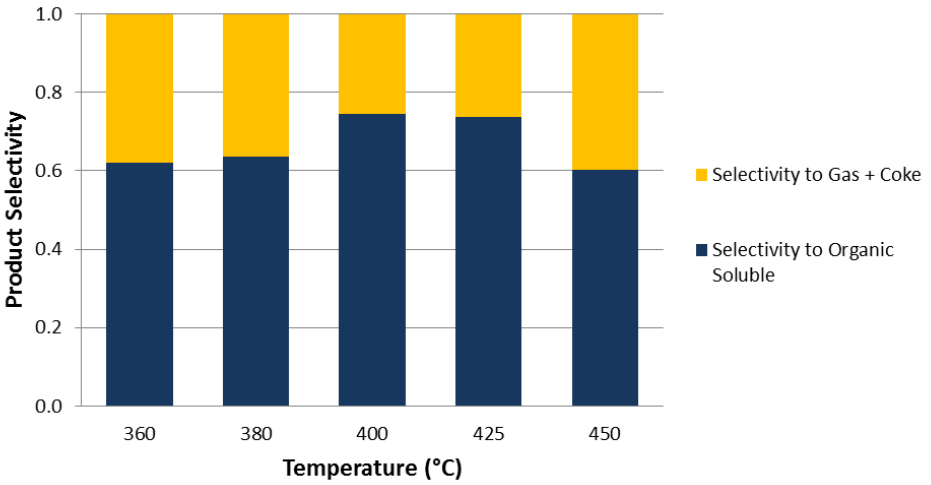


*Figure 5.15 Effect of temperature on the selectivity to organic soluble products at 230 bar, 0.2 $O/O_{stoich}$ ratio and 60 min reaction time.*

Figure 5.16 shows that an increase in reaction temperature resulted in a broader product distribution in the organic soluble fraction. This is thought to be the result of an increase in the rate of reactions such as oxygenation and cracking, which results in higher yields to organic soluble products and also in a broader product distribution.

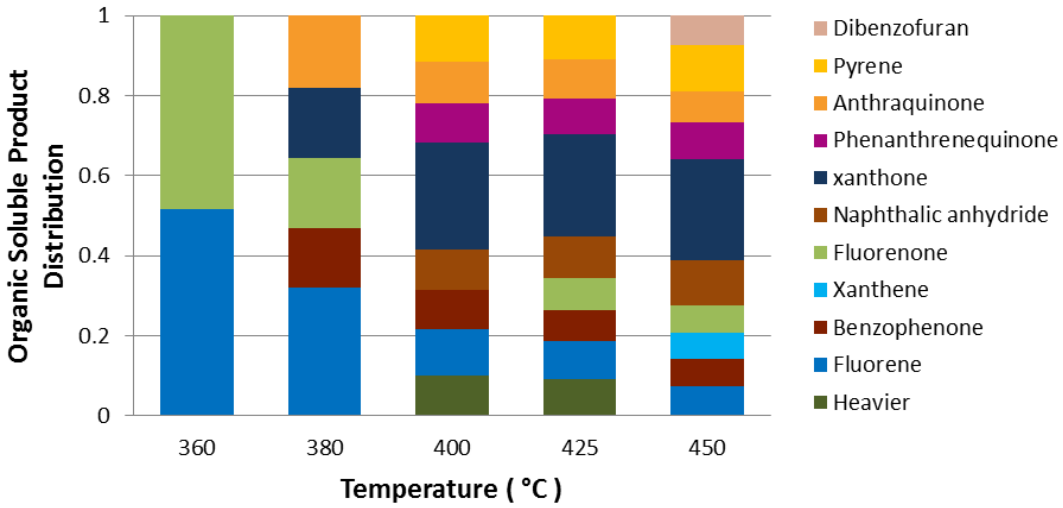


*Figure 5.16 Effect of temperature on the organic soluble product distributon at 230 bar, 0.2 $O/O_{stoich}$ ratio and 60 min reaction time.*

A relation between the O/C molar ratio in the organic soluble fraction and temperature was observed. Figure 5.17 illustrates that the amount of oxygen incorporated into the organic soluble fraction increases with an increase in temperature.

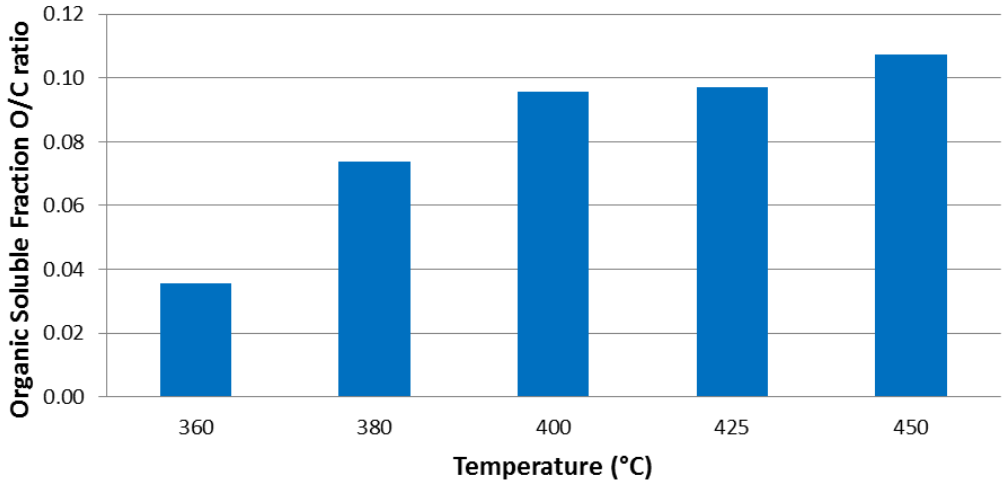


*Figure 5.17 Effect of temperature on the organic soluble product molar O/C ratio at 230 bar, 0.2 $O/O_{stoich}$ ratio and 60 min reaction time.*

In addition, considerably higher O/C molar ratios were obtained at temperatures above the critical temperature than the ones obtained at subcritical temperature. This may well be the result of the reduced mass transfer limitations encountered in SCW as well as the complete solubility of oxygen in the reaction medium, which facilitates the occurrence of oxidation reactions.

Low yields to gas below 3% were registered at all reaction temperatures with the exception of 450 °C where a yield of 10% was obtained. Analysis of the gas fraction was not performed for experiments at 360 °C due to the low amount of gas recovered. A $H_2$ rich gas product was obtained at all reaction temperatures studied as shown in Figure 5.18.

The effect of temperature on the concentration of $H_2$ and $CO_2$ with respect to $CH_4$ and CO differed greatly. An increase in temperature resulted in higher concentrations of $H_2$ and $CO_2$ in the gas fraction. In contrast, CO and $CH_4$ concentrations decreased with temperature as observed in Figure 5.18. It is thought that the increase in $H_2$ concentration could be the result of higher rates of cracking and WGSR reactions at higher temperatures. This could also explain the decrease observed in the concentration of $CH_4$ and CO with temperature. In

addition, rates of oxidation are also increased by the effect of temperature, which can potentially explain the increase observed in the concentration of $CO_2$. Similar trends in gas composition with temperature were observed by Guo et al in their work on hydrothermal gasification in the presence of an oxidizer (202,203).

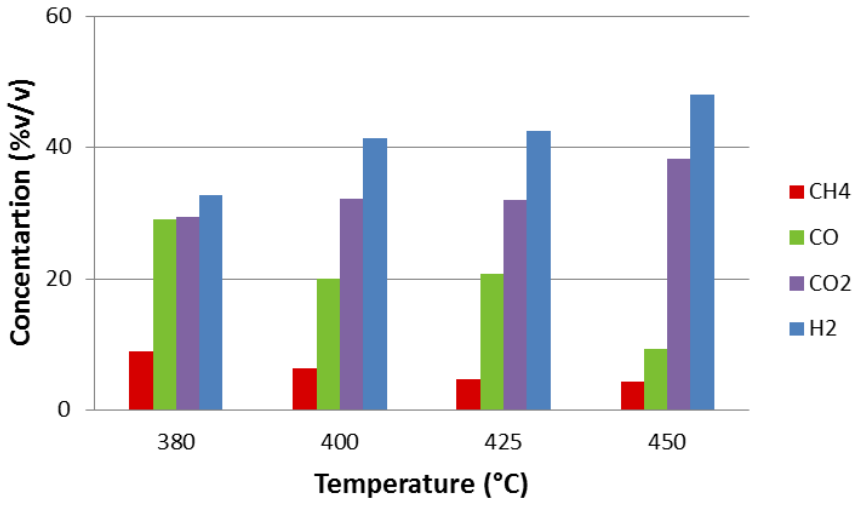


*Figure 5.18 Effect of temperature on the gas product composition at 230 bar, 0.2 $O/O_{stoich}$ ratio and 60 min reaction time.*

### 5.3.2. Effect of reaction time and determination of the reaction pathway

Table 5.2 shows the experimental conditions used to study the effect of reaction time in the oxidative cracking of phenanthrene. A pressure of 230 bar and an $O/O_{stoich}$ ratio of 0.2 were used as they were found to be optimum conditions for obtaining organic soluble products as discussed in previous sections. Experiments at different temperatures (400, 425 and 450 °C) and reaction times (0, 30, 60 and 90 min) were performed to assess the effect of reaction time in phenanthrene conversion, product yields and selectivities as well as to study the evolution of reaction products and propose a potential reaction pathway.

*Table 5.2 Experimental conditions to study oxidative cracking of phenanthrene in SCW at different reaction times and temperatures.*

| Parameter Studied | Experimental Conditions |
|---|---|
| Reaction Time (min) | 0, 30, 60 and 90 |
| Temperature (°C) | 400, 425 and 450 |
| Pressure (bar) | 230 |
| $O/O_{stoich}$ ratio | 0.2 |

### 5.3.2.1. Effect of reaction time

Figure 5.19 shows that phenanthrene conversion increased with reaction time to reach a plateau where no significant changes (within experimental error) were registered after 60 min for all reaction temperatures.

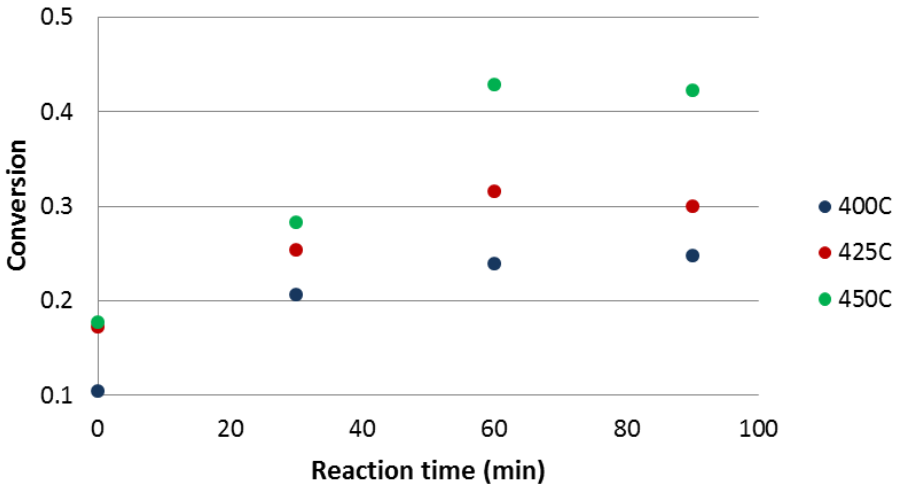


*Figure 5.19 Effect of reaction time on phenanthrene conversion varying temperature (400, 425 and 450 °C) at 230 bar and 0.2 $O/O_{stoich}$ ratio.*

The trends observed suggest that phenanthrene reacts in the presence of reactive oxygen species (ROS) abundant at early stages of reaction and stops reacting once these are consumed. In order to prove the unreactive nature of phenanthrene in SCW alone, experiments in the absence of an externally supplied oxidizer were performed at 450 °C and reaction times of 60 and 90 min. Conversion of phenanthrene during these experiments was negligible and the phenanthrene initially loaded into the reactor was recovered within experimental error. This could explain the reason for phenanthrene conversion to level off at longer reaction times (60 and 90 min) as most of the ROS in the medium have been consumed and phenanthrene stops reacting.

Yields to organic soluble products at the three temperatures increased al short reaction times until they reached 60 min where a maximum was found to then decrease sharply at 90 min, as shown in Figure 5.20. This is an indication that contrary to the trend observed with phenanthrene, intermediate oxygenated products continue to react in SCW alone to form lighter compounds leading eventually to gas. In addition, at 450 °C a sharper decrease in the yields to organic soluble products was registered between 60 and 90 min as seen in Figure 5.20. This is thought to be the result of higher rates of cracking enhanced by the higher reaction temperature.

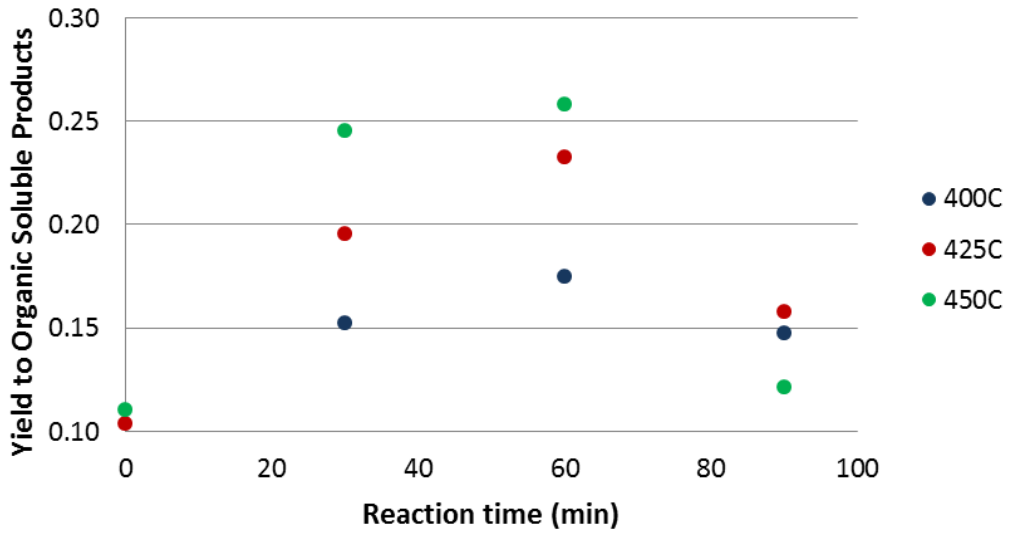


*Figure 5.20 Effect of reaction time on the yield to organic soluble products varying temperature (400, 425 and 450 °C) at 230 bar and 0.2 $O/O_{stoich}$ ratio.*

This interpretation is reinforced by the yields to gas obtained as shown in Figure 5.21.

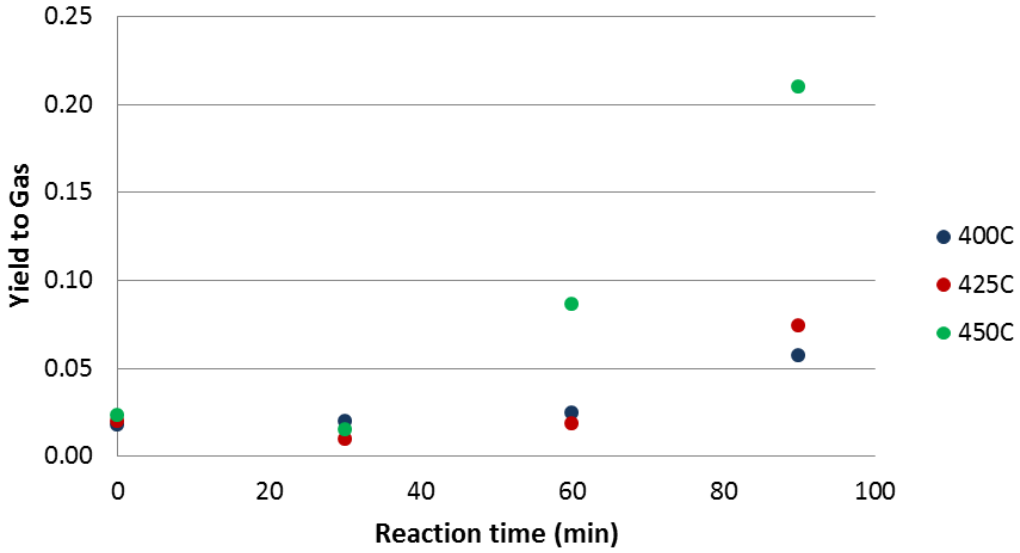


*Figure 5.21 Effect of reaction time on the yield to gas varying temperature (400, 425 and 450 °C) at 230 bar and 0.2 $O/O_{stoich}$ ratio.*

Yields to gas showed similar trends at the three reaction temperatures studied. At short reaction times (0 and 30 min) gas yields remained low and started to considerably increase after 60 min of reaction. This increment becomes highly relevant at 450 °C where a sharp increase in the yield to gas was registered between 60 and 90 min. The trends observed are in good agreement with the ones obtained for the yields to organic soluble products. The increase in the yield to gas observed after 60 min is thought to be the result of cracking reactions of intermediate products, which reduced the yields to organic soluble products as previously discussed.

A constant increase in the yields to coke with reaction time was observed at all temperatures studied. Figure 5.22 shows that after 60 min, yields to coke start to gradually level off at 400 and 425 °C. It is thought that this is the result of the decrease in the reactivity of the medium, which is linked with the reduced availability of ROS. This effect was less noticeable at 450 °C, as at higher temperatures some degree of thermal cracking can be achieved, which may result in radical recombination reactions to form coke. Overall, higher temperatures resulted in higher yields to coke.

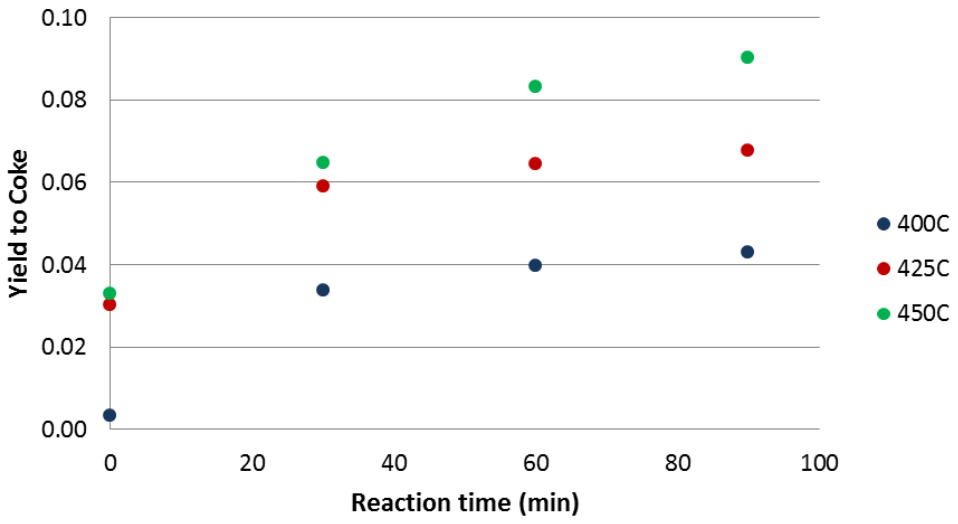


*Figure 5.22 Effect of reaction time on the yield to gas varying temperature (400, 425 and 450 °C) at 230 bar and 0.2 $O/O_{stoich}$ ratio.*

Analysis of the oxygen incorporation into the organic soluble products showed that at short reaction times, higher O/C molar ratios are achieved. An increase in reaction time at all temperatures resulted in a gradual decrease in the O/C molar ratio as shown in Figure 5.23.

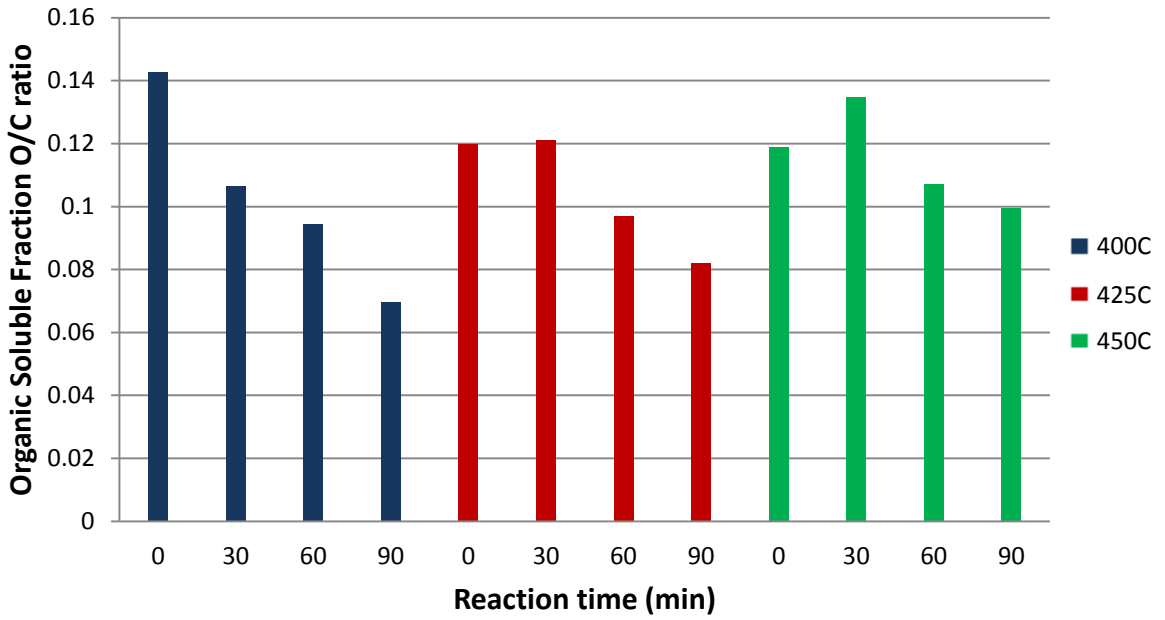


*Figure 5.23 Effect of reaction time on the organic soluble product molar O/C varying temperature (400, 425 and 450 °C) at 230 bar and 0.2 $O/O_{stoich}$ ratio.*

This suggests that at early reaction stages where high concentrations of ROS in the system are present, oxygen incorporation rates into the organic soluble product are also high. The oxygen rich organic soluble fraction was mainly composed of anthraquinone and xanthone. However, at higher reaction times, where ROS are consumed, oxygenated intermediate products continue to react to form lighter intermediates eventually leading into the formation of gas. At this stage, part of the oxygen initially incorporated is lost in cracking and reduction reactions, which result in a decrease in the O/C molar ratio of the organic soluble fraction.

Table 5.3 shows the gas compositions obtained at all reaction conditions studied. It can be observed that similar compositions were obtained regardless of the process conditions. Similar trends in gas composition have been observed at similar reaction conditions as reported in literature (204). $H_2$ concentration increased slightly with reaction time to reach a maximum between 30 and 60 min. However, an increase in reaction time to 90 min resulted in a decrease in $H_2$ concentration, which is thought to be caused by its consumption in hydrogenation reactions of intermediate products at late stages of reaction. $CH_4$ followed a similar trend by first increasing to find a maximum at the same interval to then decrease at longer reaction times. $CO_2$ showed an opposite trend with a slight decrease at shorter reaction times to find a minimum between 30 and 60 min to then increase considerably at late reaction stages especially at 425 and 450 °C. This trend is in good agreement with the one observed for the O/C molar ratio in the organic soluble product fraction (Figure 5.23),

which showed an important decrease at longer reaction times. This is thought to occur as a result of the release of oxygen, initially incorporated to the product intermediates into the gas fraction, in the form of $CO_2$.

*Table 5.3 Effect of reaction time on the gas product composition by varying temperature (400, 425 and 450 °C) at 230 bar and 0.2 $O/O_{stoich}$ ratio.*

| Temperature (°C) | Time (min) | Gas Fraction Composition (%v/v) | | | |
|---|---|---|---|---|---|
| | | $H_2$ | CO | $CH_4$ | $CO_2$ |
| **400 °C** | 0 | 38 | 15 | 5 | 42 |
| | 30 | 46 | 13 | 7 | 34 |
| | 60 | 41 | 21 | 6 | 32 |
| | 90 | 40 | 18 | 4 | 38 |
| **425 °C** | 0 | 43 | 17 | 4 | 36 |
| | 30 | 43 | 20 | 7 | 30 |
| | 60 | 43 | 21 | 5 | 31 |
| | 90 | 39 | 18 | 1 | 42 |
| **450 °C** | 0 | 45 | 21 | 2 | 32 |
| | 30 | 47 | 15 | 4 | 34 |
| | 60 | 48 | 9 | 4 | 39 |
| | 90 | 39 | 12 | 1 | 48 |

### *5.3.2.2. Reaction pathway*

The organic soluble product fraction recovered in each experiment, was analyzed through GC-MS to identify the intermediate products of reaction obtained. Then, products were organized by order of appearance according to the reaction temperature in order to follow their evolution with reaction time as shown in Table 5.4.

*Table 5.4 Products of the oxidative cracking of phenanthrene identified through GC-MS at 230 bar, 0.2 $O/O_{stoich}$, reaction times of 0, 30, 60 and 90 min and temperatures of 400, 425 and 450 °C.*

| Temperature (°C) | 400 °C | | | | 425 °C | | | | 450 °C | | | |
|---|---|---|---|---|---|---|---|---|---|---|---|---|
| Reaction time (min) | 0 | 30 | 60 | 90 | 0 | 30 | 60 | 90 | 0 | 30 | 60 | 90 |
| **Anthraquinone** | X | X | X | X | X | X | X | X | X | X | X | |
| **Xanthone** | | X | X | X | X | X | X | X | X | X | X | |
| **Fluorenone** | | X | X | X | | X | X | X | | X | X | |
| **Fluorene** | | X | X | X | | X | X | X | | X | X | X |
| **Phenanthrenequinone** | | | X | | | X | X | | | X | X | |
| **Naphthalic Anhydride** | | | X | X | | | X | | | X | X | |
| **Pyrene** | | | X | X | | | X | | | X | X | |
| **Heavier** | | | | X | | | X | | | | | |
| **Benzophenone** | | | X | | | | X | X | | | X | |
| **Xanthene** | | | | | | | | X | | | X | X |
| **Dibenzofuran** | | | | X | | | X | X | | | | X |

According to results in Table 5.4, at zero min the only product found at all temperatures was anthraquinone. In addition, at 425 °C and 450 °C xanthone was also produced. This suggests that a fast oxidation of phenanthrene to produce anthraquinone that continues to react into xanthone occurs at early stages of reaction.

Moreover, Table 5.4 also shows that product distribution varied greatly with temperature and reaction time. The broadest product distribution was registered at 425 °C and 60 min reaction time where all products, with the exception of xanthene, were recovered. Narrower product distributions were obtained at longer reaction times especially at 450 °C. Products with lower molecular weight and lower O/C molar ratio were obtained at these conditions.

The evolution of each individual organic soluble product was followed by determining its yield at the different temperatures and reaction times in order to propose a potential reaction pathway. According to their order of appearance organic soluble products were categorized as products that appear at early or late stages of reaction as shown in Figure 5.24 and Figure 5.25 respectively.

As previously discussed, the main intermediate product obtained at early reaction stages is anthraquinone. Figure 5.24 shows that high yields to anthraquinone were obtained at zero min, moment at which the reactor reaches reaction temperature. In addition, it was observed that an increase in reaction time to 30 min resulted in an increase in the yields to anthraquinone where it found a maximum at the three temperatures studied. Further increments in reaction time resulted in a decrease in the yield to anthraquinone, which suggests that it is a reaction intermediate and further reacts to form other products.

Xanthone and fluorenone showed a similar behavior increasing their yield to find a maximum at 30 min followed by a decrease in yield at longer reaction times. Interestingly, yields to xanthone between 60 and 90 min showed a slight increase at 400 °C and 425 °C. This is thought to be the result of reversible reactions from other products occurring at longer reaction times. It was noted that fluorene was produced at reaction times over 30 min and its concentration remained almost constant with changes in time and temperature. This suggest that either fluorene was formed at the same rate as it further reacted or that once formed fluorene presents as a very stable intermediate unreactive at longer reaction times where most of the ROS have been consumed.

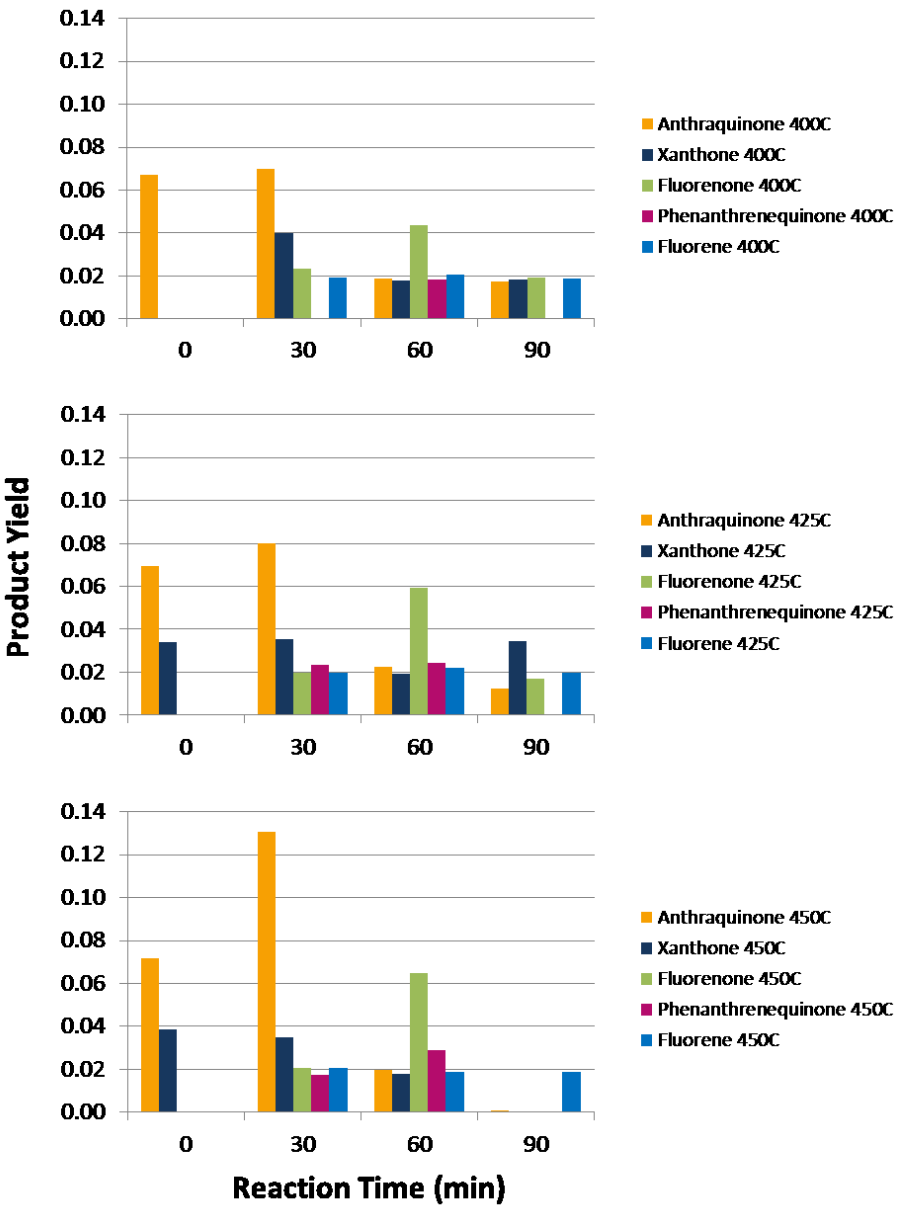


*Figure 5.24 Yield to early stage organic soluble products of phenanthrene oxidative cracking at 230 bar, 0.2 $O/O_{stoich}$ ratio, reaction time of 0, 30, 60 and 90 min and temperatures of 400, 425 and 450°C.*

The evolution of products obtained at late reaction stages is represented in Figure 5.25. Heavier products such as pyrene were obtained in reactions taking place over 60 min and temperatures of 400 °C and 425 °C. This indicates that at longer reaction times polymerization reactions into heavier products readily occur. Moreover, pyrene was recovered exclusively at 60 min when reaction took place at 450 °C, which suggests that at longer reaction times and higher temperature, pyrene may polymerize further leading to coke formation.

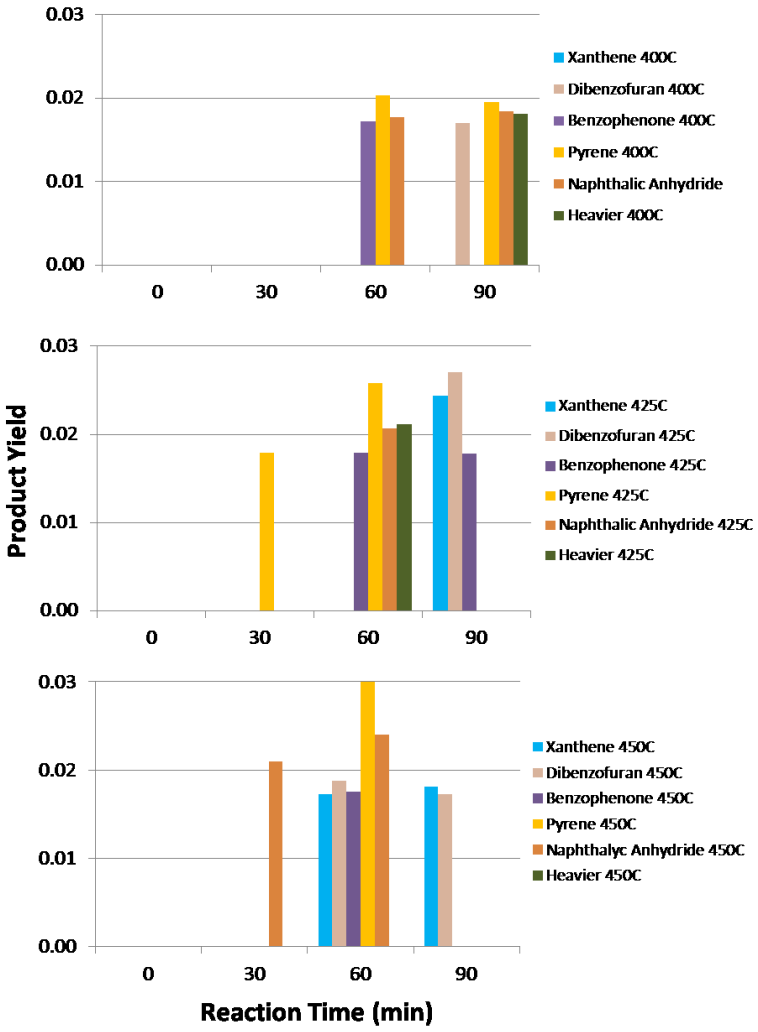


*Figure 5.25 Yield to late stage organic soluble products of phenanthrene oxidative cracking at 230 bar, 0.2 $O/O_{stoich}$ ratio, reaction time of 0, 30, 60 and 90 min and temperatures of 400, 425 and 450°C.*

Figure 5.25, shows that at 60 and 90 min (late stages of reaction), products like dibenzofuran, benzophenone, naphthalic anhydride and xanthene were obtained. It is thought that these products can potentially continue to react through cracking and ring opening to produce organic acids and other water soluble products that can further decompose into gas. In this work water soluble products were not identified and is believed that in supercritical water alone, these compounds react to produce gas especially at long reaction times studied reason why they were not recovered.

Based on the yields and product distributions obtained, a reaction pathway shown in Figure 5.26 was proposed. Potential reactions occurring in the process such as oxidation, isomerization, $H_2O$ reduction, elimination of CO and ring opening were identified. The occurrence of these reactions is in good agreement with other reaction pathways proposed

in literature for the hydrothermal oxidation of PAHs in near-critical and supercritical water conditions (106,108,109,196). The reactions proposed in Figure 5.26 are the result of comparison between the analysis of the evolution of each individual organic soluble product and information available in literature.

It is thought that the hydrothermal oxidative cracking of phenanthrene starts through the oxidation of phenanthrene into phenanthrenequinone [1]. This step can occur through hydroxylation of the initial phenanthrene followed by a tautomerism reaction (196). Once formed, phenanthrenequinone reacts through isomerization to produce anthraquinone [2] (108). It is believed that these two steps occur at very high rates as the presence of phenanthrenequinone was not detected at early reaction stages (0 min) where the main product was anthraquinone as previously shown in Figure 5.24. However, small yields of phenanthrenequinone were observed in the product mix at longer reaction times (30 and 60 min), which strongly suggests that the isomerization step [2] has some degree of reversibility. Moreover, it is thought that the reaction proceeds through the production of xanthone from anthraquinone via CO elimination followed by a hydroxylation and an epoxidation step [3] as suggested in literature (196). This reaction step also proceeds at high rates as xanthone was observed at early reaction stages (0 min) at 425 and 450 °C as shown in Figure 5.24. It is proposed that xanthone further reacts through 3 main routes, which occur at different reaction stages to give fluorenone, dibenzofuran and xanthene as products. At reaction times between 30 and 60 min xanthone yields decreased while an increase in the yield to fluorenone was observed. As previously mentioned, at long reaction time (90 min) and temperatures of 400 and 425 °C, yields to xanthone increased. This is thought to be the result of a reversible reaction from fluorenone [4] that proceeds via three consecutive reactions, hydroxylation, epoxidation and $H_2O$ loss as suggested in literature (109). Moreover, the second potential reaction route is the reduction of xanthone with loss of water to produce xanthene [5] that occurs at later stages of reactions as it was only identified at longer reaction times (60 and 90 min) and higher temperatures (425 and 450 °C). Dibenzofuran was also identified at long reaction times (60 and 90 min) and is thought to be the product of the reaction of xanthone through CO elimination [6].

Similarly, it is believed that fluorenone may react further through two main routes. First, fluorene can be formed through the reduction with loss of water of fluorenone [7], as has been suggested in literature (106). A second potential route is the reaction of fluorenone through hydroxylation and epoxidation [8] to form dibenzofuran (109). In addition, dibenzofuran could also be obtained through a decomposition, hydroxylation and epoxidation step [9] from fluorene (109).

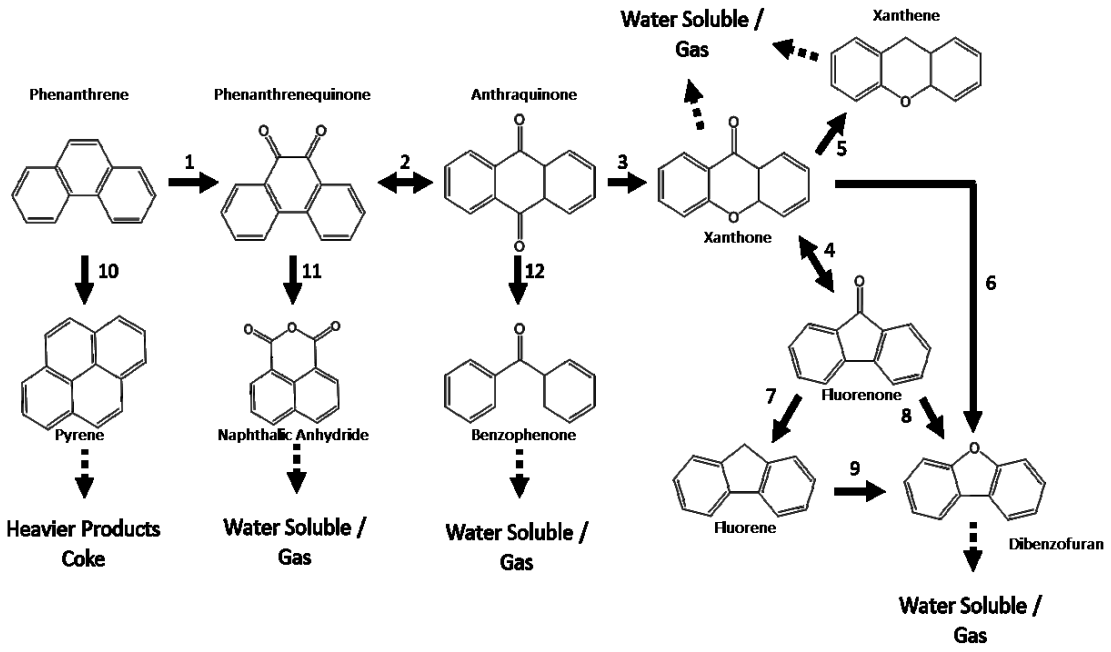


*Figure 5.26 Proposed reaction pathway for the oxidative cracking of phenanthrene in SCW.*

*Table 5.5 Summary of reactions proposed for the reaction pathway of the oxidative cracking of phenanthrene in SCW.*

| Reaction | Pathway |
|---|---|
| [1] | Oxidation of phenanthrene to phenanthrenequinone. |
| [2] | Isomerization reaction from phenanthrenequinone to anthraquinone. |
| [3] | Formation of xanthone through CO elimination + hydroxylation + epoxidation from anthraquinone. |
| [4] | Formation of fluorenone from xanthone through hydroxylation + epoxidation + $H_2O$ loss. |
| [5] | Formation of xanthene from xanthone through reduction + $H_2O$ loss. |
| [6] | Formation of dibenzofuran from xanthone through CO elimination. |
| [7] | Formation of fluorene from fluorenone through reduction + $H_2O$ loss. |
| [8] | Formation of dibenzofuran from fluorenone through hydroxylation + epoxidation. |
| [9] | Formation of dibenzofuran from fluorene through decomposition + hydroxylation + epoxidation. |
| [10] | Formation of pyrene from phenanthrene through polymerization. |
| [11] | Formation of naphthalic anhydride from phenanthrenequinone through isomerization + ring opening + hydroxylation + oxidation. |
| [12] | Formation of benzophenone from anthraquinone through ring opening + CO elimination. |

A series of secondary reactions were identified at late stages of reaction. The formation of pyrene at longer reaction times from 30 to 90 min, depending on temperature, was obtained as shown in Figure 5.25. This is thought to be the result of polymerization reactions between phenanthrene and other reaction intermediates [10] to produce larger polyaromatic structures (heavier compounds). Further polymerization reactions of these heavier compounds are thought to be the main route leading to coke formation. Formation of naphthalic anhydride was observed at long reaction times (30 to 90 min) depending on the

temperature of the system. It is thought that this may be the result of the reaction of phenanthrenequinone via isomerization, ring opening, hydroxylation and oxidation [11] to produce naphthalic anhydride as suggested in literature (196). Finally, benzophenone was also obtained at long reaction times (60 and 90 min) at all temperatures. It is thought that benzophenone is produced from the decomposition with ring opening of anthraquinone as a result of CO elimination as suggested in literature (106). In addition, it is believed that some of the oxygenated intermediate products obtained such as xanthone, xanthene, dibenzofuran and fluorenone, may react further to form water soluble products, which decompose fast into gas products.

## 5.4. CONCLUSIONS

The effect that process conditions pressure, $O/O_{stoich}$ ratio and temperature have in the hydrothermal oxidative cracking of phenanthrene in NCW and SCW were investigated.

Overall, pressure changes in the system did not have a perceptible impact in phenanthrene conversion but they did greatly influence the yields to organic soluble products and gas obtained. Yields to coke were not affected by changes in the system pressure. An optimum operating pressure, where higher yields to organic soluble products as well as a higher O/C molar ratios within the organic soluble fraction were observed at 230 bar. Gas composition showed great dependence on the system pressure. A $H_2$ rich gas was produced with the lowest $CO_2$ concentration at a reaction pressure of 230 bar.

Increments in the $O/O_{stoich}$ ratio resulted in higher phenanthrene conversions whereas yields to product fractions showed a different behavior. A maximum yield to organic soluble products was obtained at $O/O_{stoich}$ ratios between 0.2 and 0.4, which decreased with any further increment in $O/O_{stoich}$ ratio. As a result, gas yields increased considerably at high $O/O_{stoich}$ ratios. Yields to coke showed a similar trend to the organic soluble products by increasing to find a maximum at an $O/O_{stoich}$ ratio of 0.2. The initial oxygen loading had an important impact on the composition of the gas fraction, which showed high concentrations of $H_2$ at low $O/O_{stoich}$ ratios. An optimum $O/O_{stoich}$ ratio for the reaction was found at 0.2, where the selectivity to organic soluble products was higher as well as the O/C molar ratio.

An increase in reaction temperature resulted in both an increase of phenanthrene conversion and an increase in the yields to all product fractions. A maximum selectivity to organic soluble products was obtained between 400 and 425 °C. Moreover, a constant increase in the O/C molar ratio with temperature was observed. In addition, it was concluded

that gas concentration depends on reaction temperature and that $H_2$ and $CO_2$ concentrations also increased with any increase in temperature.

Phenanthrene conversion increased with reaction time to reach a plateau after 60 min at all conditions studied. This shows that at early reaction stages with high ROS concentrations, phenanthrene was highly reactive. In contrast, at longer reaction times (60 min), when ROS were consumed, phenanthrene showed to be stable and did not react further. Intermediate organic soluble product yields showed a maximum at 60 min to then decrease at longer reaction times, which shows that in the absence of ROS, intermediate products still react. Decomposition of oxygenated intermediates at long reaction times resulted in high yields to gas. These observations are in good agreement with the decrease in the O/C molar ratio in the organic soluble fraction observed, which is attributed to carbon and oxygen rejection into the gas fraction. At all conditions low yields to coke were obtained, which proves that water at near-critical and supercritical conditions can aid preventing polymerization reactions and hence coke formation.

Based on the intermediate products evolution and supported on information from literature, it was concluded that the main potential reactions occurring in the oxidative cracking of phenanthrene in NCW and SCW are oxidation, isomerization, reduction, CO elimination, cracking and ring opening. It was determined that the organic soluble product fraction was mainly composed of oxygenated hydrocarbons such as oxygen-containing heterocycles, ketones, furans as well as some PAHs. A reaction pathway for the oxidative cracking of phenanthrene was also proposed.

# Chapter 6
# Continuous Oxidative Cracking of Methyl Naphthalene in Supercritical Water

This work focuses in the study of the continuous oxidative cracking of heavy oil in SCW using methyl naphthalene as model compound. In order to do this, a continuous flow reactor was designed and built as extensively explained in Chapter 3 and Chapter 4. The main objective pursued was to gain an understanding of the process at early stages of reaction with the aim of identifying initial intermediate species and study the evolution of the reaction products.

## 6.1. INTRODUCTION

Due to the complex nature of heavy oils, getting a proper understanding of the reactions taking place at NCW and SCW conditions is not an easy task to accomplish. In order to achieve this, studies with specific model compounds that represent chemical structures commonly found in heavy oils have been performed. This has proven useful to gain some insight into the main reactions occurring in the system and also to understand the effect of process variables as reported in Chapter 5. Most of the literature available on the partial oxidation of PAHs in NCW and SCW, used batch reaction set ups (108,109,196). Some of the drawbacks of using a batch system are the heating time required to reach reaction temperature and the limitations in terms of the minimum reaction times at which the reactor can operate. This complicates the study of the process at early reaction stages and the determination of the reaction kinetics. In order to overcome this, a flow reaction system was designed and built.

Supercritical water oxidation of organic compounds in SCW has been considered extensively as a process to totally convert hazardous organic substances present in waste water streams into $CO_2$ and $H_2O$. Studies with organic compounds commonly found in waste water streams such as phenol (67,205,206), organic acids (207,208), chlorinated organic compounds (209,210) and nitrogen containing organic compounds (136,137) were performed with high conversions in continuous reaction systems. However, few studies have

been performed on the continuous partial oxidation of organic compounds to valuable intermediates (211,212).

The aim of this work is to study the oxidative cracking of heavy oil model compound methyl naphthalene in a continuous flow reactor at early reaction stages. Short residence times of up to one min and temperatures between 400 and 450 °C were studied with the aim of identifying initial reaction intermediate species and to follow the evolution of the different products obtained to determine a potential reaction pathway.

## 6.2. EXPERIMENTAL

Experiments on the oxidative cracking of heavy oil model compound methyl naphthalene in SCW were performed in a continuous flow reactor described in Section 3.2.2 and Section 4.1.2. Briefly, an organic feed composed of Sigma-Aldrich Methyl Naphthalene 97% and an aqueous feed composed of DI water and VWR $H_2O_2$ solution 30% w/v as oxidant were fed into the system according to the process conditions needed by means of a Varian LC Star 9002 and a Varian LC Star 9010 HPLC pumps respectively. Then the $H_2O_2$ solution passed through the $H_2O_2$ decomposition reactor where it was fully converted into $H_2O$ and $O_2$. The organic and the $H_2O/O_2$ stream were mixed in a mixing section to then pass through the partial oxidation reactor at SCW conditions. Products of reaction were recovered following the procedure detailed in Section 4.1.2.3. Organic soluble products were analyzed through GC-FID and GC-MS, gas products through GC-TCD and coke was determined through TGA. Analytical procedures are extensively described in Section 4.1.3.

## 6.3. RESULTS AND DISCUSSION

### 6.3.1. Oxidative cracking experiments varying temperature and residence time

In these experiments, reaction temperature and residence time were varied keeping pressure at 230 bar that is the optimum value found from the results previously discussed in Chapter 5. It was reported that the partial oxidation of PAHs begins in an initial attack of an OH radical to the aromatic ring in order to form an aromatic alcohol (196). In the results presented in Chapter 5 no aromatic alcohol species were observed among the product mix suggesting that formation and decomposition of these species are fast reactions. As one of the main objectives of this work is to gain a fundamental understanding of the process at early reaction stages and to analyze the initial intermediate products, it was considered that the reaction should be performed at lower residence times and also reducing the $O/O_{stoich}$

ratio. In order to do this, a theoretical estimation of the $O/O_{stoich}$ ratio needed to convert methyl naphthalene into methyl naphthol showed that an $O/O_{stoich}$ ratio of 0.05 should suffice. This was used to adjust the amount of oxygen fed into the system. The experimental conditions used in this study are detailed in Table 6.1.

*Table 6.1 Experimental conditions to study the continuous oxidative cracking of methyl naphthalene in SCW varying temperature and residence time.*

| Parameter | Value |
|---|---|
| Temperature (°C) | 400, 425 and 450 |
| Residence Time (s) | 15, 30, 45 and 60 |
| Pressure (bar) | 230 |
| $O / O_{stoich}$ ratio | 0.05 |
| Water / organic ratio | 12 |

Results obtained are presented in the form of methyl naphthalene conversion, yield and selectivity to different product fractions (organic soluble, gas and coke) and O/C ratio in the organic soluble products. These are calculated using Equations 6.1 to 6.4. Methyl naphthalene conversion was calculated with Equation 6.1 where $Cmol^0_{MN}$ stands for the carbon moles in the initial methyl naphthalene fed and $Cmol^f_{MN}$ stands for the carbon moles of methyl naphthalene at the outlet of the.

$$Conversion_{MN} = \frac{Cmol^0_{MN} - Cmol^f_{MN}}{Cmol^0_{MN}} \quad (6.1)$$

Yields to the different product fractions were calculated with Equation 6.2 where $Cmol_i$ stands for the carbon moles in the product fraction.

$$Yield_{prod} = \frac{Cmol_i}{Cmol^0_{MN}} \quad (6.2)$$

The selectivity to each product fraction was determined using Equation 6.3

$$Selectivity_{prod} = \frac{Cmol_i}{Cmol^0_{MN} - Cmol^f_{MN}} \quad (6.3)$$

Analysis of the organic soluble fraction showed that as expected all the organic soluble products were oxygenated compounds such as alcohols, quinones and oxygen containing heterocycles, as shown in Figure 6.1. Products of similar nature have been reported for PAH oxidation when reactions were carried out in hydrothermal conditions (105,196).

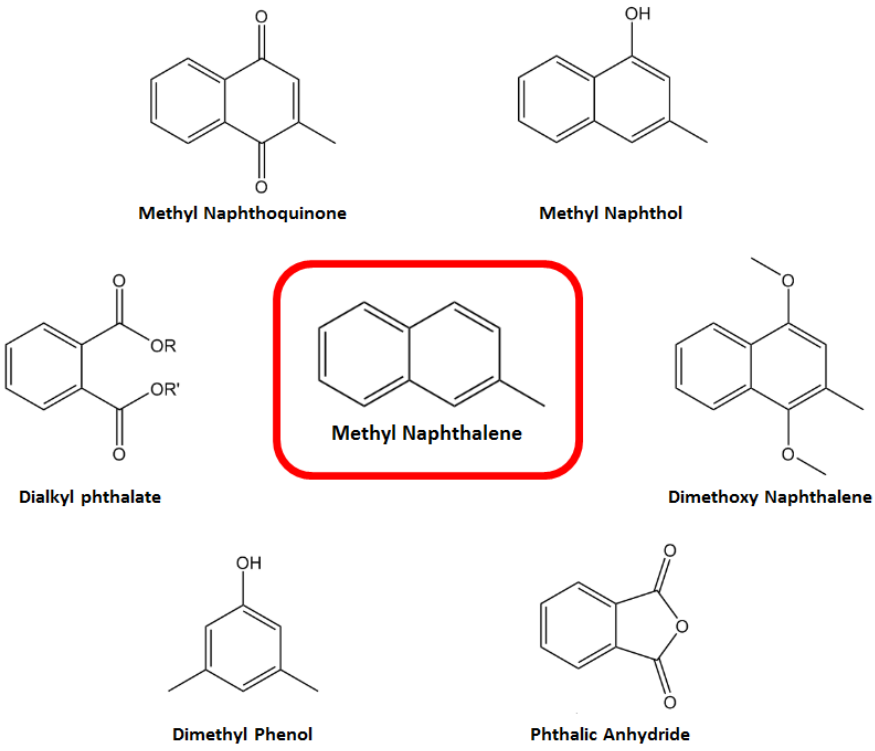


*Figure 6.1 Organic soluble products from the continuous oxidative cracking of methyl naphthalene in SCW, identified through GC-MS*

### *6.3.1.1. Methyl naphthalene conversion*

Methyl naphthalene conversion was calculated for experiments performed at different temperatures (400 °C, 425 °C and 450 °C) and residence times of 15, 30, 45 and 60 (at 400 °C only) s. As observed in Figure 6.2, methyl naphthalene conversions over 30% were achieved at all reaction conditions studied. This suggests that during the oxidative cracking process, the partial oxidation of polycyclic aromatic structures occur at high reaction rates in very short residence times. Similar observations have been reported in literature where oxidation of organic compounds in hydrothermal conditions was achieved with high conversions in short times (65,205).

It was observed that both temperature and residence time have an impact in methyl naphthalene conversion. Figure 6.2 shows that an increase in temperature results in a slight increase in conversion. This is more evident at short residence times (15 and 30 seconds) where 10 % more conversion was achieved at 450 °C than at 400 °C. At longer residence times, the effect of temperature becomes less evident. It is believed that this is related to the amount of oxygen available to react in the medium. At initial reaction stages, the amount of oxygen available is high and therefore an increase in temperature impacts oxidation rates , which results in higher conversions. However, in experiments at longer residence times, oxygen becomes the limiting reactant. Therefore, the effect of temperature is diluted as PAHs were found to be unreactive in water alone as discussed in Chapter 5.

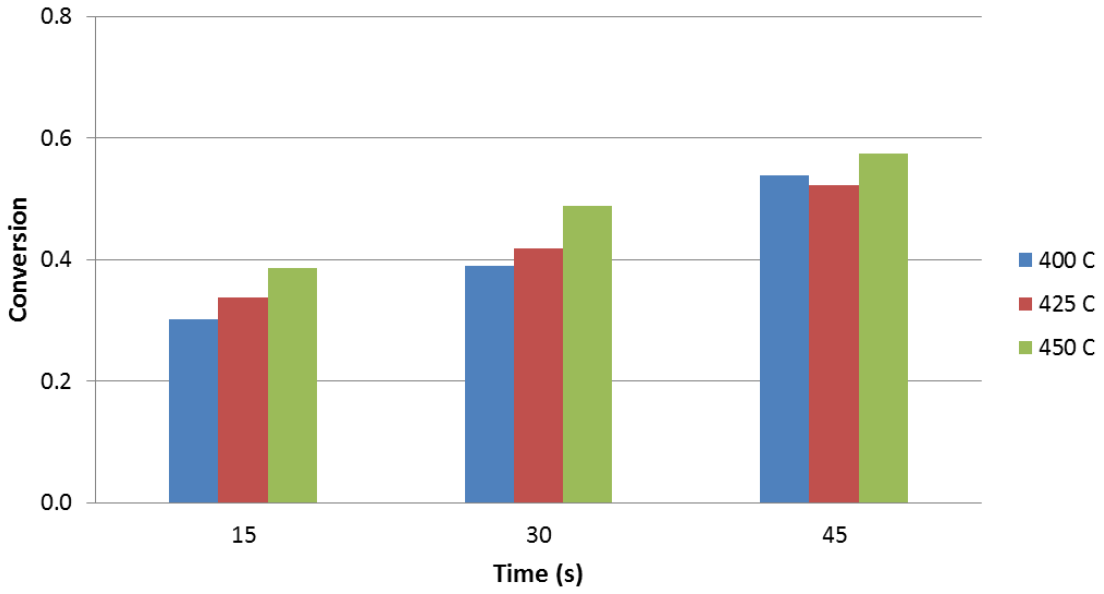


*Figure 6.2 Methyl naphthalene conversion varying temperature and residence time at 230 bar, 0.05 $O/O_{stoich}$ ratio and 12 water/org ratio.*

Methyl naphthalene conversion showed an important increase with an increase in residence time at early reaction stages until it reached a plateau as observed in experiments performed at 400 °C shown in Figure 6.3. This behaviour reinforces the explanation presented above as it makes evident that at shorter residence times, when the concentration of reactive oxygen species (ROS) in the system is high, conversion will show an important increase as occurred between 15 and 45 s. However, when most of the ROS have been consumed at longer residence time, conversion reaches a plateau as observed between 45 and 60 s.

### 6.3.1.2. Yields to reaction products

Figure 6.3 shows the evolution of methyl naphthalene conversion and the product yields as a function of residence time when reaction took place at 400 °C. At this temperature, a clear trend with two reaction regimes (reactions in SCW+$O_2$ and in SCW alone) in the oxidative cracking process can clearly be observed. In the first regime, where concentration of ROS in the medium is high, an increase in conversion results in an increase in the yield to organic soluble products, until a maximum is reached between 30 and 45 s. This is believed to be the result of the oxidation of methyl naphthalene to produce oxygenated intermediates, which is the main reaction taking place. Moreover, an increase in the yields to gas was also seen within the initial 30 s. This may be due to further oxidation or to thermal decomposition of oxygenated intermediates. At the reaction conditions studied negligible yields to coke were obtained.

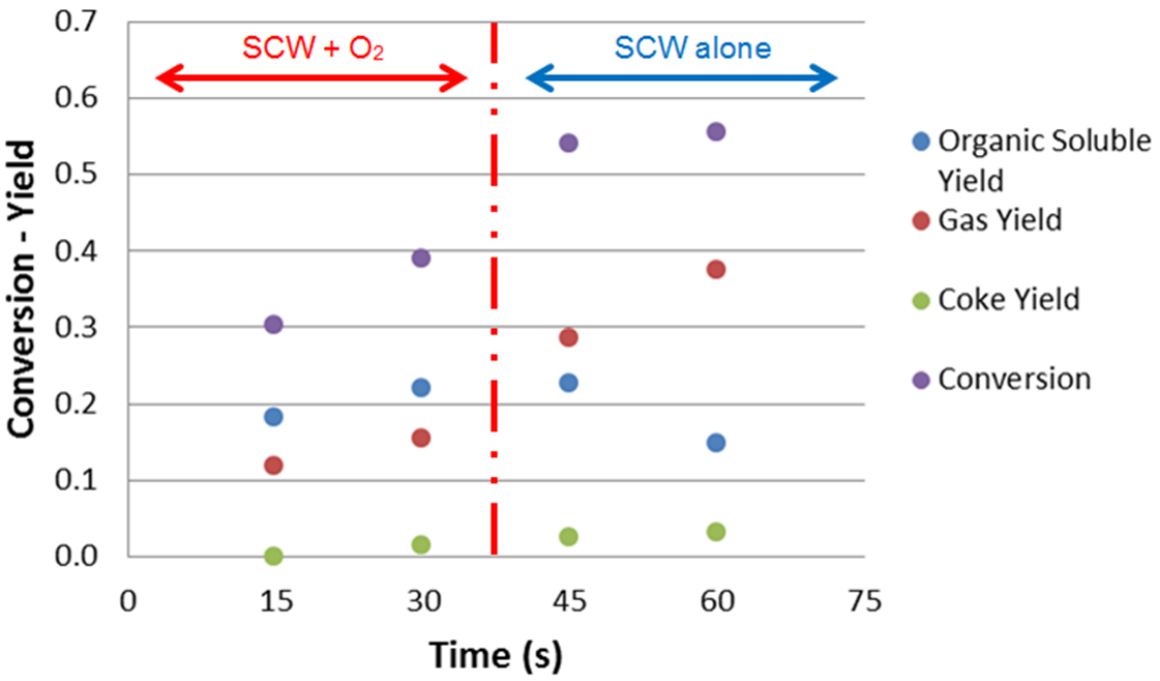


*Figure 6.3 Methyl naphthalene conversion and yield to products varying residence time at 400 °C, 230 bar, 0.05 $O/O_{stoich}$ and 12 water/org ratio.*

At residence times over 30 s, the low concentration of ROS in the medium produces a change in reaction regime in which reactions take place in SCW alone. Interestingly it was observed that while conversion of methyl naphthalene reached a plateau, yields to organic soluble compounds decreased further with increments in residence time. From this observation it can be inferred that methyl naphthalene is unreactive in SCW alone. In order

to prove this, a series of experiments at the same reaction conditions but in the absence of oxygen were performed. It was observed that in the absence of oxygen negligible conversions of methyl naphthalene were obtained proving its unreactive nature in SCW alone. However, oxygenated intermediates generated from methyl naphthalene oxidation continue to react in the absence of ROS to form lighter products and gas resulting in a decrease in its yield. This is in good agreement with the increase in gas yield with residence time as seen in Figure 6.3. However, coke yields seem not to be affected by a change in reaction regime and are kept at low values (below 4%) at the different residence times studied.

The effect of reaction temperature in the yields to organic soluble products at different residence times is shown in Figure 6.4. As previously discussed, when reaction took place at 400 °C a clear trend with a maximum between 30 and 45 s was obtained. However, at higher temperatures (425 °C and 450 °C) a steady decrease in the yields to organic soluble products was observed with any increments in residence time. It is believed that temperature has an important influence on the oxidation rates, which are especially high at early stages of reaction. This can explain the decreasing trend observed at 425 °C and 450 °C as yields to organic products could have reached a maximum at residence times below 15 s. This cannot be proved as with the current reaction set up it is not possible to work at shorter residence times.

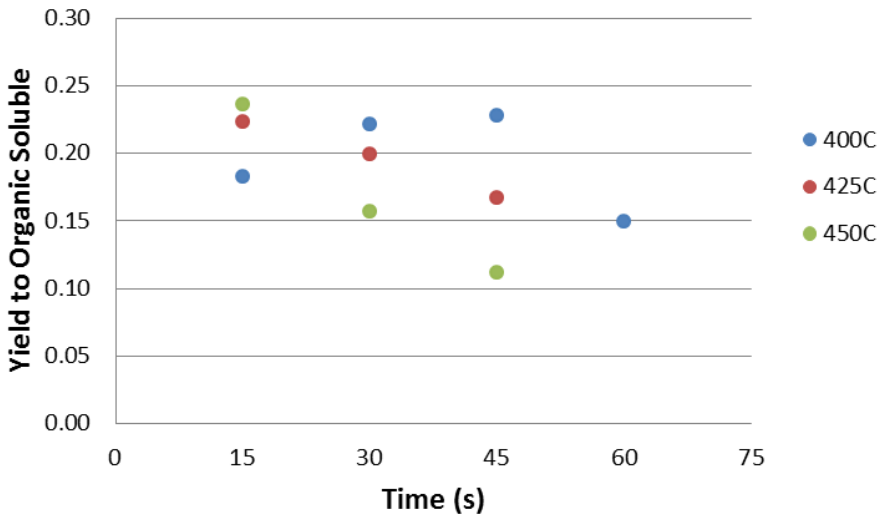


*Figure 6.4 Yield to organic soluble products varying residence time and temperature at 230 bar, 0.05 O/$O_{stoich}$ ratio and 12 water/org ratio.*

Figure 6.5 shows that yields to gas increase with an increase in residence time. This is in good agreement with the trends previously described for organic soluble products as gas production is thought to be the result of the decomposition of oxygenated intermediates, which can proceed in SCW alone leading to the formation of lighter products and eventually gas.

Moreover, an important dependence between gas yield and reaction temperature was identified. An increase in temperature results in an increase in the rate of gas formation as seen in Figure 6.5. This is evident when comparing the trends for gas production, as at higher reaction temperatures a steeper increase in the yield to gas was obtained with increasing residence time. At short residence times, when less gas was produced, differences between gas yields obtained at different reaction temperatures were less evident.

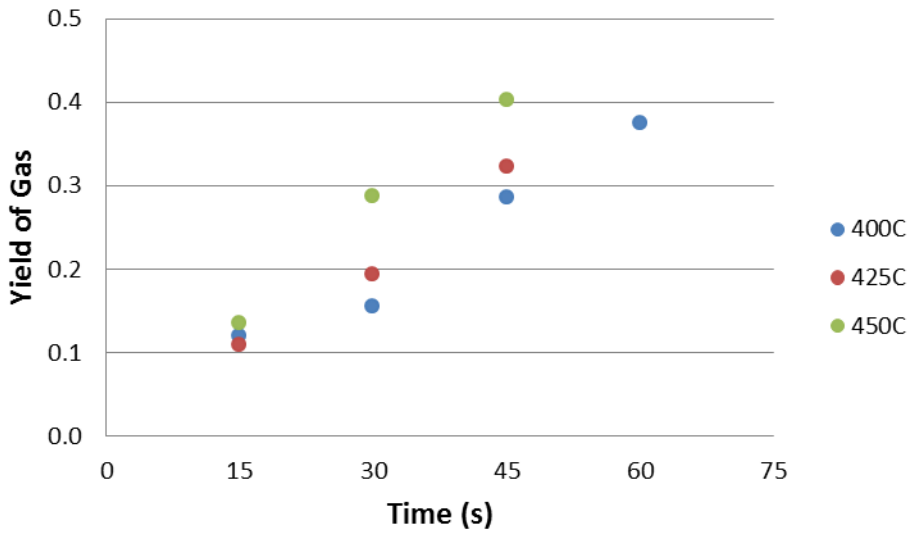


*Figure 6.5 Yield to gas varying residence time and temperature at 230 bar, 0.05 $O/O_{stoich}$ ratio and 12 water/org ratio.*

Similarly, a direct relation was observed between the yield to coke and both reaction temperature and residence time. Figure 6.6 shows that an increase in residence time resulted in an increase in coke formation. At 450 °C the increase in the yields to coke was more pronounced than the ones obtained at 425 °C and 400 °C. This suggests that higher temperatures may promote polymerization reactions that were not favored at lower reaction temperatures, which is in good agreement with the results obtained with phenanthrene

reported in Chapter 5. Overall, coke yields obtained were low, below 6%, at all reaction conditions studied.

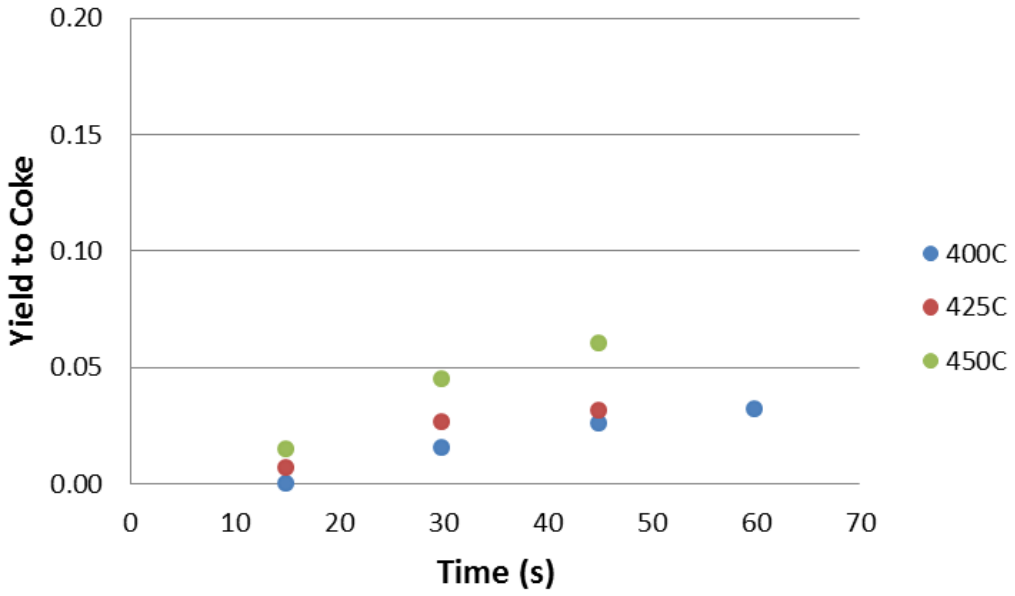


*Figure 6.6 Yield to coke varying residence time and temperature at 230 bar, 0.05 $O/O_{stoich}$ ratio and 12 water/org ratio.*

### *6.3.1.3. Selectivity to organic soluble products*

Figure 6.7 shows the selectivity to organic soluble products as a function of residence time at 400 °C. It can be observed that selectivities to organic soluble products near 60% were obtained when reaction took place at short residence times.

However, a gradual decrease in the selectivity to organic soluble products was observed when increasing residence time. This is the result of the important increments in the yield to gas registered at longer residence times. Decomposition of oxygenated intermediates leading to gas and the lack of reactivity of methyl naphthalene in the absence of ROS are thought to be the reasons for the decrease in the selectivity to organic soluble products. Values of selectivity to organic soluble products and Coke+Gas at different reaction temperatures and residence times are reported in Table 6.2. It can be observed that the decreasing trend in the selectivity to organic soluble products was obbtained at all reaction temperatures studied.

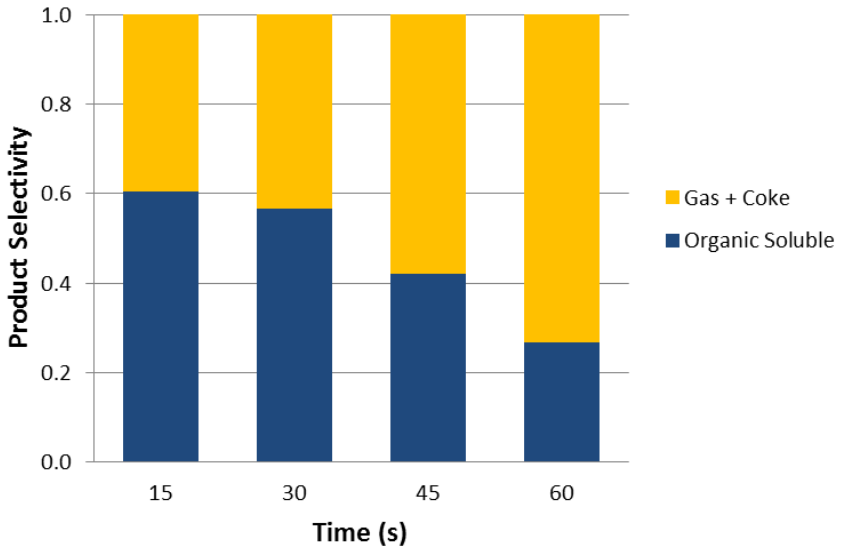


*Figure 6.7 Selectivity to organic soluble products varying residence time at 400 °C, 230 bar, 0.05 $O/O_{stoich}$ and 12 water/org ratio.*

*Table 6.2 Selectivity to organic soluble products varying residence time and temperature at 230 bar, 0.05 $O/O_{stoich}$ and 12 water/org ratio.*

| | 400°C | | 425°C | | 450°C | |
|---|---|---|---|---|---|---|
| | **Org Soluble** | **Gas+Coke** | **Org Soluble** | **Gas+Coke** | **Org Soluble** | **Gas+Coke** |
| **15s** | 0.60 | 0.40 | 0.66 | 0.34 | 0.61 | 0.39 |
| **30s** | 0.57 | 0.43 | 0.48 | 0.52 | 0.32 | 0.68 |
| **45s** | 0.42 | 0.58 | 0.32 | 0.68 | 0.19 | 0.81 |
| **60s** | 0.27 | 0.73 | - | - | - | - |

#### *6.3.1.4. O/C ratio in the organic soluble fraction*

One of the main objectives of this process is the incorporation of oxygen to the aromatic structure of the PAH with the aim to weaken it and enable its further cracking. In order to evaluate the incorporation of oxygen into the organic soluble fraction, a ratio between the moles of oxygen and the moles of carbon has been calculated and reported in Figure 6.8. It can be observed that early in the reaction an increase in the O/C ratio reflects the initial incorporation of the available ROS into the organic soluble fraction. At longer residence times, the trends observed suggest that the O/C ratio reaches a maximum and then decrease as a result of cracking and oxygen rejection reactions that form gas products. It

has to be noted that at these conditions small changes in the O/C ratio were registered (in some cases within experimental error).

In addition, it was observed that reaction temperature had an impact on the O/C ratio of the organic soluble fraction. At 400 °C, the O/C ratio increased between 15 and 45 s to then remain almost unchanged at 60 s residence time. However, at 450 °C a clear maximum in O/C ratio was observed at 30 s. Interestingly, conversion of methyl naphthalene continues to increase at 30 s residence time, which strongly suggests that the decrease in the O/C ratio at higher residence times may be caused by greater oxygen removal rates into the gas phase mainly in the form of CO and $CO_2$. This was not observed in reactions at 400 °C in which slower reaction rates are expected.

The trends observed confirm a pathway involving an initial oxidation of the PAH followed by the decomposition of the oxygenated intermediates and the partial de-oxygenation in SCW in the absence of oxygen.

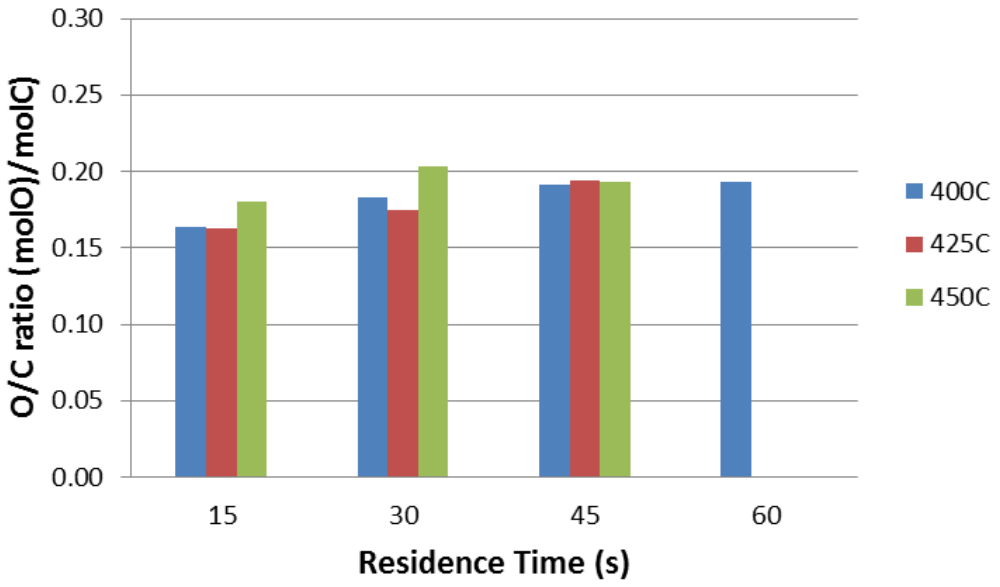


*Figure 6.8 O/C ratio in the organic soluble product fraction varying temperature and residence time at 230 bar, 0.05 $O/O_{stoich}$ ratio and 12 water/org ratio.*

### *6.3.1.5. Analysis of the gas products*

Changes in temperature and residence time have an important impact on the yields to gas produced and the composition of the gas obtained. Table 6.3 shows that at early stages of reaction the gas product is mainly composed of CO and $CO_2$ as a result of the initial

oxidation reactions. Interestingly, negligible concentrations of methane were obtained at all reaction conditions studied. It is believed that methane is mainly formed as a result of cracking and hydrogenation reactions of intermediate species that occur at later stages of reaction. Moreover, the large excess of water in the system would promote methane reforming reaction shifting its equilibrium towards CO and $H_2$. It was also reported in literature that at short residence time and in the presence of ROS in the medium, $CH_4$ concentrations near zero were obtained (136).

An important relation between $H_2$ concentration in the gas, reaction temperature and residence time was observed. An increase in residence time resulted in an important increase in the concentration of $H_2$ in the gas product. The increase in concentration of $H_2$ with residence time was more pronounced at higher temperatures.

*Table 6.3 Gas product composition varying temperature and residence time at 230 bar, 0.05 $O/O_{stoich}$ ratio and 12 water/org ratio.*

| | **400 °C** | | | | **425 °C** | | | | **450 °C** | | | |
|---|---|---|---|---|---|---|---|---|---|---|---|---|
| **Residence Time (s)** | **$H_2$** | **CO** | **$CH_4$** | **$CO_2$** | **$H_2$** | **CO** | **$CH_4$** | **$CO_2$** | **$H_2$** | **CO** | **$CH_4$** | **$CO_2$** |
| **15** | 2.6 | 23.1 | 0 | 74.3 | 2.6 | 17.7 | 0 | 79.7 | 5.2 | 21.3 | 0 | 73.5 |
| **30** | 4.0 | 33.2 | 0 | 62.8 | 3.9 | 21.6 | 0.1 | 74.4 | 7.2 | 22.3 | 0.1 | 70.4 |
| **45** | 5.4 | 32.5 | 0.1 | 62.0 | 6.8 | 16.3 | 0.1 | 76.8 | 13.8 | 16.8 | 0 | 69.4 |
| **60** | 12.1 | 26.8 | 0 | 61.1 | - | - | - | - | - | - | - | - |

Figure 6.9 presents a relation between the volume of $H_2$ produced per gram of methyl naphthalene fed and residence time. At short residence times, low $H_2$ production was achieved at all reaction temperatures. However, increments in residence time resulted in an important increase in the production of $H_2$. It is believed that $H_2$ is mainly produced as a result of a non-catalytic WGSR in SCW.

$$CO + H_2O \leftrightarrow CO_2 + H_2$$

Following Le Chatelier's principle, the great excess of water in the system will shift the equilibrium position favoring the production of $H_2$. In addition, it has been reported that at the reaction temperatures studied, equilibrium is also favorable to the forward WGSR (213). The important increase in the rate of $H_2$ production with an increase in temperature suggests that kinetics of WGSR also play an important role. An increase in the non-catalytic WGSR rates with temperature was reported in literature at similar temperature intervals (61). This shows that at the reaction conditions studied, the balance between kinetics and thermodynamics is optimum to maximize $H_2$ production.

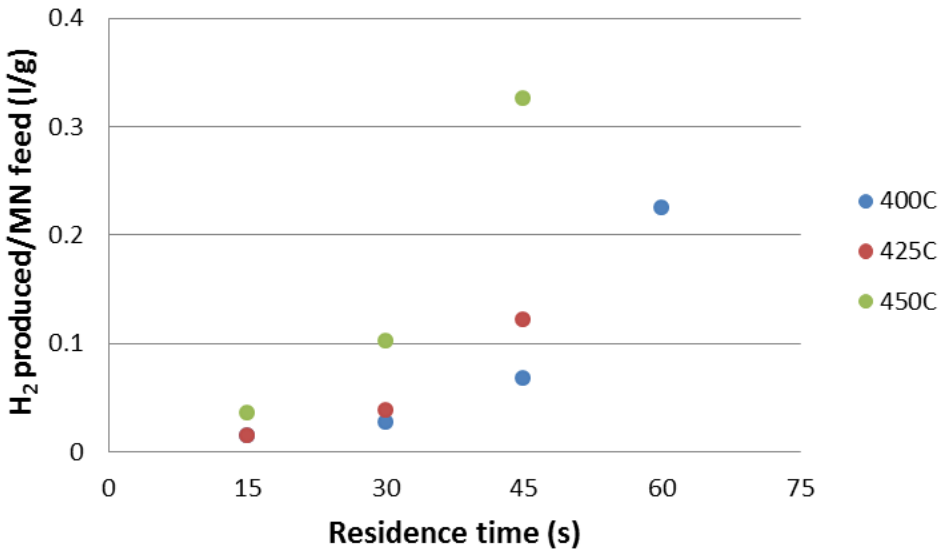


*Figure 6.9 Volume of $H_2$ produced per gram of methyl naphthalene fed varying temperature and residence time at 230 bar, 0.05 $O/O_{stoich}$ and 12 water/org ratio*

### 6.3.2. Reaction pathway

Organic soluble products obtained at different reaction conditions were analyzed in a GC-MS to identify individual products of reaction. A total of six organic soluble products of reaction (methyl naphthol, methyl naphthoquinone, phthalic anhydride, diethyl phthalate, dimetoxy naphthalene and dimethyl phenol) were identified. Yields to individual products were calculated at different temperatures and residence times in order to study their evolution as shown in Figure 6.10 and Figure 6.11. The main products obtained were methyl naphthol and methyl naphthoquinone.

Experimental results suggest that the initial stage of reaction is the oxidation of methyl naphthalene to form methyl naphthol. As can be seen in Figure 6.10, high yields to this product were observed at 15 s residence time, and then decreased sharply with an increase in residence time to become negligible at residence times of 45 s and longer. This shows that the initial oxidation reaction is a very fast process and that methyl naphthol is not a very stable intermediate. Moreover, at 30 s and 45 s residence time it can be observed that while the yield to methyl naphthol decreased an important increase in the yield to methyl naphthoquinone was registered. This shows that methyl naphthol is further oxidized to form methyl naphthoquinone. High concentrations of methyl naphthoquinone were obtained at all reaction conditions making it the main product of reaction. It was observed that at 400 °C and 425 °C yields to methyl naphthoquinone increased to find a maximum at a residence time around 45 s. At longer residence time methyl naphthoquinone decreased due to further

decomposition to form other products. At 450 °C, the highest yield to methyl naphthoquinone was obtained at 15 s and then it decreased gradually when residence time increased.

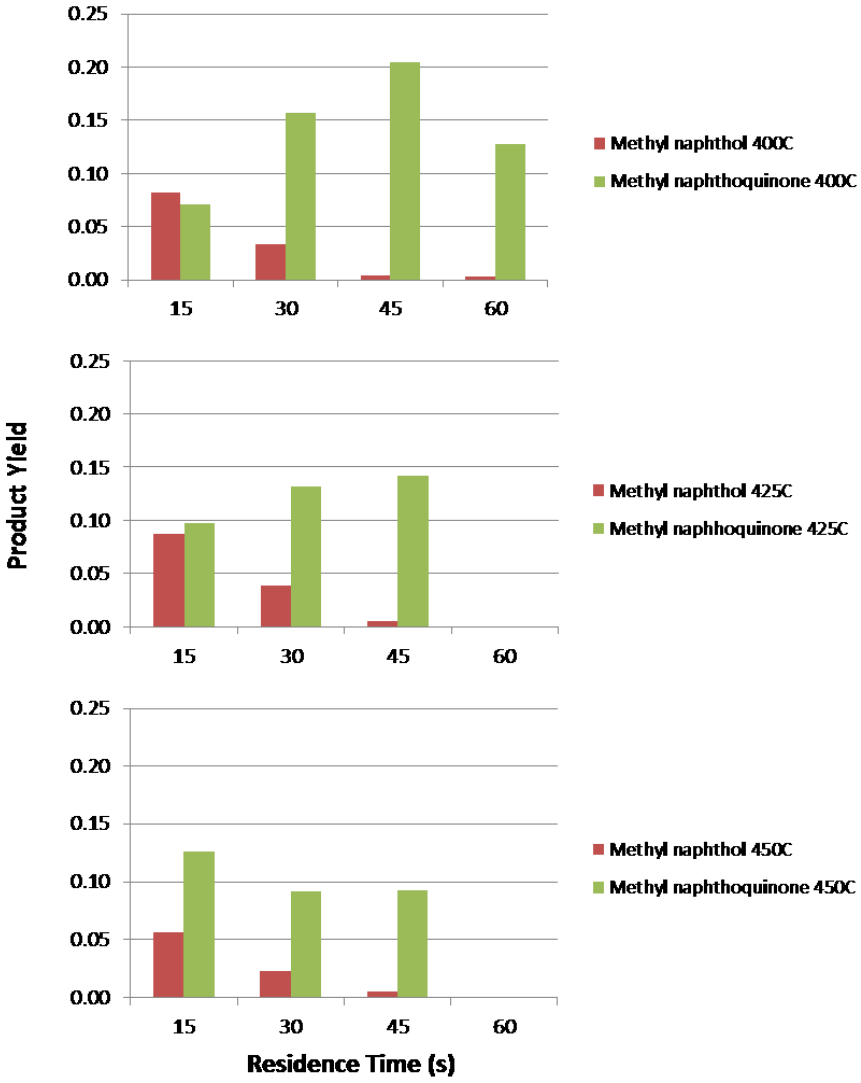


*Figure 6.10 Yields to methyl naphthol and methyl naphthoquinone at 230 bar, 0.05 $O/O_{stoich}$ ratio, water/org ratio of 12, residence times of 15, 30, 45 and 60 s and temperatures of 400, 425 and 450 °C*

The remaining products of reaction were obtained in lower concentrations, which represented yields below 2% of the initial methyl naphthalene input as seen in Figure 6.11. This is thought to be the result of a fast decomposition leading to gas products. Phthalic anhydride showed a similar trend to that of methyl naphthoquinone. It was observed that at 400 °C, yields of phthalic anhydride increased with residence time to find a maximum at around 30 s and then decreased with further increments in residence time. At higher temperature the highest yield was obtained at 15 s and a gradual decrease with residence

time was observed. Dialkyl phthalate showed higher yields at short residence times and then gradually decreased at longer residence times. The reduction in the yields to intermediate products with time is thought to be due to further thermal decomposition of the intermediate products leading to gas.

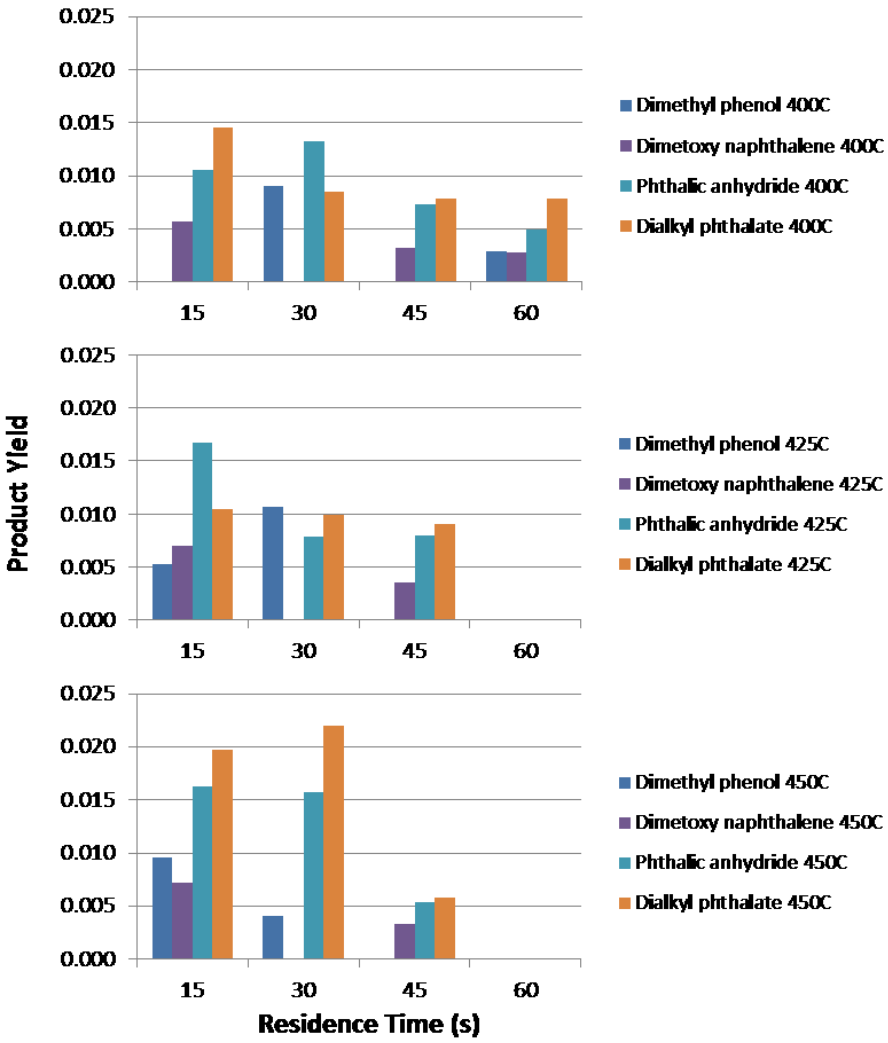


*Figure 6.11 Yields to organic soluble products at 230 bar, 0.05 $O/O_{stoich}$ ratio, water/org ratio of 12, residence times of 15, 30, 45 and 60 s and temperatures of 400, 425 and 450 °C.*

Low yields of dimethyl phenol and dimethoxy naphthalene were obtained. The trend observed with dimethyl phenol was greatly dependent on the reaction temperature. At 400 °C it was only detected at 30 s residence time. When reaction temperature increased to 425 °C an increase in the yield to dimethyl phenol was observed between 15 and 30 s, while further increases in temperature inverted the trend with higher yields to phenol at 15 s than 30 s. This behavior suggests that dimethyl phenol is not too stable and it may have

decomposed or further reacted to form gas rapidly. Dimethoxy naphthalene proved to be a minor product as very low yields, under 0.5%, were obtained at all conditions studied.

Based on the trends observed for the yields and product distribution at different residence times and reaction temperatures, a reaction pathway has been proposed in Figure 6.12. The potential reactions identified in the process are oxidation, tautomerism, $H_2O$ reduction, loss of CO, alcohol addition and ring opening. Similar reactions have been reported in literature for systems involving the oxidation of polycyclic aromatic compounds in NCW and SCW (107–109,196,214).

The initial step of reaction is the oxidation of methyl naphthalene to produce methyl naphthol [1], which involves the hydroxylation of an aromatic ring in the molecule (196). Identifying methyl naphthol as product is of great relevance as in results previously discussed for the batch system, it was suggested that hydroxylation to form an alcohol was the initial reaction step but no experimental proof was obtained. Moreover, the high yields to naphthol obtained at 15 s residence time and the important decrease in its concentration with time suggest that this reaction step proceeds fast. Once methyl naphthol has been formed, it continues to react to form methyl naphthoquinone through further hydroxylation and tautomerism [2]. High yields obtained for this product at all residence times studied give an indication that it is the main reaction intermediate. Methyl naphthoquinone could further react to produce phthalic anhydride [3]. It is thought that this reaction step consists of a series of fast reactions in which methyl naphthoquinone reacts through decarboxylation to form phthalic acid (196). Then phthalic acid would further react to form phthalic anhydride (215), which is thought to be a very fast reaction as phthalic acid was not observed during the product analysis. Further reaction of the phthalic anhydride to produce dialkyl phthalate has been considered [4]. Similarly, it is believed that this occurs through a series of fast reactions in which the addition of alcohol molecules and ring opening occur to achieve the esterification of the molecule (215). The ester formed will continue to react through cracking of aliphatic chains and ring opening to form gas products. Dimethyl phenol is thought to be produced by two potential routes, the decomposition of methyl naphthoquinone or phthalic anhydride [5, 6]. The first route is believed to follow a series of fast reactions including ring opening, oxidation and loss of CO as reported in literature (196). Similarly, the second route is thought to proceed through a series of reactions as epoxidation, condensation and ring opening with loss of water (196). Finally, the formation of dimetoxy naphthalene is thought to be the result of the reaction between methyl naphthalene and metoxy radicals formed from the cracking of other intermediate products [7] (210). This reaction is thought to be reversible based on the trend observed for the yields in Figure 6.11, where dimetoxy naphthalene was identified at 15 s and at longer residence times of 45 s and 60 s.

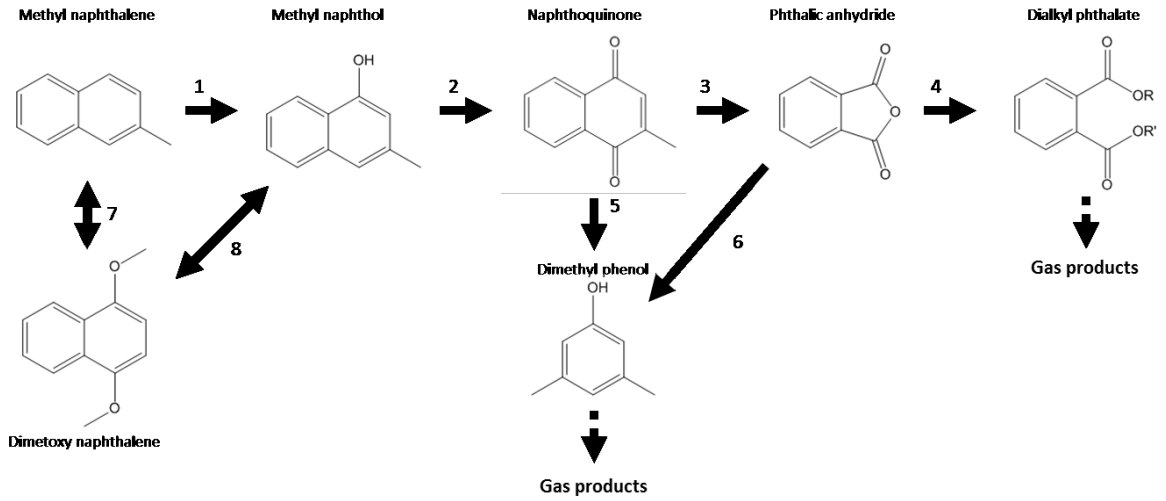


*Figure 6.12 Proposed reaction pathway for the oxidative cracking of methyl naphthalene in SCW.*

*Table 6.4 Summary of reactions proposed for the reaction pathway of the oxidative cracking of methyl naphthalene in SCW.*

| Reaction | Pathway |
|---|---|
| [1] | Formation of methyl naphthol from methyl naphthalene through oxidation. |
| [2] | Formation of methyl naphthoquinone from methyl naphthol through hydroxylation + tautomerism |
| [3] | Formation of phthalic anhydride from methyl naphthoquinone through decarboxylation forming phthalic acid. |
| [4] | Formation of dialkyl phthalate from phthalic anhydride through alcohol addition + ring opening + esterification. |
| [5] | Formation of dimethyl phenol from methyl naphthoquinone through ring opening + oxidation + loss of CO. |
| [6] | Formation of dimethyl phenol from phthalic anhydride through epoxidation + condensation + ring opening + $H_2O$ loss. |
| [7] | Formation of dimetoxy naphthalene from methyl naphthalene from metoxy radicals originated in cracking reactions. |

## 6.4. CONCLUSIONS

Experiments to study the oxidative cracking of heavy oil model compound methyl naphthalene at early reaction stages in a flow reactor were performed. The continuous flow reactor designed and built for this study enabled operation at short residence times below 1 min and facilitated the recovery and separation of the reaction products for analysis.

Experimental results showed that at the reaction conditions studied, methyl naphthalene conversions over 30% were achieved, which shows that the oxidation of the polycyclic aromatic structure is a relatively fast reaction. It was observed that the oxidative cracking process have two reaction regimes: the first at very short residence times in which an

important concentration of ROS are present and a second one where these species have been mostly consumed and the reaction medium is SCW alone. In the first regime, high conversions of methyl naphthalene are achieved and an increase in the yield to organic soluble products is observed. In SCW water alone methyl naphthalene does not react showing that PAHs are unreactive. On the contrary, oxygenated intermediate products continue to react in SCW alone to form lighter products and gas. As expected, yields to coke were low at all reaction conditions studied. Selectivity to organic soluble products was found to be high, over 60%, at short residence times (15 s) and to greatly decrease with increments in temperature and residence time. This is due to a combination of two factors, the lack of reactivity of methyl naphthalene in SCW alone and the decomposition of oxygenated intermediates mainly to produce gas.

It was observed from the molar O/C ratio in the organic soluble fraction that the incorporation of oxygen in the PAH structure effectively occurred. In addition it was concluded that the molar O/C ratio initially increases with an increase in residence time as a result of the oxidation reaction to reach a maximum and then decrease gradually at longer residence times due to the cracking and decomposition reactions of intermediate products to produce CO and $CO_2$.

Analysis of the gas product obtained showed that at early stages of the oxidative cracking reaction the gas produced is mainly composed of CO and $CO_2$. However, an important relation between $H_2$ concentration, residence time and temperature was observed. An increase in residence time and/or temperature resulted in an important increase in the amount of $H_2$ produced. It was concluded that $H_2$ produced was the result of the non-catalytic WGSR of CO produced and water available in the system.

Finally, methyl naphthol and methyl naphthoquinone were found to be the main organic soluble products of reaction. The formation of methyl naphthol was identified as the initial reaction step in the oxidative cracking of methyl naphthalene. A potential reaction pathway for the process based on experimental trends of each organic soluble product and information found in literature was proposed.

# Chapter 7
# Oxidative Cracking of Vacuum Residue in Supercritical Water

This work focuses in the study of the oxidative cracking of heavy oil in SCW using Maya oil vacuum residue as real feedstock. The main objective was to assess the potential of the process to upgrade the VR into light oil fractions with a bp < 450 °C. In addition, removal of sulfur, nitrogen and vanadium from the liquid product fraction were assessed. The work is a twofold 1) the evaluation of the oxidative cracking of VR in the absence of a catalyst at different reaction temperatures and 2) the comparison between the catalytic and non-catalytic oxidative cracking of VR using Y-zeolite and Mn-Y-zeolite as catalysts. Experiments on the non-catalytic oxidative cracking of VR were performed at 400, 425 and 450 °C in order to assess the effect of temperature on VR conversion, asphaltene conversion, yield to products, heteroatom removal, metal removal and molecular weight distribution of the liquid product. Results obtained at 425 °C in the absence of a catalyst were compared with the ones obtained in the presence of Y-Zeolite and Mn-Y-Zeolite as catalysts in order to evaluate its performance.

## 7.1. INTRODUCTION

A high percentage of the oil produced worldwide is obtained through catalytic cracking processes using zeolites (185). Zeolites are porous crystalline structures made out of alumino-silicates arranged in tetrahedral structures with Si and Al ions in the center and four oxygen atoms at the corners (216). Figure 7.1 shows a schematic representation of the basic structure of a zeolite previously described. Y-zeolite (faujasite) is the most widely used due to its high thermal stability and high concentration of acid sites, which are favorable for oil refining applications. Zeolites consist of sodalite cages joined together to form a large pore structure (super cage) with large cavities that are connected through 4 large windows as shown in Figure 7.2.

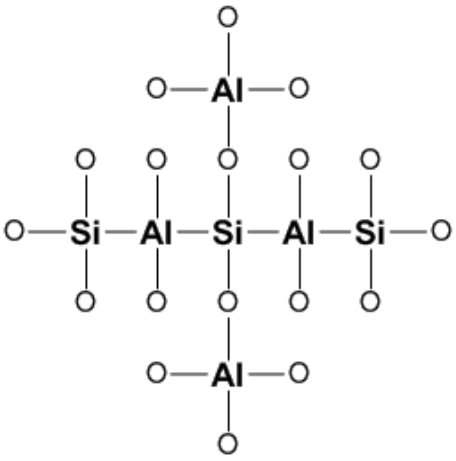


*Figure 7.1 Schematic representation of the basic tetrahedral structure of a zeolite*

The internal cavities that conform the pore structure are approximately 12 Å in diameter and the windows that link them of approximately 8 Å (217).

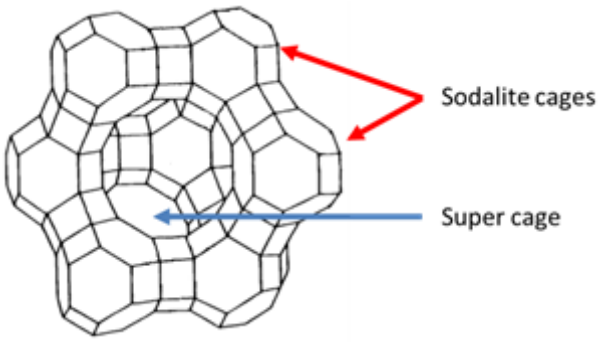


*Figure 7.2 Y-zeolite (faujasite) structure adapted with permission from (218). Copyright 1994 American Chemical Society.*

Metal oxide catalysts with zeolite as support were effectively used in the complete oxidation of chlorophenol in SCW. It was reported that the presence of this catalyst increased activity and reduced the formation of large molecular weight by-products (219,220).

Furthermore, transition metal oxides have been extensively considered for heterogeneously catalyzed oxidation reactions in SCW. It was observed that the performance of these catalysts greatly depends on the reaction conditions as the stability of the catalyst in occasions was insufficient and problems due to chemical modification and leaching were reported (144). However, manganese oxide has shown to be hydrothermally stable, highly active and resistant to metal leaching during oxidation reactions in SCW. It was reported that

the role of manganese oxide is mainly to increase the rate of formation of reaction intermediates, which results in a significant acceleration of the oxidation rates in SCW (221). Moreover, $MnO_2$ has proven to be effective in the oxidation of phenol (222), acetic acid (223) and pyridine (224) used as model compounds.

In this work, upgrading of heavy oil through oxidative cracking in SCW was studied using VR as real heavy oil feedstock. Yields to light liquid products with boiling point below 450 °C, gas and coke were determined. Changes in the molecular weight distribution of the liquid product fraction as well as in the fractionated maltene and asphaltene fractions were analyzed. Moreover, heteroatom (N and S) and metal removal (V) were also determined. Ni concentrations were not reported as the results were not conclusive due to the presence of Ni from the degradation of the reactor walls especially at high temperatures. Thermal runs were compared with the ones performed with the addition of Y-zeolite and in-house synthesized Mn-Y-zeolite catalysts. The performance of the catalyst was evaluated in terms of the yields to different products, heteroatom and metal removal.

## 7.2. EXPERIMENTAL

Experiments on the oxidative cracking of VR were performed in a SS microbomb reactor extensively described in Section 3.2.1 and Section 4.1.1. Briefly, the reactor was filled with 0.5 g of Maya oil VR and the required amount of DI water, $H_2O_2$ solution and catalyst to achieve reactions in SCW conditions at 230 bar, 60 min, O/VR ratio of 0.15 $g_{O_2}/g_{VR}$ and a cat/VR ratio of 0.25 $g_{cat}/g_{VR}$. Products of reaction were recovered and analyzed following the procedures detailed in Section 4.1.1.3.2 and Section 4.1.3 respectively. The Mn-Y-zeolite catalyst used was synthesized following a traditional ion exchange method as detailed in Section 4.2.1. The catalyst characterization was performed as described in Section 4.2.2. Different temperatures of 400 °C, 425 °C and 450 °C were implemented to assess the thermal effect on the reaction.

## 7.3. RESULTS AND DISCUSSION

### 7.3.1. Catalyst characterization

Textural properties of the catalysts were determined through $N_2$ adsorption technique and are reported in Table 7.1. It was observed that after incorporating manganese to the zeolite structure through ion exchange, the surface area of the catalyst increased 18% with respect to the original zeolite. It was observed that the introduction of Mn into the structure of the

zeolite resulted in a decrease in the pore diameter with respect to the original zeolite. However, both the Y-zeolite and the Mn-Y-zeolite remained within the microporous material range. The adsorption isotherms of the Y-zeolite and Mn-Y-zeolite can be found in Appendix 11.2.11.1.

*Table 7.1 Textural properties of the catalysts determined through $N_2$ adsorption.*

| | Y-zeolite | Mn-Y-zeolite |
|---|---|---|
| **BET Surface area ($m^2/g$)** | 430 | 510 |
| **Total pore volume ($cm^3/g$)** | 0.22 | 0.30 |
| **Pore diameter (Å)** | 7.69 | 4.73 |

Chemical composition and metal loading of the catalyst determined through ICP are presented in Table 7.2. It was observed that during ion exchange procedure Mn was successfully incorporated into the zeolite structure to produce a catalyst with 6.2 wt% of the metal. It was also noted that after the ion exchange, the Si/Al ratio of the catalyst had small changes and remained high, which is important as it determines the activity and stability of the catalyst (216).

*Table 7.2 Catalyst composition determined through ICP.*

| | Y-zeolite | Mn-Y-zeolite |
|---|---|---|
| **Si (%w/w)** | 25.1 | 22.6 |
| **Al (%w/w)** | 8.9 | 8.2 |
| **Na (%w/w)** | 1.1 | 1.3 |
| **Mn (%w/w)** | 0 | 6.2 |
| **Si/Al ratio** | 2.8 | 2.8 |

The presence of the metal in the catalyst was corroborated through EDX analysis of a sample of fresh calcined catalyst from a spot analyzed by SEM-EDX as shown in Figure 7.3. SEM analysis of the catalyst showed an irregular pseudo-spherical morphology. SEM images can be found in Appendix 11.2.11.2.

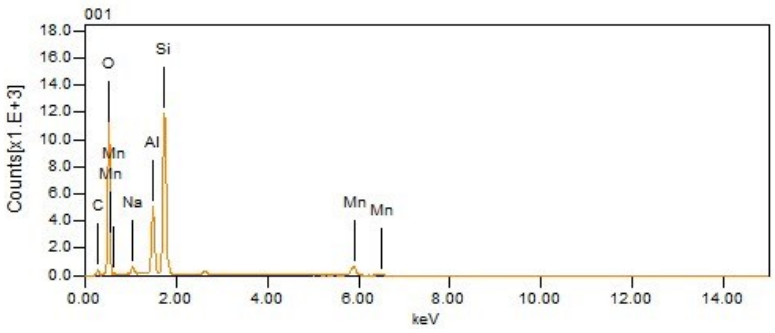


*Figure 7.3 EDX analysis of a SEM micrograph at 1.5k magnification for Mn-Y-Zeolite catalyst.*

The XRD diffraction patterns of the Y-zeolite and the Mn-Y-zeolite are shown in Figure 7.4. The diffraction analysis shows reflections at low intensity values of 2Θ around 6.2°, 15.6° and 31° for both catalysts, which are indicative of the faujasite structure of the zeolite (225). Determination of the crystal size of both catalysts showed that Y-zeolite and Mn-Y-zeolite have an average crystal size of 112.1 nm and 120.7 nm respectively. Moreover, Mn-Y-zeolite difractogram does not show any reflection specific of Mn, which suggests that the metal is completely dispersed throughout the structure and there are no perceptible metal accumulations in the material that can be detected through XRD.

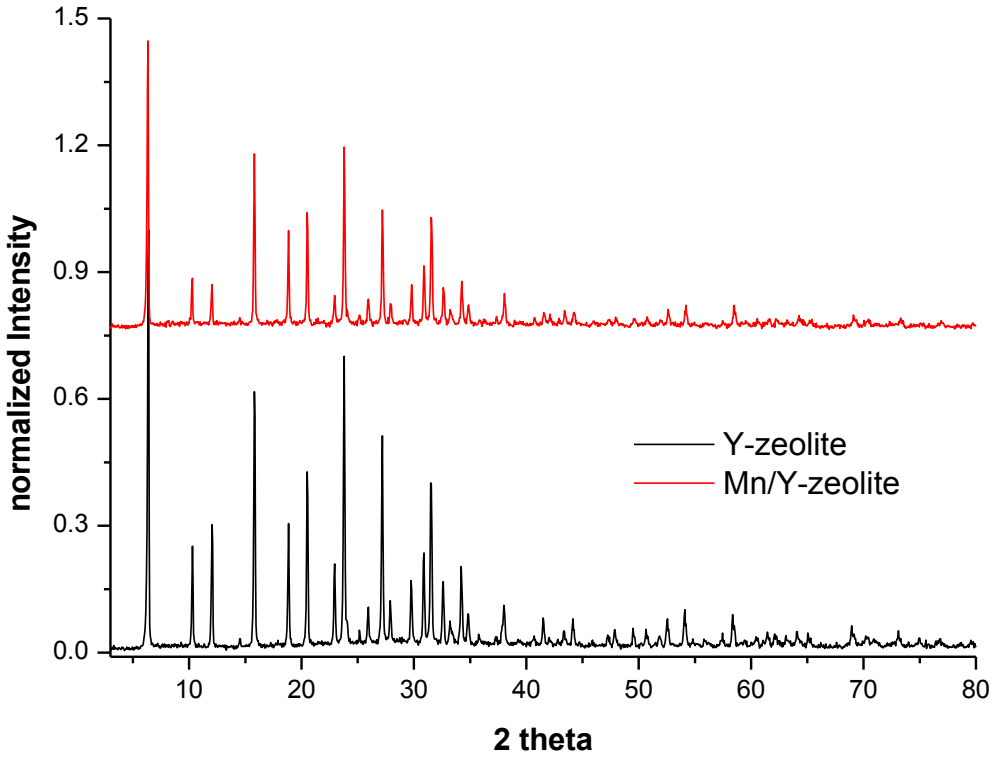


*Figure 7.4 XRD patterns of the calcined Y-zeolite and Mn-Y-zeolite catalysts.*

### 7.3.2. Experimental results

Maya oil VR as a heavy oil feedstock was upgraded through oxidative cracking in SCW. Results obtained were presented and analyzed as VR conversion, VR conversion to products with bp < 450 °C, yields to products (asphaltene, heavy maltene, liquid products with bp < 450 °C, gas and coke), heteroatom conversion (sulfur and nitrogen) and metal conversion (vanadium). These were calculated using Equations 7.1 – 7.7. In this work two different definitions of conversion were used. The first is denominated total conversion,

which considers gas, liquid product with bp < 450 °C and coke as reaction products. It was calculated using Equation 7.1 where $m^0_{VR}$ stands for the initial mass of VR, $m_A$ for the mass of asphaltenes recovered and $m_{HM}$ for the mass of heavy maltenes (bp > 450 °C).

$$Conversion_{VR} = \frac{m^0_{VR} - (m_A + m_{HM})}{m^0_{VR}} \quad (7.1)$$

The second is a conversion to light products boiling below 450 °C and considers coke as unconverted material, which means that an increase in coke formation will impact the value negatively giving a good indication of the performance of the system. It was calculated using Equation 7.2 where $m_{coke}$ stands for the mass of coke recovered as product.

$$Conversion_{bp<450C} = \frac{m^0_{VR} - (m_A + m_{HM} + m_{Coke})}{m^0_{VR}} \quad (7.2)$$

Asphaltene conversion was determined with Equation 7.3 where $m^0_A$ stands for the mass of asphaltenes in the VR originally loaded.

$$Conversion_{Asphaltene} = \frac{m^0_A - m_A}{m^0_A} \quad (7.3)$$

Heteroatom and metal removal from the liquid product was determined using Equations 7.4, 7.5 and 7.6, where $m^0_S$, $m^0_N$ and $m^0_V$ stand for initial mass of sulfur, nitrogen and vanadium respectively and $m_S$, $m_N$ and $m_V$ for the mass in the liquid product recovered.

$$Sulphur_{Removal} = \frac{m^0_S - m_S}{m^0_S} \quad (7.4)$$

$$Nitrogen_{Removal} = \frac{m^0_N - m_N}{m^0_N} \quad (7.5)$$

$$Vanadium_{Removal} = \frac{m_V^0 - m_V}{m_V^0} \quad (7.6)$$

Finally the yields to the different products obtained were calculated with Equation 7.7 where $m_n$ stand for the mass of the product analyzed.

$$Yield_{\ n} = \frac{m_n}{m_{VR}^0} \quad (7.7)$$

Products of reaction were classified first as gas, coke and liquid products. The latter was subdivided according to boiling point in liquid products bp < 450 °C (light maltenes) and heavy maltenes and asphaltenes, also considered as unconverted VR. Furthermore, the liquid products bp < 450 °C were classified in boiling point cuts through simulated distillation as clearly in Figure 7.5.

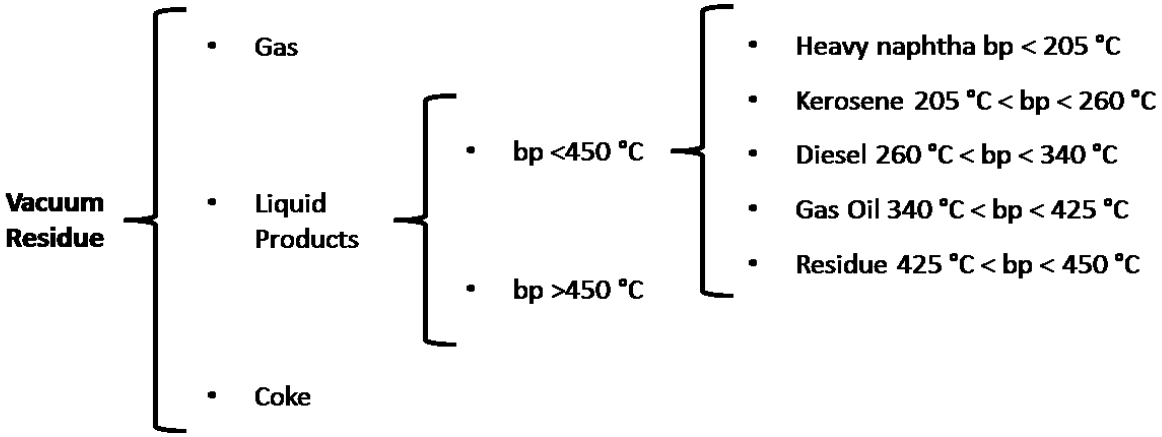


*Figure 7.5 Oxidative cracking of VR product classification according to boiling point.*

#### *7.3.2.1. Thermal oxidative cracking of vacuum residue in supercritical water*

Experiments to study the upgrading of VR through thermal oxidative cracking in SCW were performed at a pressure of 230 bar, a ratio of O/VR of 0.15 w/w and 60 min reaction time. Temperatures considered for these experiments were 400, 425 and 450 °C and no catalyst was used.

#### 7.3.2.1.1. Conversion and product yields

Figure 7.6, shows that high VR conversions above 30% were achieved at all reaction temperatures studied. As expected, an increase in temperature resulted in higher VR conversions. This behavior is well in line with the one observed for asphaltene conversion, which also increased linearly with temperature. However, an interesting trend can be observed in the conversion to liquid products with bp < 450 °C, which initially increased to find a maximum at 425 °C and then decreased with a further increase in temperature. At 400 °C it was observed that the values of both conversions are similar, which indicates that VR is mainly being converted into liquid products with bp < 450 °C and gas. This seems to be the result of a relatively low production of coke at these conditions, which is also related to the low asphaltene conversions obtained. On the contrary, at 450 °C it was observed that an important conversion difference (almost 45%) was obtained, which is mainly due to a high production of coke as product. It is thought that this can be related to the important increase in asphaltene conversion registered, which suggests that an important amount of asphaltenes polymerized to produce coke. This is supported by the high yield to coke obtained at 450 °C as shown in Figure 7.7.

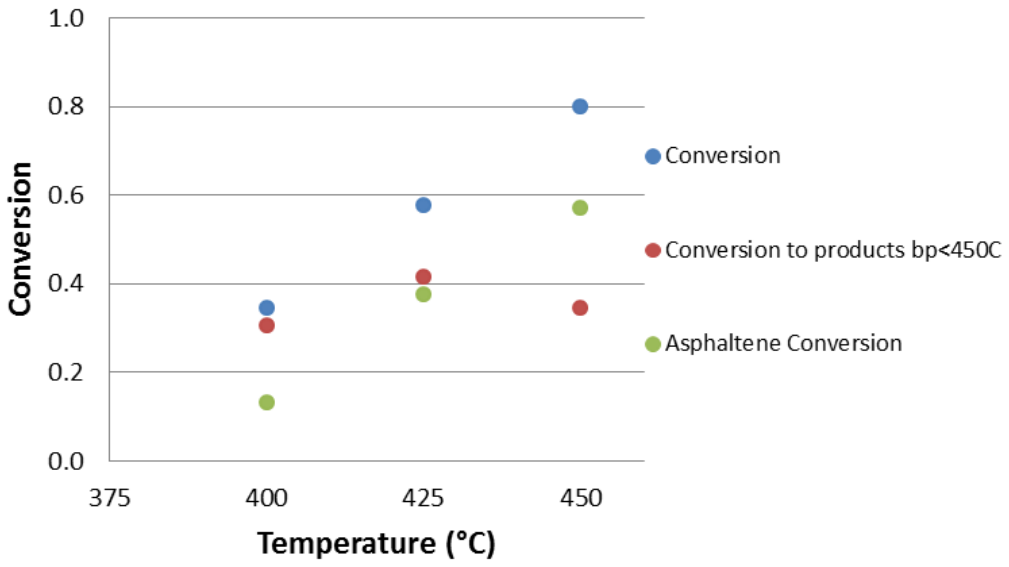


*Figure 7.6 Conversion, conversion to products with bp< 450 °C and asphaltene conversion for the thermal oxidative cracking of VR in SCW at 230 bar, 60 min and O/VR ratio of 0.15.*

Figure 7.7, shows the yields to different products at the three temperatures studied. It was observed that product distribution was greatly dependent on the process temperature. At

400 °C the heavy maltene fraction reacted to produce mainly light maltenes and some gas while the asphaltene fraction remained almost unreactive. Moreover, low yields to coke were obtained at these conditions. Overall, as expected, an increase in temperature resulted in a decrease in the yields to liquid products with bp < 450 °C and an increase in the yields to gas and coke. At 425 °C yields to light maltenes remained high, near 17%, while yields to gas and coke increased from 10% to 23% and 4% to 16% respectively. A further increase in temperature to 450 °C showed that almost all heavy maltenes and more than half of the asphaltenes were converted. However, most of the products obtained were gas and coke with a low yield to light maltenes below 5%. From these results it can be concluded that at lower temperatures closer to the critical point mainly cracking reactions of the heavy maltenes to produce liquid products with bp < 450 °C take place. However, at high temperatures gas formation and polymerization reactions leading to coke play an important role. These results are in good agreement with the trends presented in Chapter 5, where it was observed that an increase in temperature after it surpassed the critical temperature of water resulted in an increase in the yields to gas and coke.

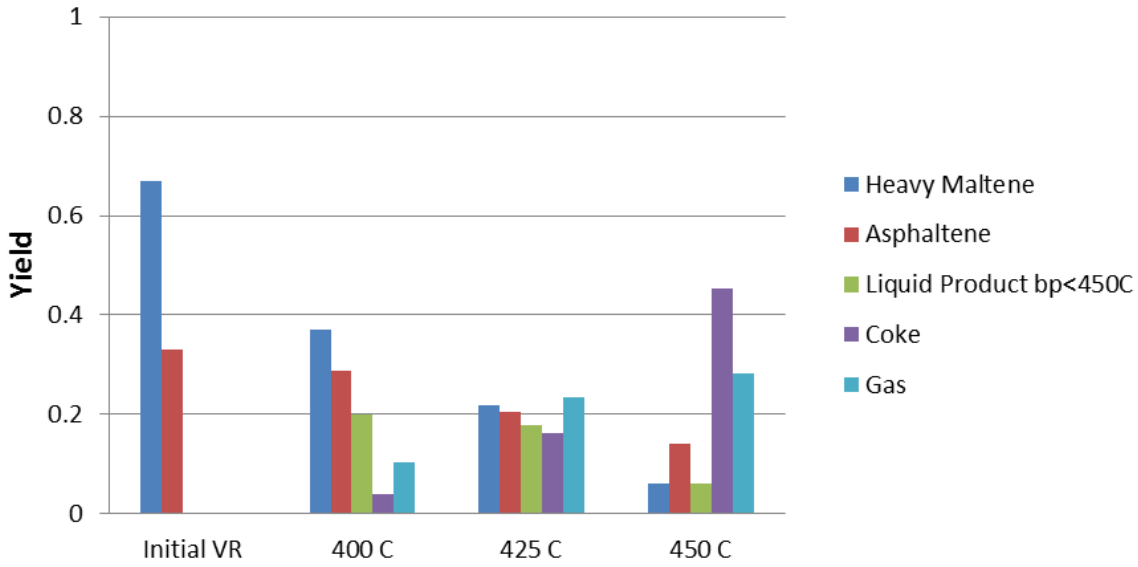


*Figure 7.7 Yields to products from the thermal oxidative cracking of VR in SCW at 230 bar, 60 min and O/VR ratio of 0.15 compared to the composition of the original VR.*

Changes in the boiling point distribution of the liquid products with bp < 450 °C fraction were observed at the different temperatures studied, as shown in Figure 7.8. At 400 °C, despite the higher yields to light maltenes obtained at this temperature, the average boiling point remained high as 40% of it was composed of residue fraction. However, an increase in

temperature produced a decrease in the yields to residue fraction, which is thought to be the result of an increase in rates of thermal cracking of heavier components.

Yields to kerosene and heavy naphtha remained low at all temperatures studied. Nevertheless, they showed a similar trend to the one observed in the residue fraction, decreasing with temperature to negligible yields at 450 °C. Similarly, it is believed that this decrease is due to an increase in the cracking rates, in this case to produce gas. This is in good agreement with the increase observed in the yields to gas. Interestingly, a completely different trend was observed in the yields to diesel and gas oil, which initially increased to find a maximum at 425 °C and decreased when temperature was further increased to 450 °C. This is a very important finding as the variation in the yields to light maltene obtained between 400 °C and 425 °C is very low as shown in Figure 7.7, but an important increase in the yield to diesel and an increase in the yield to gas oil were observed. From these observations, it can be established that 425 °C appears to be the optimum temperature to perform the oxidative cracking of VR due to the high yields to liquid products with bp < 450 °C and the higher selectivity to diesel and gas oil.

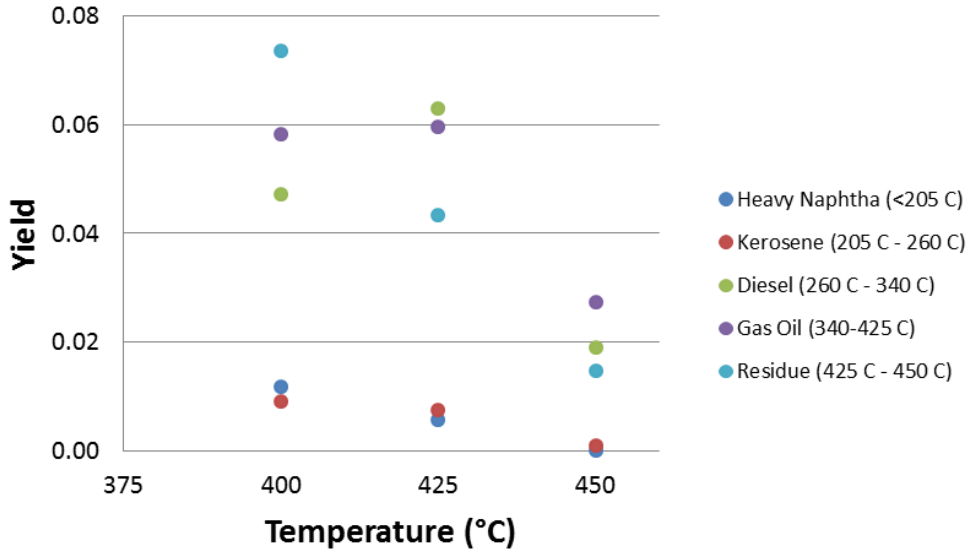


*Figure 7.8 Boiling point distribution of the light maltene fraction from the thermal oxidative cracking of VR in SCW at 230 bar, 60 min and O/VR ratio of 0.15 at different reaction temperatures.*

### *7.3.2.1.2. Molecular weight distribution*

SEC studies to determine the molecular weight distribution of the liquid product as well as the maltene and asphaltene fractions were performed. These were compared with the SEC

values obtained for the original VR. Figure 7.9 shows that the chromatogram of the VR presents a bimodal distribution in which the early eluting peak is denominated the excluded peak and the second peak is named the retained peak.

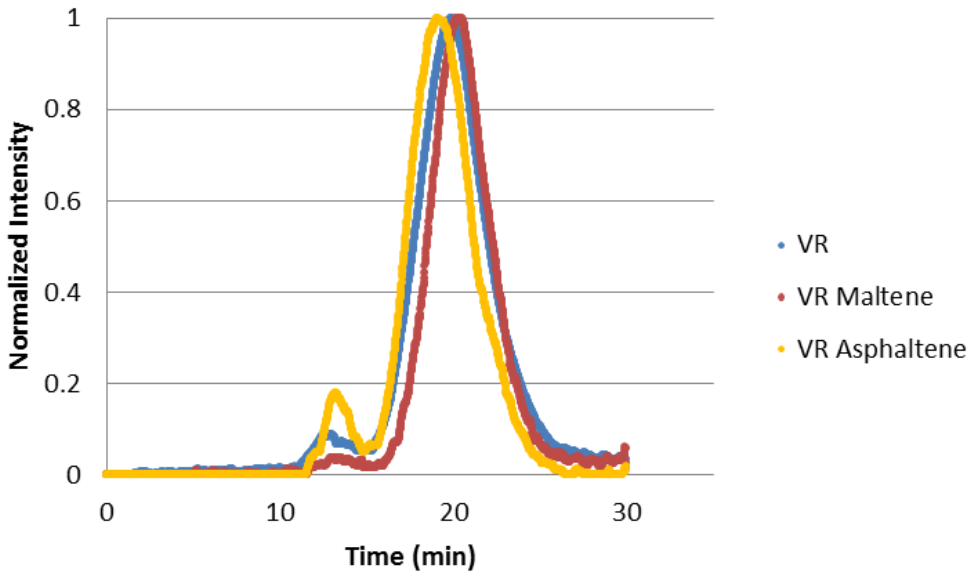


*Figure 7.9 SEC of the original VR, maltene fraction and asphaltene fraction.*

The excluded peak represents material with a high molecular mass that is unable to penetrate the column porosity and therefore present lower retention times. The retained peak corresponds to lighter products that can penetrate the pores of the column and are separated in fractions with different molecular mass, as explained in detail elsewhere (226). The retained peak of the VR showed a maximum at 19.5 min, which corresponds to an average of 520u according to the calibration shown in Appendix 11.2.5. A similar bimodal distribution was observed for the fractionated maltenes and asphaltenes, which showed a maximum in the eluted peaks corresponding to an approximate molecular weight of 280 u and 713 u respectively. In addition, it was observed that in both fractions the molecular mass range extended from a few hundred to a few thousand atomic mass units as reported in Appendix 11.2.6.

Figure 7.10$_A$, shows the SEC analysis of liquid product obtained at the three temperatures studied compared with the original VR. It was observed that a positive shift towards longer elution times was obtained with an increase in the severity of the reaction conditions, which indicates a reduction in the molecular size.

Analysis of the maltene and asphaltene fractions shown in Figure $7.10_B$ and Figure $7.10_C$ present a shift to lower molecular mass observed with an increase in reaction temperature, which is consistent with the one observed for the liquid product. Values of molecular mass ranges and maximum retained peak for each of the fractions and conditions studied can be found in Appendix 11.2.7. Interestingly the analysis of asphaltenes shown in Figure $7.10_C$ presents a shift in molecular mass with respect to the original VR asphaltenes, which corresponds to a reduction in molecular mass over 50% at all temperatures studied. This result is particularly important for reactions performed at 400 °C where low asphaltene conversions were registered, as it proves that even at low reaction temperatures cracking of asphaltenes leading to lower molecular mass products still in the range of asphaltene occurs.

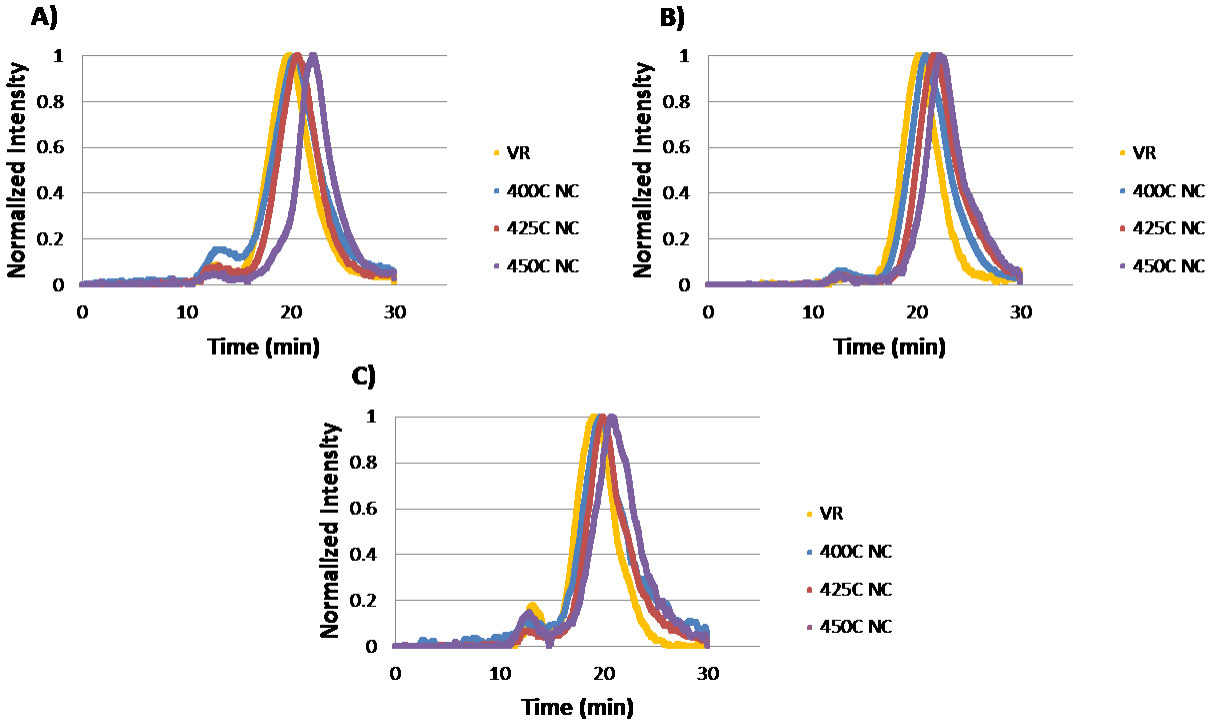


Figure 7.10 SEC analysis of A) the liquid product, B) maltene fraction and C) asphaltene fraction from the thermal oxidative cracking of VR in SCW *at 230 bar, 60 min and O/VR ratio of 0.15.*

### *7.3.2.1.3. Heteroatom and metal removal*

Sulfur and nitrogen contents in the liquid product recovered were determined through elemental analysis while vanadium concentration was determined through ICP-OES. Figure 7.11 shows an increasing trend in sulfur, nitrogen and vanadium removal from the liquid

product with an increase in temperature. It was observed that at low temperatures nitrogen and vanadium were practically unreactive, while near 20% of the sulfur was successfully removed. However, an increase in temperature showed to have a great impact especially in nitrogen and vanadium, which reached removal percentages around 80% at 450 °C. Sulfur removal also showed an increasing trend with temperature but this was less pronounced than the one observed for nitrogen and vanadium. It is thought that at the reaction conditions studied, heteroatom and metal removal is strongly linked to the yield to coke and follow a similar increasing trend with temperature.

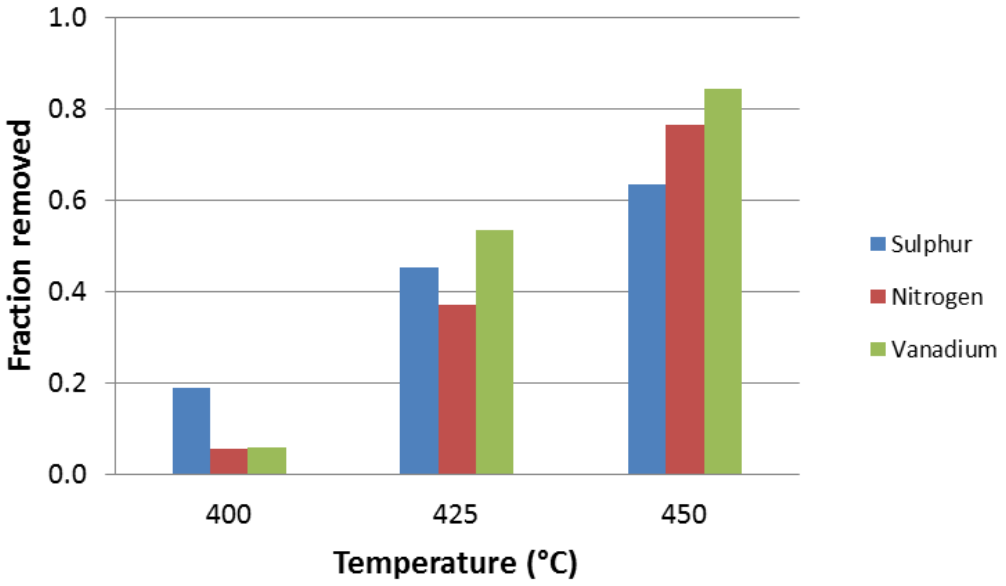


*Figure 7.11 Sulfur, nitrogen and vanadium removal for the thermal oxidative cracking of VR in SCW at 230 bar, 60 min and O/VR ratio of 0.15.*

In order to gain a better understanding on the desulfurization, denitrogenation and demetallization processes that occur during the oxidative cracking of VR a complete mass balance for S, N and V was performed. Samples of liquid product, coke and aqueous fractions were analyzed. Sulfur and nitrogen concentrations in the gas fraction were calculated by difference to close the mass balance. Results obtained for each of the components are shown in Figure 7.12.

Figure $7.12_A$ shows the sulfur distribution in the product fractions obtained. It was observed that at all temperatures the amount of sulfur removed in the gas phase remained constant in a range between 12 and 14 % w/w. However, opposing trends were observed in the weight percent of sulfur found in the liquid and coke fractions, which decreased and increased,

respectively, with an increase in reaction temperature. It is believed that the reactivity and distribution of sulfur in the different products is strongly related with the chemical form in which sulfur is found in the original VR. It was reported that sulfur in the form of alkyl sulfides and aromatic sulfides is considerably more reactive than sulfur in the form of thiophenes when treated in SCW (125,126). Based on this, it is believed that at low temperature, highly reactive sulfur found in the original VR was removed to the gas fraction while more stable forms of sulfur remained in the liquid product. Moreover, as the severity of the process increased, highly reactive sulfur was also removed into the gas fraction as suggested by the almost constant sulfur weight percent obtained at all reaction temperatures studied as shown in Figure 7.12$_A$. Furthermore, the decrease in the percentage of sulfur in the liquid fraction together with the increase observed in the sulfur content in coke with increasing temperature suggests that more stable sulfur structures remained in the asphaltenes and took part in polymerization reactions to form coke.

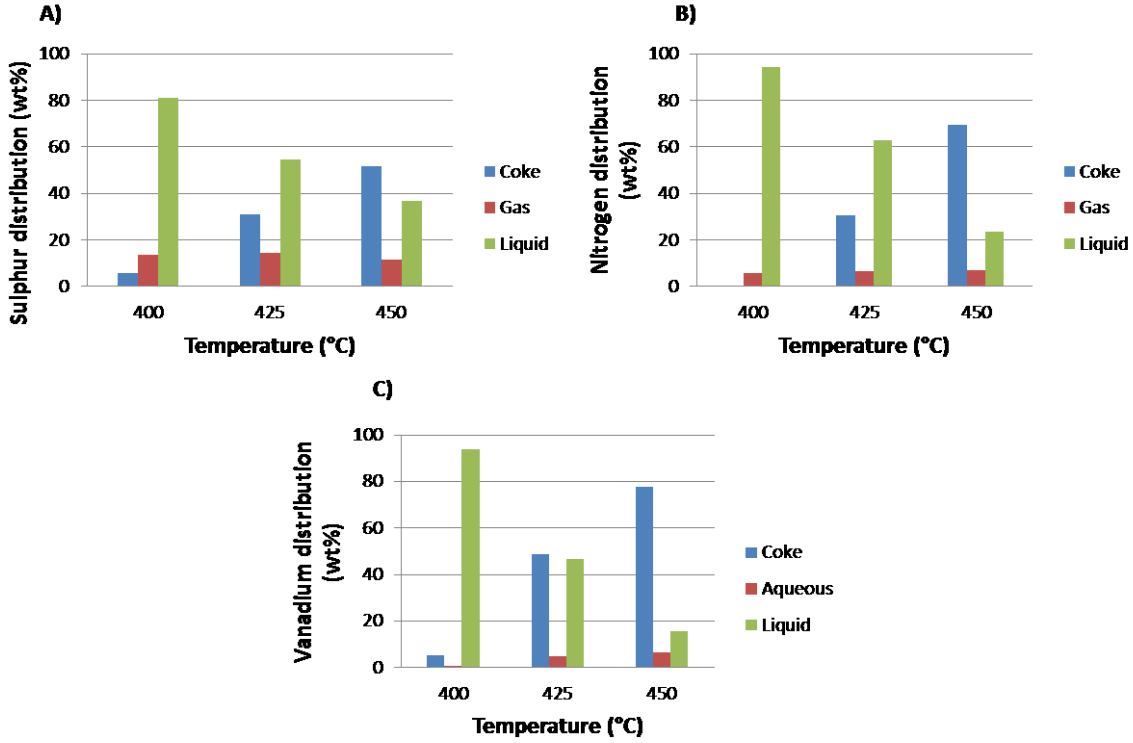


*Figure 7.12 A) Sulfur, B) nitrogen and C) vanadium mass balance for the thermal oxidative cracking of VR in SCW at 230 bar, 60 min and O/VR ratio of 0.15.*

A similar trend to that of sulfur was observed for the nitrogen distribution within the reaction products, shown in Figure 7.12$_B$. It was observed that a low percentage of nitrogen was removed into the gas fraction and it remained constant at the different reaction

temperatures. On the other hand, nitrogen presented a pronounced decrease in the percentage found in the liquid fraction and a sharp increase in the percentage found in coke. Interestingly at 400 °C no nitrogen was found in the coke fraction. This, added to the low percentage of nitrogen obtained in the gas fraction and the low nitrogen conversion at low temperature, suggests that reactivity of nitrogen found is VR was very low and most of the nitrogen present is removed through polymerization into coke. Reports in literature show that heterocyclic nitrogen and sulfur are structures with high thermal stability in SCW (110). Moreover, it was reported that sulfur containing structures tend to be more reactive than nitrogen bearing ones. This is in good agreement with the results observed, especially at 400 °C, where low yields to coke were obtained and very low nitrogen removal was achieved compared to sulfur (110).

Figure 7.12$_C$ shows that vanadium product distribution presents a similar trend as the one observed for N and S. Experimental results suggest that V is found in a very stable chemical structure in VR. This becomes evident in the low reactivity observed in reactions at low temperature where 95% of the original vanadium remained in the liquid fraction. This is in good agreement with results from Vogelaar et al, who found that Ni and V porphyrins in gas oil samples remain almost unreactive in SCW at 400 °C (125). Moreover, it was observed that an increase in temperature resulted in an important increase in the percentage of vanadium found in the coke fraction. This suggests that stable metal porphyrins remain in the asphaltene structure that polymerizes into coke. A small percentage of 4.5% and 6.5% of vanadium was removed into the aqueous phase at 425 °C and 450 °C respectively, which suggests that reactivity has a slight increase with an increase in the severity of the process.

Overall, it was concluded that heteroatom and metal bearing structures found in the original VR showed great stability during oxidative cracking in SCW. Results suggest that oxidative cracking alone was not reactive enough to break the heteroatom and metal bonds within the asphaltene molecule. It was noted that high heteroatom and metal removal, especially with increasing temperature, was mainly the result of polymerization reactions of asphaltene molecules to produce coke rather than the upgrading of the heavy liquid fraction. However, it was observed that 14 % of the sulfur in the oil was reactive at the conditions studied and was removed from the oil in the form of gas. Interestingly, this percentage remained unchanged with increments in temperature, which suggests that sulfur is found in different chemical forms and that just a fraction is reactive and the rest is stable at all conditions studied. A small percentage of nitrogen (about. 5%) showed the same behavior as sulfur and was removed into the gas phase while the rest remained mostly unreactive. Vanadium showed to be unreactive at low temperature and a marginal fraction was removed into the aqueous phase at higher temperature, which suggests a slight increase in reactivity. In

conclusion, the reactivity trend observed is as follows sulfur species > nitrogen species > vanadium species.

#### 7.3.2.2. Comparison between thermal and catalytic oxidative cracking

Experiments to study the effect that the presence of a Y-zeolite or Mn-Y-zeolite catalysts have on the upgrading of VR as compared with the thermal oxidative cracking in SCW were performed. Reaction conditions chosen for this study were 230 bar, an O/VR ratio of 0.15 w/w, 60 min and 425 °C, which was the optimum temperature found in previous experiments.

##### 7.3.2.2.1. Conversion and product yields

Results on the conversion of VR and the conversion to products with boiling point below 450 °C for the thermal and catalytic oxidative cracking of VR are shown in Figure 7.13. It was observed that in the presence of both catalysts, a slight increase of 5 % in total conversion was obtained compared to thermal oxidative cracking. However, an interesting result was observed when comparing the values of conversion to products with bp < 450 °C, which showed to increase when Mn-Y-zeolite catalyst was used but showed no change in the presence of Y-zeolite. This suggests that despite of the similar value of total conversion, the use of one or the other catalyst impacts the selectivity to the products of reaction obtained.

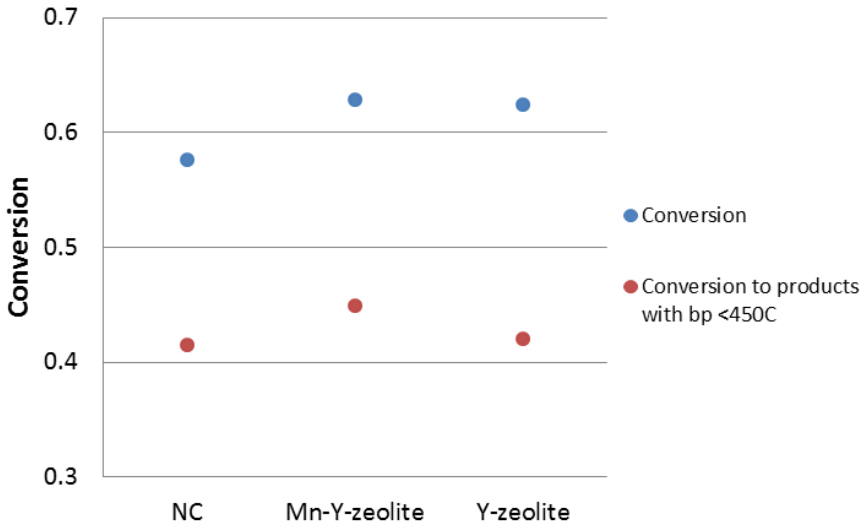


*Figure 7.13 Total conversion and conversion to products with bp < 450 °C for the thermal (NC) and catalytic oxidative cracking of VR in SCW at 230 bar, 60 min, O/VR ratio of 0.15 and 425 °C.*

The higher conversion to products with bp < 450 °C in the presence of Mn-Y-zeolite indicates that the catalyst promotes cracking reactions of VR to form lighter products. However, results in the presence of Y-zeolite catalyst show that polymerization reactions to form coke are favored.

Figure 7.14 shows the yields to the different product fractions in the presence and absence of a catalyst compared to the original VR composition. A decrease in the yield of heavy maltenes was observed in the catalytic process when compared to the one obtained in the thermal process. Interestingly, lower yields to asphaltene were obtained when reaction took place in the absence of a catalyst. Asphaltene conversion decreased 13% and 39% in reactions with Y-zeolite and Mn-Y-zeolite, respectively, compared to the one obtained through the thermal only process. It is believed that the important decrease in asphaltene conversion in the presence of a catalyst, especially for the Mn-Y-zeolite catalyst, is related to the influence that the catalyst exerts in the way asphaltenes react. The catalyst aids in the cracking of asphaltenes but also in the formation of small radicals (227) and ROS that react with large organic radicals formed preventing polymerization reactions. This can result in a reduction in the size of asphaltenes but not in the complete conversion into other products, which would explain why the yield to asphaltenes decreases in a lower proportion.

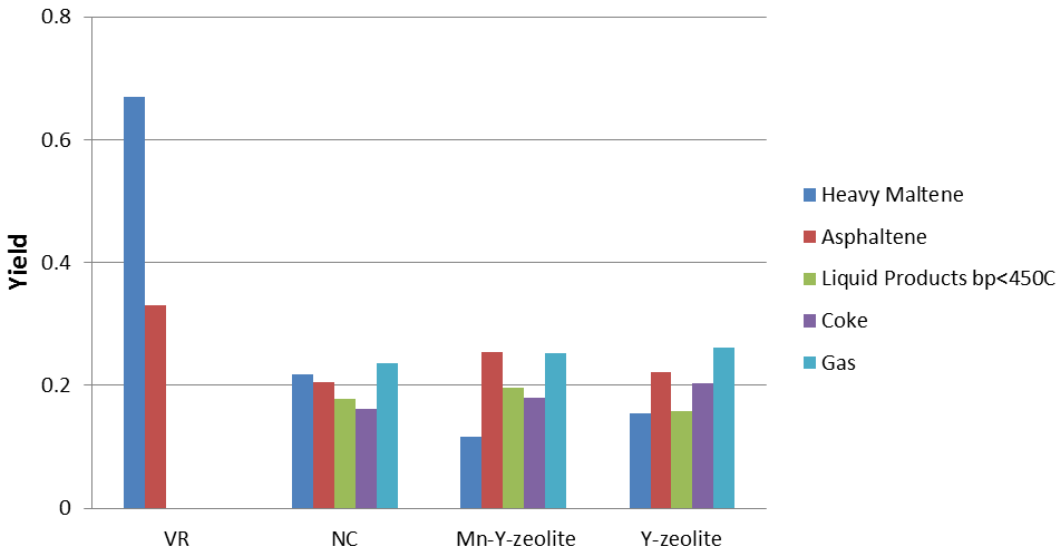


*Figure 7.14 Yields to products from the thermal (NC) and catalytic oxidative cracking of VR in SCW at 230 bar, 60 min, O/VR ratio of 0.15 and 425 °C compared to the composition of the original VR.*

Moreover, it was observed that higher yield to liquid products with bp < 450 °C around 20% was obtained when Mn-Y-zeolite catalyst was used. This represents an increment of 18% if

compared to the non-catalytic process. The opposite effect was observed when the Y-zeolite was used as it showed a decrease in the yield to liquid products with bp < 450 °C recovered of 12 % as compared to the thermal process. Yields to gas showed minor changes between catalytic and thermal processes. Only a slight increase in the yield to gas was observed when the Y-zeolite was used and this is thought to be caused by an increase in the cracking of light maltenes that can be enhanced by the acidity of the zeolite. This can explain the decrease in the yields to light maltenes observed. Similarly a slight increase in coke yield as compared to the Mn-Y-zeolite and the thermal processes was observed. This is thought to be due to the fast formation of high molecular weight organic radicals on the acid surface of the zeolite that can polymerize into coke before being stabilized.

Changes in the boiling point distribution of the light maltene fraction with the addition of both catalysts were observed, as shown in Figure 7.15. Higher yields to products with a boiling point range between 260 °C and 450 °C were obtained with the Mn-Y-zeolite catalyst, which seems to be related with the higher conversion of heavy maltenes obtained. The presence of the catalyst favored cracking reactions of heavy maltenes to lighter products, which accounts for the increase in the yields to diesel, gas-oil and residue. Negligible yields to heavy naphtha and kerosene were obtained, which suggests that at these reaction conditions in the presence or absence of a catalyst, they continue to crack mainly to form gas products.

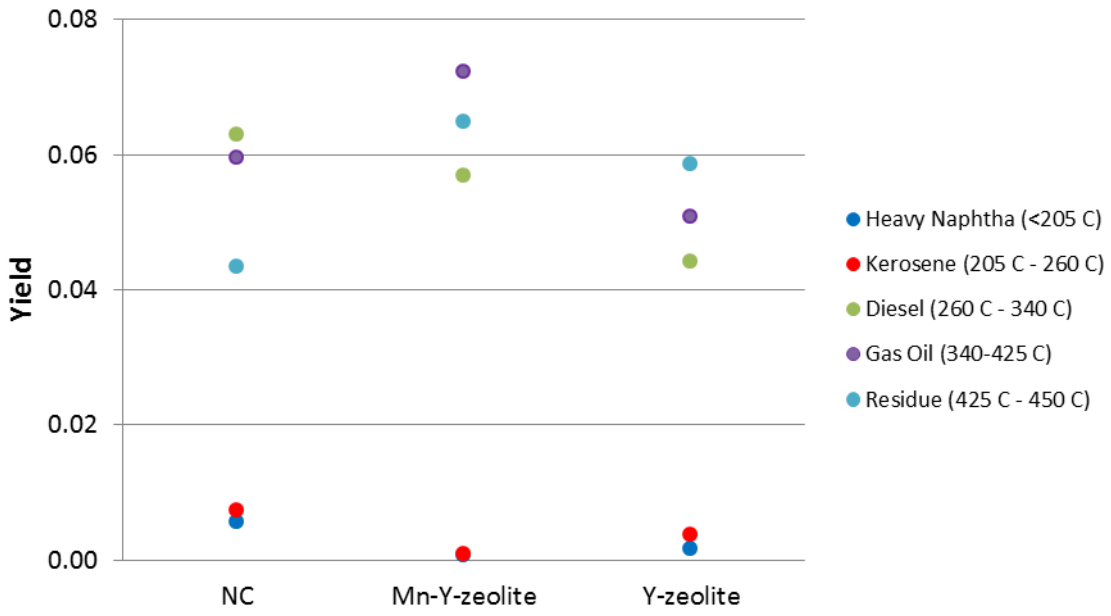


*Figure 7.15 Boiling point distribution of the light maltene fraction from the thermal (NC) and catalytic oxidative cracking of VR in SCW at 230 bar, 60 min, O/VR ratio of 0.15 and 425 °C.*

In particular, it can be said that the addition of Mn-Y-zeolite as catalyst seems to have a positive effect as it increases the yields to light maltene (residue, gas-oil and diesel) with a high commercial value mainly from an increase in the conversion of heavy maltenes. On the contrary, Y-zeolite seems to promote the cracking of light liquids to gas, which results in lower yields to light maltenes. Moreover, the higher yields to coke obtained with Y-zeolite suggest that polymerization reactions rather than cracking of heavy molecules occurs. This can be related to the role that manganese oxide plays in the reaction enhancing oxidation, which weakens heavy molecules making them prone to cracking into lighter products. This is in good agreement with reports from literature that suggest that manganese oxide play an important role as oxidizer in SCW oxidation reactions and that provides oxygen into the process (228).

#### *7.3.2.2.2. Molecular weight distribution*

Figure 7.16 shows the results of the SEC studies on the liquid product (A), maltene fraction (B) and asphaltene fraction (C) to determine the molecular weight distribution obtained compared to the values of the original VR. Retention times in the chromatograms were converted into molecular weight with a calibration curve in Appendix 11.2.5.

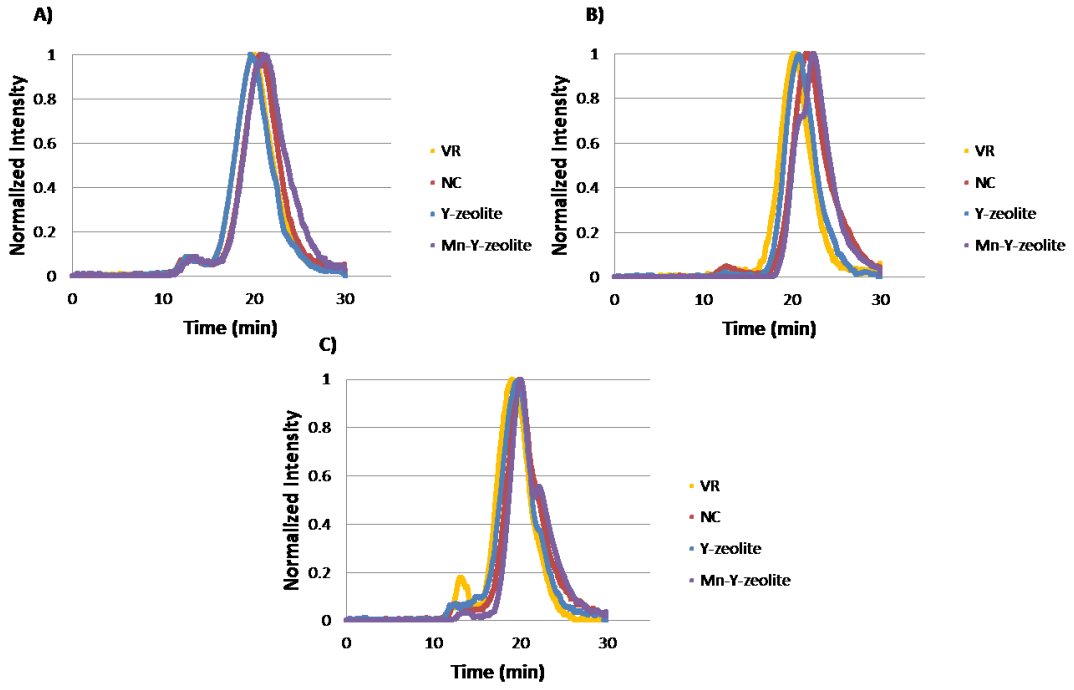


*Figure 7.16 SEC analysis of the A) liquid product, B) maltene fraction and C) asphaltene fraction from the thermal (NC) and catalytic oxidative cracking of VR in SCW at 230 bar, 60 min, O/VR ratio of 0.15 and 425 °C.*

Results of the analysis of the liquid product in Figure 7.16$_A$, show a shift to longer retention times after reaction without a catalyst and with Mn-Y-zeolite as catalyst. The greatest shift was obtained with Mn-Y-zeolite, which represents an important reduction on the average molecular weight if compared to the original VR. Interestingly, the liquid product obtained after reaction with Y-zeolite did not show a shift to longer retention times when compared to the original vacuum residue. The previous result was unexpected as the presence of the zeolite was expected to promote cracking of heavy fractions. On the contrary, it appears that the presence of Y-zeolite promotes polymerization reactions that increase the molecular weight of the sample. This is in good agreement with the higher yields to coke obtained with Y-zeolite compared to other experiments.

SEC plots of the maltene and asphaltene fractions of the product from the catalytic and non-catalytic reactions as well as the fractions of the original VR are shown in Figure 7.16$_B$ and Figure 7.16$_C$.

Results from the maltene fraction show that after reaction, a shift to longer retention times was obtained in the presence or absence of a catalyst. The magnitude of the shift observed for the maximum in the retained peak was as follows: Mn-Y-zeolite > No catalyst > Y-zeolite. Interestingly, the SEC plot obtained for the maltene fraction after reaction with Mn-Y-zeolite; show the formation of a shoulder at a lower molecular weight range apart from the maximum in the retained peak. The existence of this shoulder and the important shift in the retained peak maximum gives evidence that the Mn-Y-zeolite catalyst plays an important role in cracking reactions that result in maltenes with a lower average molecular weight.

A similar trend to the one observed for the maltene fraction was obtained for the asphaltene fraction where the magnitude of the shift in the retained peak also presents a shift in the following order: Mn-Y-zeolite > No catalyst > Y-zeolite. Similarly, it was observed that when Mn-Y-zeolite was used a shoulder at a lower molecular weight range was formed indicating that an important amount of lighter asphaltenes was formed, which suggests that cracking reactions are being promoted by the catalyst presence.

Overall, SEC results show that a reduction in molecular weight of the liquid product is achieved through oxidative cracking in SCW in the presence or absence of a catalyst at the reaction conditions studied. It was also concluded that the presence of Mn-Y-zeolite has a positive effect and produces a greater shift to a liquid product with a lower molecular weight. On the contrary, the presence of the Y-zeolite alone seems to have a negative effect if compared to the thermal only process. Analysis of the maltene and asphaltene fractions suggest that this is mainly due to the lower shift achieved in the maltene fraction as the reduction in asphaltene size was similar in all cases. This may be due to the fact that Y-

zeolite promotes cracking but also re-polymerization reactions. In contrast, Mn-Y-zeolite, apart from promoting cracking reactions, seems to prevent re-polymerization reactions which may be attributed to the role manganese oxide plays in the oxidation reaction (228). The addition of the Mn-Y-zeolite enhances oxidation reactions, which weakens the structure of heavy molecules making them prone to cracking reducing the average molecular weight of the liquid product and each of the fractions.

#### *7.3.2.2.3. Heteroatom and metal removal*

Based on the results previously discussed, it was decided to study the effect that the addition of Mn-Y-zeolite catalyst has on the removal of metals and heteroatoms as compared to the thermal process in the absence of a catalyst. Figure 7.17 shows the overall sulfur, nitrogen and vanadium removal from the liquid product in reactions with and without Mn-Y-zeolite. It was observed that an increase of 11%, 8% and 20% in the removal of sulfur, nitrogen and vanadium, respectively, were achieved in the presence of the catalyst. This combined with the small change in coke yields observed suggest that a higher percentage of heteroatoms and metals were removed from the asphaltene fraction.

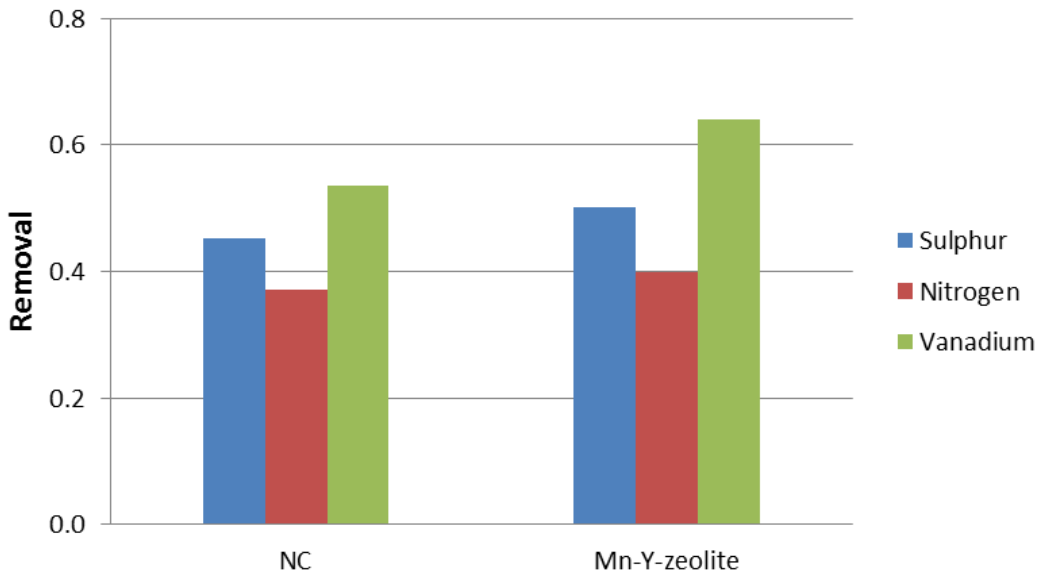


*Figure 7.17 Sulfur, nitrogen and vanadium removal for the catalytic and thermal oxidative cracking of VR in SCW at 230 bar, 60 min, O/VR ratio of 0.15 and 425 °C.*

In order to determine the effect the catalyst has on the way heteroatoms and metals are removed from VR, a complete mass balance of S, N and V was performed, as shown in Figure 7.18.

Figure 7.18$_A$, shows the percent in weight of sulfur in the different product fractions obtained in reactions with and without Mn-Y-zeolite as catalyst. It was observed that when the catalyst was used, sulfur content in the liquid fraction obtained was 5% lower. Interestingly, analysis of the coke fraction showed that the percentage of the total sulfur removed that was found in the coke was reduced from 69% to 51% in the presence of the catalyst. No sulfur was obtained in the aqueous phase, which means that an increment in the percentage of the sulfur removed in the gas increased from 31% to 49%. This suggests that the presence of the catalyst aids in the decomposition of some stable sulfur species found in VR that are not reactive in SCW alone, causing an increase in sulfur removal into the gas product fraction. Similar conclusions were reached by Timko et al, who observed that SCW alone can promote decomposition of some sulfur bearing compounds present in heavy oil but thiophenic species remain unreactive. However, when a desulfurization catalyst was added decomposition of thiophenes species was achieved (124).

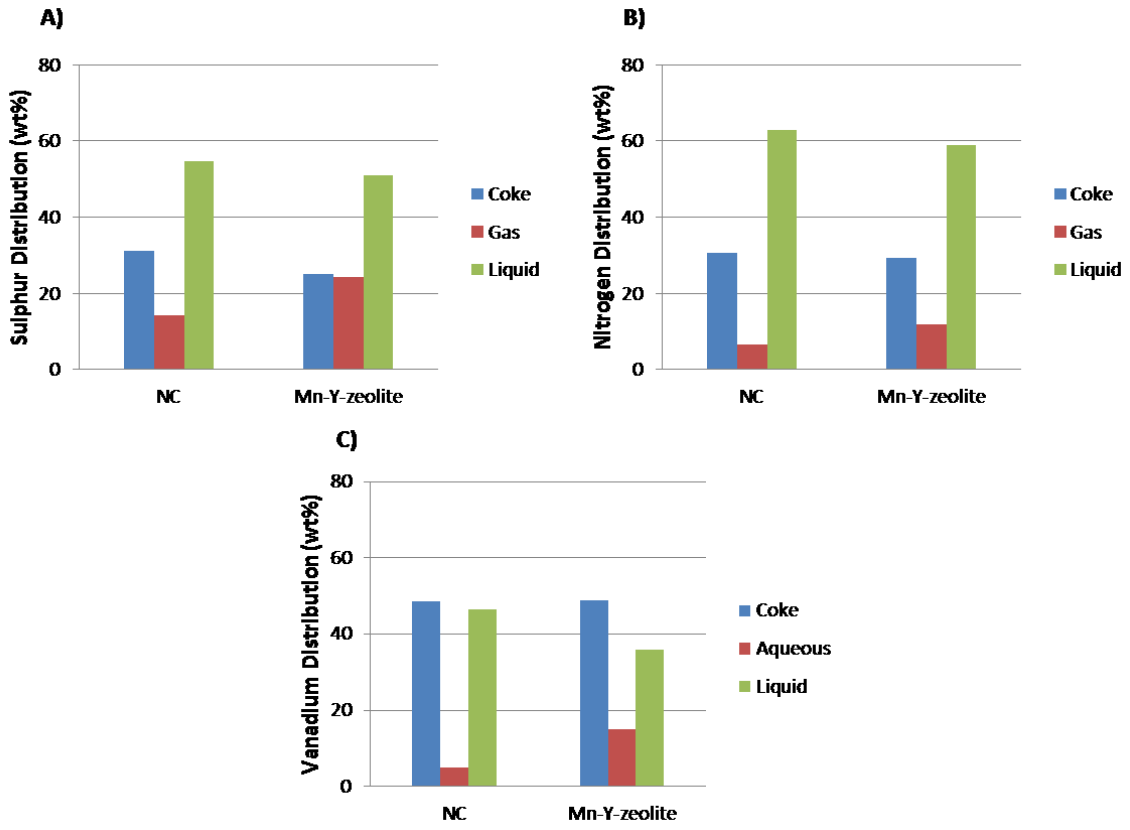


*Figure 7.18 A) Sulfur, B) nitrogen and C) vanadium mass balance for the catalytic and thermal oxidative cracking of VR in SCW at 230 bar, 60 min, O/VR ratio of 0.15 and 425 °C.*

Nitrogen removal showed a similar trend as the one previously discussed for sulfur, as observed in Figure 7.18$_B$. A decrease of 4% in the amount of nitrogen found in the liquid product was obtained when catalyst was used. This shows that the presence of the catalyst aids in the removal process of nitrogen from the original VR. Moreover, the percentage of nitrogen removed found in the coke fraction showed a decrease from 83% in the thermal process to 71% in the catalytic process. Analysis of the aqueous phase showed that no nitrogen was transferred into the aqueous phase in both the thermal and catalytic processes. These results in an increase on the percentage of the total nitrogen removed that goes into the gas phase from 17% in the thermal process to 29% in the catalytic process. This suggests that in a similar case as sulfur removal, the presence of the catalyst aids in the decomposition of highly stable nitrogen species present in VR, which results in an increase in the percentage of nitrogen in the gas phase. However, the smaller changes registered in the distribution of nitrogen within the different product fractions compared with sulfur,suggests that nitrogen species are more stable than sulfur bearing compounds, which is in good agreement with trends previously reported in literature (110).

As previously mentioned, the presence of Mn-Y-zeolite has a greater effect on the removal of vanadium than it does on S and N. This is clearly observed in Figure 7.18$_C$ where a 10% reduction in the amount of vanadium found in the liquid product was obtained in the presence of Mn-Y-zeolite as catalyst. Despite the overall increase in vanadium removal from the liquid product, the total mass of vanadium removed into the coke remained constant. This accounts for a significant decrease in the percentage of the total vanadium removed that goes into the coke fraction from 91% to 76% in the catalytic process. On the other hand, the amount of vanadium found after analysis of the aqueous phase shows an increase from 9% to 24% of the total vanadium removed from the liquid fraction. This suggests that the presence of the catalyst aids in the cleavage of N-C bonds in the porphyrin, which enables the removal of vanadium from porphyrin structures found in asphaltenes. Similar trends were reported in literature (125).

## 7.4. CONCLUSIONS

Experiments on the upgrading of vacuum residue through oxidative cracking in SCW with and without a catalyst were performed.

Results of the thermal oxidative cracking at different temperatures (400, 425 and 450 °C) showed that as expected, an increase in temperature resulted in an increase of VR conversion and asphaltene conversion. Interestingly, a maximum at 425 °C was observed for the conversion to products with bp < 450 °C, which decreased at higher temperature.

This is mainly caused by an important increase in the yields to coke observed when reaction took place at 450 °C. An optimum process temperature was found at 425 °C based on the high conversion and the high yields to gas and light maltene products obtained. Moreover, a maximum production of diesel and gas-oil within the light maltene fraction was also achieved. SEC studies on the liquid product showed a shift to lower molecular weight products with an increase in reaction temperature. Similar behavior was observed when the maltene and asphaltene fractions were analyzed separately from which was concluded that both maltene and asphaltene fractions in oil can be upgraded to lower molecular weight compounds through oxidative cracking in SCW.

Furthermore, it was concluded that heteroatom and metal species found in VR are highly stable in oxidative cracking in SCW conditions. In addition, their removal from the liquid product proceeds mainly due to polymerization reactions of asphaltenes to end up in the coke fraction rather than decomposition of large heteroatom and metal bearing compounds. Based on the percentage of S, N or V removed into the gas or aqueous phase, respectively, the following reactivity trend was observed; sulfur species > nitrogen species > vanadium species.

Catalytic oxidative cracking experiments in SCW using Y-zeolite and Mn-Y-zeolite as catalysts were conducted at 425 °C. The presence of any of the catalysts increased the overall conversion of VR. However, conversion to products with bp < 450 °C only increased over non-catalytic runs with Mn-Y-zeolite and remained unchanged with Y-zeolite. It was concluded that the presence of Y-zeolite promotes thermal cracking of heavy molecules but does not prevent recombination and polymerization reactions to occur, which is supported by the higher yields to coke obtained. On the contrary, the presence of Mn-Y-zeolite as catalyst resulted beneficial as it also has the cracking function of the Y-zeolite but the presence of manganese oxide promotes oxidation reactions through the formation of ROS with the heavy organic species.

SEC plots of the liquid product, the maltene fraction and the asphaltene fraction showed that Mn-Y-zeolite produced an important shift to lighter products compared to the thermal only process, while the Y-zeolite had a negative effect. Moreover, analysis of the maltene and asphaltene fractions showed an important molecular weight decrease compared to the VR fractions of 40% and 60% respectively after reaction with Mn-Y-zeolite as catalyst. The shape of the plot also presents the formation of a shoulder at longer elution times in the maltene and asphaltene fractions that show that the catalyst promotes cracking reactions to form lower molecular weight hydrocarbons.

Finally, the presence of Mn-Y-zeolite increased the removal of metals and heteroatoms from the liquid product. The mass balance of S, N and V showed an important increase in the percentage of S and N removed that goes into the gas fraction and in the case of V an increase in the one that is removed into the aqueous phase. This shows that the catalyst promotes the decomposition of large S, N and V bearing compounds, which enables the upgrading of the liquid fraction through size reduction and metal – heteroatom removal.

# Chapter 8
# Catalytic Oxidative Cracking of Vacuum Residue in Supercritical Water

The work presented in this chapter focuses on the effect of reaction time and temperature in the catalytic oxidative cracking of VR in SCW using Mn-Y-zeolite as catalyst. This work represents the direct continuation of the studies performed on the catalytic and non-catalytic upgrading of VR presented in Chapter 7. The main objective pursued was to determine the optimum process conditions (reaction time and temperature) at which yields to liquid products with boiling point below 450 °C (light maltene) were maximized and low yields to gas and coke were obtained. In addition, the effect of these two process variables on the conversion of VR, product distribution, average molecular weight of maltene and asphaltene fractions as well as in the removal of S, N and V from the liquid fraction are discussed.

## 8.1. INTRODUCTION

In order to fully understand the process of upgrading heavy oil through oxidative cracking in SCW, it is necessary to study the evolution of products at different stages of reaction. Recent studies on the kinetics of the pyrolysis of heavy oil in SCW (229,230), showed that the overall process kinetics aligns well with a pseudo first order of reaction. It was also reported that variations in temperature have a dominant role in the final product distribution obtained. Moreover, it was reported that the maltene fraction of heavy oils is more reactive than the asphaltene fraction, which was completely stable at temperatures below 400 °C. The authors observed that an increase in temperature to 430 °C had a large impact on both the conversion of maltenes and asphaltenes at the expense of higher yields to coke and gas products.

The aim of this work is to elucidate the effect that changes in temperature and reaction time have in the catalytic oxidative cracking of VR in SCW. In these experiments, Mn-Y-zeolite was used as catalyst, as it enhanced the upgrading process as discussed in Chapter 7. The upgrading of the VR and the evolution of the different product fractions was assessed based on the yields to different products, the capacity to remove heteroatoms (S and N) and metals

(V) from the liquid phase as well as the reduction in the average molecular weight of the asphaltene and maltene fractions. Optimum reaction conditions were determined where the highest yields to liquid products with boiling point below 450 °C are obtained.

## 8.2. EXPERIMENTAL

The experimental procedure used for this work is the same as the one for experiments discussed in Chapter 7. Briefly, experiments were performed in a SS microbomb reactor extensively described in Section 3.2.1 and Section 4.1.1. Experiments at reaction temperatures of 400, 425 and 450 °C and reaction times of 10, 30, 60 and 90 min were performed. Pressure, O/VR ratio and catalyst/VR ratio were kept constant at 230 bar, 60 min, 0.15 $g_{O2}/g_{VR}$ and a 0.25 $g_{cat}/g_{VR}$ respectively. Reaction products were recovered and analyzed following the procedures detailed in Section 4.1.1.3.2 and Section 4.1.3 respectively.

## 8.3. RESULTS AND DISCUSSION

### 8.3.1. Experimental results

In this section, experimental findings on the upgrading of VR through oxidative cracking in SCW are discussed. Experiments varying reaction temperature and time were performed at the experimental conditions reported in Table 8.1.

*Table 8.1 Experimental conditions to study the effect of reaction time and reaction temperature in the catalytic oxidative cracking of vacuum residue in SCW.*

| Parameter | Value |
|---|---|
| **Temperature (°C)** | 400, 425 and 450 |
| **Residence Time (min)** | 10*, 30*, 60 and 90* |
| **Pressure (bar)** | 230 |
| **O / VR ratio ($gO_2/g_{VR}$)** | 0.15 |
| **Cat / VR ratio ($g_{cat}/g_{VR}$)** | 0.25 |

*Experiments at 10, 30 and 90 min for the three temperatures studied were performed in collaboration with a MSc student project (231).

Analysis of results was made following the same approach as the one extensively explained in Chapter 7. Especial emphasis was placed on the influence that changes in reaction time and temperature have in VR conversion, yields to products, heteroatom removal, metal

removal and changes in the average molecular weight of the maltene and asphaltene fractions. These were calculated with Equations 7.1 – 7.7. Similarly, two different definitions of conversion were considered. The first (Equation 7.1) defines the total conversion considering gas, liquid product with bp < 450 °C and coke as reaction products. The second (Equation 7.2) is for conversion to light products with boiling point below 450 °C including gas but considering coke as unconverted material. Reaction products were divided and classified as gas, coke and liquid products. Liquid products were further divided into asphaltenes and maltenes which were also classified depending on boiling point range as previously shown in Figure 7.5.

#### *8.3.1.1. Conversion*

Figure 8.1 shows that process variables temperature and reaction time have an important impact in the conversion of VR. As expected an increase in conversion was registered with increments in reaction time at the different temperatures studied.

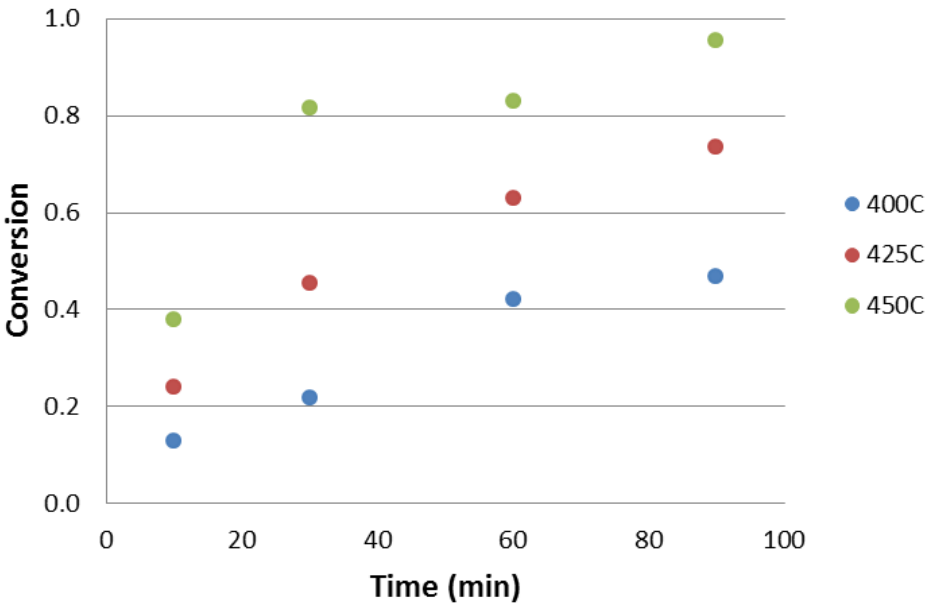


*Figure 8.1 VR conversion through catalytic oxidative cracking in SCW varying reaction temperature and reaction time at 230 bar, 60 min, cat/VR ratio of 0.25 and O/VR ratio of 0.15.*

At 400 °C, it was observed that conversion increased fast between 10 and 60 min and gradually started to level off with further increments in reaction time. This is thought to be

related with the concentration of ROS that are completely consumed at longer reaction times decreasing greatly the reactivity of the system. When reactions were carried out at longer reaction times, the availability of ROS in the medium was limited decreasing its reactivity. These observations are in good agreement with the trends observed in Chapters 5 and 6, where it was concluded that PAH structures have no reactivity in the absence ROS. However, at 425 °C and especially at 450 °C, the trend observed showed that conversion had a constant increase with an increase in reaction time. This suggests that at higher reaction temperatures, other reactions like thermal cracking and polymerization become more relevant than at lower temperatures, contributing to the increase in conversion even at longer reaction times. This is further addressed when analyzing the product distribution as it was observed that conversion is closely related to the product distribution obtained.

Figure 8.2 shows the values of conversion to products with bp < 450 °C. At all reaction temperatures, conversion to products with bp < 450 °C increased between 10 and 60 min. Interestingly, further increase in reaction time had a different effect depending on the temperature at which the experiment was carried out.

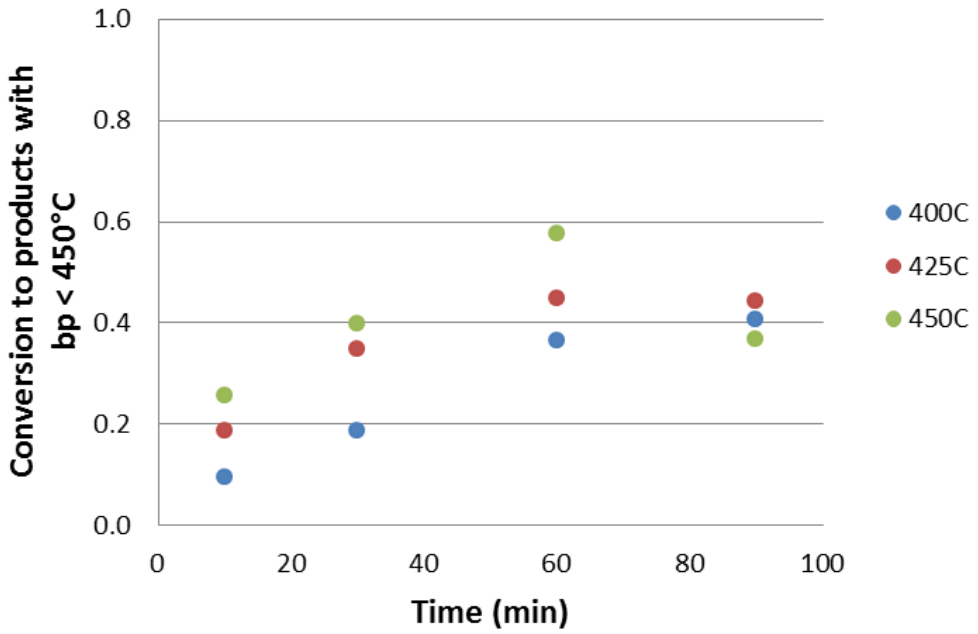


*Figure 8.2 VR conversion to products with bp < 450 °C through catalytic oxidative cracking in SCW varying reaction temperature and time at 230 bar, 60 min, cat/VR ratio of 0.25 and O/VR ratio of 0.15.*

At 400 °C, it was observed that conversion to products with bp < 450 °C started to level off after 60 min. The trend observed is similar to the one followed by total conversion (Figure

8.1) mainly due to the low production of coke at this temperature. However, at 425 °C and 450 °C conversion to products with bp < 450 °C reached a maximum after 60 min to decrease afterwards. This trend was more pronounced at 450 °C where a sharp decrease of more than 20% in conversion to products with bp < 450 °C was registered. Therefore, dependence between the conversion to products with bp < 450 °C and temperature was observed. It was concluded that the decrease in conversion to products with bp < 450 °C was due to the increase in the amount of coke produced with increasing temperature

### 8.3.2. Product yields

Figure 8.3 shows the evolution with time of the different product fractions (asphaltenes, heavy maltenes, light maltenes, gas and coke) obtained at different temperatures compared to the composition of the original VR. The original feedstock is composed of a mixture of asphaltenes and heavy maltenes with a boiling point of 540 °C or higher. Overall, it was observed that the trends in the yields to the different products are strongly related to the reaction temperature.

At 400 °C the yield to heavy maltenes decreased with an increase in reaction time, while the yield to asphaltenes remained almost unchanged as shown in Figure $8.3_A$. An increase in the yield to liquid products with bp < 450 °C with time was observed until it reached a plateau after 60 min. A further increase in reaction time from 60 to 90 min produced no change in the yields to liquid with bp < 450 °C. This is believed to be strongly related with the concentration of ROS in the system that was high at early stages of reaction and decreased with time. It is thought that initially heavy maltenes are cracked into lighter fractions aided by the incorporation of oxygen into the structure. At longer reaction times cracking of heavy molecules slow down and occur mainly as a result of thermal cracking. Moreover, light fractions may continue to thermally crack to form gas. The constant yield to liquid with bp < 450 °C observed at long reaction times is thought to be the result of a balance between the production of light maltenes by cracking and their decomposition into gas. Yields to coke remained low below 6 % at all conditions studied.

Figure $8.3_B$ shows that an increase in reaction temperature to 425 °C resulted in a faster decrease in the yield to heavy maltenes, which was lower than 20% after just 10 min of reaction. Interestingly, at short times an increase in the yield to asphaltenes was registered to then decrease with further increase in reaction time. This may be due to the effect of polymerization reactions that occur at early reaction stages.

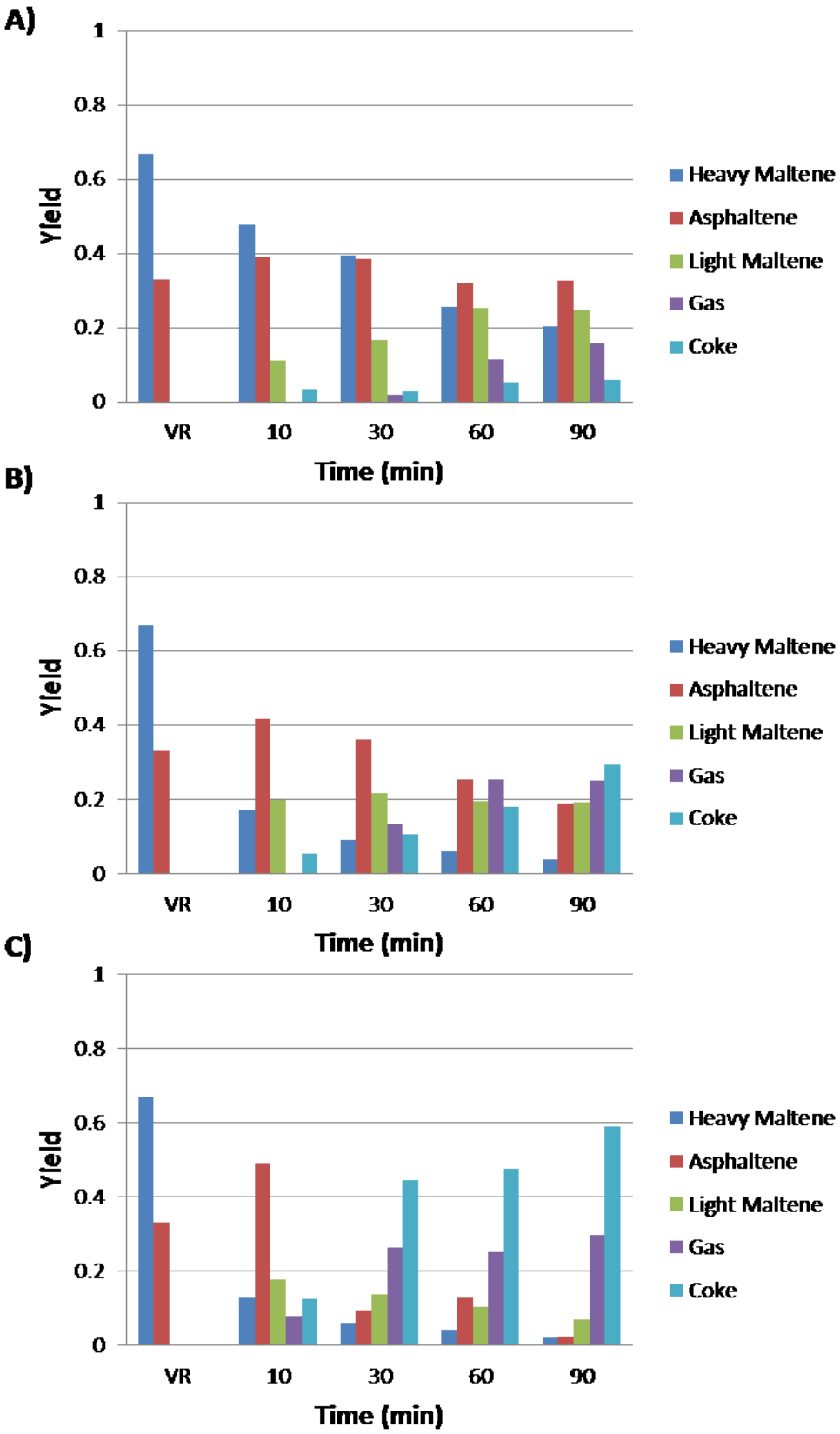


*Figure 8.3 Yield to products from the catalytic oxidative cracking of VR in SCW at 230 bar, cat/VR ratio 0.25, O/VR ratio of 0.15 varying reaction time at temperatures of A) 400 °C, B) 425 °C and C) 450 °C.*

At longer reaction times the yields to asphaltene decreased, which is thought to be the result of two potential processes, the condensation of asphaltenes to form coke and the cracking of asphaltenes into lighter fractions. It was also observed that the yields to light maltenes remained unchanged with an increase in reaction time. Similarly as at 400 °C, it is thought that this is the result of a balance between the formation of light maltenes from cracking of heavier compounds and their further decomposition into gas. This is in good agreement with the increase in gas yields with reaction time. Yields to coke showed an increasing trend with reaction time, which matches the decrease in the yields to asphaltenes suggesting that asphaltene polymerization is responsible for coke formation as was reported in literature (100).

Further increments in reaction temperature to 450 °C boosted the trends observed at 425 °C as shown in Figure 8.3$_C$. It was observed that heavy maltenes reacted fast and had yields lower than 12 % at all reaction times studied. Moreover, an important increase in the yield to asphaltenes was registered in the initial 10 min of reaction. As previously mentioned, this is thought to be caused by an increase in the polymerization rates at initial reaction stages and during the initial heating of the reactor. At longer reaction times, yields to asphaltenes decreased to almost achieve complete conversion. This is directly linked with the important increase registered in the yields to coke at reaction times over 30 min. Yields to light maltenes decreased progressively as reaction time increased. On the contrary, an increase in reaction time resulted in an increase in the yields to gas mainly as a result of the decomposition of light maltenes.

Based on trends observed for the yields to different products, a general reaction pathway for the upgrading of VR through oxidative cracking in SCW was proposed, as shown in Figure 8.4. The reaction pathway considers as unconverted VR any liquid product (heavy maltene and asphaltene) with a boiling point over 450 °C.

Asphaltene molecules are thought to react through two main processes: through cracking to form heavy maltenes and through polymerization to form coke. The second was proven to be strongly dependent on reaction temperature as yields to coke remained low below 6% when reaction took place at 400 °C. On the contrary, high yields to coke of up to 58% were obtained when temperature increased to 450 °C. Similarly, two processes are thought to occur with the heavy maltene fraction. These are the polymerization to form asphaltenes and the cracking to form light maltene products with a boiling point lower than 450 °C. Finally, light maltenes are thought to further crack to form gas products. It was observed that this reaction is strongly dependent on reaction time as low gas yields were obtained at early reaction stages. Temperature also had influence on the yield to gas especially at 450 °C,

where gas yields over 20% were obtained at reaction times of 30 min or longer. The reaction pathway and product trends observed are in good agreement with similar works published in literature (100,229,230).

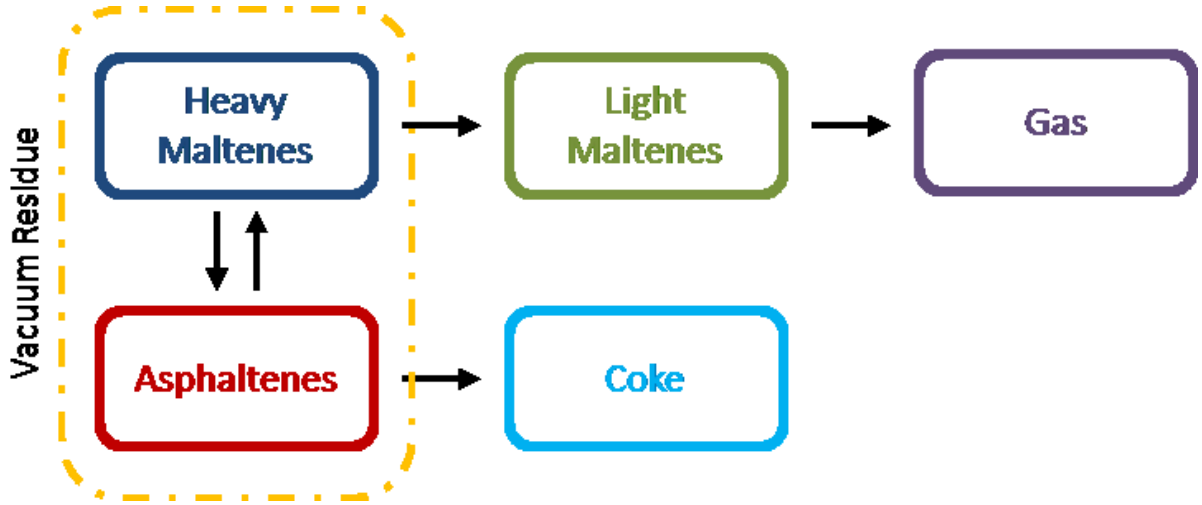


Figure 8.4 Proposed reaction pathway for the upgrading of VR through catalytic oxidative cracking in SCW.

As previously mentioned, one of the main objectives of this work was the optimization of reaction conditions to produce liquid products with bp < 450 °C. In order to gain a further insight into the effect of temperature and reaction time, the maltene fraction was further analyzed through simulated distillation and classified according to boiling point range into residue (425 – 450 °C), gas oil (340 – 425 °C), diesel (260 – 340 °C), kerosene (205 – 260 °C), heavy naphtha (< 205 °C). Figure 8.5 shows the yields to different boiling point fractions obtained at the different reaction temperatures. It was observed that in all cases light maltenes were mainly composed of diesel, gas oil and residue fractions with a boiling point between 260 °C and 450 °C. Negligible yields to heavy naphtha and kerosene were obtained. Figure $8.5_A$ shows that at 400 °C, yields to residue, diesel and gas oil increased between 10 and 60 min. When reaction time was further increased to 90 min the three fractions showed a different behavior: the yield to residue fraction decreased while the yield to diesel kept increasing and the yield to gas oil remained steady. This suggests that at long reaction times, cracking within the light maltene fraction takes place, reducing the average boiling point of the fraction.

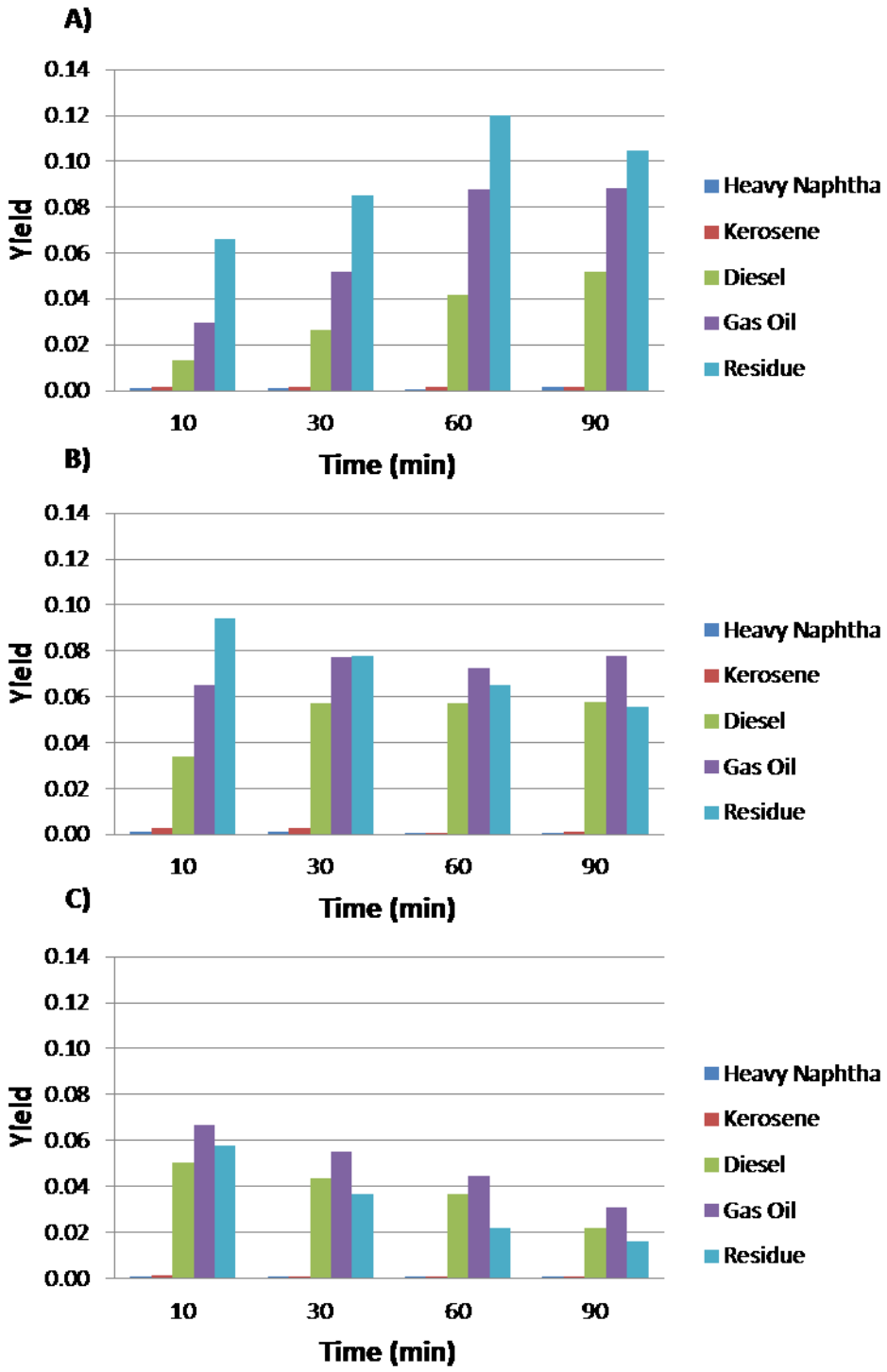


*Figure 8.5 Yield to light maltene fractions for the catalytic oxidative cracking of vacuum residue in SCW at 230 bar, cat/VR ratio 0.25, O/VR ratio of 0.15 varying reaction time at temperatures of A) 400 °C, B) 425 °C and C) 450 °C.*

Figure $8.5_B$ and Figure $8.5_C$ show that an increment in reaction temperature increased cracking reactions within the light maltene fraction. At 425 °C, the yield to residue fraction

decreased with an increase in reaction time, which is thought to be the result of cracking reactions mainly to produce gas oil and diesel. Interestingly, at these conditions an initial increase with time was observed in the yield to gas oil between 10 and 30 min, which then levelled off at values of 7%. It is believed that at these conditions, the decomposition of maltenes within the residue fraction to form gas oil and its subsequent cracking to form diesel reached a balance. On the other hand, yields to maltenes with boiling point within the diesel fraction increased with reaction time as consequence of the thermal cracking of the previous two fractions.

It was observed that at 450 °C, any increment in reaction time resulted in a decrease in the yields to the different light maltene fractions. This shows that at high reaction temperature, the main reaction pathways in the process change and reactions like the thermal cracking of light maltenes to form gas become more relevant.

Overall, it was concluded that the optimum process conditions to carry out the oxidative cracking of VR in SCW, where high yields to liquid products with bp < 450 °C were obtained keeping low yields to gas and coke, were 425 °C and 30 min. Moreover, high yields to valuable fractions as diesel and gas-oil were obtained at these conditions.

### 8.3.3. Molecular weight distribution

The maltene and asphaltene fractions recovered were analyzed through size exclusion chromatography in order to determine the molecular weight distribution of the fractions compared to the values obtained in the original VR. Values of the molecular weight ranges and the average molecular weight for the whole liquid product as well as the asphaltene and maltene fractions independently were obtained using the calibration curve in Appendix 11.2.5 and are reported in Appendix 11.2.7.

Overall it was observed that both, reaction time and temperature have an important influence on the average molecular size of the maltene and asphaltene fractions as seen in Figure 8.6. Results on the analysis of the maltene fractions for experiments at 400 °C, 425 °C and 450 °C are shown in Figure $8.6_A$, Figure $8.6_C$ and Figure $8.6_E$ respectively. An increase in reaction time resulted in a shift to longer elution times at the three temperatures studied, which represents a decrease in the average molecular weight of the maltene fraction. Moreover, it was observed that increasing reaction temperature had an important impact reducing the average molecular weight of the final maltene product compared to the one of the original VR. Figure $8.6_A$ shows that at 400 °C a shoulder was formed at longer elution times, which indicates that maltenes with a lower molecular weight were obtained. The

intensity of the shoulder increased at longer reaction times showing an evolution with time towards lighter maltene products. This provided with further evidence of the existence of cracking reactions of heavy maltenes into lighter products.

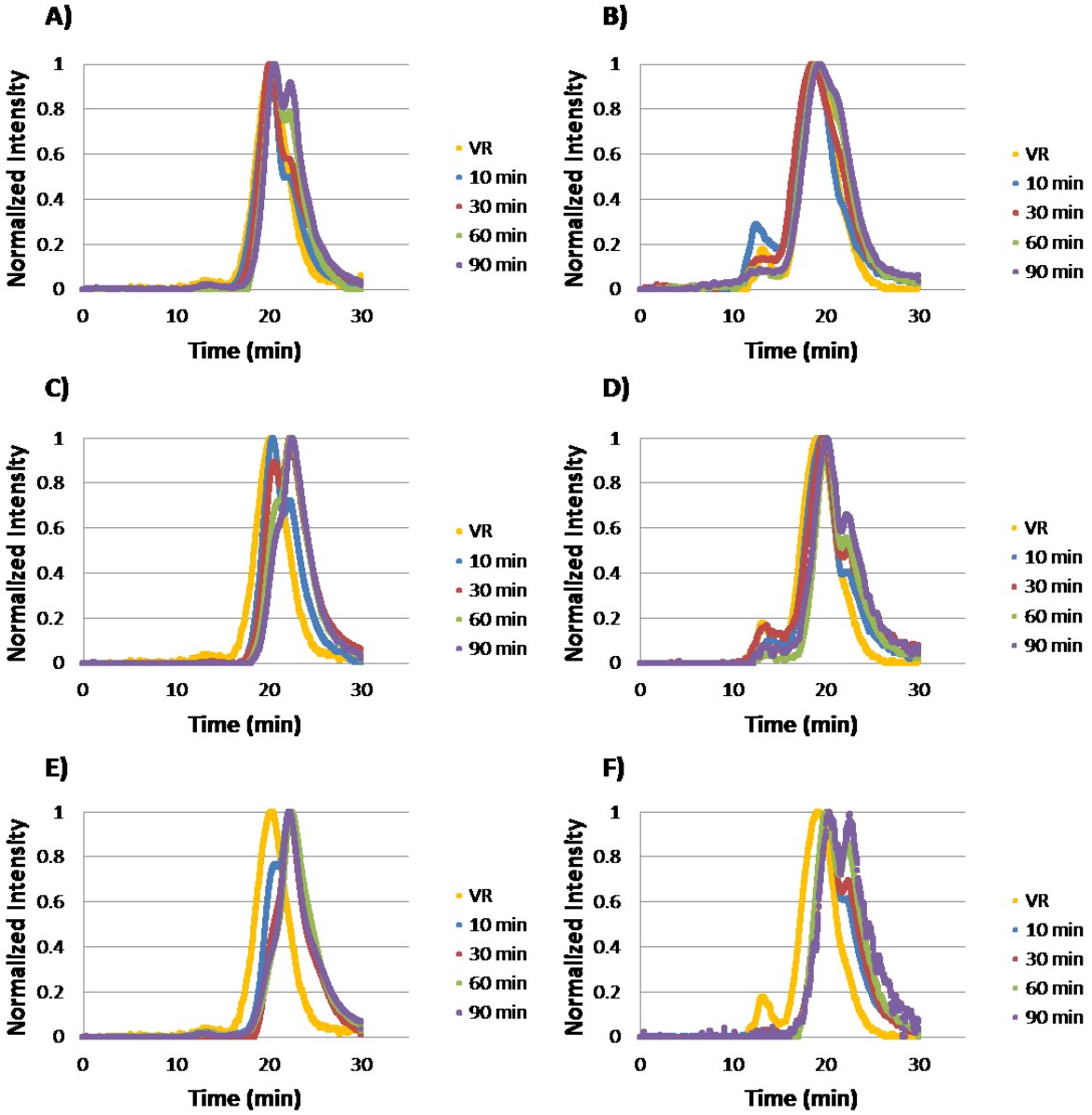


*Figure 8.6* SEC analysis of the maltene (A,C,E) and asphaltene (B,D,F) fractions from the catalytic oxidative cracking of VR in SCW at 230 bar, O/VR ratio of 0.15 and cat/VR ratio of 0.25 at 400 °C (A,B), 425 °C (C,D) and 450 °C (E,F) at reaction times of 10, 30, 60 and 90 min.

At 425 °C, a clear trend of the evolution towards lighter maltenes with time was obtained, as shown in Figure 8.6$_C$. It can be observed that after 10 min a slight shift to longer elution times was observed with the formation of a shoulder at longer elution times. However, when reaction time increased to 30 min, the peaks were shifted showing that an important

reduction in the average molecular weight of the maltene fraction occurred. The presence of a shoulder at shorter elution times shows clearly the transition from heavy to lighter maltenes. Further increase in reaction time to 60 and 90 min resulted in an important reduction of the shoulder at shorter elution time, which showed the occurrence of further thermal cracking to lighter maltenes. The average molecular weight obtained for the maltene fraction at 60 and 90 min was approximately 60% lighter than the one of the maltenes in the original VR.

At 450 °C, thermal cracking of heavy maltenes occurred at higher rates since early stages of reaction, as shown in Figure $8.6_E$. It was observed that from 10 min reaction time an important shift towards longer elution times was observed. This corresponds to a reduction of more than half of the molecular weight of the maltenes in the original VR. At this temperature, increments in reaction time had lesser effect than at other temperatures only narrowing slightly the molecular weight range of the fraction. This is thought to be the result of further cracking of heavy maltenes and the loss of light maltenes that continue to crack into gas.

SEC analysis of the asphaltene fraction for experiments at 400 °C, 425 °C and 450 °C are presented in Figure $8.6_B$, Figure $8.6_D$ and Figure $8.6_F$ respectively. It was observed that reaction temperature had an important effect on the molecular weight distribution of the asphaltene fraction. Moreover, at all temperatures a reduction in the molecular weight range with reaction time was registered. Figure $8.6_B$ shows that in experiments at 400 °C, a slight shift towards longer elution times was observed with longer reaction times, which indicates a reduction in the average molecular weight. However, important evidence of asphaltene cracking and size reduction was obtained at 425 °C and 450 °C where a shoulder at longer retention times was observed. At 425 °C, an increase in reaction time resulted in a greater intensity of the shoulder showing that the proportion of lighter asphaltenes within the fraction increased, as shown in Figure $8.6_D$. An increase in temperature to 450 °C resulted in an important reduction in the average molecular weight of the asphaltene fraction. In addition it was also observed that the intensity of the shoulder at longer elution time increased at higher reaction times, which shows that cracking of asphaltene molecules occurred, as seen in Figure $8.6_F$. The important reduction in the average molecular weight of asphaltenes at 450 °C is thought to be the result of two main phenomena; first the thermal cracking of the molecule to produce lighter asphaltenes and second the potential polymerization of the heaviest asphaltenes to produce coke leaving the liquid product fraction.

### 8.3.4. Heteroatom and metal removal

The effect of temperature and reaction time in the removal of sulfur, nitrogen and vanadium from the liquid product obtained was studied. Overall it was observed that both exert an important influence on the total removal of heteroatoms and metals from the original VR.

Figure 8.7 shows the fraction of the original sulfur removed from the original VR at different temperatures and reaction times.

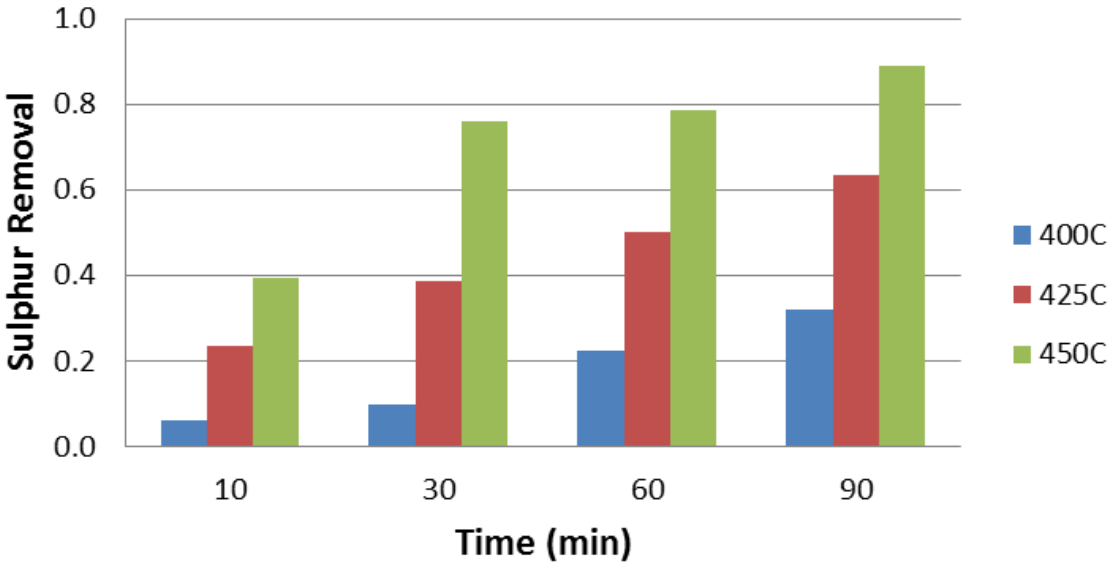


*Figure 8.7* Sulfur removal for the catalytic oxidative cracking of vacuum residue in SCW at 230 bar, cat/VR ratio 0.25, O/VR ratio of 0.15 at temperatures of 400 °C, 425 °C and 450 °C and reaction times of 10, 30, 60 and 90 min.

At 400 °C, it was observed that sulfur removal was almost negligible at early reaction stages achieving 6% after 10 min. However, at longer reaction times sulfur removal reached values over 30% at 90 min. At intermediate reaction times of 30 min and 60 min, a removal of sulfur of 10% and 22% was achieved, which is in good agreement with results reported in literature for SCW desulfurization of Arabian heavy oil in a similar reaction set up (89). The low desulfurization achieved at this condition suggests that sulfur present in the original VR is part of aromatic structures commonly found in asphaltenes. These type of molecules were studied independently and were reported to be highly stable in SCW at similar reaction conditions (125,126). Interestingly, it was noted that an increase in reaction time, results in a proportional increase in the removal of sulfur at the three reaction temperatures studied. It was evident that an increase in temperature had an important impact, achieving sulfur

removal from the liquid product of up to 90% at 450 °C and 90 min. This is believed to be related to the increase in the yields to coke obtained at higher temperatures and reaction times, as most of the sulfur was removed into the coke fraction due to polymerization of heavy asphaltenes as concluded in Chapter 7.

Results on nitrogen removal at different conditions studied are reported in Figure 8.8. It was observed that temperature exerts an important influence in the removal of nitrogen from the liquid fraction of the oil. At 400 °C, nitrogen removal was below 16% at all reaction times studied. However, an increase in temperature resulted in a significant increase in nitrogen removal. Large extents of de-nitrogenation over 70 % were achieved at 450 °C and reaction times over 30 min. As in the case of sulfur, this result is thought to be directly related with the important increase observed in the yields to coke. This suggests that the mechanism of nitrogen removal is strongly related to polymerization reactions of asphaltenes to coke that are promoted at higher reaction temperatures. At short reaction times and lower temperatures the extent of de-nitrogenation was lower than that of de-sulfurization. The latter is believed to be directly linked with the higher stable nature presented by nitrogen containing organic compounds over sulfur-containing ones, as was suggested in literature (110).

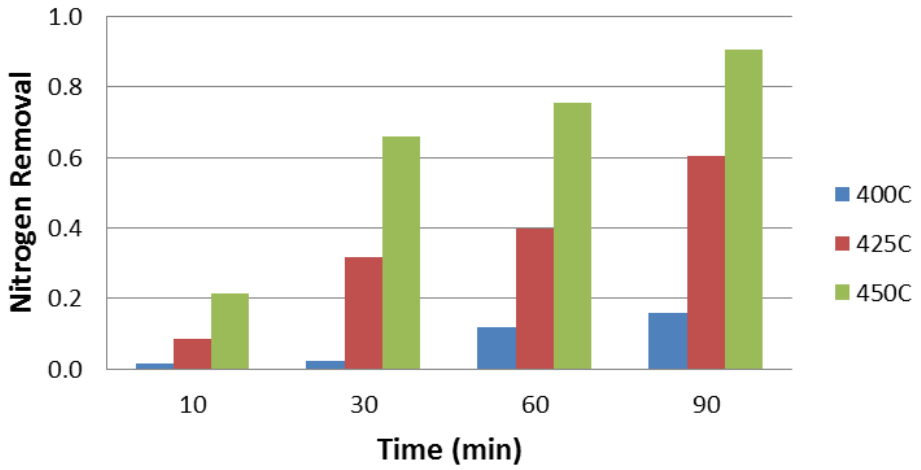


*Figure 8.8 Nitrogen removal for the catalytic oxidative cracking of vacuum residue in SCW at 230 bar, cat/VR ratio 0.25, O/VR ratio of 0.15 at temperatures of 400 °C, 425 °C and 450 °C and reaction times of 10, 30, 60 and 90 min.*

A similar trend as the one of sulfur and nitrogen was observed in the removal of vanadium from the liquid fraction as shown in Figure 8.9. It was noted that an increase in temperature

had a greater impact on the de-metallization process than the one observed in the heteroatom removal. This was particularly evident in reactions at 425 °C and 450 °C where more than 40% of the vanadium found in the original VR was removed from the liquid fraction at reaction times of 30 min or longer. These results are well in line with observations in literature reporting that metal complexes as porphyrins commonly found in asphaltene molecules undergo chemical reactions in the presence of SCW and a catalyst. In addition, it was reported that metal porphyrins are normally more reactive than S and N containing organic molecules (125). Nevertheless, as concluded in Chapter 7, most of the vanadium present in the original oil was removed from the liquid fraction in the form of coke or was deposited in the surface of the catalyst. This explains the high extent of de-metallization above 70% achieved at 450 °C and reaction times over 30 min where high yields to coke over 40% were obtained.

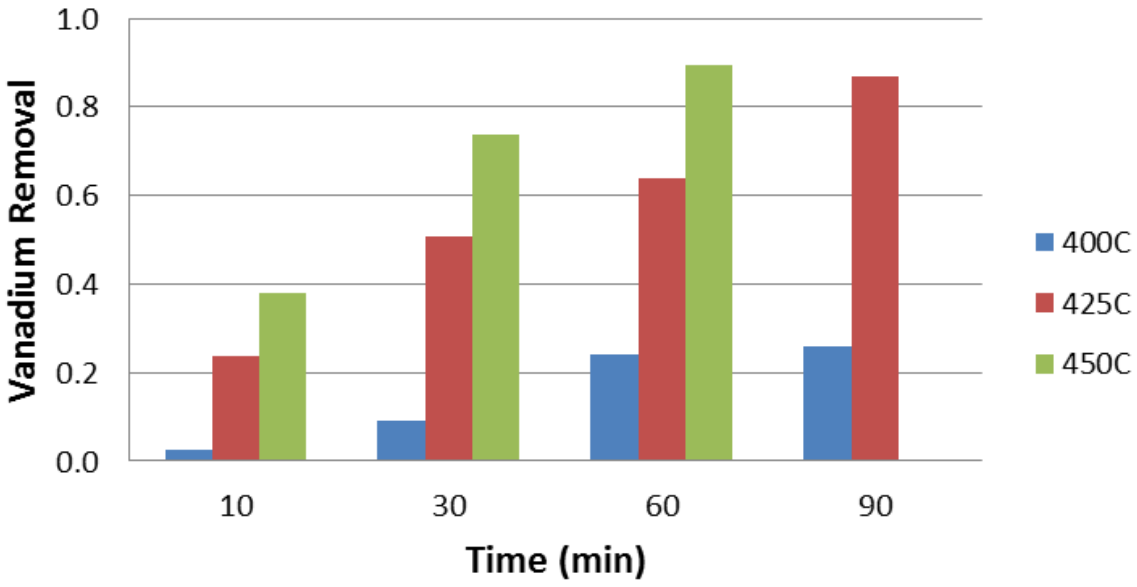


*Figure 8.9 Vanadium removal for the catalytic oxidative cracking of vacuum residue in SCW at 230 bar, cat/VR ratio 0.25, O/VR ratio of 0.15 at temperatures of 400 °C, 425 °C and 450 °C and reaction times of 10, 30, 60 and 90 min.*

## 8.4. CONCLUSIONS

Experiments on the upgrading of VR through oxidative cracking in SCW with Mn-Y-zeolite at different reaction times and temperatures were performed.

Experimental results showed that both variables studied exert an important influence in the conversion of VR and the product distribution obtained. Increments in reaction time and temperature resulted in an important increase in the total conversion of VR. However, conversion to products with bp < 450 °C increased until it reached a maximum at 60 min to then level off or decrease at 450 °C due to the formation of coke. In addition the asphaltene fraction of the VR showed to be stable at 400 °C and required higher reaction temperatures to decrease its yield. It was concluded that the sharp decrease in the yield to asphaltenes is related to an increase in the yield to coke, which shows that an important fraction of the asphaltenes that reacted were converted into coke through polymerization. Trends in the yields to liquid with bp < 450 °C showed to depend greatly on the reaction temperature. It was observed that higher reaction temperature resulted in an increase in the rate of formation of liquid products with bp < 450 °C but also increased their decomposition into gas products. As a result a gradual increase in the yield to liquid with bp < 450 °C with reaction time was observed at 400 °C, a relatively constant yield at 425 °C and a gradual decrease at 450 °C. Yields to gas and coke showed to increase with any increment in reaction time and temperature and became especially relevant at 450 °C. Results on the simulated distillation of the light maltene fraction showed that it was mainly composed of diesel, gas oil and residue, which represent a liquid product with a bp range between 260 °C and 450 °C. Based on conversion and product distribution, it was concluded that the process conditions, where a favorable balance between high yields to light maltenes (over 20%) keeping yields to coke and gas low, were 425 °C and 30 min. In addition, selectivity to diesel and gas oil within the light maltene fraction was high at these conditions.

Size exclusion chromatography analysis of the maltene and asphaltene fractions recovered showed that increasing reaction time or temperature resulted in a reduction in the average molecular weight of the fraction. The analysis of the maltene fraction at all temperatures showed the formation of a shoulder at longer elution times that increased in area for experiments at longer reaction times proving that cracking reactions take place to produce an important amount of lighter maltenes. Similar conclusions were made for the analysis of the asphaltene fraction, which also showed a displacement to longer elution times with an increase in reaction time as well as the formation of a shoulder when the reaction took place at 425 °C and 450 °C. Thus an increase in temperature or reaction time resulted in a decrease in the average molecular weight of the asphaltene fraction. The increase in the intensity of the shoulder with time is proof that cracking of asphaltene molecules into lighter ones took place.

Finally, an increase in reaction time or temperature resulted in an increased heteroatom and metal removal capacity of the process. Overall temperature showed to play the most

important role in the removal of heteroatoms and metals as it is directly related to the production of coke. The trends observed at low temperature suggest that sulfur containing compounds had a slightly higher reactivity than nitrogen and vanadium compounds. However at higher temperature the percentage of removal for S, N and V is high in all cases.

# Chapter 9
# Conclusions and Future Work Recommendations

The research developed in this thesis was set to explore the potential of a process that takes advantage of the solvent properties of supercritical water to perform the upgrading of heavy oil feedstocks. The process principle is founded in the partial oxidation of heavy molecules such as polycyclic aromatic molecules commonly found in heavy oil feedstocks to weaken their structure and facilitate their cracking into lighter and more valuable compounds. A twofold approach was followed during the project: First, polycyclic aromatic hydrocarbons were used as heavy oil model compounds in order to proof concept, gain deeper understanding of the process and optimize reaction conditions. Second, the process was tested using Maya oil VR as real heavy oil feedstock. For this, a continuous flow reactor was designed, built and tested and also an existing microbomb batch reactor was improved.

## 9.1. GENERAL CONCLUSIONS

Upgrading of heavy oil feedstocks through oxidative cracking in hydrothermal conditions, namely near-critical and supercritical water, is a promising process that gives rise to important yields to lighter and more valuable liquid fractions. It is thought that it can be implemented as an alternative to traditional heavy oil refining processes or as an addition into the actual refining scheme, aiming to upgrade residue and heavy oil fractions before being fed into the hydrotreating processes.

Water near or above its critical point is a good reaction medium for heavy oil upgrading reactions as it prevents coke formation and simplifies product separation stages after reaction. Changes in process conditions exert an important influence in the process performance, especially in the final product distribution. This is of great relevance as it shows that the system can be finely tuned to fulfill process needs with slight changes in operating conditions. When reaction takes place near the critical point of water high yields to liquid fractions and low yields to coke are obtained regardless of reaction time. However, if the temperature increases, condensation and polymerization reactions become more relevant, which results in an increment in the yields to coke. Moreover, it was observed that

depending on reaction conditions high yields to gas are obtained. Analysis of the gas fraction showed that it was rich in $H_2$, making it a high value by-product of the process.

Furthermore, results obtained with heavy oil model compounds showed that the upgrading through oxidative cracking in SCW consists of two main reaction stages. First, a partial oxidation step that occurs at early reaction stages when the concentration of reactive oxygen species in the system is high. This step is followed by the thermal cracking of the oxygenated compounds with carbon and oxygen rejection to produce a lighter organic fraction and gas as main products. Based on the experimental evidence obtained from this work, it is believed that water mainly plays the role of solvent in the process and that oxygen reacts with the heavy organic compounds present in heavy oils weakening its structure and enabling its cracking into lighter fractions and gas.

### 9.1.1. Conclusions obtained from the work performed with model compounds

As shown in Chapters 5 and 6, the work performed with heavy oil model compounds enabled a deep understanding of the effect of operating conditions in the overall performance of the process. It also provided valuable information to gain insight on the potential reaction pathways that will enable further improvement of the process.

Analysis of reaction products showed that they are the result of a partial oxidation of the polycyclic aromatic compounds and that the reaction proceeds preferentially through the central ring. This presents a great advantage as it weakens the polycyclic aromatic structures in central positions, breaking its aromaticity and enabling its cracking into lighter compounds. It is believed that this makes the process more efficient than other processes that preferentially proceed through the periphery of the molecule incurring in further loss of carbon.

In addition, it was observed that polycyclic aromatic compounds are not reactive in water alone at near-critical or supercritical conditions. However, in the presence of reactive oxygen species, fast reaction occurs and high conversions are observed at residence times as short as 15 s. Interestingly, experimental evidence shows that oxygen-containing products from the partial oxidation of polycyclic aromatic hydrocarbons continue to react in NCW or SCW alone. It was observed that at longer reaction times, the O/C ratio in the liquid product fraction decreases, which shows that some degree of de-oxygenation of the final product can be achieved within the same process.

Reaction conditions have an important impact in the overall performance of the oxidative cracking process. The effect with changes in pressure, initial oxygen loading ($O/O_{stoich}$ ratio),

temperature and time have in conversion and product distribution was extensively studied. It was concluded that changes in pressure have a small influence in conversion showing a slight increase in the transition between near-critical and supercritical conditions and remaining almost unchanged at pressures above the critical pressure of water. However, pressure affects directly the product distribution obtained showing that the higher selectivity to organic soluble products is obtained at pressures slightly above the critical point. It was observed that the initial amount of oxygen loaded into the system has an important impact in conversion and product distribution. High $O/O_{stoich}$ ratios result in high conversion and also high yields to gas product, which decreases the selectivity to organic soluble products. In this work, it was concluded that operation at an $O/O_{stoich}$ ratio between 0.2 and 0.4 results in high selectivities to organic soluble products. As expected, an increase in temperature resulted in an increase in conversion and in the different product yields. However, a higher selectivity to organic soluble products was obtained at temperatures between 400 °C and 425 °C.

In both reaction set ups (batch and continuous) two main reaction regimes were observed. At early reaction stages, where the concentration of reactive oxygen species in the system is high, conversion of polycyclic aromatic hydrocarbons increases with time, same as the yield to organic soluble products. At later stages of reaction, where most of the reactive oxygen species in the medium have reacted, conversion of polycyclic aromatic hydrocarbons levels off and remains constant while the yields to organic soluble products decrease mainly due to the decomposition of oxygen containing intermediate products. From this it can be concluded that the oxidative cracking process occur at two regimes depending on the availability of reactive oxygen species and that reaction and residence time (depending on the reaction system used) have an important impact on conversion and especially on the selectivity to different products.

### 9.1.2. Conclusions from the work performed with vacuum residue

Results from the work discussed in Chapters 7 and 8 showed that the oxidative cracking process in SCW can be implemented in the upgrading of real heavy oil feedstocks achieving important yields to light oil fractions. It was observed that the heavy maltene fraction in the vacuum residue is reactive at all conditions mainly to produce lighter liquid fractions or gas. On the contrary, asphaltenes were less reactive especially at lower temperatures. An increase in temperature results in a considerable decrease in the yields to asphaltenes at the expense of an increase in coke yields. The light maltene fractions obtained from the

upgrading of vacuum residue had a boiling point range between 260 °C and 450 °C and were composed of fractions of gas oil, diesel and residue.

Moreover, it was resolved that the average molecular weight of both maltene and asphaltene fractions decreases after reaction if compared to the ones in the original vacuum residue. This shows that even though yields to asphaltenes remain almost unchanged at low temperatures, size reduction within the fraction is achieved.

Overall, it was observed that heteroatoms and metals found in vacuum residue show high stability especially at lower temperatures and reaction times. However, an increase in reaction time or temperature resulted in an increased capacity of the system to remove heteroatoms and metals. This is directly related to the parallel increase in the yields to coke where most of the metals and heteroatoms removed were found. Thus, it was concluded that the removal of heteroatoms and metals from the liquid phase is mainly due to polymerization reactions of asphaltenes to form coke rather than the decomposition of the heteroatom or metal bearing compound. Moreover, the percentage of S, N and V determined in the gas and aqueous phases showed that sulphur species have a slightly higher reactivity than nitrogen and vanadium bearing compounds.

Furthermore, the addition of a zeolite based catalyst (Mn-Y-zeolite or Y-zeolite) increased vacuum residue conversion compared to the non-catalytic process. However, each catalyst presented a different effect on the product distribution obtained. It was concluded that the Mn-Y-zeolite improved the upgrading process as it increased the yields to products with bp < 450 °C without increasing the yields to coke. On the contrary, the addition of Y-zeolite had a negative effect increasing the yields to coke and gas and decreasing the yield to liquid products with bp < 450 °C compared to the non-catalytic process. From this it was concluded that the addition of Mn-Y-zeolite had a positive effect in the system increasing the selectivity to products with bp < 450 °C and was decided to be studied further.

The addition of Mn-Y-zeolite produced a further decrease in the average molecular weight of both maltene and asphaltene fractions compared to the ones obtained in the absence of a catalyst as the presence of the catalyst enhanced the cracking of both asphaltene and maltene fractions. Increments in temperature and reaction time resulted in further reduction of the average molecular weight of both fractions. However, despite of the evident upgrading of the asphaltene fraction, it is believed that the presence of the catalyst and the severity of the process are not enough to fully convert asphaltenes into lighter and more valuable liquid fractions. Finally, it was resolved that the presence of Mn-Y-zeolite catalyst increases the removal of heteroatom and metals from the liquid phase into the gas or aqueous phases. This provides evidence that the catalyst aids in the decomposition of large heteroatom and

metal bearing organic compounds enabling the upgrading of the liquid fraction through size reduction and the removal of metals and heteroatoms.

## 9.2. RECOMMENDATIONS FOR FUTURE WORK

This section focuses on the description of future work that can be performed in order to further improve the oxidative cracking process. During the development of this work some great challenges such as the design, commissioning and testing of a flow reaction system to carry out reactions in supercritical water as well as the development of catalyst to further improve the oxidative cracking process were tackled. Moreover, the development of standard operating procedures and methodologies to recover and analyze products of experiments with model compounds and vacuum residue required an important effort and time input. In addition, some intrinsic limitations encountered during the development of this project such as time constraints, equipment and material availability and other situations out of the author control left room for further work and process improvement.

### 9.2.1. Improvement of reaction set-ups

Some potential improvements to the current reaction systems used were identified. These are aimed to facilitate operation, increase safety when operating and increase the reliability of the results obtained.

#### *9.2.1.1. Microbomb reactor*

During operation it was observed that the spring and seal of the relief valve was worn out after 4 to 5 experiments and needed to be replaced. In order to improve the system and avoid having to replace these fittings in a regular basis the installation of a rupture disc instead of the relief valve is being proposed as shown in Figure 9.1.

The installation of a rupture disc will ensure that leaks do not occur during operation due to worn out fittings in the relief valve section. Moreover, they increase the safety of operation against a sudden increase in the system pressure, as the rupture disc will break protecting the rest of the set-up. Rupture discs made out of Inconel are corrosion resistant and retain 90% of the room temperature rating at temperatures as high as 450 °C (232). This is of great importance as the system requires that the rupture disc operate at reaction temperatures of up to 450 °C and to bare the corrosive nature of the sand used in the bath.

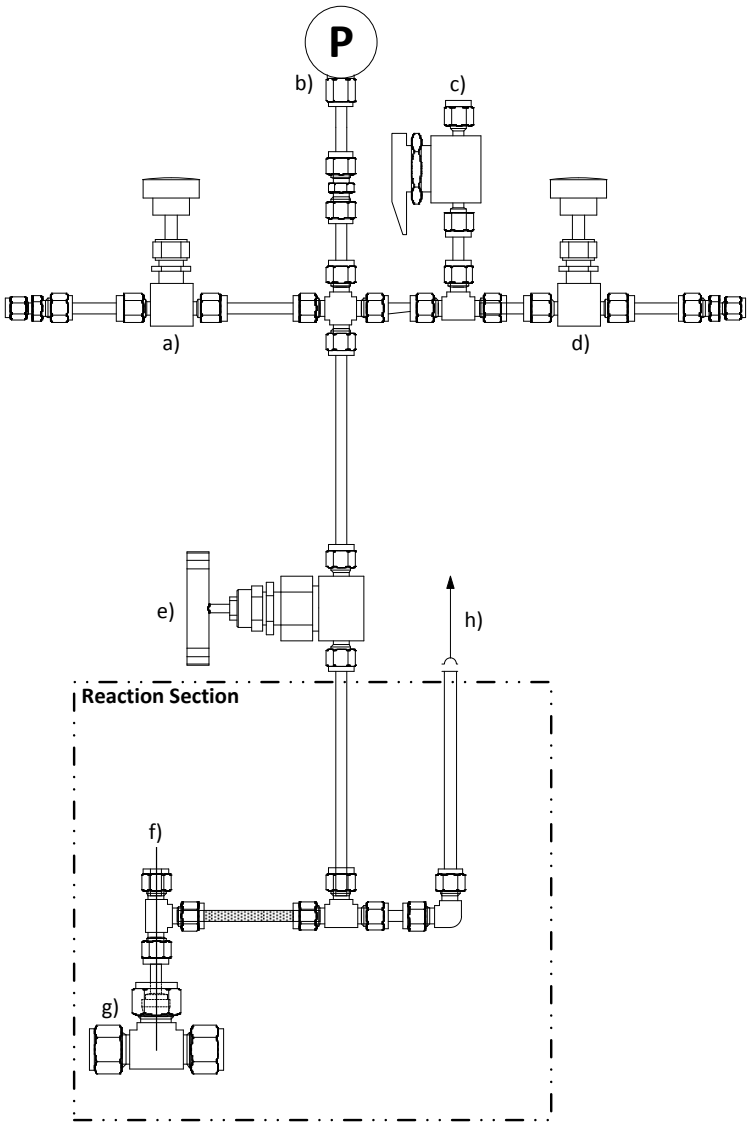


*Figure 9.1 Scheme of the proposed modification to the microbomb reaction system that consists of a) inlet purge valve, b) pressure gauge, c) gas sampling port, d) outlet purge valve, e) high P and high T valve, f) thermocouple, g) reactor main body, h) rupture disc.*

#### *9.2.1.2. Oxidative cracking reactor*

It would be desirable in order to perform stability tests of the catalysts in the process, to modify the configuration of the oxidative cracking reactor in order to fit a catalytic packed bed. A design of a prototype on how to attach a packed bed into the reactor is shown in Figure 9.2. It is thought that the catalyst fixed bed should be placed in a vertical orientation after the mixer, taking care that the bed is located in a position where it is well immersed in the sand-bath, in order to avoid temperature gradients and hot spots as much as possible.

The prototype for the packed bed is built out of two ½" to ¼" stainless steel Swagelok reducing unions. The catalyst would be contained in a ½" stainless steel tube with a stainless steel disc with holes covered with wire mesh to avoid any loss of catalyst. The vertical orientation of the reactor with the feed of reactants flowing from the bottom is intended to avoid plugging within the catalytic bed, which would increase the pressure in the system.

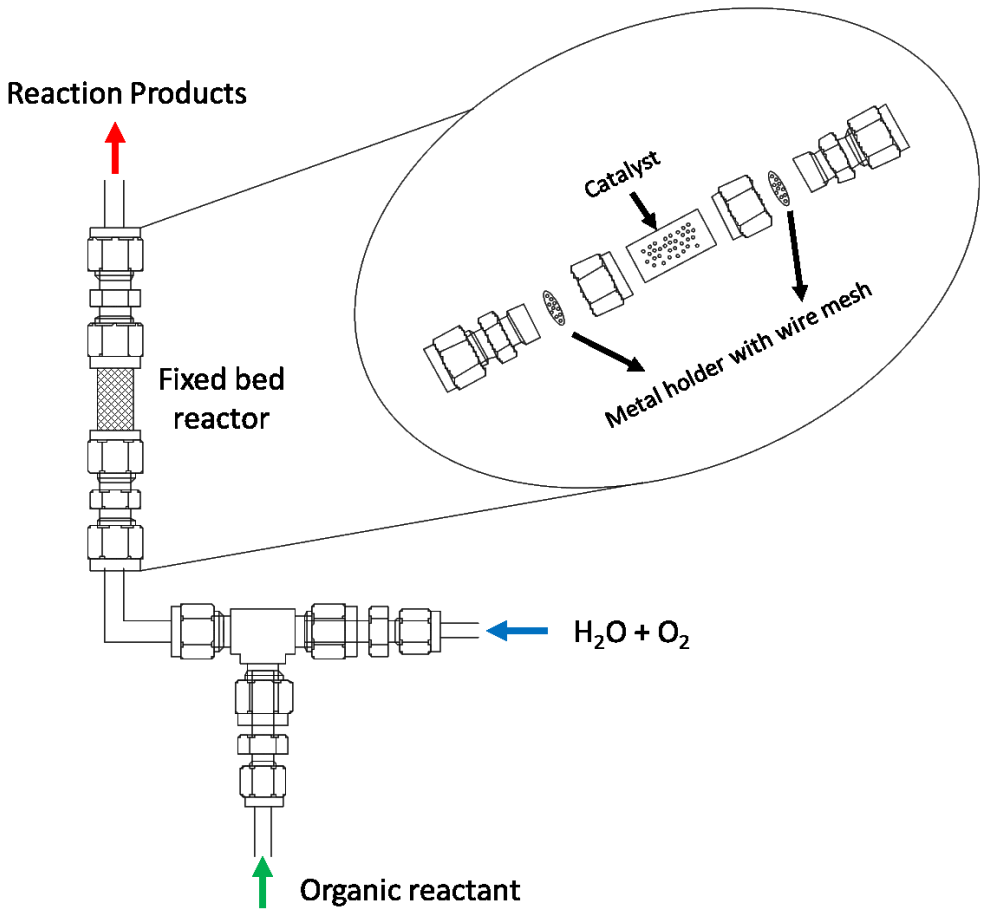


*Figure 9.2 Design of a catalyst packed bed incorporated into the oxidative cracking flow reactor.*

### 9.2.2. Catalyst development and testing

In this work, the Mn-Y-zeolite catalyst tested with vacuum residue showed to improve the upgrading capacity of the process facilitating the cracking of heavy maltene and asphaltene molecules as well as increasing the metal and heteroatom removal capacity of the process. However, some work is still needed in order to fully understand the role of the catalyst in the process and also the resistance of the catalyst to the harsh reaction environment.

In order to do this, further analysis of the catalyst post reaction should be done in order to study the stability of the material. This will provide with information to relate the experimental findings with the catalyst and the state of the catalyst at different conditions. Information from the catalyst analysis post-reaction may prove useful to modify the catalyst with the aim of improving its performance in the process.

Apart from the Mn-Y-zeolite catalyst, it would be interesting to test different catalysts varying the nature of the support and the metal used. For this purpose a series of catalysts have already been prepared but due to time constraints they were not tested as part of this work. Different supports, including Y-zeolite, mesoporous $Al_2O_3$, carbon nanofibres and $TiO_x$ were used to synthetize the catalysts. Likewise, manganese, iron and vanadium were selected as metals due to their good properties as oxidation catalysts. Zeolite-based catalysts were synthesized through ion exchange and the rest of the catalysts through wet impregnation. It would be of great interest to evaluate the effect that changes in the support or metal have in conversion, product selectivity, metal and heteroatom removal. Moreover, depending on the differences observed between the catalysts, it would be of great interest to carry out a series of experiments using model compounds to gain an insight on how the catalyst affects the reaction pathways and impacts the product selectivity.

Finally, after selection of the catalyst with the best performance, a series of tests in the flow reaction system to evaluate the long operation performance of the catalyst would be desirable. This will indicate if the catalyst is stable at the process conditions and if it is prone to de-activation.

# References


1. U.S. Energy Information Administration. International Energy Outlook 2013 [Internet]. Washington D.C.: U.S. Department of Energy; Report No.: DOE/EIA-0484(2013). Available from: http://www.eia.gov/forecasts/ieo/

2. U.S. Energy Information Administration. International Energy Outlook 2014 [Internet]. Washington D.C.: U.S. Department of Energy; Report No.: DOE/EIA-0484(2013). Available from: http://www.eia.gov/forecasts/ieo/

3. Radial Drilling. UNCONVENTIONAL RESOURCES [Internet]. [cited 2015 Nov 16]. Available from: http://www.radialdrilling.com/?page_id=17130

4. Hart Energy Research Group. Heavy Crude Oil: Global Perspective, Analysis & Outlook to 2035 | Hart Energy [Internet]. Houston USA: Hart Energy; [cited 2015 Aug 14]. Available from: http://www.hartenergy.com/Upstream/Research-And-Consulting/Heavy-Crude-Oil-A-Global-Analysis-And-Outlook/

5. Owen NA, Inderwildi OR, King DA. The status of conventional world oil reserves—Hype or cause for concern? Energy Policy. 2010 Aug;38(8):4743–9.

6. Hirsch R. The Inevitable Peaking of World Oil Production [Internet]. USA: The Atlantic Council of the United States; 2005. Report No.: Vol. XVI, No. 3. Available from: http://www.isn.ethz.ch/Digital-Library/Publications/Detail/?ots591=0c54e3b3-1e9c-be1e-2c24-a6a8c7060233&lng=en&id=13958

7. Ancheyta J, Centeno G, Trejo F, Marroquín G, García JA, Tenorio E, et al. Extraction and Characterization of Asphaltenes from Different Crude Oils and Solvents. Energy Fuels. 2002 Sep 1;16(5):1121–7.

8. Briggs PJ, Baron PR, Fulleylove RJ, Wright MS. Development of Heavy-Oil Reservoirs. Journal of Petroleum Technology. 1988;40(02):206–14.

9. Meyer RF, Witt WD. Definition and world resources of natural bitumens [Internet]. G.P.O. ; Books and Open- File Reports Section [distributor],; 1990 [cited 2015 Nov 16]. Report No.: 1944. Available from: http://pubs.er.usgs.gov/publication/b1944

10. Trejo F, Centeno G, Ancheyta J. Precipitation, fractionation and characterization of asphaltenes from heavy and light crude oils. Fuel. 2004 Nov;83(16):2169–75.

11. Exxon Mobil. A Simple Guide to Oil Refining [Internet]. Exxon Mobil; Available from: http://www.exxonmobil.com/europe-english/files/simple_guide_to_oil_refining.pdf

12. Ancheyta J, Speight JG. Hydroprocessing of heavy oils and residua. CRC Press; 2007. 366 p.

13. Gary JH, Handwerk GE, Kaiser MJ. Petroleum Refining: Technology and Economics, Fifth Edition. CRC Press; 2007. 488 p.

14. Castañeda LC, Muñoz J, Ancheyta J. Combined process schemes for upgrading of heavy petroleum. Fuel. 2012;100(0):110–27.

15. Rana MS, Sámano V, Ancheyta J, Diaz JAI. A review of recent advances on process technologies for upgrading of heavy oils and residua. Fuel. 2007 Jun;86(9):1216–31.

16. Hammel KE, Kalyanaraman B, Kirk TK. Oxidation of polycyclic aromatic hydrocarbons and dibenzo[p]-dioxins by Phanerochaete chrysosporium ligninase. J Biol Chem. 1986 Dec 25;261(36):16948–52.

17. Haritash AK, Kaushik CP. Biodegradation aspects of Polycyclic Aromatic Hydrocarbons (PAHs): A review. Journal of Hazardous Materials. 2009 Sep 30;169(1–3):1–15.

18. Field JA, Jong E de, Costa GF, Bont JA de. Biodegradation of polycyclic aromatic hydrocarbons by new isolates of white rot fungi. Appl Environ Microbiol. 1992 Jan 7;58(7):2219–26.

19. Hammel KE. Mechanisms for polycyclic aromatic hydrocarbon degradation by ligninolytic fungi. Environ Health Perspect. 1995 Jun;103(Suppl 5):41–3.

20. Speight JG. The Chemistry and Technology of Petroleum, Fourth Edition. CRC Press; 2006. 994 p.

21. Hsu CS, Robinson PR, editors. Practical Advances in Petroleum Processing [Internet]. New York, NY: Springer New York; 2006 [cited 2015 Aug 14]. Available from: http://link.springer.com/10.1007/978-0-387-25789-1

22. Ancheyta J. Modeling and Simulation of Catalytic Reactors for Petroleum Refining. John Wiley & Sons; 2011. 526 p.

23. Fan T, Wang J, Buckley JS. Evaluating Crude Oils by SARA Analysis. In Society of Petroleum Engineers; 2002 [cited 2015 Aug 16]. Available from: http://www.onepetro.org/doi/10.2118/75228-MS

24. Fan T, Buckley JS. Rapid and Accurate SARA Analysis of Medium Gravity Crude Oils. Energy Fuels. 2002 Nov 1;16(6):1571–5.

25. McKenna AM, Marshall AG, Rodgers RP. Heavy Petroleum Composition. 4. Asphaltene Compositional Space. Energy Fuels. 2013 Mar 21;27(3):1257–67.

26. Acevedo S, Mendez B, Rojas A, Layrisse I, Rivas H. Asphaltenes and resins from the Orinoco basin. Fuel. 1985 Dec;64(12):1741–7.

27. Zhao B, Shaw JM. Composition and Size Distribution of Coherent Nanostructures in Athabasca Bitumen and Maya Crude Oil. Energy Fuels. 2007 Sep 1;21(5):2795–804.

28. Paspek SC, Klein MT. Shale Oil Upgrading in Supercritical Water Solutions. Fuel Science and Technology International. 1990 Jan 1;8(6):673–87.

29. Speight JG, Long RB. The Concept of Asphaltenes Revisited. Fuel Science and Technology International. 1996 Jan 1;14(1-2):1–12.

30. Kandiyoti R, Herod AA, Bartle KD. Chapter 2 - Fossil Fuels: Origins and Characterization Methods. In: Kandiyoti R, Bartle AAHD, editors. Solid Fuels and Heavy Hydrocarbon

Liquids [Internet]. Oxford: Elsevier Science Ltd; 2006 [cited 2015 Aug 18]. p. 13–35. Available from: http://www.sciencedirect.com/science/article/pii/B9780080444864500027

31. President KJLPD. The Asphaltene and Wax Deposition Envelopes. Fuel Science and Technology International. 1996 Jan 1;14(1-2):13–39.

32. Shirokoff JW, Siddiqui MN, Ali MF. Characterization of the Structure of Saudi Crude Asphaltenes by X-ray Diffraction. Energy Fuels. 1997 May 1;11(3):561–5.

33. Mullins OC, Sheu EY, Hammami A, Marshall AG. Asphaltenes, Heavy Oils, and Petroleomics. Springer; 2007. 677 p.

34. Demirbaş A. Physical and Chemical Characterizations of Asphaltenes from Different Sources. Petroleum Science and Technology. 2002 Jan 6;20(5-6):485–95.

35. Ancheyta J, Rana M, Trejo F. Asphaltenes: Chemical Transformation During Hydroprocessing of Heavy Oils [Internet]. C R C Press LLC; 2009. Available from: http://books.google.com/books?id=idlcfpknjsgC

36. Sharma BK, Sharma CD, Bhagat SD, Erhan SZ. Maltenes and Asphaltenes of Petroleum Vacuum Residues: Physico-Chemical Characterization. Petroleum Science and Technology. 2007 Jan;25(1-2):93–104.

37. Calemma V, Iwanski P, Nali M, Scotti R, Montanari L. Structural Characterization of Asphaltenes of Different Origins. Energy Fuels. 1995 Mar 1;9(2):225–30.

38. Zhao S, Kotlyar LS, Woods JR, Sparks BD, Hardacre K, Chung KH. Molecular transformation of Athabasca bitumen end-cuts during coking and hydrocracking. Fuel. 2001 Jun;80(8):1155–63.

39. Rogel E, Carbognani L. Density Estimation of Asphaltenes Using Molecular Dynamics Simulations. Energy Fuels. 2003 Mar 1;17(2):378–86.

40. Gawrys KL, Spiecker PM, Kilpatrick PK. The Role of Asphaltene Solubility and Chemical Composition on Asphaltene Aggregation. Petroleum Science and Technology. 2003 Jan 5;21(3-4):461–89.

41. Sheremata JM, Gray MR, Dettman HD, McCaffrey WC. Quantitative Molecular Representation and Sequential Optimization of Athabasca Asphaltenes. Energy Fuels. 2004 Sep 1;18(5):1377–84.

42. Solari RB, Marzin R, Zbinden H. Comparison of Carbon Rejection and Hydrogen Addition Processes in Production-Upgrading Complexes. In: 15th World Petroleum Congress. World Petroleum Congress; 1997.

43. Speight JG. New approaches to hydroprocessing. Catalysis Today. 2004 Nov 24;98(1–2):55–60.

44. Speight JG. Visbreaking: A technology of the past and the future. Scientia Iranica. 2012 Jun;19(3):569–73.

45. Rodríguez-Reinoso F, Santana P, Palazon ER, Diez M-A, Marsh H. Delayed coking: Industrial and laboratory aspects. Carbon. 1998;36(1–2):105–16.

46. Ancheyta J. Modeling of Processes and Reactors for Upgrading of Heavy Petroleum. CRC Press; 2013. 565 p.

47. Chen Y-M. Recent advances in FCC technology. Powder Technology. 2006 Apr 25;163(1–2):2–8.

48. Puron H, Arcelus-Arrillaga P, Chin KK, Pinilla JL, Fidalgo B, Millan M. Kinetic analysis of vacuum residue hydrocracking in early reaction stages. Fuel. 2014 Jan 30;117, Part A:408–14.

49. Clar E. Polycyclic Hydrocarbons. Academic Press; 1964. 532 p.

50. Lee ML, Novotny MV, Bartle KD. Analytical chemistry of polycyclic aromatic compounds. Academic Press; 1981. 490 p.

51. Harvey RG. Polycyclic aromatic hydrocarbons. Wiley-VCH; 1997. 696 p.

52. Aihara J. Reduced HOMO−LUMO Gap as an Index of Kinetic Stability for Polycyclic Aromatic Hydrocarbons. J Phys Chem A. 1999 Sep 1;103(37):7487–95.

53. Haddon RC, Fukunaga T. Unified theory of the thermodynamic and kinetic criteria of aromatic character in the [4n+2]annulenes. Tetrahedron Letters. 1980 Jan 1;21(13):1191–2.

54. Zhou Z, Parr RG. New measures of aromaticity: absolute hardness and relative hardness. J Am Chem Soc. 1989 Sep 1;111(19):7371–9.

55. Weingärtner H, Franck EU. Supercritical Water as a Solvent. Angewandte Chemie International Edition. 2005 Apr 29;44(18):2672–92.

56. Savage PE. Organic Chemical Reactions in Supercritical Water. Chem Rev. 1999 Feb 1;99(2):603–22.

57. Bellissent-Funel M-C, Tassaing T, Zhao H, Beysens D, Guillot B, Guissani Y. The structure of supercritical heavy water as studied by neutron diffraction. The Journal of Chemical Physics. 1997 Aug 22;107(8):2942–9.

58. Fraga-Dubreuil J, Poliakoff M. Organic reactions in high-temperature and supercritical water. Pure and Applied Chemistry [Internet]. 2006 Jan 1 [cited 2014 Jul 28];78(11). Available from: http://www.iupac.org/publications/pac/78/11/1971/

59. Brunner G. Near critical and supercritical water. Part I. Hydrolytic and hydrothermal processes. The Journal of Supercritical Fluids. 2009 Jan;47(3):373–81.

60. Klein MT, Torry LA, Wu BC, Townsend SH, Paspek SC. Hydrolysis in supercritical water: Solvent effects as a probe of the reaction mechanism. The Journal of Supercritical Fluids. 1990 Dec;3(4):222–7.

61. Sato T, Kurosawa S, Smith Jr. RL, Adschiri T, Arai K. Water gas shift reaction kinetics under noncatalytic conditions in supercritical water. The Journal of Supercritical Fluids. 2004 Apr;29(1–2):113–9.

62. Rice SF, Steeper RR, Aiken JD. Water Density Effects on Homogeneous Water-Gas Shift Reaction Kinetics. J Phys Chem A. 1998 Apr 1;102(16):2673–8.

63. Melius CF, Bergan NE, Shepherd JE. Effects of water on combustion kinetics at high pressure. Symposium (International) on Combustion. 1991;23(1):217–23.

64. Bermejo MD, Cocero MJ. Supercritical water oxidation: A technical review. AIChE J. 2006 Nov 1;52(11):3933–51.

65. Rice SF, Steeper RR. Oxidation rates of common organic compounds in supercritical water. Journal of Hazardous Materials. 1998 Apr;59(2–3):261–78.

66. Portela JR, Nebot E, Martínez de la Ossa E. Kinetic comparison between subcritical and supercritical water oxidation of phenol. Chemical Engineering Journal. 2001 Jan 1;81(1–3):287–99.

67. Koo M, Lee WK, Lee CH. New reactor system for supercritical water oxidation and its application on phenol destruction. Chemical Engineering Science. 1997 Apr;52(7):1201–14.

68. Krajnc M, Levec J. On the kinetics of phenol oxidation in supercritical water. AIChE J. 1996 Jul 1;42(7):1977–84.

69. Oshima Y, Hori K, Toda M, Chommanad T, Koda S. Phenol oxidation kinetics in supercritical water. The Journal of Supercritical Fluids. 1998 Jun 15;13(1–3):241–6.

70. Li L, Chen P, Gloyna EF. Generalized kinetic model for wet oxidation of organic compounds. AIChE J. 1991 Nov 1;37(11):1687–97.

71. Boock LT, Klein MT. Lumping strategy for modeling the oxidation of C1-C3 alcohols and acetic acid in high-temperature water. Ind Eng Chem Res. 1993 Nov 1;32(11):2464–73.

72. Brock EE, Savage PE, Barker JR. A reduced mechanism for methanol oxidation in supercritical water. Chemical Engineering Science. 1998 Feb 6;53(5):857–67.

73. Vogel F, Blanchard JLD, Marrone PA, Rice SF, Webley PA, Peters WA, et al. Critical review of kinetic data for the oxidation of methanol in supercritical water. The Journal of Supercritical Fluids. 2005 Jul;34(3):249–86.

74. Ardali M, Barrufet MA, Mamora DD, Qiu F. A critical review of hybrid steam-solvent processes to recover heavy oil. In: Proceedings - SPE Annual Technical Conference and Exhibition. 2012. p. 1829–40.

75. Hemmati Sarapardeh A, Hashemi Kiasari H, Alizadeh N, Mighani S, Kamari A. Application of fast-SAGD in naturally fractured heavy oil reservoirs: A case study. In: SPE Middle East Oil and Gas Show and Conference, MEOS, Proceedings. 2013. p. 1946–53.

76. Rivera JA, Mamora DD. Production Acceleration and Injectivity Enhancement Using Steam-Propane Injection for Hamaca Extra-Heavy Oil. In: Proceedings - SPE Symposium on Improved Oil Recovery. 2002. p. 64–76.

77. Deng X, Huang H, Zhao L, Law DH-S, Nasr TN. Simulating the ES-SAGD process with solvent mixture in Athabasca reservoirs. Journal of Canadian Petroleum Technology. 2010;49(1):38–46.

78. Gupta SC, Gittins SD. Christina lake solvent aided process pilot. Journal of Canadian Petroleum Technology. 2006;45(9):15–8.

79. Ayodele OR, Nasr TN, Beaulieu G, Heck G. Laboratory experimental testing and development of an efficient low pressure ES-SAGD process. Journal of Canadian Petroleum Technology. 2009;48(9):54–61.

80. Jonasson HP, Kerr RK. SAGDOX - Steam assisted gravity drainage with the addition of oxygen injection. In: Society of Petroleum Engineers - SPE Heavy Oil Conference Canada 2013. 2013. p. 1543–617.

81. Mu HS, Wang YNN, Zhang Z, Zhou ZY, Liu YX. Feasibility study on development of heavy oil reservoir by steam-nitrogen assisted gravity drainage. 2014. 224 p.

82. Du Y, Wang Y, Jiang P, Ge JJ, Zhang GC. Mechanism and feasibility study of nitrogen assisted cyclic steam stimulation for ultra-heavy oil reservoir. In: Society of Petroleum Engineers - SPE Enhanced Oil Recovery Conference, EORC 2013: Delivering the Promise NOW! 2013. p. 36–45.

83. Miller JD, Misra M. Hot water process development for Utah tar sands. Fuel Processing Technology. 1982 Apr;6(1):27–59.

84. Lewan M, Winters J, Mc Donald J. Generation of oil-like pyrolyzates from organic-rich shales. Science. 1979;203(4383):897–9.

85. Park JH, Son SH. Extraction of bitumen with sub- and supercritical water. Korean J Chem Eng. 2010 Dec 23;28(2):455–60.

86. Canel M, Missal P. Extraction of solid fuels with sub- and supercritical water. Fuel. 1994 Nov 1;73(11):1776–80.

87. Meng, Hu H, Zhang Q, Ding M. Extraction of Tumuji Oil Sand with Sub- and Supercritical Water. Energy Fuels. 2006 May 1;20(3):1157–60.

88. Morimoto M, Sugimoto Y, Saotome Y, Sato S, Takanohashi T. Effect of supercritical water on upgrading reaction of oil sand bitumen. The Journal of Supercritical Fluids. 2010 Nov;55(1):223–31.

89. Ates A, Azimi G, Choi K-H, Green WH, Timko MT. The role of catalyst in supercritical water desulfurization. Applied Catalysis B: Environmental. 2014 Apr 5;147:144–55.

90. Kozhevnikov IV, Nuzhdin AL, Martyanov ON. Transformation of petroleum asphaltenes in supercritical water. The Journal of Supercritical Fluids. 2010 Nov;55(1):217–22.

91. Mandal PC, Wahyudiono, Sasaki M, Goto M. Non-catalytic vanadium removal from vanadyl etioporphyrin (VO-EP) using a mixed solvent of supercritical water and toluene: A kinetic study. Fuel. 2012 Feb;92(1):288–94.

92. Mandal PC, Wahyudiono, Sasaki M, Goto M. Nickel removal from nickel etioporphyrin (Ni-EP) using supercritical water in the absence of catalyst. Fuel Processing Technology. 2012 Dec;104:67–72.

93. Kruse A, Dinjus E. Hot compressed water as reaction medium and reactant: Properties and synthesis reactions. The Journal of Supercritical Fluids. 2007 Jan;39(3):362–80.

94. Ederer HJ, Kruse A, Mas C, Ebert KH. Modelling of the pyrolysis of tert-butylbenzene in supercritical water. The Journal of Supercritical Fluids. 1999 Jul 15;15(3):191–204.

95. Watanabe M, Kato S, Ishizeki S, Inomata H, Smith Jr. RL. Heavy oil upgrading in the presence of high density water: Basic study. The Journal of Supercritical Fluids. 2010 Jun;53(1–3):48–52.

96. Sato T, Mori S, Watanabe M, Sasaki M, Itoh N. Upgrading of bitumen with formic acid in supercritical water. The Journal of Supercritical Fluids. 2010 Nov;55(1):232–40.

97. Sato T, Trung PH, Tomita T, Itoh N. Effect of water density and air pressure on partial oxidation of bitumen in supercritical water. Fuel. 2012 May;95:347–51.

98. Trejo F, Rana MS, Ancheyta J. Thermogravimetric determination of coke from asphaltenes, resins and sediments and coking kinetics of heavy crude asphaltenes. Catalysis Today. 2010 Mar 30;150(3–4):272–8.

99. Rahmani S, McCaffrey W, Gray MR. Kinetics of Solvent Interactions with Asphaltenes during Coke Formation. Energy Fuels. 2002 Jan 1;16(1):148–54.

100. Vilcáez J, Watanabe M, Watanabe N, Kishita A, Adschiri T. Hydrothermal extractive upgrading of bitumen without coke formation. Fuel. 2012 Dec;102:379–85.

101. Speight JG, Moschopedis SE. Some observations on the molecular nature of petroleum asphaltenes. Am Chem Soc, Div Pet Chem, Prepr; (United States) [Internet]. 1979 Sep 1 [cited 2015 Sep 3];24:4. Available from: http://www.osti.gov/scitech/biblio/5720200

102. Brons GB, Siskin M, Wrzeszczynski KO. Upgrading of bitumen asphaltenes by hot water treatment containing carbonate (C-2726) [Internet]. US5326456 A, 1994 [cited 2015 Sep 3]. Available from: http://www.google.com.ar/patents/US5326456

103. Yi Y, Li S, Ding F, Yu H. Change of asphaltene and resin properties after catalytic aquathermolysis. Pet Sci. 2009 May 8;6(2):194–200.

104. Sato T, Adschiri T, Arai K, Rempel GL, Ng FTT. Upgrading of asphalt with and without partial oxidation in supercritical water☆. Fuel. 2003 Jul;82(10):1231–9.

105. Yang Y, Hildebrand F. Phenanthrene degradation in subcritical water. Analytica Chimica Acta. 2006 Jan 12;555(2):364–9.

106. Katritzky AR, Ignatchenko ES, Allin SM, Barcock RA, Siskin M, Hudson CW. Aqueous High-Temperature Chemistry of Carbo- and Heterocycles. 29.1 Reactions of Aryl Hydrocarbons, Aryl N-Oxides, and Aryl Carbonyl Compounds in Supercritical Water at 460 °C. Energy Fuels. 1997 Jan 1;11(1):160–73.

107. Katritzky AR, Barcock RA, Balasubramanian M, Greenhill JV, Siskin M, Olmstead WN. Aqueous High-Temperature Chemistry of Carbo- and Heterocycles. 20. Reactions of Some Benzenoid Hydrocarbons and Oxygen-Containing Derivatives in Supercritical Water at 460 .degree.C. Energy Fuels. 1994 Mar 1;8(2):487–97.

108. Onwudili JA, Williams PT. Flameless supercritical water incineration of polycyclic aromatic hydrocarbons. Int J Energy Res. 2006 Jun 10;30(7):523–33.

109. Onwudili JA, Williams PT. Reaction mechanisms for the hydrothermal oxidation of petroleum derived aromatic and aliphatic hydrocarbons. The Journal of Supercritical Fluids. 2007 Nov;43(1):81–90.

110. Ogunsola OM, Berkowitz N. Removal of heterocyclic S and N from oil precursors by supercritical water. Fuel. 1995 Oct;74(10):1485–90.

111. Patel KM, Bekker AY, Murthy AKS, Gefri FJ. Process for production of hydrogenated light hydrocarbons by treatment of heavy hydrocarbons with water and carbon monoxide [Internet]. US4675097 A, 1987 [cited 2015 Sep 4]. Available from: http://www.google.com.sv/patents/US4675097

112. He Z, Li L. Simultaneous Metal, Sulfur and Nitrogen Removal Using Supercritical Water [Internet]. WO/2009/085436, 2009 [cited 2015 Sep 4]. Available from: https://patentscope.wipo.int/search/en/detail.jsf?docId=WO2009085436

113. Jr SCP, Coker CD. Conversion of high boiling organic materials to low boiling materials [Internet]. US4557820 A, 1985 [cited 2015 Sep 4]. Available from: http://www.google.com.ar/patents/US4557820

114. Jr SCP. Conversion of high boiling organic materials to low boiling materials [Internet]. US4559127 A, 1985 [cited 2015 Sep 4]. Available from: http://www.google.com.sv/patents/US4559127

115. McCollum JD, Quick LM. Process for recovering and upgrading hydrocarbons from oil shale and tar sands [Internet]. US3948754 A, 1976 [cited 2015 Sep 4]. Available from: http://www.google.com.sv/patents/US3948754

116. McCollum JD, Quick LM. Process for recovering and upgrading hydrocarbons from oil shale and tar sands [Internet]. US3948755 A, 1976 [cited 2015 Sep 4]. Available from: http://www.google.com.sv/patents/US3948755

117. Clark PD, Hyne JB, Tyrer JD. Chemistry of organosulphur compound types occurring in heavy oil sands:: 1. High temperature hydrolysis and thermolysis of tetrahydrothiophene in relation to steam stimulation processes. Fuel. 1983 Aug 1;62(8):959–62.

118. Katritzky AR, Lapucha AR, Greenhill JV, Siskin M. Aqueous high-temperature chemistry of carbo- and heterocycles. 13. Sulfides and disulfides. Energy Fuels. 1990 Sep 1;4(5):562–71.

119. Katritzky AR, Lapucha AR, Luxem FJ, Greenhill JV, Siskin M. Aqueous high-temperature chemistry of carbo- and heterocycles. 14. Mercaptans and sulfonic acids. Energy Fuels. 1990 Sep 1;4(5):572–7.

120. Katritzky AR, Murugan R, Siskin M. Aqueous high-temperature chemistry of carbo- and heterocycles. 15. Aquathermolysis of arenethiols and aryl sulfides in the presence and absence of sodium bisulfite. Energy Fuels. 1990 Sep 1;4(5):577–84.

121. Katritzky AR, Murugan R, Balasubramanian M, Greenhill JV, Siskin M, Brons G. Aqueous high-temperature chemistry of carbo- and heterocycles. Part 16. Model sulfur compounds: a study of hydrogen sulfide generation. Energy Fuels. 1991 Nov 1;5(6):823–34.

122. Katritzky AR, Balasubramanian M, Siskin M. Aqueous high-temperature chemistry of carbo- and heterocycles. 17. Thiophene, tetrahydrothiophene, 2-methylthiophene, 2,5-dimethylthiophene, benzo[b]thiophene, and dibenzothiophene. Energy Fuels. 1992 Jul 1;6(4):431–8.

123. Katritzky AR, Barcock RA, Balasubramanian M, Greenhill JV, Siskin M, Olmstead WN. Aqueous High-Temperature Chemistry of Carbo- and Heterocycles. 21. Reactions of Sulfur-Containing Compounds in Supercritical Water at 460 .degree.C. Energy Fuels. 1994 Mar 1;8(2):498–506.

124. Timko MT, Ghoniem AF, Green WH. Upgrading and desulfurization of heavy oils by supercritical water. The Journal of Supercritical Fluids. 2015 Jan;96:114–23.

125. Vogelaar BM, Makkee M, Moulijn JA. Applicability of supercritical water as a reaction medium for desulfurisation and demetallisation of gasoil. Fuel Processing Technology. 1999 Nov;61(3):265–77.

126. Patwardhan PR, Timko MT, Class CA, Bonomi RE, Kida Y, Hernandez HH, et al. Supercritical Water Desulfurization of Organic Sulfides Is Consistent with Free-Radical Kinetics. Energy Fuels. 2013 Oct 17;27(10):6108–17.

127. Kida Y, Class CA, Concepcion AJ, Timko MT, Green WH. Combining experiment and theory to elucidate the role of supercritical water in sulfide decomposition. Physical Chemistry Chemical Physics. 2014;16(20):9220.

128. Hook BD, Akgerman A. Desulfurization of dibenzothiophene by in-situ hydrogen generation through a water gas shift reaction. Ind Eng Chem Proc Des Dev. 1986 Jan 1;25(1):278–84.

129. Adschiri T, Shibata R, Sato T, Watanabe M, Arai K. Catalytic Hydrodesulfurization of Dibenzothiophene through Partial Oxidation and a Water−Gas Shift Reaction in Supercritical Water. Industrial & Engineering Chemistry Research. 1998 Jul 1;37(7):2634–8.

130. Prins R. Catalytic hydrodenitrogenation. In: Advances in Catalysis [Internet]. Academic Press; 2001 [cited 2014 Jan 17]. p. 399–464. Available from: http://www.sciencedirect.com/science/article/pii/S0360056402460257

131. Katritzky AR, Lapucha AR, Siskin M. Aqueous high-temperature chemistry of carbo- and heterocycles. 18. Six-membered heterocycles with one nitrogen atom: pyridine, quinoline, acridine, and phenanthridine systems. Energy Fuels. 1992 Jul 1;6(4):439–50.

132. Katritzky AR, Luxem FJ, Murugan R, Greenhill JV, Siskin M. Aqueous high-temperature chemistry of carbo- and heterocycles. 19. Pyrroles and indoles. Energy Fuels. 1992 Jul 1;6(4):450–5.

133. Katritzky AR, Barcock RA, Siskin M, Olmstead WN. Aqueous High-Temperature Chemistry of Carbo- and Heterocycles. 23.Reactions of Pyridine Analogs and Benzopyrroles in Supercritical Water at 460 .degree.C. Energy Fuels. 1994 Jul 1;8(4):990–1001.

134. Katritzky AR, Shipkova PA, Allin SM, Barcock RA, Siskin M, Olmstead WN. Aqueous High-Temperature Chemistry. 24. Nitrogen-Containing Heterocycles in Supercritical Water at 460 .degree.C. Energy Fuels. 1995 Jul 1;9(4):580–9.

135. Yuan P-Q, Cheng Z-M, Zhang X-Y, Yuan W-K. Catalytic denitrogenation of hydrocarbons through partial oxidation in supercritical water. Fuel. 2006 Feb;85(3):367–73.

136. Pinto LD, dos Santos LMF, Al-Duri B, Santos RC. Supercritical water oxidation of quinoline in a continuous plug flow reactor—part 1: effect of key operating parameters. J Chem Technol Biotechnol. 2006 Jun 1;81(6):912–8.

137. Pinto LD, dos Santos LMF, Santos RC, Al-Duri B. Supercritical water oxidation of quinoline in a continuous plug flow reactor—part 2: kinetics. J Chem Technol Biotechnol. 2006 Jun 1;81(6):919–26.

138. Houser TJ, Tiffany DM, Li Z, McCarville ME, Houghton ME. Reactivity of some organic compounds with supercritical water. Fuel. 1986 Jun;65(6):827–32.

139. Li Z, Houser TJ. Kinetics of the catalyzed supercritical water-quinoline reaction. Ind Eng Chem Res. 1992 Nov 1;31(11):2456–9.

140. Ramirez de Agudelo MM, Galarraga C. A stable catalyst for heavy oil processing: III. Activity and selectivity. The Chemical Engineering Journal. 1991 Jun;46(2):61–8.

141. Kobayashi S, Kushiyama S, Aizawa R, Koinuma Y, Inoue K, Shimizu Y, et al. Kinetic study on the hydrotreating of heavy oil. 2. Effect of catalyst pore size. Ind Eng Chem Res. 1987 Nov 1;26(11):2245–50.

142. Mandal PC, Wahyudiono, Sasaki M, Goto M. Nickel removal from nickel-5,10,15,20-tetraphenylporphine using supercritical water in absence of catalyst: A basic study. Journal of Hazardous Materials. 2011 Mar 15;187(1–3):600–3.

143. Savage PE. A perspective on catalysis in sub- and supercritical water. The Journal of Supercritical Fluids. 2009 Jan;47(3):407–14.

144. Kruse A, Vogel H. Heterogeneous Catalysis in Supercritical Media: 2. Near-Critical and Supercritical Water. Chem Eng Technol. 2008 Sep 1;31(9):1241–5.

145. Clark PD, Kirk MJ. Studies on the Upgrading of Bituminous Oils with Water and Transition Metal Catalysts. Energy Fuels. 1994 Mar 1;8(2):380–7.

146. Jian C, Yihong L, Yunhua L, Guohe Q. Hydrocracking of Gudao Residual Oil with Dispersed Catalysts Using Supercritical Water-Syngas as a Hydrogen Source. Part II: The Comparison of Residue Hydrocracking in Different Hydrogen Sources. Petroleum Science and Technology. 2006 Nov 1;24(11):1339–46.

147. Fumoto E, Tago T, Tsuji T, Masuda T. Recovery of Useful Hydrocarbons from Petroleum Residual Oil by Catalytic Cracking with Steam over Zirconia-Supporting Iron Oxide Catalyst. Energy Fuels. 2004 Nov 1;18(6):1770–4.

148. Fumoto E, Tago T, Masuda T. Production of Lighter Fuels by Cracking Petroleum Residual Oils with Steam over Zirconia-Supporting Iron Oxide Catalysts. Energy Fuels. 2006 Jan 1;20(1):1–6.

149. Fumoto E, Matsumura A, Sato S, Takanohashi T. Kinetic Model for Catalytic Cracking of Heavy Oil with a Zirconia−Alumina−Iron Oxide Catalyst in a Steam Atmosphere. Energy Fuels. 2009 Nov 19;23(11):5308–11.

150. Fumoto E, Matsumura A, Sato S, Takanohashi T. Recovery of Lighter Fuels by Cracking Heavy Oil with Zirconia−Alumina−Iron Oxide Catalysts in a Steam Atmosphere†. Energy Fuels. 2009 Mar 19;23(3):1338–41.

151. Fumoto E, Sato S, Takanohashi T. Production of Light Oil by Oxidative Cracking of Oil Sand Bitumen Using Iron Oxide Catalysts in a Steam Atmosphere. Energy Fuels. 2011 Feb 17;25(2):524–7.

152. Funai S, Fumoto E, Tago T, Masuda T. Recovery of useful lighter fuels from petroleum residual oil by oxidative cracking with steam using iron oxide catalyst. Chemical Engineering Science. 2010 Jan 1;65(1):60–5.

153. Fedyaeva ON, Vostrikov AA. Hydrogenation of bitumen in situ in supercritical water flow with and without addition of zinc and aluminum. The Journal of Supercritical Fluids. 2012 Dec;72:100–10.

154. Vostrikov AA, Fedyaeva ON. Mechanism and kinetics of Al2O3 nanoparticles formation by reaction of bulk Al with H2O and CO2 at sub- and supercritical conditions. The Journal of Supercritical Fluids. 2010 Nov;55(1):307–15.

155. Vostrikov AA, Fedyaeva ON, Shishkin AV, Sokol MY. ZnO nanoparticles formation by reactions of bulk Zn with H2O and CO2 at sub- and supercritical conditions: I. Mechanism and kinetics of reactions. The Journal of Supercritical Fluids. 2009 Mar;48(2):154–60.

156. Vostrikov AA, Fedyaeva ON, Shishkin AV, Sokol MY. ZnO nanoparticles formation by reactions of bulk Zn with H2O and CO2 at sub- and supercritical conditions: II. Morphology and properties of nanoparticles. The Journal of Supercritical Fluids. 2009 Mar;48(2):161–6.

157. Striegel A, Yau WW, Kirkland JJ, Bly DD. Modern Size-Exclusion Liquid Chromatography: Practice of Gel Permeation and Gel Filtration Chromatography. John Wiley & Sons; 2009. 513 p.

158. Kandiyoti R, Herod A, Bartle K. Solid Fuels and Heavy Hydrocarbon Liquids: Thermal Characterisation and Analysis: Thermal Characterisation and Analysis. Elsevier; 2006. 365 p.

159. Berrueco C, Venditti S, Morgan TJ, Álvarez P, Millan M, Herod AA, et al. Calibration of Size-Exclusion Chromatography Columns with 1-Methyl-2-pyrrolidinone (NMP)/Chloroform Mixtures as Eluent: Applications to Petroleum-Derived Samples. Energy Fuels. 2008 Sep 17;22(5):3265–74.

160. Karaca F, Islas CA, Millan M, Behrouzi M, Morgan TJ, Herod AA, et al. The Calibration of Size Exclusion Chromatography Columns: Molecular Mass Distributions of Heavy Hydrocarbon Liquids. Energy Fuels. 2004 May 1;18(3):778–88.

161. Thompson M. CHNS Elemental Analysers. The Royal Society of Chemistry. 2008 Apr; AMCTB No 29. ISSN 1757-5958.

162. Boss CB, Freeden KJ Concepts, Instrumentation and Techniques in Inductively Coupled Plasma Optical Emission Spectrometry. Perkin Elmer; 2004. Third Edition. USA. pp 120.

163. Sun C, Hui R, Qu W, Yick S. Progress in corrosion resistant materials for supercritical water reactors. Corrosion Science. 2009 Nov;51(11):2508–23.

164. Kritzer P, Boukis N, Dinjus E. Factors controlling corrosion in high-temperature aqueous solutions: a contribution to the dissociation and solubility data influencing corrosion processes. The Journal of Supercritical Fluids. 1999 Jul 15;15(3):205–27.

165. Marrone PA, Hong GT. Corrosion control methods in supercritical water oxidation and gasification processes. The Journal of Supercritical Fluids. 2009 Dec;51(2):83–103.

166. Yin K, Qiu S, Tang R, Zhang Q, Zhang L. Corrosion behavior of ferritic/martensitic steel P92 in supercritical water. The Journal of Supercritical Fluids. 2009;50(3):235–9.

167. Hwang SS, Lee BH, Kim JG, Jang J. SCC and corrosion evaluations of the F/M steels for a supercritical water reactor. Journal of Nuclear Materials. 2008;372(2-3):177–81.

168. Asselin E, Alfantazi A, Rogak S. Corrosion of nickel–chromium alloys, stainless steel and niobium at supercritical water oxidation conditions. Corrosion Science. 2010;52(1):118–24.

169. Watanabe Y, Kobayashi T, Adschiri T. Significance of Water Density on Corrosion Behavior of Alloys in Supercritical Water. In: Corrosion 2001. Houston, Texas: NACE International; 2001.

170. Saito N, Tsuchiya Y, Akai Y, Omura H, Takada T, Hara N. Corrosion Performance of Metals for Supercritical Water, Oxidation-Utilized Organic Waste-Processing Reactors. Corrosion. 2006;62(5):383–94.

171. Eliaz N, Bryce Mitton D, Latanison RM. Review of Materials Issues in Supercritical Water Oxidation Systemsand the Need for Corrosion Control. Trans Indian Inst Met. 2003;56(3):1–10.

172. Daud A. Partial Oxidative Cracking of Polycyclic Aromatic Compounds under Supercritical Water Conditions for Heavy Hydrocarbons Upgrading. [London UK]: Imperial College London; 2011.

173. Pinilla JL, Arcelus-Arrillaga P, Puron H, Millan M. Selective Catalytic Steam Cracking of anthracene using mesoporous Al2O3 supported Ni-based catalysts doped with Na, Ca or K. Applied Catalysis A: General. 2013 May 24;459:17–25.

174. Swagelok. Gaugeable Tube Fittings and Adapter Fittings [Internet]. Swagelok; [cited 2015 Apr 30]. Available from: http://www.swagelok.com/downloads/webcatalogs/en/ms-01-140.pdf

175. Swagelok. Stainless Steel Seamless Tubing [Internet]. Swagelok; [cited 2015 Apr 30]. Available from: http://www.swagelok.com/downloads/webcatalogs/en/MS-01-181.pdf

176. Croiset E, Rice SF, Hanush RG. Hydrogen peroxide decomposition in supercritical water. AIChE J. 1997 Sep 1;43(9):2343–52.

177. Azadi P, Farnood R, Vuillardot C. Estimation of heating time in tubular supercritical water reactors. The Journal of Supercritical Fluids. 2011 Jan;55(3):1038–45.

178. Patrick WA, Wagner HB. Method for Complete Deoxygenation of Water. Anal Chem. 1949 Jun 1;21(6):752–3.

179. Amin VM, Olson NF. Spectrophotometric Determination of Hydrogen Peroxide in Milk1. Journal of Dairy Science. 1967 Apr;50(4):461–4.

180. Satterfield CN, Bonnell AH. Interferences in Titanium Sulfate Method for Hydrogen Peroxide. Anal Chem. 1955 Jul 1;27(7):1174–5.

181. ASTM International. Standard Test Method for n-Heptane Insolubles. Report No.: ASTM D3279.

182. ASTM International. Standard Test Method for Boiling Range Distribution of Petroleum Fractions by Gas Chromatography. Report No.: ASTM D2887.

183. Puron H. Novel Mesoporous Catalysts for Vacuum Residue Hydrocracking. [London UK]: Imperial College London; 2013.

184. Pine LA, Maher PJ, Wachter WA. Prediction of cracking catalyst behavior by a zeolite unit cell size model. Journal of Catalysis. 1984 Feb;85(2):466–76.

185. Corma A, Díaz-Cabañas MJ, Martínez-Triguero J, Rey F, Rius J. A large-cavity zeolite with wide pore windows and potential as an oil refining catalyst. Nature. 2002 Aug 1;418(6897):514–7.

186. Marcilly C. Present status and future trends in catalysis for refining and petrochemicals. Journal of Catalysis. 2003 May;216(1–2):47–62.

187. Einaga H, Futamura S. Catalytic oxidation of benzene with ozone over Mn ion-exchanged zeolites. Catalysis Communications. 2007 Mar;8(3):557–60.

188. Neamţu M, Zaharia C, Catrinescu C, Yediler A, Macoveanu M, Kettrup A. Fe-exchanged Y zeolite as catalyst for wet peroxide oxidation of reactive azo dye Procion Marine H-EXL. Applied Catalysis B: Environmental. 2004 Apr 8;48(4):287–94.

189. Kondru AK, Kumar P, Chand S. Catalytic wet peroxide oxidation of azo dye (Congo red) using modified Y zeolite as catalyst. Journal of Hazardous Materials. 2009 Jul 15;166(1):342–7.

190. Heinrichs C, Hölderich WF. Novel zeolitic hosts for ‘ship-in-a-bottle’ catalysts. Catalysis Letters. 1999 Apr 1;58(2-3):75–80.

191. Knops-Gerrits PP, Trujillo CA, Zhan BZ, Li XY, Rouxhet P, Jacobs PA. Oxidation catalysis with well-characterised vanadyl bis-bipyridine complexes encapsulated in NaY zeolite. Top Catal. 1996 Aug 1;3(3-4):437–49.

192. Daud M, Pinilla JL, Arcelus-Arrillaga P, Hellgardt K, Kandiyoti R, Millan M. Heavy oil upgrading in subcritical and supercritical water: Studies on model compounds. American Chemical Society, Division of Energy and Fuels Preprints. 2012;57(2):22–6.

193. Gloyna EF, Li L. Supercritical water oxidation research and development update. Environ Prog. 1995;14(3):182–92.

194. Thomason TB, Modell M. Supercritical Water Destruction of Aqueous Wastes. Hazardous Waste. 1984 Jan 1;1(4):453–67.

195. Rivas FJ. Polycyclic aromatic hydrocarbons sorbed on soils: A short review of chemical oxidation based treatments. Journal of Hazardous Materials. 2006 Nov 16;138(2):234–51.

196. Onwudili JA, Williams PT. Reaction mechanisms for the decomposition of phenanthrene and naphthalene under hydrothermal conditions. The Journal of Supercritical Fluids. 2007 Jan;39(3):399–408.

197. Kronholm J, Kuosmanen T, Hartonen K, Riekkola ML. Destruction of PAHS from soil by using pressurized hot water extraction coupled with supercritical water oxidation. Waste Manag. 2003;23(3):253–60.

198. Pinilla JL, Arcelus-Arrillaga P, Puron H, Millan M. Reaction pathways of anthracene selective catalytic steam cracking using a NiK/Al2O3 catalyst. Fuel. 2013 Jul;109:303–8.

199. Lee D-S, Gloyna EF, Li L. Efficiency of H2O2 and O2 in supercritical water oxidation of 2,4-dichlorophenol and acetic acid. The Journal of Supercritical Fluids. 1990 Dec;3(4):249–55.

200. Kobayashi S. Science of Synthesis: Water in Organic Synthesis. Georg Thieme Verlag; 2014. 1621 p.

201. García Jarana MB, Sánchez-Oneto J, Portela JR, Nebot Sanz E, Martínez de la Ossa EJ. Supercritical water gasification of industrial organic wastes. The Journal of Supercritical Fluids. 2008 Oct;46(3):329–34.

202. Guo LJ, Lu YJ, Zhang XM, Ji CM, Guan Y, Pei AX. Hydrogen production by biomass gasification in supercritical water: A systematic experimental and analytical study. Catalysis Today. 2007 Dec 15;129(3–4):275–86.

203. Lu Y, Guo L, Zhang X, Yan Q. Thermodynamic modeling and analysis of biomass gasification for hydrogen production in supercritical water. Chemical Engineering Journal. 2007 Jul 1;131(1–3):233–44.

204. Williams PT, Onwudili J. Composition of Products from the Supercritical Water Gasification of Glucose: A Model Biomass Compound. Ind Eng Chem Res. 2005;44(23):8739–49.

205. Thornton TD, Savage PE. Phenol oxidation in supercritical water. The Journal of Supercritical Fluids. 1990 Dec;3(4):240–8.

206. Matsumura Y, Nunoura T, Urase T, Yamamoto K. Supercritical water oxidation of high concentrations of phenol. Journal of Hazardous Materials. 2000 Apr 28;73(3):245–54.

207. Meyer JC, Marrone PA, Tester JW. Acetic acid oxidation and hydrolysis in supercritical water. AIChE J. 1995 Sep 1;41(9):2108–21.

208. Park T-J, Lim JS, Lee Y-W, Kim S-H. Catalytic supercritical water oxidation of wastewater from terephthalic acid manufacturing process. The Journal of Supercritical Fluids. 2003 Aug;26(3):201–13.

209. Li R, Savage PE, Szmukler D. 2-Chlorophenol oxidation in supercritical water: Global kinetics and reaction products. AIChE J. 1993 Jan 1;39(1):178–87.

210. Yang HH, Eckert CA. Homogeneous catalysis in the oxidation of p-chlorophenol in supercritical water. Ind Eng Chem Res. 1988 Nov 1;27(11):2009–14.

211. Hamley PA, Ilkenhans T, Webster JM, Garcia-Verdugo E, Venardou E, Clarke MJ, et al. Selective partial oxidation in supercritical water: the continuous generation of terephthalic acid from para-xylene in high yield. Green Chem. 2002 Jun 28;4(3):235–8.

212. Garcia-Verdugo E, Fraga-Dubreuil J, Hamley PA, Thomas WB, Whiston K, Poliakoff M. Simultaneous continuous partial oxidation of mixed xylenes in supercritical water. Green Chem. 2005 May 3;7(5):294–300.

213. Hirth T, Franck EU. Oxidation and Hydrothermolysis of Hydrocarbons in Supercritical Water at High Pressures. Berichte der Bunsengesellschaft für physikalische Chemie. 1993 Sep 1;97(9):1091–7.

214. Pehlivan D, Olcay A. Reactions of Methoxy-Substituted Aromatic Coal Mooels in Supercritical Solvents. Fuel Science and Technology International. 1994 Jan 1;12(3):375–88.

215. Çomak G. The Synthesis of Phthalate Derivatives in High-Pressure, High-Temperature Water. [Turkey]: Institute of Natural and Applied Sciences University of Cukurova; 2008.

216. Primo A, Garcia H. Zeolites as catalysts in oil refining. Chem Soc Rev. 2014 Oct 20;43(22):7548–61.

217. Kaduk JA, Faber J. Crystal Structure of Zeolite Y as a Function of Ion Exchange. Rigaku J. 1995;12(2):14–34.

218. Klein H, Kirschhock C, Fuess H. Adsorption and Diffusion of Aromatic Hydrocarbons in Zeolite Y by Molecular Mechanics Calculation and X-ray Powder Diffraction. J Phys Chem. 1994 Nov 1;98(47):12345–60.

219. Lin K-S, Wang HP. Shape selectivity of trace by-products for supercritical water oxidation of 2-chlorophenol effected by CuO/ZSM-48. Applied Catalysis B: Environmental. 1999 Oct 4;22(4):261–7.

220. Lin K-S, Wang HP. Byproduct Shape Selectivity in Supercritical Water Oxidation of 2-Chlorophenol Effected by CuO/ZSM-5. Langmuir. 2000 Mar 1;16(6):2627–31.

221. Savage PE, Dunn JB, Yu J. Recent Advances in Catalytic Oxidation in Supercritical Water. Combustion Science and Technology. 2006 Jan 1;178(1-3):443–65.

222. Oshima Y, Tomita K, Koda S. Kinetics of the Catalytic Oxidation of Phenol over Manganese Oxide in Supercritical Water. Ind Eng Chem Res. 1999 Nov 1;38(11):4183–8.

223. Yu J, Savage PE. Kinetics of MnO2-Catalyzed Acetic Acid Oxidation in Supercritical Water. Ind Eng Chem Res. 2000 Nov 1;39(11):4014–9.

224. Aki S, Abraham MA. Catalytic Supercritical Water Oxidation of Pyridine: Comparison of Catalysts. Ind Eng Chem Res. 1999 Feb 1;38(2):358–67.

225. Hildebrando EA, Andrade CGB, Junior R, Da CAF, Angélica RS, Valenzuela-Diaz FR, et al. Synthesis and characterization of zeolite NaP using kaolin waste as a source of silicon and aluminum. Materials Research. 2014 Aug;17:174–9.

226. Purón H, Pinilla JL, Berrueco C, Montoya de la Fuente JA, Millán M. Hydrocracking of Maya Vacuum Residue with NiMo Catalysts Supported on Mesoporous Alumina and Silica–Alumina. Energy Fuels. 2013 Jul 18;27(7):3952–60.

227. Su H-Y, Gorlin Y, C. Man I, Calle-Vallejo F, K. Nørskov J, F. Jaramillo T, et al. Identifying active surface phases for metal oxide electrocatalysts: a study of manganese oxide bi-functional catalysts for oxygen reduction and water oxidation catalysis. Physical Chemistry Chemical Physics. 2012;14(40):14010–22.

228. Tomita K, Oshima Y. Stability of Manganese Oxide in Catalytic Supercritical Water Oxidation of Phenol. Ind Eng Chem Res. 2004 Nov 1;43(24):7740–3.

229. Tan X-C, Liu Q-K, Zhu D-Q, Yuan P-Q, Cheng Z-M, Yuan W-K. Pyrolysis of heavy oil in the presence of supercritical water: The reaction kinetics in different phases. AIChE J. 2015 Mar 1;61(3):857–66.

230. Liu Q-K, Zhu D-Q, Tan X-C, Yang J-Y, Yuan P-Q, Cheng Z-M, et al. Lumped reaction kinetic models for pyrolysis of heavy oil in the presence of supercritical water. AIChE J. 2015 Aug 1;n/a – n/a.

231. De Sa Martins C. Partial Oxidative Cracking of Vacuum Residue in Supercritical Water using MNO2-Y-Zeolite Caalyst. [London UK]: Imperial College London; 2013.

232. Safety Rupture Discs [Internet]. Parr Instrument Company. [cited 2016 Jan 18]. Available from: http://www.parrinst.com/products/stirred-reactors/options-accessories/safety-rupture-discs/

233. Brunauer S, Deming LS; Deming WE, Teller E. On a Theory of the van der Waals Adsorption of Gases . J. Am. Chem. Soc. 1940; 62: 1723-32.

# Appendix

## 11.1. REACTION SYSTEMS

### 11.1.1. Microbomb reactor part inventory

| | Part Description | Supplier | Supplier Code | Number |
|---|---|---|---|---|
| 1 | 1/2” Union tee bored through | Swagelok | SS-810-3-BT | 1 |
| 2 | 1/2” Plug | Swagelok | SS-810-P | 2 |
| 3 | 1/2” to 1/4” Reducing port connector | Swagelok | SS-811-PC4 | 1 |
| 4 | 1/4” Union tee | Swagelok | SS-400-3 | 3 |
| 5 | 1/16” to 1/4" OD, Bored through reducer | Swagelok | SS-100-R4-BT | 1 |
| 6 | 1/8” to 1/4" OD, Reducer | Swagelok | SS-200-R4 | 2 |
| 7 | 1/4" High pressure needle valve, grafoil packing | Swagelok | SS-3HNRS4-G | 1 |
| 8 | 1/4" Relief valve | Swagelok | SS-4R3A-NE | 1 |
| 9 | Red spring kit 4000 – 5000 psig | Swagelok | 177-R3A-K1-G | 1 |
| 10 | 1/4" Union cross | Swagelok | SS-400-4 | 1 |
| 11 | 1/4" Ball valve, 0.6 Cv | Swagelok | SS-42GS4 | 3 |
| 12 | 1/4" Tube OD to 1/4" female connector | Swagelok | SS-400-7-4 | 1 |
| 13 | 1/4" Port connector | Swagelok | SS-401-PC | 5 |
| 14 | 1/4” Tube 0.065” wall | Swagelok | SS-T4-S-065-6ME-Z | 0.5 m |
| 15 | 1/4" NPT digital pressure gauge 0-9999 psig | Omega | DPG8000-DK | 1 |
| 16 | 1.5mm x 300mm type K thermocouple | TC | 405-004 | 1 |

### 11.1.2. Oxidative cracking reactor part inventory

| | Part Description | Supplier | Supplier Code | Number |
|---|---|---|---|---|
| 1 | 1/4” to 1/8” Reducing union | Swagelok | SS-400-6-2 | 4 |
| 2 | 1/4" to 3/8” Reducing union | Swagelok | SS-400-6-4 | 1 |
| 3 | 1/4” Union elbow | Swagelok | SS-400-9 | 18 |
| 4 | 1/4” Union cross | Swagelok | SS-400-4 | 1 |
| 5 | 1/4” Union tee | Swagelok | SS-400-3 | 20 |
| 6 | 1/2" Union tee | Swagelok | SS-810-3 | 3 |
| 7 | 3/8” Union tee | Swagelok | SS-600-3 | 1 |
| 8 | 1/4" Straight union | Swagelok | SS-400-6 | 1 |
| 9 | 1/4" to 1/2" OD, Reducer | Swagelok | SS-400-R-8 | 3 |
| 10 | 1/8” to 1/4" OD, Reducer | Swagelok | SS-200-R-4 | 4 |
| 11 | 1/16” to 1/4" OD, Bored through reducer | Swagelok | SS-100-R4-BT | 4 |
| 12 | 1/4" Port connector | Swagelok | SS-401-PC | 30 |
| 13 | 3/8” Port connector | Swagelok | SS-601-PC | 1 |
| 14 | 1/4" Tube OD to 1/4" female connector | Swagelok | SS-400-7-4 | 3 |
| 15 | 1/4" to 1/4" Male connector | Swagelok | SS-400-1-4RS | 4 |
| 16 | 3/8” to 1/4" Male connector | Swagelok | SS-600-1-4RS | 1 |
| 17 | 1/2" to 1/4" Male connector | Swagelok | SS-810-1-4RS | 1 |
| 16 | 1/4" Plug | Swagelok | SS-400-P | 2 |
| 17 | 1/4" Relief valve | Swagelok | SS-4R3A-NE | 3 |
| 18 | Red spring kit 4000 – 5000 psig | Swagelok | 177-R3A-K1-G | 3 |
| 19 | 1/4" Check valve 6000 psig | Swagelok | SS-CHS4-25 | 4 |
| 20 | 1/4" Tee type 7 micron filter | Swagelok | SS-4TF-7 | 2 |
| 21 | 1/4" Needle valve with grafoil packing | Swagelok | SS-3NBS4-G | 15 |
| 22 | SPL Med/High Back Pressure Regulator | Swagelok | KPB1S0A422P20000 | 1 |
| 23 | 1/4" 3-way valve 0.35 cv | Swagelok | SS-42GXS4 | 1 |
| 24 | 1/4" Sample vessel, 50 $cm^3$, 1800 psig | Swagelok | 304L-HDF4-50 | 1 |
| 25 | 1/4" Sample vessel, 150 cm3, 1800 psig | Swagelok | 304L-HDF4-150 | 1 |
| 26 | 1/2” Tube 0.065” wall | Swagelok | SS-T8-S-065-6ME | 0.5 m |
| 27 | 3/8” Tube 0.065” wall | Swagelok | SS-T6-S-065-6ME | 0.5 m |
| 28 | 1/4” Tube 0.065” wall | Swagelok | SS-T4-S-065-6ME | 4.0 m |
| 29 | 1/8” Tube 0.028” wall | Swagelok | SS-T2-S-028-6ME | 3.0 m |
| 30 | 1/4" NPT digital pressure gauge 0-9999 psig | Omega | DPG8000-DK | 3 |
| 31 | 1.5mm x 150mm type K thermocouple | TC | 405-001 | 1 |
| 32 | 1.5mm x 300mm type K thermocouple | TC | 405-004 | 3 |

### 11.1.3. $H_2O_2$ concentration analysis through UV-VIS spectrophotometry using $Ti(SO_4)_2/H_2SO_4$ solution calibration curve

| % w/w | Absorbance (AU) | | | | | |
|---|---|---|---|---|---|---|
| % | 1 | 2 | 3 | 4 | 5 | AVE |
| 1.50 | 3.35 | 3.35 | 3.65 | 3.66 | 3.66 | 3.53 |
| 1.25 | 2.75 | 2.95 | 2.87 | 2.96 | 2.96 | 2.90 |
| 1.00 | 2.36 | 2.40 | 2.40 | 2.38 | 2.40 | 2.39 |
| 0.80 | 1.95 | 1.96 | 1.96 | 1.95 | 1.97 | 1.96 |
| 0.60 | 1.43 | 1.43 | 1.44 | 1.44 | 1.44 | 1.44 |
| 0.40 | 0.91 | 0.91 | 0.91 | 0.91 | 0.91 | 0.91 |
| 0.20 | 0.47 | 0.47 | 0.47 | 0.48 | 0.47 | 0.47 |

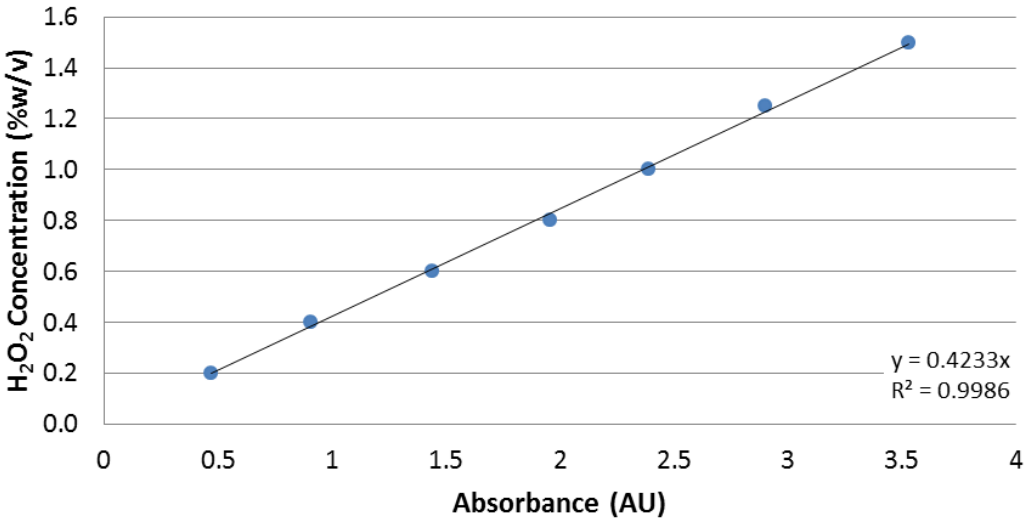


### 11.1.4. Microbomb reactor heating time curves

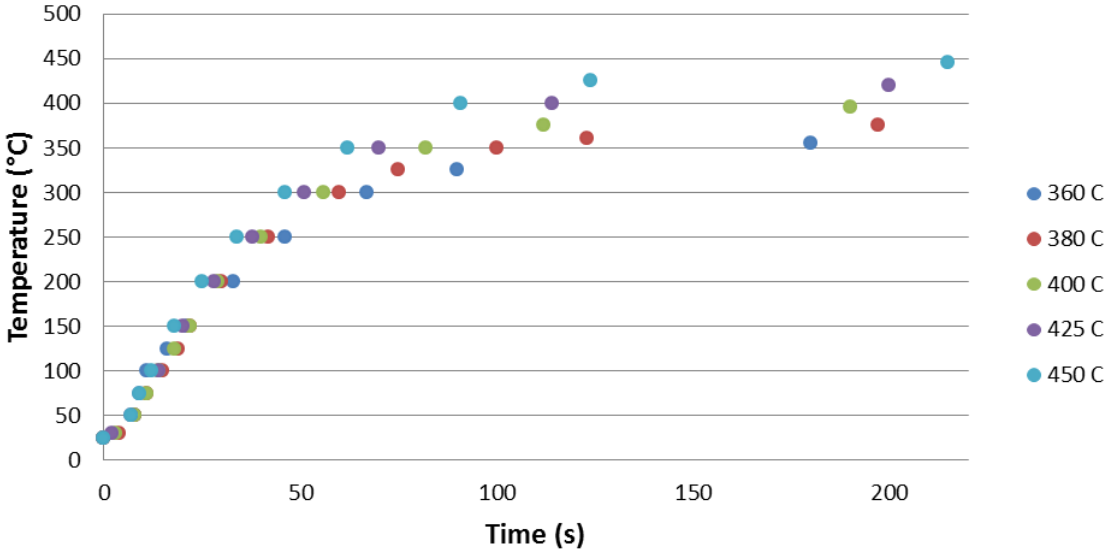

### 11.1.5. Microbomb system pressure calibration curves

In order to determine the volume of DI water required to reach the desired reaction pressure, calibration curves at different reaction temperatures were built from experimental data. In order to do this, 1.2 mL of $H_2O_2$ 30% w/v were added to the reactor as well as different DI water loadings. Temperature in the reactor was varied and the pressure obtained was registered. A calibration curve of DI water volume added to Pressure obtained was built for the reaction temperatures studied.

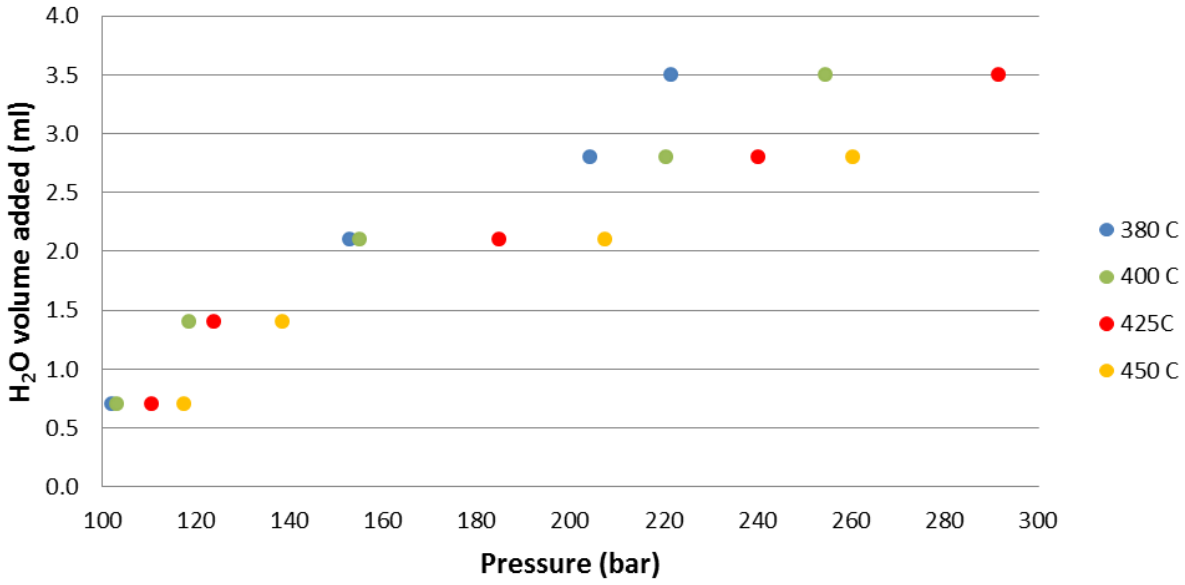


The equations to determine the amount of water required in order to reach a desired operation pressure at a fixed temperature in the microbomb reaction are reported in the following table.

| Reaction Temperature | Equation | $R^2$ coefficient |
|---|---|---|
| 380°C | $V_{H_2O} = 0.0219\, P_{380} - 1.44$ | 0.98 |
| 400°C | $V_{H_2O} = 0.0166\, P_{400} - 0.7358$ | 0.96 |
| 425°C | $V_{H_2O} = 0.0142\, P_{425} - 0.6072$ | 0.97 |
| 450°C | $V_{H_2O} = 0.0135\, P_{450} - 0.7031$ | 0.96 |

## 11.2. PRODUCT RECOVERY AND ANALYSIS

### 11.2.1. Nitrogen drying system

The custom made nitrogen drying system was designed in order to concentrate or dry liquid samples under an inert gas flow (N2 oxygen free) at room temperature and pressure. The system has the capacity to process eight samples at the same time, each with a valve to control the gas flow and an individual lifting mechanism that enables the adequate positioning of the vial depending on the volume of liquid product to dry.

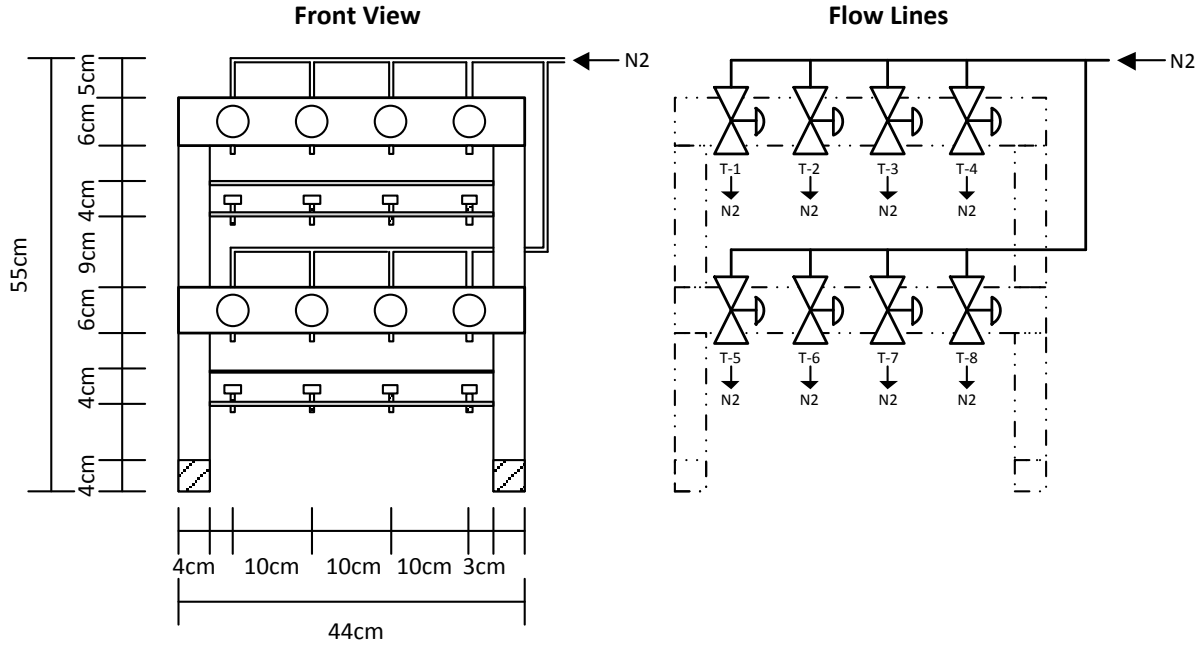


### 11.2.2. Calibration gas composition and response factors

The following table shows the standard gas mixture composition supplied by BOC and balanced with helium. In addition the response factors obtained for each gas from the analysis of calibration gas done through the injection of 100 □l of the gas standard 10 times are reported.

| | Calibration Gas Concentration | Response Factors |
|---|---|---|
| Hydrogen | 20% | 1.54E-04 |
| Carbon Monoxide | 20% | 2.29E-06 |
| Methane | 10% | 2.58E-06 |
| Carbon Dioxide | 20% | 1.73E-06 |
| Ethane, Propane, Propylene and n-Butane | 4% | N/A |

### 11.2.3. Liquid organic products calibration curves

Calibration curves for the main reactants and products obtained in reactions with model compounds are presented in the following table.

| Compound | Calibration Curve | Concentration Range | Linearity Coeffcient |
|---|---|---|---|
| Phenanthrene | $C_{ph} = 2E\text{-}09\ A_{ph} + 0.001$ | 0.002 – 0.012 g/ml | 0.997 |
| Methyl Naphthalene | $C_{mn} = 2E\text{-}09\ A_{mn} + 0.0001$ | 0.002 – 0.012 g/ml | 0.995 |
| Naphthalene | $C_{nph} = 2E\text{-}09\ A_{nph} - 1E\text{-}05$ | 0.002 – 0.012 g/ml | 0.985 |
| Anthraquinone | $C_{ant} = 4E\text{-}09\ A_{ant} - 2E\text{-}05$ | 0.002 – 0.012 g/ml | 0.999 |
| Phenanthrenequinone | $C_{phq} = 5E\text{-}09\ A_{phq} + 0.0004$ | 0.002 – 0.012 g/ml | 0.993 |
| Fluorenone | $C_{fln} = 4E\text{-}09\ A_{fln} - 0.0001$ | 0.002 – 0.012 g/ml | 0.999 |
| Fluorene | $C_{flu} = 3E\text{-}09\ A_{flu} - 0.0009$ | 0.002 – 0.012 g/ml | 0.990 |
| Dibenzofuran | $C_{dib} = 5E\text{-}09\ A_{dib} - 8E\text{-}05$ | 0.002 – 0.012 g/ml | 0.999 |
| Xanthone | $C_{xan} = 4E\text{-}09\ A_{xan} + 7E\text{-}05$ | 0.002 – 0.012 g/ml | 0.991 |
| Xanthene | $C_{xnt} = 5E\text{-}09\ A_{xnt} - 0.0003$ | 0.002 – 0.012 g/ml | 0.996 |
| Naphthalyc anhydride | $C_{nan} = 5E\text{-}09\ A_{nan} - 0.0002$ | 0.002 – 0.012 g/ml | 0.988 |
| pyrene | $C_{pyr} = 2E\text{-}09\ A_{pyr} - 4E\text{-}05$ | 0.002 – 0.012 g/ml | 0.994 |
| naphtoquinone | $C_{npq} = 3E\text{-}09\ A_{npq} + 0.0004$ | 0.002 – 0.012 g/ml | 0.999 |
| Methyl naphthol | $C_{mnp} = 4E\text{-}09\ A_{mnp} + 0.0001$ | 0.002 – 0.012 g/ml | 0.993 |

### 11.2.4. Boiling point distribution for gas-oil standard

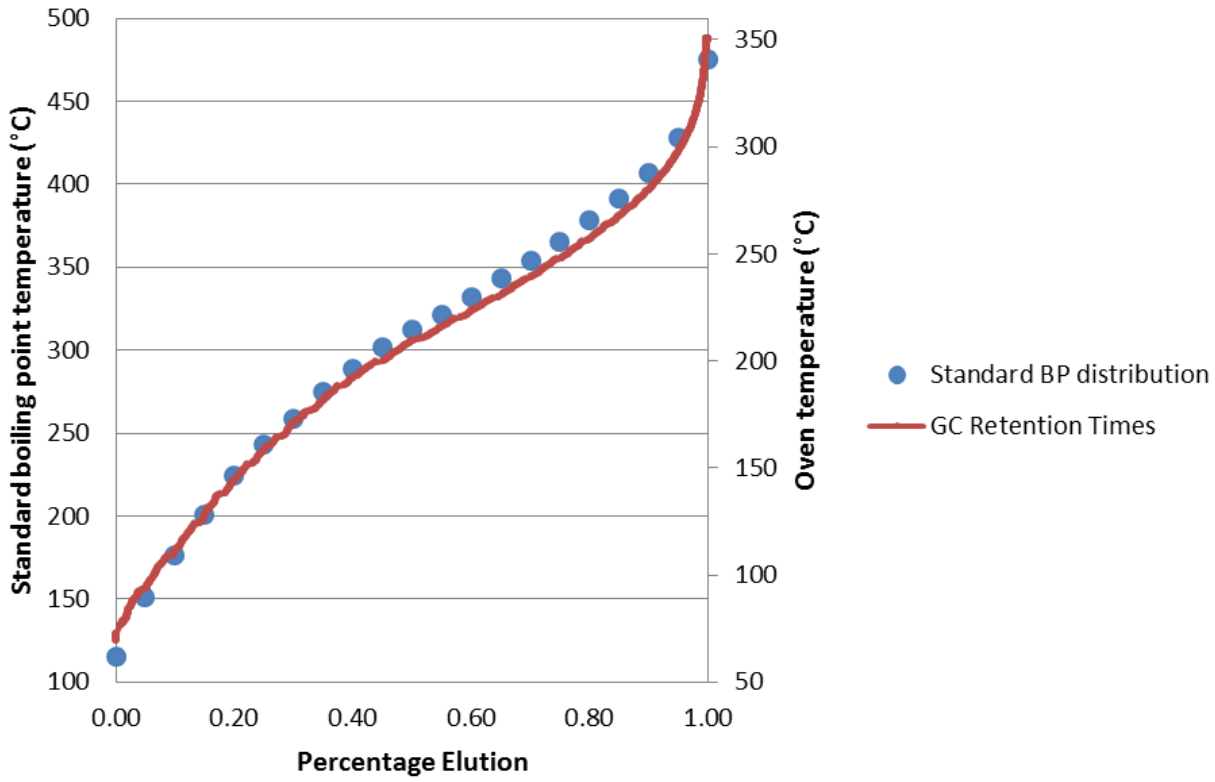

### 11.2.5. Size exclusion chromatography calibration curve

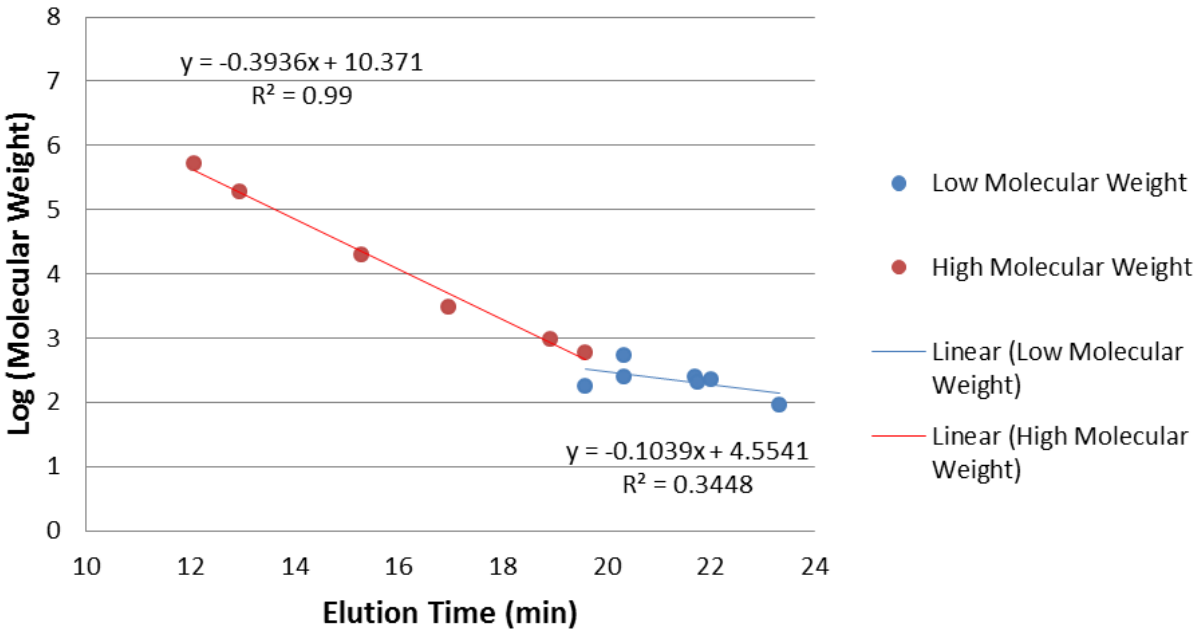


### 11.2.6. Experimental error estimation and repeatability

Experiments with model compounds in the microbomb reactor (T=450 °C, P=230 bar, $O/O_{stoich}$=0.4 and 60 min).

| N = 4 experiments | Mean | Std Deviation | Std Error | Error % |
|---|---|---|---|---|
| Phenanthrene recovery | 0.5122 | 0.0203 | 0.0102 | 1.98 |
| Liquid organic products yield | 0.2604 | 0.0106 | 0.0053 | 2.04 |
| Coke yield | 0.1058 | 0.0041 | 0.002 | 1.92 |
| Gas yield | 0.1217 | 0.0085 | 0.0043 | 3.49 |

Experiments with heavy oil in the microbomb reactor (T=425 °C, P=230 bar, O/VR=0.15 and 60 min)

| N = 4 experiments | Mean | Std Deviation | Std Error | Error % |
|---|---|---|---|---|
| Liquid organic products yield | 0.5661 | 0.0242 | 0.0121 | 2.14 |
| Coke yield | 0.1768 | 0.0112 | 0.0056 | 3.16 |
| Gas yield | 0.2606 | 0.0194 | 0.0097 | 3.71 |
| Maltene yield | 0.3221 | 0.0136 | 0.0068 | 2.12 |
| Asphaltene yield | 0.2440 | 0.0141 | 0.0071 | 2.89 |
| Sulfur removal | 0.5310 | 0.0358 | 0.0206 | 3.89 |
| Nitrogen removal | 0.4347 | 0.0310 | 0.0185 | 4.24 |
| Vanadium removal | 0.6671 | 0.0240 | 0.0139 | 2.08 |

Experiments with model compounds in the oxidative cracking flow reactor (T=425 °C, P=230 bar, $O/O_{stoich}$=0.03 and 0.75 min residence time)

| N = 3 experiments | Mean | Std Deviation | Std Error | Error % |
|---|---|---|---|---|
| Met Naphthalene recovery | 0.4326 | 0.0320 | 0.0185 | 4.27 |
| Liquid organic products yield | 0.1831 | 0.0134 | 0.0077 | 4.23 |
| Coke yield | 0.0304 | 0.0017 | 0.0010 | 3.18 |
| Gas yield | 0.3539 | 0.0187 | 0.0108 | 3.05 |

### 11.2.7. Molecular weight distribution obtained in experiments on oxidative cracking of VR in SCW

| | Liquid Product | | Maltene Fraction | | | Asphaltene Fraction | | |
|---|---|---|---|---|---|---|---|---|
| | BP Range (u) | Max Peak (u) | BP Range (u) | Max Peak (u) | Shoulder (u) | BP Range (u) | Max Peak (u) | Shoulder (u) |
| **Original Vacuum Residue** | | | | | | | | |
| Vacuum Residue | 23017 - 117 | 520 | 6471 - 91 | 289 | - | 32578 - 187 | 713 | - |
| **Reactions without Catalyst (230 bar, 60 min, O/VR ratio 0.15)** | | | | | | | | |
| 400°C | 6729 - 107 | 264 | 1847 - 82 | 293 | - | 7527 - 140 | 308 | - |
| 425°C | 3182 – 107 | 253 | 781 - 67 | 297 | - | 3591 - 107 | 297 | - |
| 450°C | 936 - 74 | 178 | 318 - 57 | 173 | - | 2388 - 86 | 245 | - |
| **Reactions with Mn-Y-Zeolite Catalyst (230 bar, 400°C, O/VR ratio 0.15, VR/cat ratio 0.25)** | | | | | | | | |
| 10 min | 25973 - 95 | 299 | 2736 - 85 | 269 | 176 | 34088 – 131 | 682 | - |
| 30 min | 27177 - 99 | 299 | 1687 – 83 | 266 | 171 | 16018 – 101 | 569 | - |
| 60 min | 17015 - 90 | 269 | 1473 - 73 | 263 | 166 | 8754 – 99 | 519 | - |
| 90 min | 6471 - 68 | 253 | 1451 - 60 | 259 | 165 | 9441 - 101 | 512 | - |
| **Reactions with Mn-Y-Zeolite Catalyst (230 bar, 425°C, O/VR ratio 0.15, VR/cat ratio 0.25)** | | | | | | | | |
| 10 min | 17015 - 60 | 259 | 1386 – 74 | 266 | 197 | 6185 – 97 | 327 | 174 |
| 30 min | 10029 – 59 | 241 | 817 – 61 | 168 | 250 | 6001 – 86 | 300 | 171 |
| 60 min | 6481 – 56 | 220 | 632 – 52 | 167 | 236 | 3230 – 87 | 297 | 170 |
| 90 min | 3537 - 58 | 198 | 613 - 52 | 162 | 236 | 3279 - 79 | 286 | 169 |
| **Reactions with Mn-Y-Zeolite Catalyst (230 bar, 450°C, O/VR ratio 0.15, VR/cat ratio 0.25)** | | | | | | | | |
| 10 min | 15541 - 74 | 237 | 1010 – 46 | 175 | 246 | 2820 -74 | 277 | 173 |
| 30 min | 6185 - 69 | 202 | 936 – 44 | 173 | - | 2906 -73 | 276 | 167 |
| 60 min | 3279 - 64 | 195 | 922 - 43 | 170 | - | 2695 -57 | 279 | 175 |
| 90 min | | | 936 - 37 | 175 | - | 2575 - 43 | 259 | 163 |

### 11.2.8. Conversion, yield to products, heteroatom removal and metal removal on the oxidative cracking of VR in the absence of catalyst at 230 bar

| | 400 °C | 425 °C | 450 °C |
|---|---|---|---|
| Conversion | 0.34 | 0.58 | 0.80 |
| Conversion to product bp < 450 °C | 0.30 | 0.41 | 0.34 |
| Yield to maltenes | 0.56 | 0.40 | 0.12 |
| Yield to asphaltenes | 0.29 | 0.21 | 0.14 |
| Yield to liquid with bp < 450 °C | 0.20 | 0.18 | 0.06 |
| Yield to gas | 0.10 | 0.24 | 0.28 |
| Yield to coke | 0.04 | 0.16 | 0.45 |
| Yield to heavy naphtha (bp < 205 °C) | 0.01 | 0.01 | 0.00 |
| Yield to kerosene (205 °C < bp < 260 °C) | 0.01 | 0.01 | 0.00 |
| Yield to diesel (260 °C < bp < 340 °C) | 0.05 | 0.06 | 0.02 |
| Yield to gas-oil (340 °C < bp < 425 °C) | 0.06 | 0.06 | 0.03 |
| Yield to residue ( 425 °C < bp < 450 °C) | 0.07 | 0.04 | 0.02 |
| Sulfur removal | 0.19 | 0.45 | 0.63 |
| Nitrogen removal | 0.06 | 0.37 | 0.76 |
| Vanadium removal | 0.06 | 0.53 | 0.84 |

### 11.2.9. Comparison between results with no catalyst, Y-Zeolite and Mn-Y-Zeolite as catalysts at 425 °C and 230 bar in the oxidative cracking of VR

| | No catalyst | Y-Zeolite | Mn-Y-Zeolite |
|---|---|---|---|
| Conversion | 0.58 | 0.62 | 0.63 |
| Conversion to product bp < 450 °C | 0.41 | 0.42 | 0.45 |
| Yield to maltenes | 0.40 | 0.31 | 0.31 |
| Yield to asphaltenes | 0.21 | 0.22 | 0.26 |
| Yield to liquid with bp < 450 °C | 0.18 | 0.16 | 0.20 |
| Yield to gas | 0.24 | 0.26 | 0.25 |
| Yield to coke | 0.16 | 0.20 | 0.17 |
| Yield to heavy naphtha (bp < 205 °C) | 0.01 | 0.00 | 0.00 |
| Yield to kerosene (205 °C < bp < 260 °C) | 0.01 | 0.00 | 0.00 |
| Yield to diesel (260 °C < bp < 340 °C) | 0.06 | 0.04 | 0.06 |
| Yield to gas-oil (340 °C < bp < 425 °C) | 0.06 | 0.05 | 0.07 |
| Yield to residue ( 425 °C < bp < 450 °C) | 0.04 | 0.06 | 0.06 |
| Sulfur removal | 0.45 | 0.49 | 0.50 |
| Nitrogen removal | 0.37 | 0.38 | 0.40 |
| Vanadium removal | 0.53 | 0.58 | 0.64 |

## 11.2.10. Conversion, yield to products, heteroatom removal and metal removal on the oxidative cracking of VR with Mn-Y-Zeolite as catalyst at 230 bar

### *11.2.10.1. Experiments at 400 °C*

| | 10 min | 30 min | 60 min | 90 min |
|---|---|---|---|---|
| Conversion | 0.13 | 0.22 | 0.42 | 0.47 |
| Conversion to product bp < 450 °C | 0.09 | 0.19 | 0.37 | 0.41 |
| Yield to maltenes | 0.59 | 0.56 | 0.51 | 0.45 |
| Yield to asphaltenes | 0.39 | 0.39 | 0.32 | 0.33 |
| Yield to liquid with bp < 450 °C | 0.11 | 0.17 | 0.25 | 0.25 |
| Yield to gas | 0.00 | 0.02 | 0.11 | 0.16 |
| Yield to coke | 0.03 | 0.04 | 0.06 | 0.05 |
| Yield to heavy naphtha (bp < 205 °C) | 0.00 | 0.00 | 0.00 | 0.00 |
| Yield to kerosene (205 °C < bp < 260 °C) | 0.00 | 0.00 | 0.00 | 0.00 |
| Yield to diesel (260 °C < bp < 340 °C) | 0.01 | 0.03 | 0.04 | 0.05 |
| Yield to gas-oil (340 °C < bp < 425 °C) | 0.03 | 0.05 | 0.09 | 0.09 |
| Yield to residue ( 425 °C < bp < 450 °C) | 0.07 | 0.09 | 0.12 | 0.10 |
| Sulfur removal | 0.06 | 0.10 | 0.23 | 0.32 |
| Nitrogen removal | 0.02 | 0.02 | 0.12 | 0.16 |
| Vanadium removal | 0.02 | 0.09 | 0.24 | 0.26 |

### *11.2.10.2. Experiments at 425 °C*

| | 10 min | 30 min | 60 min | 90 min |
|---|---|---|---|---|
| Conversion | 0.24 | 0.46 | 0.63 | 0.74 |
| Conversion to product bp < 450 °C | 0.19 | 0.35 | 0.45 | 0.44 |
| Yield to maltenes | 0.54 | 0.40 | 0.31 | 0.27 |
| Yield to asphaltenes | 0.42 | 0.36 | 0.25 | 0.19 |
| Yield to liquid with bp < 450 °C | 0.20 | 0.22 | 0.20 | 0.19 |
| Yield to gas | 0.00 | 0.13 | 0.25 | 0.25 |
| Yield to coke | 0.05 | 0.11 | 0.18 | 0.29 |
| Yield to heavy naphtha (bp < 205 °C) | 0.00 | 0.00 | 0.00 | 0.00 |
| Yield to kerosene (205 °C < bp < 260 °C) | 0.00 | 0.00 | 0.00 | 0.00 |
| Yield to diesel (260 °C < bp < 340 °C) | 0.03 | 0.06 | 0.06 | 0.06 |
| Yield to gas-oil (340 °C < bp < 425 °C) | 0.07 | 0.08 | 0.07 | 0.08 |
| Yield to residue ( 425 °C < bp < 450 °C) | 0.09 | 0.08 | 0.06 | 0.05 |
| Sulfur removal | 0.23 | 0.39 | 0.50 | 0.64 |
| Nitrogen removal | 0.09 | 0.32 | 0.40 | 0.06 |
| Vanadium removal | 0.24 | 0.51 | 0.64 | 0.87 |

### 11.2.10.3. Experiments at 450 °C

| | 10 min | 30 min | 60 min | 90 min |
|---|---|---|---|---|
| Conversion | 0.38 | 0.84 | 0.83 | 0.96 |
| Conversion to product bp < 450 °C | 0.26 | 0.40 | 0.58 | 0.38 |
| Yield to maltenes | 0.31 | 0.20 | 0.15 | 0.09 |
| Yield to asphaltenes | 0.49 | 0.10 | 0.13 | 0.02 |
| Yield to liquid with bp < 450 °C | 0.18 | 0.14 | 0.10 | 0.07 |
| Yield to gas | 0.08 | 0.26 | 0.25 | 0.30 |
| Yield to coke | 0.12 | 0.45 | 0.48 | 0.59 |
| Yield to heavy naphtha (bp < 205 °C) | 0.00 | 0.00 | 0.00 | 0.00 |
| Yield to kerosene (205 °C < bp < 260 °C) | 0.00 | 0.00 | 0.00 | 0.00 |
| Yield to diesel (260 °C < bp < 340 °C) | 0.05 | 0.04 | 0.03 | 0.02 |
| Yield to gas-oil (340 °C < bp < 425 °C) | 0.07 | 0.05 | 0.04 | 0.03 |
| Yield to residue ( 425 °C < bp < 450 °C) | 0.06 | 0.04 | 0.02 | 0.02 |
| Sulfur removal | 0.39 | 0.76 | 0.79 | 0.89 |
| Nitrogen removal | 0.21 | 0.66 | 0.75 | 0.91 |
| Vanadium removal | 0.38 | 0.74 | 0.89 | - |

## 11.2.11. Appendix 11.2.11 Catalyst Characterization

### 11.2.11.1. Appendix 11.2.11.1 BET Isotherms

BET isotherm for the Mn-Y-zeolite catalyst

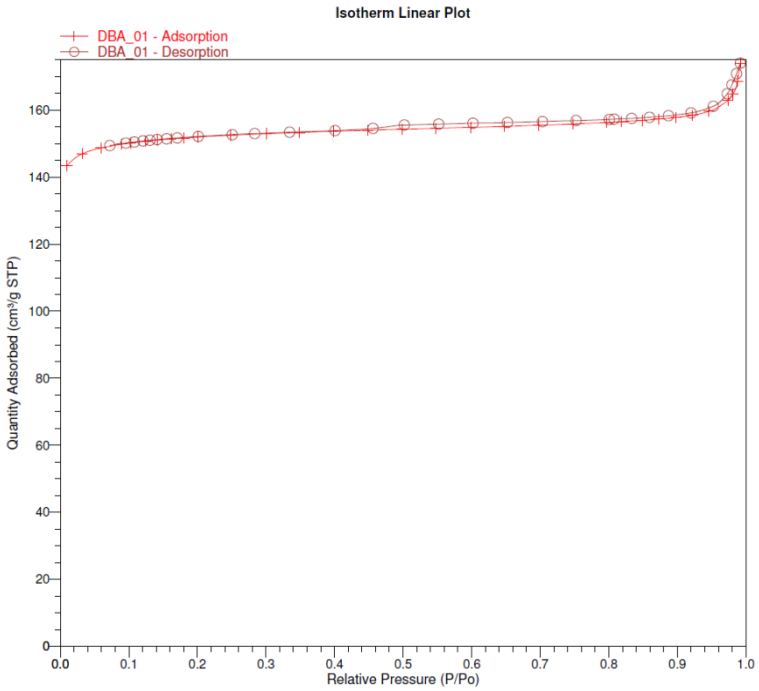

BET isotherm for the Mn-Y-zeolite catalyst

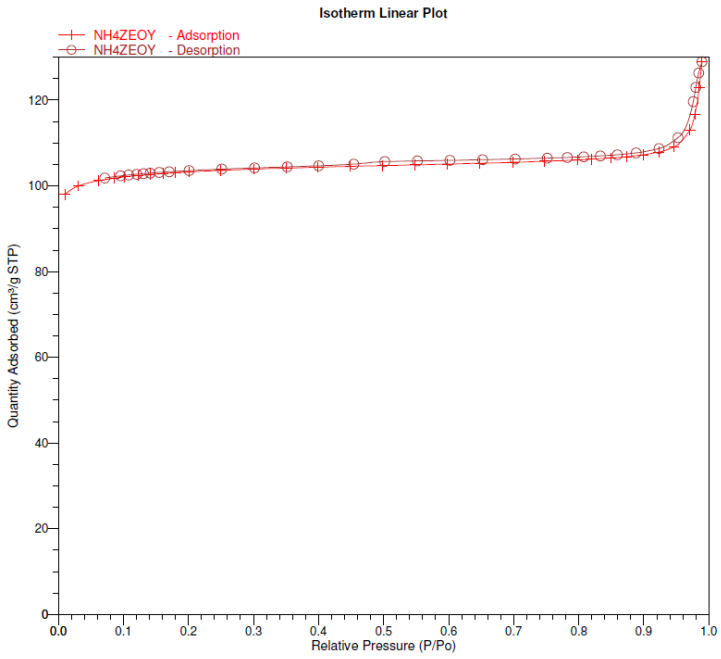


The isotherms present a combination of both a type I and IV isotherms based on the Brunauer Deming Deming Teller classification, which corresponds to a material with micropores and mesopores (233).

### *11.2.11.2. Appendix 11.2.11.2 SEM Images*

SEM images of the A) Mn-Y-zeolite catalyst at 1000x and B) the Y-zeolite catalyst at 900x.

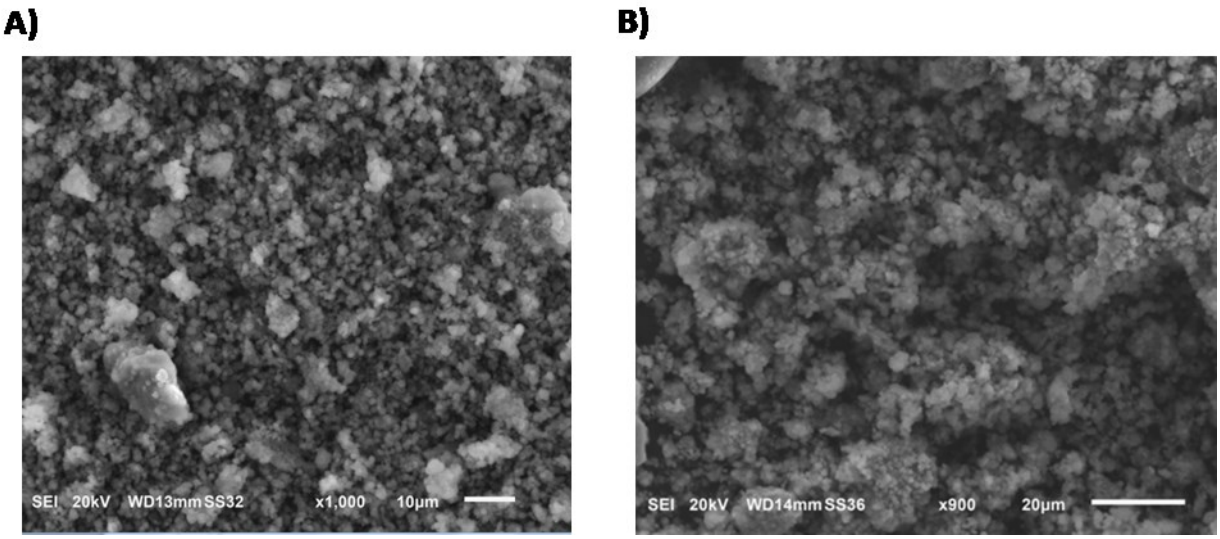

## 11.3. WORKS AND PUBLICATIONS RELATED TO THIS PROJECT

### 11.3.1. Accepted / submitted journal articles

- H Puron, P Arcelus-Arrillaga, K K Chin, J L Pinilla, B Fidalgo, M Millan: Kinetic analysis of vacuum residue hydrocracking in early reaction stages. Fuel. 01/2014; 117(PARTA):408-414. URL:http://www.sciencedirect.com/science/article/pii/S001623611300896X
- J L Pinilla, P Arcelus-Arrillaga, H Puron, M Millan: Selective Catalytic Steam Cracking of anthracene using mesoporous $Al_2O_3$ supported Ni-based catalysts doped with Na, Ca or K. Applied Catalysis A: General. 01/2013; 459:17-25. URL:http://www.sciencedirect.com/science/article/pii/S0926860X13001877
- J L Pinilla, P Arcelus-Arrillaga, H Puron, M Millan: Reaction pathways of anthracene selective catalytic steam cracking using a $NiK/Al_2O_3$ catalyst. Fuel. 01/2013; URL:http://www.sciencedirect.com/science/article/pii/S0016236113000434
- ARM Daud, J L Pinilla, P Arcelus-Arrillaga, K Hellgardt, R Kandiyoti, M Millan: Heavy oil upgrading in subcritical and supercritical water: studies on model compounds. American Chemical Society, Division of Energy and Fuels Preprints. 08/2012; 57(2):22.
- B Patel, P Arcelus-Arrillaga, A Izadpanah, K Hellgardt: Catalytic Hydrotreatment of Fast Liquefaction Algal Biocrude from Continuous Flow Reactor. (submitted to Applied Energy, 2016).
- J Remon, P Arcelus-Arrillaga, L Garcia, J Arauzo: Production of gaseous and liquid bio-fuels from the upgrading of lignocellulosic bio-oil in sub- and supercritical water: Effect of operating conditions on the process. Energy Conversion and Management. 2016; 119:14-36.
- T R Reina, P Yeletsky, J M Bermudez, P Arcelus-Arrillaga, V A Yakovlev, M Millan: Anthracene aquacracking using NiMo/SiO2 catalysts in supercritical water conditions. Fuel. 2016; 182:740-748.

### 11.3.2. Journal articles in preparation

- J. Remón, J. Arauzo, L. García, P. Arcelus-Arrillaga, M. Millan, I. Suelves, JL. Pinilla: Bio-oil upgrading in supercritical water using Ni-Co catalysts supported on carbon nanofibres.
- P Arcelus-Arrillaga, JL Pinilla, K Hellgardt, M Millan: Application of Hydrothermal and Supercritical Water for the Upgrading of Heavy and Unconventional Oils: A Review.

- P Arcelus-Arrillaga, K Hellgardt, M Millan: Effect of Process Conditions on the Hydrothermal Partial Oxidation of Heavy Oil Model Compound Phenanthrene.
- P Arcelus-Arrillaga, K Hellgardt, M Millan: Reaction Pathways of the Oxidative Cracking of Phenanthrene in Supercritical Water.
- P Arcelus-Arrillaga, K Hellgardt, M Millan: Continuous Oxidative Cracking of Naphthalene in Supercritical Water.
- P Arcelus-Arrillaga, JL Pinilla, K Hellgardt, M Millan: Oxidative Cracking of Vacuum Residue in Supercritical Water.
- P Arcelus-Arrillaga, JL Pinilla, C Sa-Martins, K Hellgardt, M Millan: Catalytic Oxidative Cracking of Vacuum Residue in Supercritical Water.
- E Fernandez-Puertas, P Arcelus-Arrillaga, N Murtuza, J Strang, M Millan: Oxidative Cracking of Heavy Oil in Supercritical Water, A Kinetic Study.

### 11.3.3. Contributions to Conferences

- P Arcelus-Arrillaga, JL Pinilla, I Suelves, K Hellgardt, M Millan. Catalytic Upgrading of Maya Oil Vacuum Residue through Partial Oxidation in Supercritical Water. AIChE Annual Meeting, Salt Lake City (USA), Nov 2015 (Oral).
- P Arcelus-Arrillaga, K Hellgardt, M Millan. Partial Oxidation of Heavy Oil Model Compounds in Supercritical Water. AIChE Annual Meeting, Salt Lake City (USA), Nov 2015 (Oral).
- T Ramirez-Reina, P Yeletsky, J Bermudez-Menendez, P Arcelus-Arrillaga, V Yakovlev, M Millan. Anthracene Aquacracking Using NiMo/$SiO_2$ Catalysts in Supercritical Water Conditions. AIChE Annual Meeting, Salt Lake City (USA), Nov 2015 (Oral).
- J Remón, P Arcelus-Arrillaga, J Arauzo, L García, M Millan. Liquid and Gas Biofuels from the Catalytic Reforming of Pyrolysis Bio-oil in Supercritical Water. Effect of the Operating Conditions on the Process. Med Green Forum III, Florence (Italy), Aug 2015 (Oral).
- J Remon, P Arcelus-Arrillaga, J Arauzo, a Garcia, M Millan. Pyrolysis Bio-oil Upgrading to Renewable Liquid Fuels by Catalytic Hydrocracking. Effect of Operating Conditions on the Process. Med Green Forum III, Florence (Italy), Aug 2015 (Oral).
- P Arcelus-Arrillaga, M Millan, K Hellgardt. Effect of Pressure, O/Ostoich Ratio and Temperature on the Partial Oxidation of Heavy Oil Model Compound Phenanthrene. AIChE Annual Meeting, Atlanta (USA), Nov 2014 (Oral).

- B Patel, P Arcelus-Arrillaga, K Hellgardt. Batch Catalytic Hydroprocessing of Algal Biocrude Produced Via Fast Hydrothermal Liquefaction. AIChE Annual Meeting, Atlanta (USA), Nov 2014 (Oral).
- JL Pinilla, H Puron, D Torres, P Arcelus-Arrillaga, B Fidalgo, M Millan, I Suelves. Carbon Nanofilaments (CNF & MWCNT) Supported Ni-MoS2 as Heavy Oil Hydroprocessing Catalysts. 6th International Symposium on Carbon for Catalysis CARBOCAT-IV, Trondheim (Norway), Jun 2014 (Oral).
- P Arcelus-Arrillaga, B Fidalgo, M Millan, K Hellgardt. Effect of Pressure and O/Ostoich ratio on the Partial Oxidation of Heavy Oil Model Compounds Phenantrene. ChemEng Day UK, Manchester (UK), Apr 2014 (Poster).
- P Arcelus-Arrillaga, AR Mohamad Daud, JL Pinilla, M Millan, K Hellgardt. Upgrading of Heavy Oil Model Compounds through Partial Oxidation in Supercritical Water. International Symposium of Chemical Reaction Engineering ISCREE22, Maastricht (Netherlands), Sep 2012 (Poster).
- JL Pinilla, AR Mohamad Daud, H Puron, P Arcelus-Arrillaga, M Millan, K Hellgardt. Catalytic steam cracking of anthracene using nickel based catalysts, 15th International Congress on Catalysis ICC2012, Munich (Germany), July 2012 (Poster).
- P Arcelus-Arrillaga, JL Pinilla, F Zemichael, M Millan, K Hellgardt. Design and Commissioning of a Flow Reactor to Upgrade Heavy Oil Model Compounds in Supercritical Water, IChemE Applied Catalysis and Reaction Engineering, Coventry (UK), April 2012 (Poster).
- P Arcelus-Arrillaga, AR Mohamad Daud, M Millan, K Hellgardt. Upgrading of Anthraquinone through Hydrolysis Reaction in Water at Supercritical Conditions, 12th International Conference on Petroleum Phase Behavior and Fouling PETROPHASE, London (UK), July 2011, (Poster).

### 11.3.4. Thesis Co-Supervised

- Oct 2014 – Sep 2015, Leonard Van Thiele, Upgrading of Heavy Oil in Supercritical Water (Imperial College London, Master Thesis).
- Oct 2014 – Sep 2015, Chiara Heide, Heavy Oil Hydrocracking (Imperial College London, Master Thesis).
- Oct 2013 – Sep 2014, Arran Marais-Gilchrist, Catalytic Upgrading of Vacuum Residue by Partial Oxidation in Supercritical Water (Imperial College London, Master Thesis).

- Oct 2013 – Sep 2014, Gemma Vinnicombe, Catalytic Hydrocracking of Heavy Oil Model Compounds in a Continuous Reactor (Imperial College London, Master Thesis).
- Oct 2012 – Sep 2013, Carla de Sa Martins, Partial oxidative cracking of Vacuum Residue in Supercritical Water using $MnO_2$-Y-Zeolyte Catalyst (Imperial College London, Master Thesis).